

The University of Southern Queensland
Faculty of Health, Engineering and Sciences

Use of Fibre-Optic (FBG) Sensors in Structural Health Monitoring – High Grade Reinforced Concrete Beams

A dissertation submitted by

Miss Amy Bernier

In fulfilment of the requirements of
Bachelor of Civil Engineering (Honours)

October 2015

Abstract

Natural disasters such as fires, floods and terrorist activities can cause some critical civil infrastructures to be exposed to extreme loading conditions and/or extreme temperatures. After such exposure these structures may become unsafe for general use. Currently there are limited mechanisms to evaluate the integrity of these structures after such disasters. Fibre Bragg Grating (FBG) Sensors could be used as in-situ sensing systems for reviewing the structural health of these damaged structures.

The aim of this research is to design a viable method of embedding FBG Sensors within a concrete structure. This technique will be utilised to analyse the structural health of concrete when curing, under normal operating conditions, and when heated to simulate the extreme condition of a fire. The application will be used to predict damage accumulation and conditions inside the concrete structure before, during, and after such an event.

The technique chosen to be tested was to encase FBG Sensors in concrete capsules before embedding them in a concrete structure. It was believed that such a technique would be superior to current and previous methods because it would be flexible and would move with the concrete. This technique thus was compared to an inflexible method of encasing that would encourage crack propagation and prove that FBG Sensors are capable of detecting internal deformities.

A reinforced concrete beam was chosen as the structure to be analysed. Three dimensional static and thermal models of the beam were created in Abaqus/CAE. These models were used to determine the locations of the most critical stresses, strains and temperatures. FBG Sensors, as well as thermocouples and strain gauges for result comparison, were then placed throughout the beam structure accordingly as measuring devices.

Only replicas of the sensor fibre were able to be successfully embedded in the beam with this unique concrete encasing. This is because the initial design failed. The experimental analysis suggests the modified method that was successfully embedded would be superior to alternate methods of encasing and embedding FBG Sensors, and could be a viable method for industry use. Further work would include the embedding of an actual FBG Sensor encased with the modified method of concrete encasing.

Disclaimer Page

University of Southern Queensland

Faculty of Health, Engineering and Sciences

ENG4111/ENG4112 Research Project

Limitations of Use

The Council of the University of Southern Queensland, its Faculty of Health, Engineering & Sciences, and the staff of the University of Southern Queensland, do not accept any responsibility for the truth, accuracy or completeness of material contained within or associated with this dissertation.

Persons using all or any part of this material do so at their own risk, and not at the risk of the Council of the University of Southern Queensland, its Faculty of Health, Engineering & Sciences or the staff of the University of Southern Queensland.

This dissertation reports an educational exercise and has no purpose or validity beyond this exercise. The sole purpose of the course pair entitled “Research Project” is to contribute to the overall education within the student’s chosen degree program. This document, the associated hardware, software, drawings, and other material set out in the associated appendices should not be used for any other purpose: if they are so used, it is entirely at the risk of the user.

Candidates Certification

I certify that the ideas, designs, theoretical and experimental work, results, analyses and conclusions presented in this dissertation are entirely my own, except where otherwise acknowledged.

I further certify that the work is original and has not been formerly submitted for assessment in any other course or institution, except where stated.

Amy Bernier

Student Number: 0061033255

Signature

Date

Acknowledgements

I would like to acknowledge the assistance and contribution of all that have aided the development of this dissertation.

A special thank-you to my supervisors Jayantha Epaarachchi and Sourish Banerjee who have been invaluable throughout the duration of this project.

I would also like to acknowledge The University of Southern Queensland for allowing me to use their facilities.

Table of Contents

Abstract	3
Candidates Certification	5
Acknowledgements	6
List of Tables.....	11
List of Figures	12
List of Appendices	15
Nomenclature and Acronyms	16
Chapter 1: Introduction.....	18
1.1 Background Information	18
1.2 The Problem	19
1.3 Research Significance	19
1.4 Research Scope and Objectives	20
1.5 Structure of Dissertation	22
Chapter 2: Literature Review – Structural Health Monitoring of Concrete.....	24
2.1 Introduction	24
2.2 The Constituents of Concrete	25
2.3 Properties of Concrete.....	26
2.3.1 Plastic State Properties	26
2.3.2 Hardened State Properties.....	28
2.4 Making a Reinforced Concrete Beam.....	33
2.4.1 Slump Test.....	33
2.4.2 Formwork.....	35
2.4.3 Compaction	36
2.5 The Curing of a Reinforced Concrete Beam.....	37
2.5.1 Procedure	37
2.5.2 Structural Behaviour.....	38
2.5.3 Thermal Behaviour.....	39
2.6 Loading of a Reinforced Concrete Beam	43
2.6.1 Structural Behaviour.....	43
2.7 Reinforced Concrete Beams and Heat.....	45
2.7.1 The Risks Associated with Heat Exposure Altering the Structural Properties of Concrete.....	45
2.7.2 Thermal Behaviour.....	47

2.8 Analysing Concrete Structural Health	52
2.8.1 Why Analyse Concrete Structural Health.....	52
2.8.2 Finite Element Analysis Techniques	53
2.8.3 Methods of Analysing the Behaviour of Reinforced Concrete Beams Insitu	54
2.8.4 Methods of Measuring Concrete Structural Health.....	67
Chapter 3: Dissertation Methodology.....	71
3.1 Design of Concrete Structure to be Analysed	72
3.2 How the Concrete Structure will be Analysed.....	73
3.3 Theoretical Analysis Techniques.....	74
3.3.1 Finite Element Analysis Techniques	74
3.3.2 Calculations.....	78
3.3.3 Information Purely from Literature.....	83
3.4 Experimental Analysis Technique	84
3.4.1 FBG Sensor Encasing Techniques	84
3.4.2 Placement of FBG Sensors, Strain gauges and Thermocouples.....	88
3.4.3 Casting of Concrete Structures	91
3.4.4 Sensor Calibration and Interrogation	92
3.4.5 Heat Test.....	94
3.4.6 Structural Health Tests	96
3.4.7 Calculations.....	97
Chapter 4: Project Organisation.....	101
4.1 Timelines	101
4.2 Resource Requirements	103
4.3 Risk Register	108
4.4 Consequential Effects	109

Chapter 5: Models and Results	110
5.1 Theoretical Analysis	111
5.1.1 Performance of FBG Encasing Techniques	111
5.1.2 Concrete Curing Temperatures	113
5.1.3 Heating Profile of Beam	115
5.1.4 Modulus of Elasticity of Beam	117
5.1.5 Midpoint Deflections Associated with Loading Beam	118
5.1.6 Maximum Principal Strains Associated with Loading Beam and Appropriate Placement of FBG Sensor	120
5.1.7 Maximum Principal Stresses Associated with Loading Beam	126
5.1.8 Tensile Strength of Beam	131
5.1.9 Flexural Strength of Beam	133
5.1.10 Compressive Strength of Beam	135
5.2 Experimental Analysis	137
5.2.1 Performance of FBG Encasing Techniques	137
5.2.2 Concrete Curing Temperatures	144
5.2.3 Heating Profile of Beam	148
5.2.4 Midpoint Deflections Associated with Loading Beam	151
5.2.5 Modulus of Elasticity of Beam	153
5.2.6 Principal Strains Associated with Loading Beam	155
5.2.7 Principal Stresses Associated with Loading Beam	159
5.2.8 Tensile Strength of Beam	162
5.2.9 Flexural Strength of Beam	164
5.2.10 Compressive Strength of Beam	167

Chapter 6: Discussion and Recommendations	170
6.1 Discussion of Theoretical and Experimental Results	170
6.1.1 Concrete Curing Temperatures	171
6.1.2 Heating Profile of Beam	172
6.1.3 Midpoint Deflections Associated with Loading Beam	172
6.1.4 Modulus of Elasticity of Beam	173
6.1.5 Maximum Principal Strains Associated with Loading Beam	174
6.1.6 Maximum Principal Stresses Associated with Loading Beam	176
6.1.7 Tensile Strength of Beam	177
6.1.8 Flexural Strength of Beam	178
6.1.9 Compressive Strength of Beam	179
6.1.10 Performance of FBG Sensor Encasing Techniques	180
6.2 Comparison with the Aim of the Research	182
6.3 Limitations and Improvements	184
Chapter 7: Conclusion	185
7.1 Overall Conclusion	185
7.2 Recommendations	186
7.3 Further Research	187
Chapter 8: List of References	188
Appendices	190

List of Tables

Table 1 - Stirrup, Reinforcement and Concrete Requirements	72
Table 2 - Specifications of FBG Sensor	92
Table 3 - Specifications of Strain Gauges to be used	93
Table 4 - Timelines	102
Table 5 - Resource Requirements	103
Table 6 - Theoretical Flexural Strengths and Failure Loads	133
Table 7 - Theoretical Compressive Strengths and Failure Loads	135
Table 8 - Surface Temperatures along the Length of the Side Face of the Beam Whilst at Maximum Temperature	149
Table 9 - Experimental Compression Test Results	167
Table 10 - Comparison of Theoretical and Experimental Modulus of Elasticity	173
Table 11 - Comparison of Theoretical and Experimental Strains	174
Table 12 - Comparison of Theoretical and Experimental Stresses	176
Table 13 - Comparison of Theoretical and Experimental Tensile Strengths	177
Table 14 - Comparison of Theoretical and Experimental Flexural Strengths	178
Table 15 - Comparison of Theoretical and Experimental Compressive Strengths	179
Table 16 – Theoretical Midpoint Deflections Associated with Loading Beam	203
Table 17 - Theoretical Maximum Principal Strains as Per Static Model	205
Table 18 - Validation of Theoretical Strains via Hand Calculations	206
Table 19 – Theoretical Maximum Principal Stresses as Per Static Model	209
Table 20 - Validation of Theoretical Stresses via Hand Calculations	210
Table 21 - Experimental Curing Temperatures of Beam 1	211
Table 22 - Experimental Curing Temperatures of Beam 2	231
Table 23 - Ambient Temperatures Whilst Curing (Started after 1 week)	251
Table 24 - Experimental Heating Temperatures	266
Table 25 - Experimental Midpoint Deflections Associated with Loading Beam	278
Table 26 - Experimental Maximum Principal Strains	280
Table 27 - Experimental Maximum Principal Stresses	281

List of Figures

Figure 1 - Relative Strength of Concrete Members at Various Locations (Millard, 1996)	29
Figure 2 - The Influence of Water-Cement Ratio on 28 Day Compressive Strength (Australia, 2002)	30
Figure 3 - The Effect of Air Voids on Potential Strength of Concrete (Australia, 2002)	31
Figure 4 - Typical Mould for Slump Test (Australia, 2002)	33
Figure 5 - Performing the Slump Test (Australia, 2002)	34
Figure 6 - Method of Measuring Slump (Australia, 2002)	34
Figure 7 - Examples of Slump (Australia, 2002)	34
Figure 8 - Loss of Strength through Incomplete Compaction (Australia, 2002)	36
Figure 9 - The Effect of Curing Temperature on Strength Gain (Australia, 2002)	39
Figure 10 - Typical Internal and Surface Temperatures Generated as Concrete Cures (Yadav, 2015)	41
Figure 11 - Typical Internal Temperatures of Differing Concrete Specimens Whilst Curing ((APEE), 2005)	42
Figure 12 - Types of Stresses (Australia, 2002)	43
Figure 13 - Vertical Shear Stresses (Australia, 2002)	43
Figure 14 - Horizontal Shear Stresses (Australia, 2002)	44
Figure 15 - Diagonal Tension Cracks (Australia, 2002)	44
Figure 16 - Concrete Compressive Strength after Heating for Different Temperatures (Yao, 2006)	48
Figure 17 - Compressive Strength of Concrete after Various Temperature Exposures (Association, 2002)	48
Figure 18 - Concrete Tensile Strength after Heating for Different Temperatures (Yao, 2006)	49
Figure 19 - Concrete Stress-Strain Curves after Heating for Different Temperatures (Yao, 2006)	50
Figure 20 - The Relationship between Temperature Exposure and Concrete Flexural Strength (Association, 2002)	50
Figure 21 - The Relationship Between Temperature Exposure and Modulus of Elasticity (Association, 2002)	51
Figure 28 - Measurement Principal of FBG Sensor (Su and Han, 2014)	54
Figure 30 - FBG Sensors Grating Structures (Erdogan, 1997)	56
Figure 22 - Basic Thermocouple Circuit (Engineering, N/D)	62
Figure 23 - NI cDAQ-9174 Used for Thermocouple Interrogation	63
Figure 24 - Basic Strain Gauge Circuit (Dasar, 2013)	64
Figure 25 - How to Orientate Strain Gauges to Read Bending Strain (Inc, 2015a)	65
Figure 26 - Strain Gauge Interrogator Unit	66
Figure 27 - Quarter Bridge Layout	66
Figure 31 - Configuration of a General Compression Test (Australia, 2002)	67
Figure 32 - Modes of Failure of Standard Concrete Cylinders (M. Nadim Hassoun, 2012)	68

Figure 33 - Standard Configuration of a Three Point Bending Test (Kopeliovich, 2012)	69
Figure 34 - Examples of Shear and Flexural Cracks	69
Figure 35 - Concrete Beam Structure	72
Figure 36 - Method of Encasing FBG Sensor in Concrete Capsule Moulds	85
Figure 37 - Aluminium Encasing of FBG Sensor	86
Figure 38 - Positioning of FBG Sensor	88
Figure 39 - Positioning of Thermocouples	89
Figure 40 - Positioning of Strain gauges	90
Figure 41 - Comparable Theoretical Internal Curing Temperatures ((APEE), 2005)..	113
Figure 42 – Theoretical Temperature Profile of Reinforced Concrete Beam	115
Figure 43 - Theoretical Midspan Deflections at Various Loads	118
Figure 44 – Theoretical Maximum Principal Strain of Entire Beam Structure	120
Figure 45 – Theoretical Maximum Principal Strain through Centre of Beam	121
Figure 46 - Theoretical Maximum Principal Strains for Various Loads	122
Figure 47 - Verification of Theoretical Maximum Principal Strains for Various Loads	124
Figure 48 - Theoretical Maximum Principal Stresses for Various Loads	126
Figure 49 - Verification of Theoretical Maximum Principal Stresses for Various Loads	129
Figure 50 – Modified Concrete Capsule Moulds	138
Figure 51 - Replica Fibre Shown to Survive Modified Method of Concrete Encasing	139
Figure 52 - Replica Fibre Tied in Position Using Fishing Line	139
Figure 53 - Replica Fibre Shown to Survive Pouring and Compaction	140
Figure 54 - Proof Replica Fibre is embedded in Concrete Beam	140
Figure 55 - Concrete Encasing Shown to Bond when Embedded in Concrete	141
Figure 56 - Uninterrupted FBG Sensor Spectra	142
Figure 57 – Interrupted FBG Sensor Reading Suggesting Internal Crack within Beam	143
Figure 58 - Experimental Curing Temperatures of Beam One Week One	144
Figure 59 - Theoretical Curing Temperatures of Beam 1 Week 2	146
Figure 60 - Experimental Temperature Variation of Concrete Beam over Time due to Heating	148
Figure 61 - Experimental Midpoint Deflections with Varying Loads	151
Figure 62 - Comparison of Maximum Principal Strains on Control and Heated Beams	155
Figure 63 - Maximum Principal Strains Read by the FBG Sensor during the Three Point Bending Test	156
Figure 64 - Comparison of Maximum Principal Stresses of Control and Heated Beam Specimens	159
Figure 65 - Maximum Principal Stresses Read by FBG Sensor during the Three Point Bending Test	160
Figure 66 - Flexural and Shear Cracking of Control Beam	165
Figure 67 - Flexural and Shear Cracking of Heated Beam	165
Figure 68 - Concrete Cylinder under Compression Tests at Failure Load	168

Figure 69 - Failure Planes of Control and Heated Concrete Cylinders	168
Figure 70 - Optical Sensing Interrogator Specifications (Micron Optics Inc, 2009) ...	202
Figure 71 - Theoretical Maximum Principal Strain through Reinforcement Bars	204
Figure 72 – Theoretical Maximum Principal Strain through Reinforcement Bars	204
Figure 73 – Theoretical Maximum Principal Stress over Entire Beam Structure	207
Figure 74 – Theoretical Maximum Principal Stress through Centre of Beam	207
Figure 75 – Theoretical Maximum Principal Stress through Reinforcement.....	208
Figure 76 – Theoretical Maximum Principal Stress through Reinforcement.....	208

List of Appendices

Appendix A - Project Specification	190
Appendix B – Risk Assessment Documentation	191
Appendix C – Interrogation Unit Specifications	202
Appendix D – Additional Theoretical Analysis Results	203
Appendix D1 – Midpoint Deflections Associated with Loading Beam	203
Appendix D2 – Maximum Principal Strains Associated with Loading Beam ..	204
Appendix D3 – Maximum Principal Stresses Associated with Loading Beam .	207
Appendix E – Additional Experimental Analysis Results	211
Appendix E1 – Curing Temperatures of Beams	211
Appendix E2 – Heating Temperatures	266
Appendix E3 – Midpoint Deflections	278
Appendix E4 – Maximum Principal Strains Associated with Loading Beam ..	280
Appendix E5 – Maximum Principal Stresses Associated with Loading Beam .	281

Nomenclature and Acronyms

The following list details the nomenclature and acronyms used in the following text.

α	Coefficient of Thermal Expansion of Glass
A	Area of Cylinder
A _s	Area of Tensile Reinforcing Steel
B	Width of Beam
d _i	Diameter of Cylinder
D	Depth of Beam
ξ	Thermooptic Coefficient
e	Maximum Principal Strain
Δe	Change in Strain
E	Modulus of Elasticity
E _c	Theoretical Modulus of Elasticity of Concrete
E _s	Theoretical Modulus of Elasticity of Reinforcing Steel
FBG	Fibre Bragg Grating
f _c	Compressive Strength
f _y	Yielding Strength of Steel
kN	Kilo Newtons
kW	Kilo Watts
L	Length of Beam
L _s	Length of Beam Supports
m	Metres
m ³	Cubic Metres
mm	Millimetres
MPa	Mega Pascals
M _U	Ultimate Moment Capacity
N	Newtons

P	Applied Load
Pa	Pascals
P_U	Ultimate Applied Load
SG	Strain Gauge
ΔT	Change in Temperature
TC	Thermocouple
3D	Three Dimensional
I	Moment of Inertia
σ	Maximum Principal Stress
δ	Midpoint Deflection
λ_B	Original Wavelength of FBG Sensor
$\Delta\lambda_B$	Change in Wavelength of FBG Sensor
p_e	Strain Optic Coefficient

Chapter 1: Introduction

Chapter one will provide background information, detail the problem, discuss the significance, scope and objectives, and give an overview of the structure of the dissertation.

1.1 Background Information

Natural disasters such as fires, floods and terrorist activities can cause some critical civil infrastructures to be exposed to extreme loading conditions and/or extreme temperatures. After such exposure these structures may become unsafe for general use. In some cases though, the structural integrity of the structure may be intact, and thus not need repair. Structural health monitoring can allow for the determination of the integrity of a structure after such an event (Su and Han, 2014).

Structural health monitoring can be applied to a variety of infrastructures. Such infrastructures include bridges, buildings, dams, mines, underpasses, pipelines and aerospace structures. Monitoring the structural health of such infrastructures leads to greater safety as it means engineers are aware of when damages have occurred. It may also lead to reduced maintenance, since whether there is in fact a problem and its source is able to be determined. This means unnecessary maintenance will not be performed. Since damages can be fixed at early onset, structural health monitoring can lead to increased structural longevity and health (Su and Han, 2014).

1.2 The Problem

Natural disasters such as fires, floods and terrorist activities can cause some critical civil infrastructures to be exposed to extreme loading conditions and/or extreme temperatures. After such exposure these structures may become unsafe for general use. Currently there are limited mechanisms to evaluate the integrity of these structures after such disasters. The structural integrity/health of these damaged structures, however, can be reviewed if there is an in-situ sensing and measuring system. FBG Sensors, for example, could be embedded in a structure and used to measure strain and temperature.

The aim of this research is to design a viable method of embedding FBG Sensors within a concrete structure. This technique will be utilised to analyse the structural health of concrete when curing, under normal operating conditions, and when heated to simulate the extreme condition of a fire. The application will be used to predict damage accumulation and conditions inside the concrete structure before, during, and after such an event.

1.3 Research Significance

Currently there are limited mechanism to evaluate the integrity and health of structures in-situ. Most evaluation techniques for concrete structures involve partially destructive tests (Millard, 1996). There has been limited research regarding the embedding of FBG Sensors within a concrete structure. If a design was made that ensured the movement of the FBG Sensors coincide with the movement of the concrete structure, this would be a technique that could be utilised for monitoring structural health and integrity of concrete worldwide. The utilisation of this technique would, however, depend on necessity and affordability.

1.4 Research Scope and Objectives

The following is the defined scope of this investigation into structural health monitoring of concrete structures:

1. Conduct an extensive literature review on the behaviour of concrete when curing, when loaded, and when subjected to heat. Also include an overview of structural health monitoring techniques with a focus on FBG Sensors, strain gauges, thermocouples, three point bending tests, and compression tests.
2. Determine an appropriate testing temperature and method of heating.
3. Model a chosen concrete beam structure using Abaqus 3D finite element analysis in order to predict structural and thermal behaviours and thus determine appropriate placement of FBG Sensors, strain gauges and thermocouples.
4. Perform relevant hand calculations to theoretically analyse the effects of temperature on the chosen beam structure.
5. Design a method for placing FBG Sensors within the concrete beam structures.
6. Build two concrete beam structures with embedded FBG Sensors and thermocouples.
7. Monitor internal temperature changes of the two concrete beam structures for 28 days as they cure.
8. Keep one beam as the control and with the other simulate the situation of heat and monitor the temperature variation inside the structure using embedded FBG sensor(s) & thermocouples.
9. Carry out compression and three point bending tests to concrete specimens.

10. Analyse experimental data.

11. Submit an academic dissertation on the project findings.

As time permits:

12. Analyse a third concrete beam structure with a deliberately made internal crack.

Chapter 3 outlines the methodology and how these research objectives will be achieved.

1.5 Structure of Dissertation

Chapter one of this dissertation has introduced the problem. The chapter then discussed the research significance, scope and objectives of this paper. The remainder of the dissertation will be structured as follows:

- **Chapter 2: Literature Review – Structural Health Monitoring of Concrete**
This chapter will discuss the constituents of concrete, the structural and thermal behaviour of concrete when curing and when subjected to heat, and the risk of heat exposure altering the structural and thermal properties of concrete. It will also discuss how to analyse concrete structural health and why. The finite element analysis techniques that will be used will be discussed, as will the methods chosen to analyse concrete behaviour insitu and to measure concrete structural health.
- **Chapter 3: Dissertation Methodology**
This chapter will discuss the design of the concrete structure to be analysed. It will outline the theoretical and experimental techniques that will be used to analyse the structure.
- **Chapter 4: Project Organisation**
This chapter will outline project timelines for testing and research. It will discuss the resources required for the project, and an assessment of the risks involved with any experimental testing as well as the possible consequential effects of this project.
- **Chapter 5: Models and Results**
This chapter will display the theoretical results, in the form of the finite element analysis and hand calculations, as well as the experimental results. The assumptions and findings will be discussed.

- **Chapter 6: Discussion and Recommendations**

This chapter will discuss, compare, and make recommendations based on the findings of the theoretical and experimental results. It will compare these results with the aims of this paper and outline any suggested limitations and improvements.

- **Chapter 7: Conclusion**

This chapter will conclude on all research and analysis findings. It will discuss any related recommendations and make suggestions for further research.

Chapter 2: Literature Review – Structural Health Monitoring of Concrete

2.1 Introduction

This chapter will discuss the constituents of concrete, the structural and thermal behaviour of concrete when curing, when loaded, and when subjected to heat, and the risk of heat exposure altering the structural and thermal properties of concrete. It will also discuss how to analyse concrete structural health and why. The finite element analysis techniques that will be used will be discussed, as will the methods chosen to analyse concrete behaviour insitu and to measure concrete structural health.

2.2 The Constituents of Concrete

Cement, water, and fine and coarse aggregates are mixed to form concrete. The chemical reaction between cement and water, is known as hydration, and causes the concrete to begin setting and form a plastic state. Whilst in this state it can be moulded as wanted (Australia, 2002, SJ Foster, 2010).

After time concrete hardens into a solid mass. It is kept moist, or cured, for 28 days to ensure rapid strength increase. After this, the rate of strength increase declines. Not only is concrete strong when hardened, it is also durable and resistant to deterioration caused by weather, wear, heat, and other such effects. It is also able to support significant loads. Concrete is, therefore, able to be used for a variety of applications (Australia, 2002, SJ Foster, 2010).

Cement is typically known as the binder for concrete. In modern times, it is typically a mixture of Portland cement, fly ash, and blast furnace slag. This mixture is cheaper and results in better properties than non-blended cement (SJ Foster, 2010). The amount of water added to cement to create a paste must be kept to a minimum because just like any glue it is weakened by excessive dilution. Enough must be added, however, to ensure workability (Australia, 2002).

Fine aggregates act as a filler and improve the flow properties of fresh concrete so it can be transported placed and compacted. Sand is generally the fine aggregate of choice. Coarse aggregates function as an inert filler. They generally take the form of crushed rock or natural gravel. Sometimes expanded, heated clay is used because it is lightweight and reduces the self-weight of the concrete. Crushed concrete may also be used (SJ Foster, 2010).

Fresh concrete of a viscous, readily flowing nature is achieved by using appropriate relative quantities of the above discussed ingredients (SJ Foster, 2010). The proper development of chemical bonds between water and cement during the hydration of concrete is required to ensure desirable hardened state properties are achieved. As the concrete hardens, the physical bonds between the cement paste and aggregate must develop properly to allow for desirable hardened state properties. The addition of steel reinforcement is also used to enhance the strength capabilities of concrete (Australia, 2002).

2.3 Properties of Concrete

The plastic and hardened state properties of concrete will be discussed in the following section.

2.3.1 Plastic State Properties

Workability, consistence and cohesiveness are typical plastic state properties of concrete.

2.3.1.1 Workability

The workability of concrete is influenced by water and cement content, as well as aggregate particle shape, size and distribution (Australia, 2002).

Increased water content increases concrete workability but lessens concrete strength and durability. It also has the ability to induce cracking via drying shrinkage. The addition of water is only recommended for minor adjustments to workability, and is recommended to always be accompanied by an addition of cement. Cement paste has the ability to lubricate aggregate particles. This means that at a fixed water-cement ratio, the higher the cement content, the greater the concrete workability (Australia, 2002).

Flaky or elongated aggregate particles require large amounts of cement paste to attain decent workability, and are thus undesirable. Rounded or approximately cubical aggregate particles are better at enhancing concrete workability. Larger particles relative to water-cement ratio are also desirable. It is recommended to use smoothly graded aggregates, or aggregates of relatively consistent size, to enhance workability. This is because the larger the surface area of the aggregates, the more water required to lubricate them (Australia, 2002).

2.3.1.2 Consistence

The degree of wetness of the concrete influences the ease with which it flows. This is termed the consistence of the concrete. High consistence refers to a high degree of wetness. Consistence and workability of concrete, although different, are referred to the slump of the concrete (Australia, 2002). The desired amount of concrete slump, and methods to measure slump will be discussed in section 2.4.1.

2.3.1.3 Cohesiveness

During handling, placing and compacting, the components of concrete must resist segregation. The cohesiveness of concrete is a measure of how well it is able to do this. Segregation may be in the form of bleeding, which is the movement of water to the surface, or may involve the parting of coarse aggregates from the cement paste. The cohesiveness of concrete may be influenced by specific gravities of the constituents, consistence, or aggregate grading (Australia, 2002).

Whilst placing concrete, abrupt changes in velocity and/or the direction of the concrete can cause particles of dissimilar specific gravities to become dislodged or segregated. This can create honeycomb patches within the structure (Australia, 2002).

The higher the consistence of the concrete, the more probable segregation and bleeding is to occur. Excessive water dilutes the cement paste, thereby decreasing its ability to bind aggregate particles. It also retards the early stiffening of concrete. This can lead to concrete bleeding, as it can cause long periods of sedimentation of heavier particles. Low consistence can also lead to concrete segregation due to poor binding of particles (Australia, 2002).

Segregation and bleeding may also occur due to a lack of very fine aggregate particles. Too many fine particles, however, may lead to the concrete being too thick to move, place and compact easily (Australia, 2002).

2.3.2 Hardened State Properties

Strength and durability are the hardened state properties of concrete which will be discussed.

2.3.2.1 Strength

The strength of concrete can be measured in terms of compressive strength, characteristic strength, tensile strength, or flexural strength. Compressive strength is a measure of concrete's capacity to resist crushing loads, whereas tensile strength is a measure of concrete's capacity to resist stretching or bending forces. Characteristic strength refers to the level of compressive strength above which 95 percent of the concrete is expected to have after a 28 day analysis. Flexural strength refers to concrete's ability to resist bending. Relative strength is sometimes used to describe the general overall strength of concrete (Australia, 2002).

Mature, hardened concrete typically has a high compressive strength of between 30 and 60 Megapascals. In tension, however, concrete has limited strength. Steel reinforcement, is therefore, embedded into a concrete structure to increase its tensile strength (SJ Foster, 2010).

The relative strength of concrete members varies depending on the location in the structure. This is due to the structural design and may also be influenced by inconsistencies in the concrete caused by improper preparation (Millard, 1996).

The following figure shows that the relative strength of a concrete beam is typically 100 percent at the bottom and decreases throughout the member to reach approximately 60 percent at the top of the member (Millard, 1996).

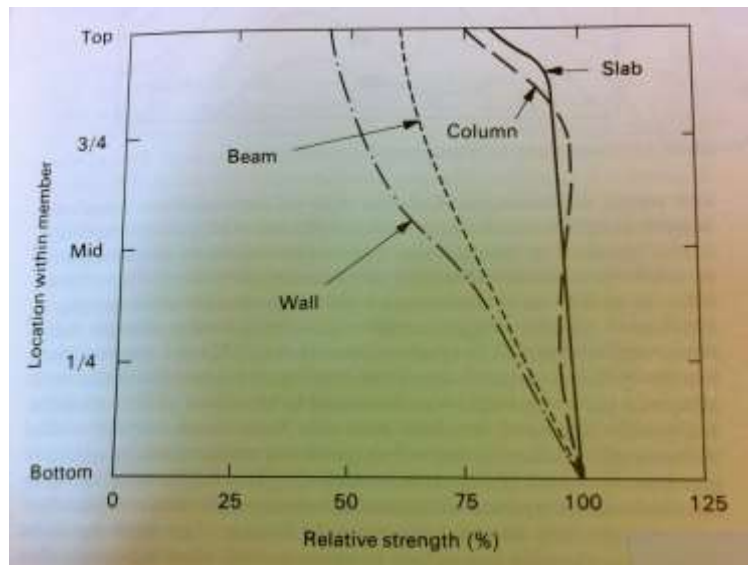


Figure 1 - Relative Strength of Concrete Members at Various Locations (Millard, 1996)

When loads are applied, the steel reinforcement and concrete act as one due to bonding. These loads cause stresses within the structure. In order to resist these, suitable amounts of reinforcement must be located appropriately throughout the structure (Australia, 2002).

In a concrete beam the main reinforcement consists of straight bars placed close to the faces of the member and extending longitudinally over the members length. Stirrups are then used as secondary reinforcement and placed transversely to the main reinforcement (SJ Foster, 2010). An adequate thickness of concrete cover must also be applied to protect the steel from environmental exposures (Australia, 2002).

The strength of concrete can be affected by water-cement ratio, the extent of voids, the degree of hydration, and the quality of its constituents (Australia, 2002).

Water-cement ratio is calculated by dividing the amount of free water by the mass of the cement. The following figure displays that for standard compaction and curing, the lower the water-cement ratio, the higher the 28 day compressive strength (Australia, 2002).

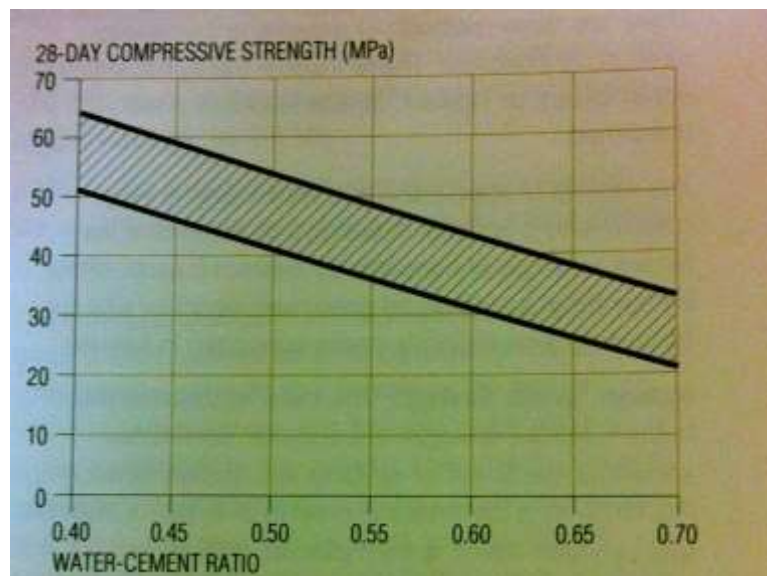


Figure 2 - The Influence of Water-Cement Ratio on 28 Day Compressive Strength (Australia, 2002)

High water-cement ratio can lead to voids and capillaries caused by bleeding. The maximum potential strength of concrete can only be reached if all air is expelled from the system, i.e. no voids. The following figure shows that the greater the percentage of air voids present in the concrete, the lower the relative strength (Australia, 2002).

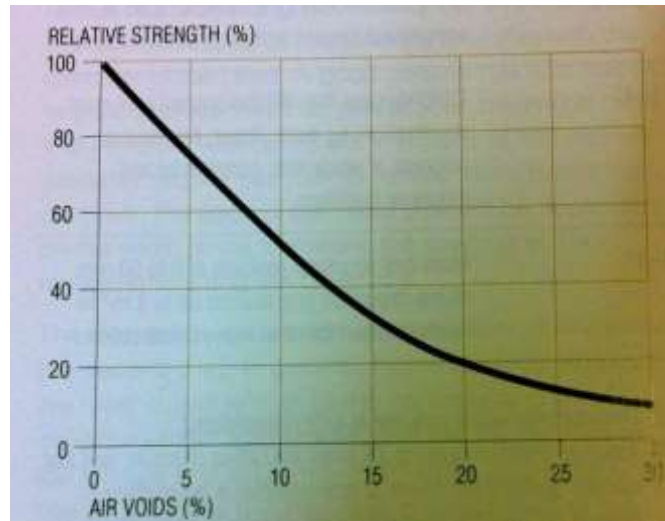


Figure 3 - The Effect of Air Voids on Potential Strength of Concrete (Australia, 2002)

Excess water within the concrete mix can degrade concrete strength, but hydration of the concrete once set is important for full strength development. The presence of water is recommended for at least 28 days to allow sufficient reaction between the cement and water. This process of hydration is known as curing (Australia, 2002).

The higher the quality of the cement, aggregate and water, the better they will be at enhancing the strength of the concrete. Admixtures and additives may also be used to enhance concrete strength but will not be further discussed in this dissertation (Australia, 2002).

2.3.2.2 Durability

Durability refers to concrete's ability to withstand wear, pressure or damage. Concrete must be durable against volume changes, reinforcement corrosion, chemical attack, abrasion, freezing and thawing, and other such environmental effects (Australia, 2002).

Two of concrete's most important durable properties are its permeability and absorptivity. Permeability is used to describe concrete's ability to repel the passage of gas or liquid through it. Absorptivity, on the other hand, refers to the amount of liquid concrete will soak up when submerged. Although they are separate properties, they tend to follow similar trends as they are affected similarly. They are both influenced by water-cement ratio, the extent of voids and capillaries, and cement type (Australia, 2002).

The greater the water-cement ratio, the higher the concrete permeability and absorptivity. This is because excess water either bleeds to the surface, thus making passages or capillaries, or it dries out and forms voids. The more capillaries or voids in concrete, the higher its permeability and absorptivity. Proper hydration, curing and compaction of concrete are thus necessary (Australia, 2002).

The use of blended cements is also recommended to produce low permeability concrete. Their pozzolanic materials react with the hydration products to form new insoluble materials that may embed themselves in voids thus reducing their extent (Australia, 2002).

2.4 Making a Reinforced Concrete Beam

“A beam is a member that supports transverse loads, that is, loads perpendicular to its longitudinal axis, and transfers the loads to its supports by bending action, shear and possibly torsion. The supports may consist of another beam, a column, a wall or a footing (SJ Foster, 2010).”

In order to make a reinforced concrete beam, the concrete must pass the slump test, be encased in appropriate formwork, and be compacted appropriately (SJ Foster, 2010). This will be discussed throughout this section of the literature review.

2.4.1 Slump Test

The slump test is performed on fresh concrete in order to determine its workability and consistency. The desired slump for a high strength concrete beam is within the range of 10 to 50 millimetres (Australia, 2002).

In order to perform the test a steel tamping rod, ruler, scoop, steel tray and container are required. A mould made of galvanised sheet metal of the dimensions shown in the below figure is also required (Australia, 2002).

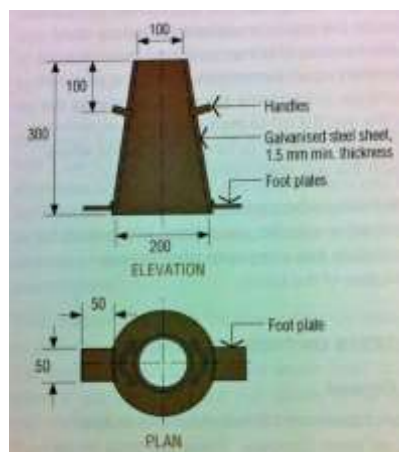


Figure 4 - Typical Mould for Slump Test (Australia, 2002)

The test is performed as per AS 1012. The concrete to be tested is scooped into the mould in three layers of approximately the same size. Each layer is compacted using the steel tamping rod by dropping it from just above the level of the mould thirty times (Australia, 2002).

The top of the mould is then struck to ensure the concrete fits the mould as perfectly as possible. The mould is carefully lifted ensuring the concrete is not influenced by this movement. Without the support of the mould the concrete then slumps. The amount of slump is measured by comparing the height of the concrete with the height of the mould (Australia, 2002). This procedure is shown in the following figure:



Figure 5 - Performing the Slump Test (Australia, 2002)

The following figure shows the method of measuring slump:

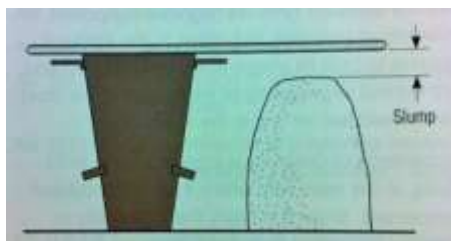


Figure 6 - Method of Measuring Slump (Australia, 2002)

If the slump of the concrete is unacceptable, the quantities of the concrete constituents should be altered accordingly and then the test should be repeated (Australia, 2002). The following figure shows typical acceptable and unacceptable slumps:

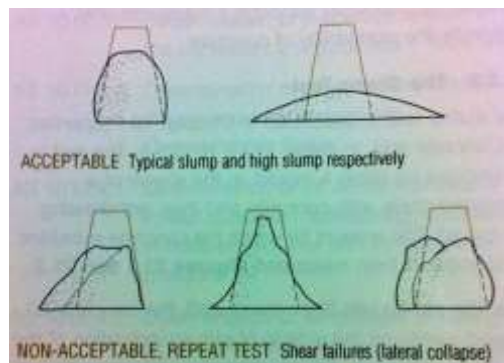


Figure 7 - Examples of Slump (Australia, 2002)

2.4.2 Formwork

Fresh concrete is poured into formwork before it sets. This formwork moulds the outer dimensions of the concrete by supporting it as it hardens. When the concrete has gained sufficient strength to support itself, the formwork is removed. The geometry of formwork may be altered so as to form members of varying shape. Almost any complex shape can be made (SJ Foster, 2010).

2.4.3 Compaction

The process of compaction sets the aggregate particles in motion and liquifies concrete. This allows it to fill the formwork, thus creating a level top surface. Trapped air is then expelled from the system. Achievement of desirable hardened state characteristics occurs when all air is expelled from the system (Australia, 2002).

The following figure shows that the greater the percentage of air voids in concrete the greater the decline in relative strength of that concrete:

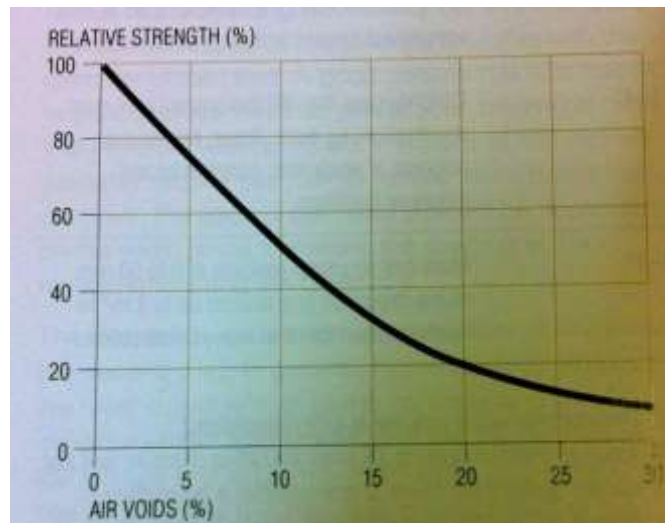


Figure 8 - Loss of Strength through Incomplete Compaction (Australia, 2002)

Proper compaction thus leads to improved relative concrete strength. Permeability of concrete is also enhanced by compaction. This is because pores are more evenly distributed throughout the mixture. This also leads to increased concrete durability and abrasion resistance (Australia, 2002).

Compaction may be done by rodding, tamping, vibration, or another method. The method of vibration is generally used as it is much more efficient. The relative amounts of the concrete constituents has a large effect on how much compaction is needed. If desirable plastic state properties of concrete are achieved generally 10 to 20 seconds of vibration is recommended for appropriate compaction. Appropriate compaction is achieved when air bubbles no longer appear on the concrete's surface. If concrete is compacted too much, segregation and/or bleeding may occur (Australia, 2002).

2.5 The Curing of a Reinforced Concrete Beam

The procedure of curing and the structural and thermal behaviour of concrete whilst curing will be discussed in the following section.

2.5.1 Procedure

There are three types of curing generally used (Australia, 2002):

- Covering concrete with an impermeable membrane.
- Continuously wetting the surface of the concrete.
- A combination of either of the above two methods with the raising of the temperature of the concrete.

The covering of concrete with an impermeable membrane is effective and cheap. It is ideal for laboratory testing and thus will be the only method of curing further discussed. The easiest way to perform this type of curing is to leave the formwork in place for as long as possible. Any exposed surfaces are then recommended to be kept moist via the covering with hessian cloth or plastic sheeting. Plastic sheeting of at least 0.10 millimetre thickness forms an effective barrier against water loss if kept securely in place (Australia, 2002).

The effects of insufficient curing are not easily determined. It is known, however, that it can lead to poor abrasion resistance, unexpected cracking, or corrosion of reinforcement. Curing for 28 days is the best practice but AS/NZS 3600-2009 sets out minimum periods for which concrete must be cured depending on the required strength of the concrete and the conditions to which it is likely to be exposed (Australia, 2002).

2.5.2 Structural Behaviour

The duration of curing has a direct effect on the strength of the concrete. If no curing method is emplaced and concrete is left to dry out it is likely to only achieve 40 percent of its potential compressive strength. Concrete which is kept moist, however, generally reaches approximately 95 percent of its potential compressive strength within 28 days (Australia, 2002).

The duration of curing also has a direct effect on the durability of concrete. By keeping concrete moist, over time hydration products fill the pores and capillaries in the concrete. This leads to greater durability (Australia, 2002).

2.5.3 Thermal Behaviour

The following section will discuss the effect of external temperature on the strength and durability of concrete whilst it cures. Typical internal temperatures generated within a concrete specimen whilst curing will also be discussed.

2.5.3.1 External Temperature Effect

The temperature at which concrete is cured has an effect on the rate at which concrete hydrates. This means it therefore effects concrete's strength and durability (Australia, 2002). The following figure shows the effect of external temperature on the compressive strength gain of concrete over the 28 day curing period:

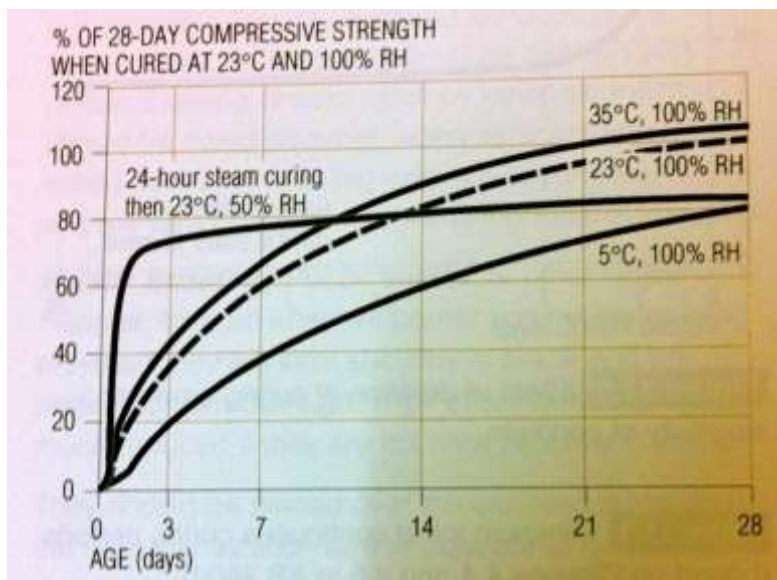


Figure 9 - The Effect of Curing Temperature on Strength Gain (Australia, 2002)

Lower curing temperatures reduce the rate at which hydration occurs, which thus reduces the rate at which strength gain occurs. This may lead to concrete never reaching its potential strength. This is represented in the above figure by the concrete cured at a temperature of five degrees Celsius only reaching approximately 80 percent of its potential compressive strength (Australia, 2002).

Higher curing temperatures cause hydration to occur too fast thus reducing the potential strength gain. This is represented in the above figure by the concrete that was initially cured at a high temperature via the use of steam curing. It can be seen that the concrete initially gains strength rapidly but then this slows and stops with the concrete only reaching approximately 80 percent of its potential compressive strength (Australia, 2002).

It can be seen from the above figure that concrete cured at 35 degrees Celsius produces the best results. Concrete cured at 23 degrees Celsius produces results of comparable nature. It is, therefore, recommended to cure concrete at a temperature approximately between 23 and 35 degrees Celsius. This is the normal range of ambient temperatures encountered in Australia (Australia, 2002).

2.5.3.2 Internal Temperature Generated

As concrete cures, temperature is generated due to the reaction of cement and water (Australia, 2002). The following schematic displays the typical interior and surface temperatures of a concrete specimen:

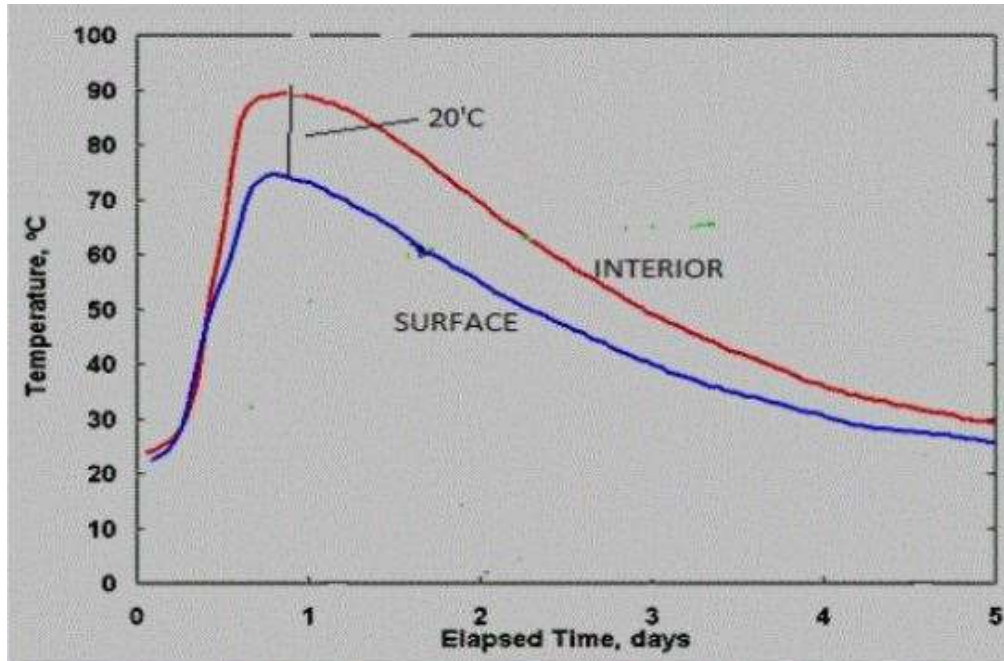


Figure 10 - Typical Internal and Surface Temperatures Generated as Concrete Cures (Yadav, 2015)

From the above schematic it can be viewed that the concrete's surface and internal temperatures displayed a similar trend. As the concrete cured, the temperature rapidly increased to reach a maximum after approximately 24 hours of curing. The temperature then declined and returned to its comparative starting temperature after roughly five days. The maximum internal temperature of the concrete was approximately 90 degrees Celsius, with a 20-degree Celsius drop in temperature on the surface (Yadav, 2015). The central point of the beam is thus suggested to be the ideal location for reading the greatest variance in temperature.

The relative properties of the concrete specimen in the above schematic is unknown. The following schematic thus shows the curing temperatures of concrete for differing specimen properties. The specimen properties of interest are:

- Normal weight concrete test block of dimension 1m³
- Normal weight concrete footing of dimensions 8.7m x 13.6 m x 2.9 m

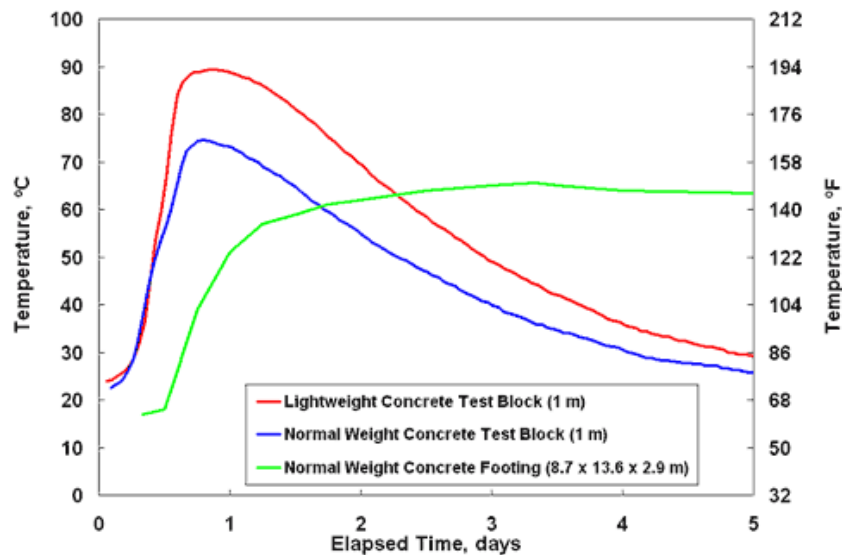


Figure 11 - Typical Internal Temperatures of Differing Concrete Specimens Whilst Curing ((APEE), 2005)

From the above schematic it can be viewed that in a larger concrete specimen the internal temperature rise is more delayed and further prolonged. This is suggested to be due to the fact that more reactions (between the cement and water) must occur due to the larger surface area. Both larger specimen was also recorded to only reach a maximum internal temperature rise of approximately 65 degrees Celsius, whereas, the smaller specimen reached a maximum internal temperature rise of approximately 75 degrees Celsius ((APEE), 2005).

The following factors may inhibit internal temperature rise within a curing concrete specimen (Yadav, 2015):

- High cement to aggregate content (80 – 85%)
- Cold mixing water
- Cold external temperatures
- Unideal cement composition
- Cement fineness

2.6 Loading of a Reinforced Concrete Beam

The structural behaviour of a reinforced concrete beam when loaded will be discussed in this section.

2.6.1 Structural Behaviour

When a concrete structure is loaded stresses are likely to be induced. These stresses may be of compressive, tensile or shear nature. Stresses of compressive nature are those that cause the member to compact, whereas stresses of tensile nature are those that cause the member to stretch, and those of shear nature cause adjacent portions of the member to slide across each other (Australia, 2002). These are summarised in the below figure.

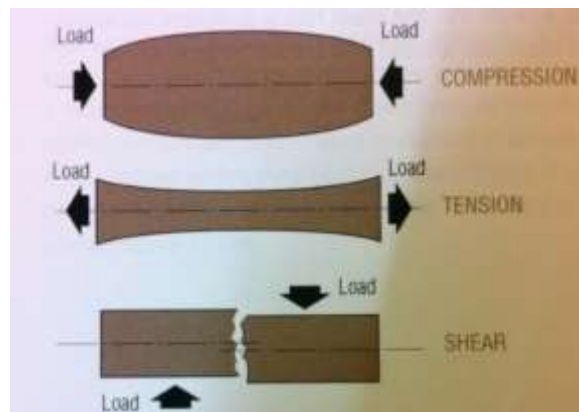


Figure 12 - Types of Stresses (Australia, 2002)

Shear stresses may be vertical, horizontal or diagonal, and may lead to concrete cracking of a similar nature. When the central portion of the beam slides across the end portion of the beam this is known as a vertical shear stress (Australia, 2002). This is shown in the below figure:

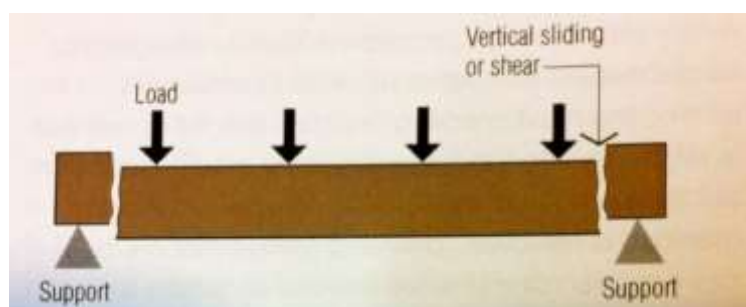


Figure 13 - Vertical Shear Stresses (Australia, 2002)

Horizontal shear stresses, however, are when the beam bends. It is as if horizontal layers are present within the structure and that they are sliding over one another (Australia, 2002). This is shown in the below figure:

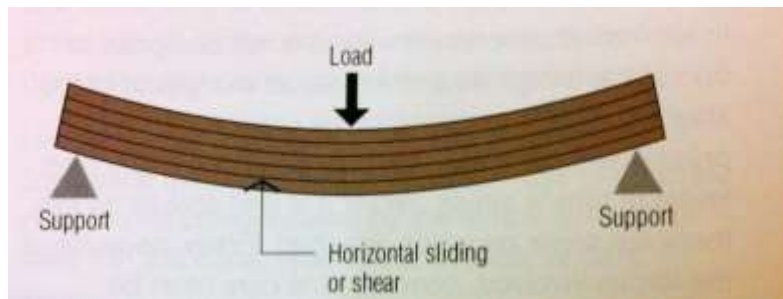


Figure 14 - Horizontal Shear Stresses (Australia, 2002)

Diagonal tensile cracking occurs when vertical and shear stresses react with one another (Australia, 2002). This is shown in the below figure.

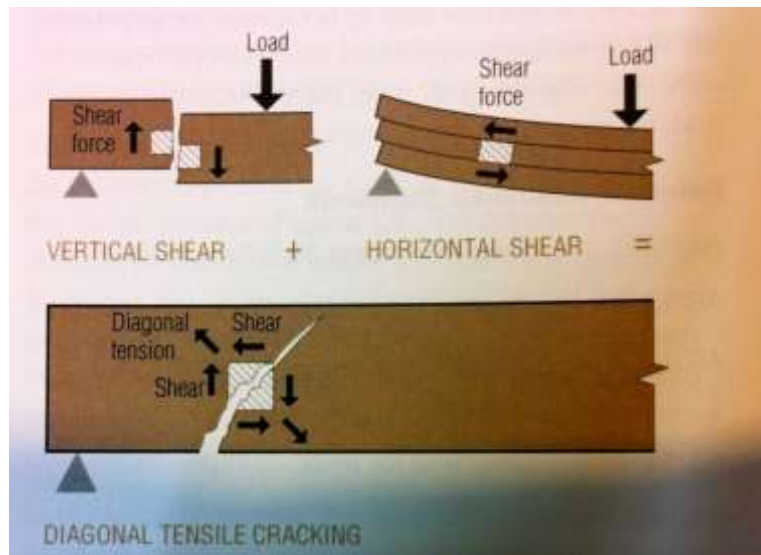


Figure 15 - Diagonal Tension Cracks (Australia, 2002)

When concrete is under loading, cracks begin to occur when its maximum tensile stress reaches the modulus of rupture of concrete. Steel bars are thus used to increase the moment capacity of the beam (M. Nadim Hassoun, 2012).

2.7 Reinforced Concrete Beams and Heat

The risks associated with heat exposure altering the structural properties of concrete and the actual behaviour of concrete under heat will be discussed in the following section.

2.7.1 The Risks Associated with Heat Exposure Altering the Structural Properties of Concrete

The thickness of the concrete, its type and size of aggregates, its cement content, and its age effects concrete's ability to resist heat. Concrete is known to have a relatively high heat resistance due to its low thermal conductivity and high specific heat (M. Nadim Hassoun, 2012, Hamerlinck, 1991).

(APEE), 2005, suggests that the properties of concrete are substantially unaffected when subjected to temperatures of up to 100 degrees Celsius. Temperature exposure between 100 and 300 degrees Celsius has the potential to cause degradation in concrete strength. When exposed to temperatures between 300 and 600 degrees Celsius significant loss of strength begins. Concrete subjected to temperatures above 600 degrees Celsius is said to completely lose its strength, thus leading to structural failure ((APEE), 2005). It must be noted that proportional loss in concrete strength is not believed to be dependent on the initial compressive strength of the concrete (Association, 2002).

When concrete has been exposed temperatures above 300 degrees Celsius it is generally recognisable due to it forming a light pink colour. Concrete exposed to temperatures above 600 degrees Celsius generally displays a light grey or yellow brown colour((APEE), 2005). This puts forward the question then, how can concrete that has been exposed to potentially damaging temperatures between 100 and 300 degrees Celsius be recognised and how can its structural integrity be determined. Especially since steel reinforcement gives concrete the ability to remain in shape due to it having similar expansion and contraction properties (Australia, 2002).

Temperature exposure has the potential to cause loss of concrete strength due to the heat causing thermal expansion and dehydration, which leads to shrinkage as the concrete cools and contracts. Aggregate type has a large impact on the effects that temperature exposure can have. This is because typically the aggregate continues expanding after the concrete has begun to contract. Trapped moisture also has the ability to cause internal pressures if it forms steam and bursts internally (Association, 2002).

The faster the temperature rises, and the longer the structure is exposed to high temperatures the more detrimental the effects on the concrete. Concrete subjected to thermal cycling, when cooled generally shows the greatest degradation in strength (Association, 2002). Concrete exposed to rapidly increasing temperature generally begins to spall. If exposure time is low though, the structure may not be affected by those temperatures that are believed to be dangerous ((APEE), 2005). Special consideration must be given to structures in which portions of the structure are exposed to temperature changes, and other portions are partially or fully protected (Association, 2002).

It should be noted that if concrete is under design load whilst heated its degradation in strength should be minimal in comparison to unloaded concrete. It is believed that the compressive stresses created by the load to some extent prevent the advancement of cracks (M. Nadim Hassoun, 2012, Association, 2002).

A concrete structure partially exposed to cyclic temperatures between 100 and 300 degrees Celsius, and that is not under load during this exposure time, is a prime example of a structure that may have unrecognisable loss of strength that could deem it potentially unsafe ((APEE), 2005, Association, 2002). The question is, however, how can it be recognised that concrete has been exposed to potentially damaging conditions such as this and the like, and how can the integrity of the structure be determined.

2.7.2 Thermal Behaviour

When a building is exposed to fire, the temperatures that it is exposed to will be unknown. Different structural elements will be subjected to different temperatures (Yao, 2006). As discussed in section 2.7.1, concrete exposed to temperatures between 100 and 300 degrees Celsius has the potential to be unrecognisably unsafe ((APEE), 2005). The following section will thus discuss the effect of various temperatures on the properties of concrete, with a particular focus on the external temperature of 200 degrees Celsius.

Yao, 2006, formed the following schematic to show the relative loss in compressive strength of concrete when subjected to various temperatures:

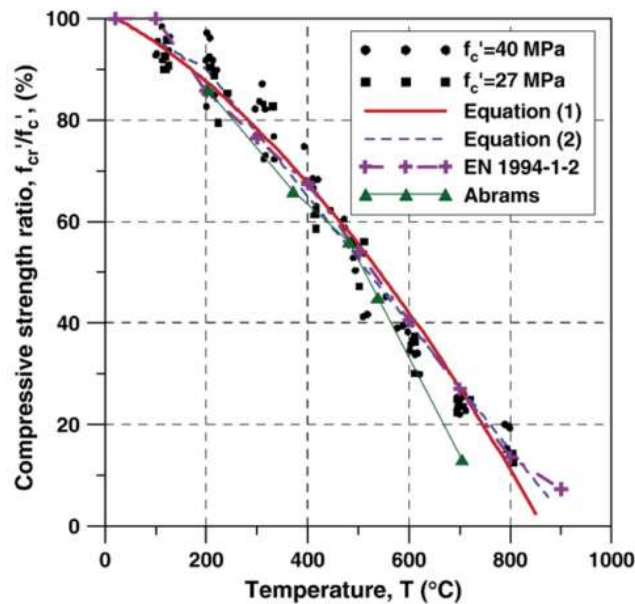


Figure 16 - Concrete Compressive Strength after Heating for Different Temperatures (Yao, 2006)

It can be viewed from the above schematic that concrete exposed to 200 degrees Celsius has the potential to degrade in compressive strength by approximately 10 percent (Yao, 2006). Association, 2002 supports this, as shown by the dotted average line in the below schematic:

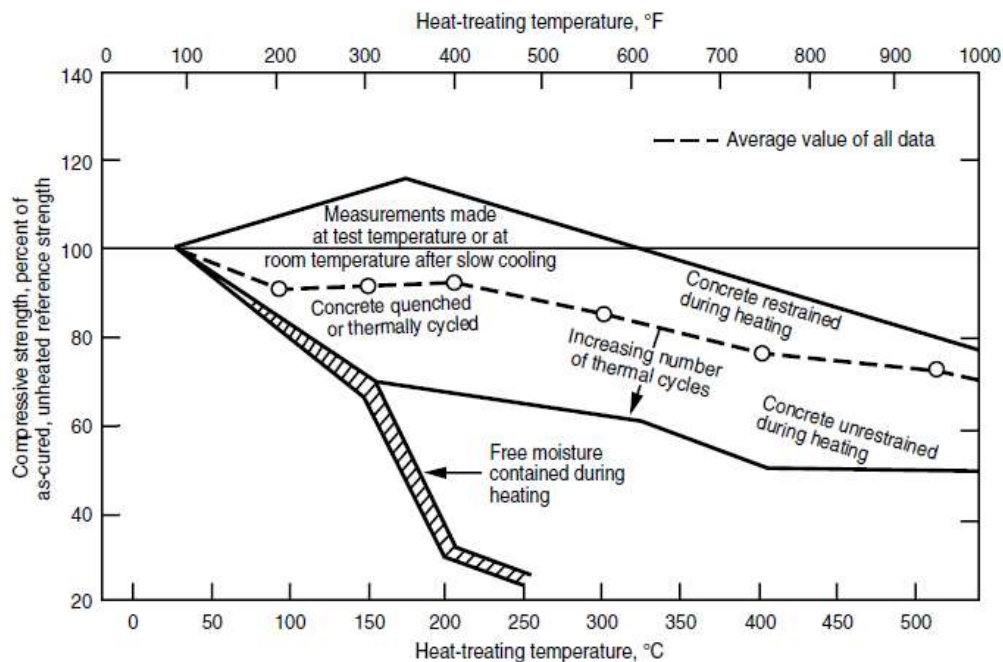


Figure 17 - Compressive Strength of Concrete after Various Temperature Exposures (Association, 2002)

Yao, 2006 also developed a schematic of the relationship between temperature exposure and tensile strength:

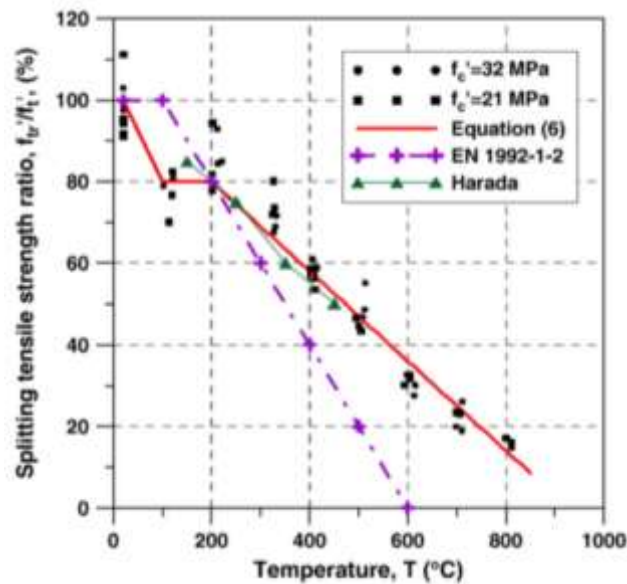


Figure 18 - Concrete Tensile Strength after Heating for Different Temperatures(Yao, 2006)

Yao, 2006, suggests that a temperature of 200 degrees Celsius can lead to a degradation in splitting tensile strength of a cylinder of approximately 20 percent. Assuming the tensile strength of a beam will be affected similarly, it must be noted that tensile strength may also be decreased due to deformation of steel reinforcement. This is because the steel used to reinforce concrete has a relatively low heat resistance (Australia, 2002).

The figure below shows that increased temperatures lead to increased strain within a concrete structure. This is because as the stress is decreasing the tensile stress within the structure is increasing (Yao, 2006).

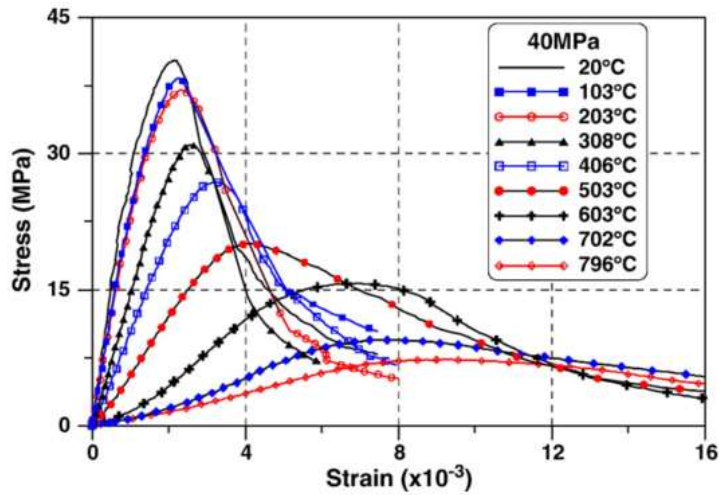


Figure 19 - Concrete Stress-Strain Curves after Heating for Different Temperatures (Yao, 2006)

The flexural strength of a member is also subject to degradation due to temperature exposure. Association, 2002, developed the following relationship for temperature exposure and flexural strength:

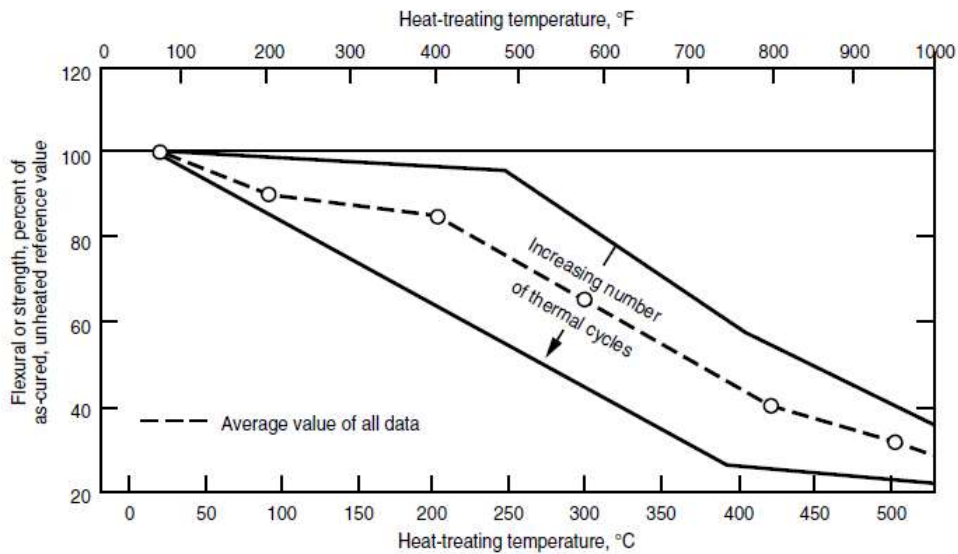


Figure 20 - The Relationship between Temperature Exposure and Concrete Flexural Strength (Association, 2002)

The dotted line in the above schematic suggests that concrete exposed to a temperature of 200 degrees Celsius will have a relative reduction in flexural strength of approximately 15 percent (Association, 2002).

The property of concrete that is suggested to be most greatly affected by temperature exposure is the modulus of elasticity. Association, 2002, have developed the following figure to show the effects of temperature rise on modulus of elasticity:

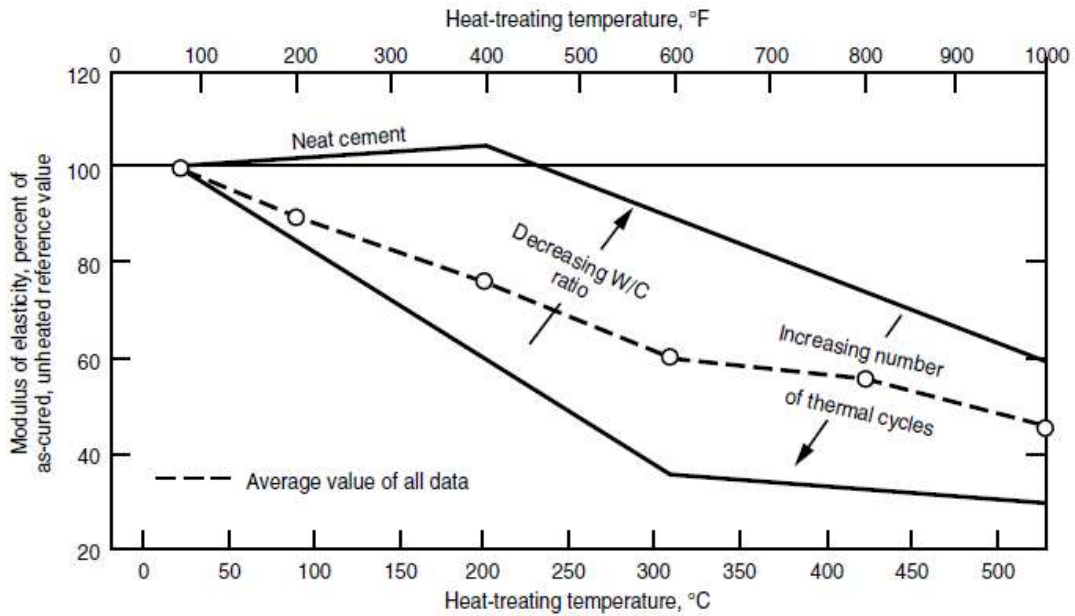


Figure 21 - The Relationship Between Temperature Exposure and Modulus of Elasticity (Association, 2002)

The dotted average line in the above figure suggests that concrete exposed to an external temperature of 200 degrees Celsius will show a reduction in modulus of elasticity of 25 percent. It must be noted that the higher the aggregate to cement ratio, the lesser the reduction in compressive strength but the greater reduction in modulus of elasticity (Association, 2002).

If concrete can be degraded in strength whilst maintaining shape and appearance, being able to internally monitor a structure and determine the extent of damage to that structure is of great importance.

2.8 Analysing Concrete Structural Health

The following section will discuss why the analysis of structural health is important, the methods chosen to analyse the concrete beams structural health insitu, and the methods chosen to measure the concrete structural health.

2.8.1 Why Analyse Concrete Structural Health

After exposure to high temperatures concrete structures may become unsafe for general use. In some cases though the structural integrity of the structure may be intact, and thus not need repair. Structural health monitoring can allow for the determination of the integrity of a structure after such an event (Su and Han, 2014).

Monitoring the structural health of concrete structures can lead to greater safety as it means engineers are aware of when damages have occurred to a structure. It may also lead to reduced maintenance, as whether a problem exists and its source is able to be determined. This means unnecessary maintenance will not be performed. Since damages can be fixed at early onset, structural health monitoring can lead to increased structural longevity and health (Su and Han, 2014).

2.8.2 Finite Element Analysis Techniques

The program Abaqus/CAE was chosen to perform a finite element analysis of the reinforced beam structure. This program was chosen due to its three dimensional capabilities. Dassault Systems 2015 describe the capabilities of Abaqus/CAE as follows:

“With Abaqus/CAE you can quickly and efficiently create, edit, monitor, diagnose, and visualize advanced Abaqus analyses. The intuitive interface integrates modeling, analysis, job management, and results visualization in a consistent, easy-to-use environment that is simple to learn for new users, yet highly productive for experienced users. Abaqus/CAE supports familiar interactive computer-aided engineering concepts such as feature-based, parametric modeling, interactive and scripted operation, and GUI customization.

Users can create geometry, import CAD models for meshing, or integrate geometry-based meshes that do not have associated CAD geometry. Associative Interfaces for CATIA V5, SolidWorks, and Pro/ENGINEER enable synchronization of CAD and CAE assemblies and enable rapid model updates with no loss of user-defined analysis features.

The open customization toolset of Abaqus/CAE provides a powerful process automation solution, enabling specialists to deploy proven workflows across the engineering enterprise. Abaqus/CAE also offers comprehensive visualization options, which enable users to interpret and communicate the results of any Abaqus analysis (Systems, 2015).”

Abaqus/CAE’s high capabilities is ideal for generating three dimensional models in order to analyse theoretical static and thermal behaviours of structures (Systems, 2015).

2.8.3 Methods of Analysing the Behaviour of Reinforced Concrete Beams Insitu

Methods of analysing the behaviour of the reinforced concrete beam insitu include thermocouples, strain gauges, and FBG Sensors. Their relative abilities will be discussed in this section.

2.8.3.1 FBG Sensors

The Fibre Bragg Grating Sensor (FBG Sensor) is able to measure both strain and temperature (Su and Han, 2014).

2.8.3.1.1 Layout

The below figure shows the general layout and measurement principal of an FBG Sensor:

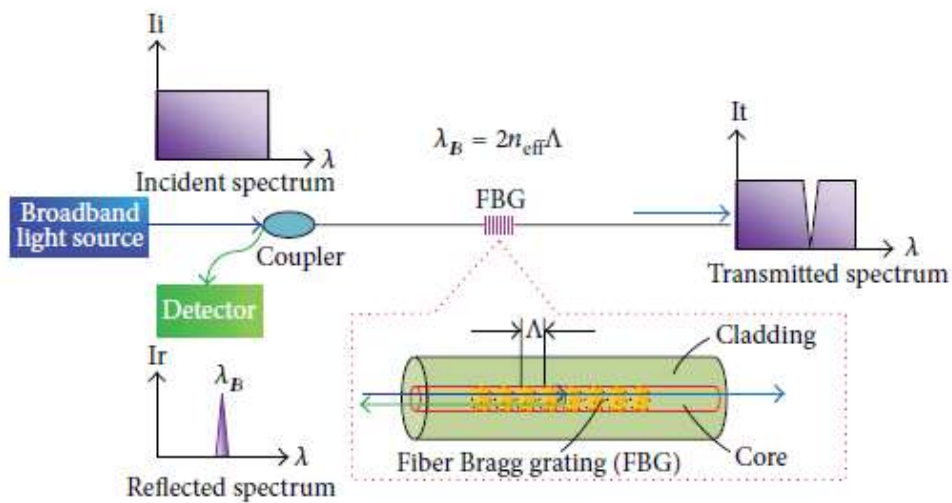


Figure 22 - Measurement Principal of FBG Sensor (Su and Han, 2014)

The above figure displays that FBG Sensors have an inner core, and cladding typically made of silica glass or polymer material. The inner core is typically four to nine micrometres thick and has a high refractive index which causes light to propagate. The cladding is typically 125 micrometres in diameter. In order to protect the FBG Sensor from hydrogen and water, a coating typically made of acrylate or polyamide is applied to the cladding (Su and Han, 2014).

If the refractive index in the fibre core experiences a permanent periodic change this induces reflection of a spectral component of a broadband light source. This reflected light is centred on the Bragg wavelength. It can, therefore, be related to the inscribed grating period, and the effective refractive index through the Bragg condition. A shift in Bragg wavelength without any degradation of the spectrum shape indicates axial strain or temperature change (Su and Han, 2014).

The following specifications about an FBG Sensor must be known (Su and Han, 2014):

- Control Wavelength (CW)
- FBG Length
- Reflectivity
- Fibre Type
- Recoat Type
- Connector Type

2.8.3.1.2 Grating Structures

There are several different grating structures available depending on the desired application for the FBG Sensor. These variations in grating structures are achieved by altering the induced index change along the fibre axis (Erdogan, 1997). The most common FBG Sensor grating structures are shown in the below figure:

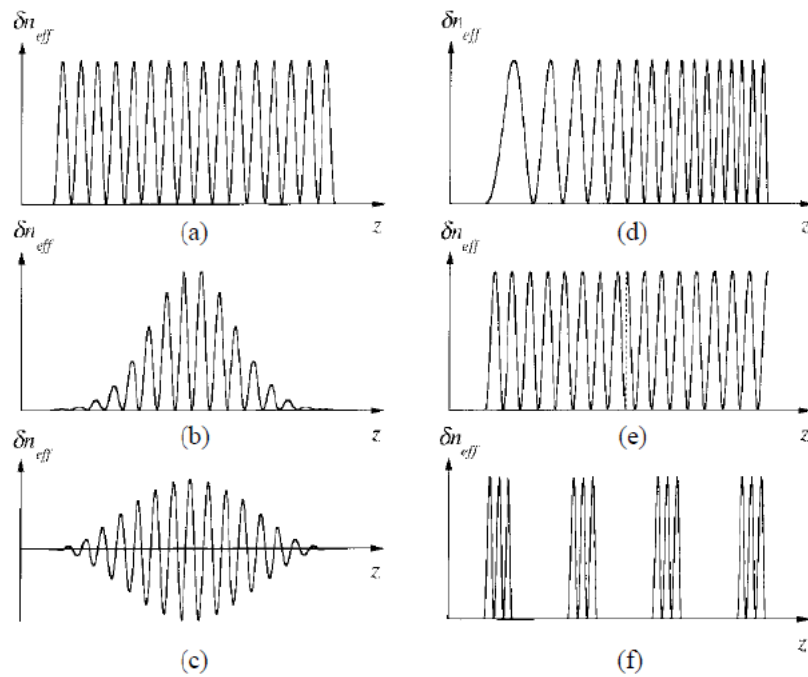


Figure 23 - FBG Sensors Grating Structures (Erdogan, 1997)

Erdogan, 1997 states that the above FBG Sensor grating structures are:

- a) Uniform with positive only index change – basic form of grating.
- b) Gaussian apodised – used to suppress sidelobes and suited to telecommunications applications.
- c) Raised cosine apodised – used to suppress sidelobes and suited to telecommunications applications.
- d) Chirped – increase the bandwidth of the reflected spectrum and are suited to telecommunications applications.
- e) Discrete phase shift – used as dispersion filters in telecommunications applications.
- f) Superstructure – used as dispersion filters in telecommunications applications.

Since FBG Sensors with uniform gratings are the most commonly used they are thus easily sourced and will be used in this research.

2.8.3.1.3 Physics

The Bragg wavelength is reflected and correlated to the grating period in accordance with Bragg's law. According to this law it occurs when the light from the broadband source passes through the grating at a particular wavelength (Su and Han, 2014).

The Bragg wavelength may be calculated as follows (Su and Han, 2014):

$$\lambda_B = 2n_{\text{eff}}\Lambda,$$

Where:

n_{eff} = the effective index of refraction

Λ = the grating period.

The Bragg wavelength varies linearly with strain and/or temperature. The amount of strain and/or temperature change present determines the degree of external disturbance and thus the amount of grating period and Bragg wavelength variance (Su and Han, 2014).

The variation of the Bragg wavelength can be calculated from the following equation (Su and Han, 2014):

$$\Delta\lambda_B = \lambda_B \{(\alpha + \xi) \Delta T + (1 - p_e) \Delta\varepsilon\},$$

Where:

$\Delta\varepsilon$ = strain variation

ΔT = temperature change

α = coefficient of thermal expansion

ξ = thermo-optic coefficient

p_e = strain optic coefficient

2.8.3.1.4 Interrogation

The Centre of Excellence in Engineered Fibre Composites Micron Optics Optical Sensing Interrogator (model sm125) was used for interrogation of FBG Sensors. This interrogator is designed to measure full spectrum of fibre optic gratings. It has a wavelength range from 1510-1590 nanometres with 1 picometre wavelength accuracy (Inc, 2009). Refer to Appendix C to view full details of the interrogators specifications.

This interrogator works by transferring the information from the FBG Sensor to a computer. It is connected to these via an Ethernet cable. The MOI Enlight Sensing Analysis software published by Micron Optics must be present on the computer in order for data to be viewable. Text files may then be exported from MOI Enlight to other software packages for analysis (Inc, 2009).

2.8.3.1.5 Performance

In comparison to other mechanisms utilised to measure strain and temperature, FBG Sensors have the following advantages (Biswas et al., 2010, Su and Han, 2014):

- Small size
- Light weight
- Immune to electromagnetic interference
- Immune to corrosion
- Do not require calibration
- Embedding capability
- Long term stability – 100 year design life
- High reliability
- Can be used for multi-point sensing through a single optical channel.

FBG Sensors do, however, have the following disadvantages (Su and Han, 2014):

- Exhibit high temperature dependence (a one degrees Celsius change corresponds to approximately eight micro strains.
- High stiffness which causes increased parallel forces.
- Highly sensitive to lateral forces and pressure which may cause multiple peaks in the spectra.

“In structural health monitoring (SHM) it is essential that placement of the sensors are appropriately chosen so that the measured strains and/or vibrations provide valuable information about the integrity of the structural system. Concrete structures are generally large in dimension and geometrically complex and in this respect, to get meaningful data, it is often required that the sensors be embedded into the concrete structure at proper location. suitable protective housing is necessary for embedding in concrete structures (Biswas et al., 2010).”

FBG Sensor placement and orientation is thus of high importance. They can be orientated longitudinally to read bending or maximum principal strains but must be in a position where such strains are evident (Biswas et al., 2010).

2.8.3.1.6 Methods of Encasing FBG Sensors

The chemicals in cement and the process of moulding a concrete beam may cause damage to the FBG Sensors. A method of protecting them from damage must, therefore, be introduced. It must be ensured that a proper technique is chosen to encase the FBG Sensors because incorrect encasing can inhibit the capabilities of the sensor (Biswas et al., 2010).

(Biswas et al., 2010) found that first coating the FBG Sensors in a layer of epoxy (EPO-TEK 353ND), then encapsulating it in a stainless steel housing with a diameter of 3.5 millimetres, wall thickness of 0.5 millimetres and length of 100 millimetres, worked to protect sensors embedded in concrete.

One issue with this technique, however, is the risk that the encasing will move within the beam structure. This is of particular concern when subjecting the concrete to vibration to rid it of air voids. If the sensor is not orientated correctly it will not translate any readings, and if its location shifts its readings will not be comparable to theoretical results (Biswas et al., 2010). HBM Australia, 2010, have, therefore, suggested welding FBG Sensors to the reinforcement. This, however, could cause the sensors to be reading false strain values. The sensor would actually be picking up the strain associated with the steel reinforcement rather than the concrete itself (Biswas et al., 2010).

In order to embed the sensor away from the reinforcement, a technique that has been utilised is to weld stainless steel cylinders to either end of the stainless steel housing. This provided stability and a mechanism for tying the sensors in place. Cylinders were chosen because their smooth edges ensure that they do not cause flaws within the concrete structure (Australia, 2002).

It must be noted that encasing an FBG Sensor in steel leads to the sensor picking up false strains. The FBG Sensor will be picking up the strains of the steel rather than the true strains of the concrete (Biswas et al., 2010).

It must also be noted that coating the FBG Sensors in epoxy coating must be done so carefully, taking into account the epoxy type, bonding length and bonding thickness. Imperfect bonding may inhibit strain transfer from the concrete beam to the sensor thus leading to unreliable readings (Biswas et al., 2010).

If the epoxy has any voids or experiences any shrinkage this can also lead to unreliable strain readings. This is because non-uniform strain will be induced on the FBG Sensor and thus will cause distortion and/or broadening in the corresponding wavelength spectra. This would create increased system noise and thus false measurements. Specialist techniques would be required to demodulate the sensor signal (Biswas et al., 2010).

It must also be noted that if the stainless steel housing commonly used to encase an FBG Sensor comes into contact with the reinforcing steel, it would cause corrosion of the reinforcing steel and thus internal structural deformities. This is because the reinforcing steel has a lower electrochemical activity than stainless steel. This may still occur without direct contact being made because the concrete can act as an active electrolyte (Association, 2002).

The use of dissimilar metals in the same active electrolyte such as concrete, thus is not ideal. This is because each metal has a unique electrochemical potential, and with the concrete acting as an active electrolyte, the metal with the lower electrochemical activity may corrode and cause an internal structural deformity (Association, 2002).

A list of metals in order of electrochemical activity is as follows (Association, 2002):

1. Zinc
2. Aluminium
3. Steel
4. Iron
5. Nickel
6. Tin
7. Lead
8. Brass
9. Copper
10. Bronze
11. Stainless Steel
12. Gold

A technique of encasing that avoids dissimilar metals being within the steel reinforced concrete, does not use epoxy which can encourage shrinkage, and allows the FBG Sensor to be in direct contact with the concrete it is embedded within would be the ideal method of FBG Sensor encasing.

2.8.3.2 Thermocouples

Thermocouples can be used to verify temperatures recorded by FBG Sensors.

2.8.3.2.1 Layout

Thermocouples comprise two dissimilar metal wires joined at the sensing junction. At the reference junction the wires are terminated. It is called the reference end because it is maintained at a known constant temperature. When a temperature variance exists between the sensing and reference junctions, an emf is produced which creates a current in the circuit. A meter or recorder is connected to the reference junction and gives an indication proportional to the temperature variance between the sensing and reference junctions (Engineering, N/D). This is illustrated in the below picture.

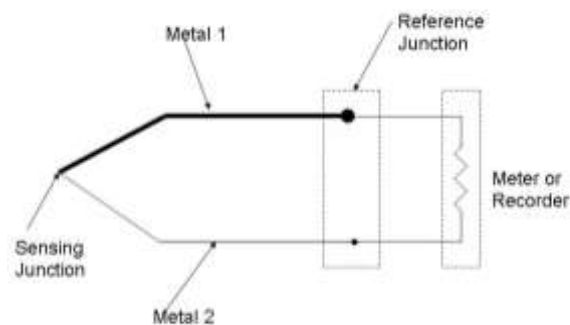


Figure 24 - Basic Thermocouple Circuit (Engineering, N/D)

Type K thermocouples have an ability to read high temperatures. They are capable of reading temperatures between the ranges of negative 200 to positive 1250 degrees Celsius. This is thanks to the use of nickel-chromium and nickel-aluminium as the two dissimilar metal wires (Inc, 2015b). Type K thermocouples will thus be utilised to record temperatures throughout the reinforced concrete beam structure.

2.8.3.2.2 Interrogation

Thermocouples require calibration. This is generally done by recording the amf produced by the thermocouple at various temperatures, and correlating the recorded values to a calibration curve. From this calibration curve a calibration equation can be determined.

An NI cDAQ-9174 can also be used for interrogation in conjunction with the program LabVIEW (Corporation, 2015). An NI cDAQ-9174 is shown in the below figure:



Figure 25 - NI cDAQ-9174 Used for Thermocouple Interrogation

In order to interpret data from the NI cDAQ-9174, a script must be written in LabVIEW. LabVIEW is short for Laboratory Virtual Instrument Engineering Workbench. It is a system design platform and development environment for visual programming. It has high data acquisition abilities and is rather simple and fast for multi-core programming (Corporation, 2015)..

How it works is a compiler that produces native code for the CPU platform, which is then translated into machine code by interpreting and compiling the syntax. The syntax is compiled into machine code when requested to run or upon saving (Corporation, 2015).

2.8.3.3 Strain Gauges

As the name suggests, strain gauges measure strain. They can be used to verify strains recorded by FBG Sensors.

2.8.3.3.1 Layout

The most common type of strain gauge consists of a flexible backing that provides insulation to a metallic foil pattern which it supports. The gauge is attached to an object whose strain needs to be analysed via the use of an adhesive on the solder tabs. An electrical resistance change occurs in the metal foil as it deforms in relation to the deformation of the object. This resistance change is usually measured using a Wheatstone bridge. It is correlated to the strain by the gauge factor (Dasar, 2013). This is illustrated in the below diagram.

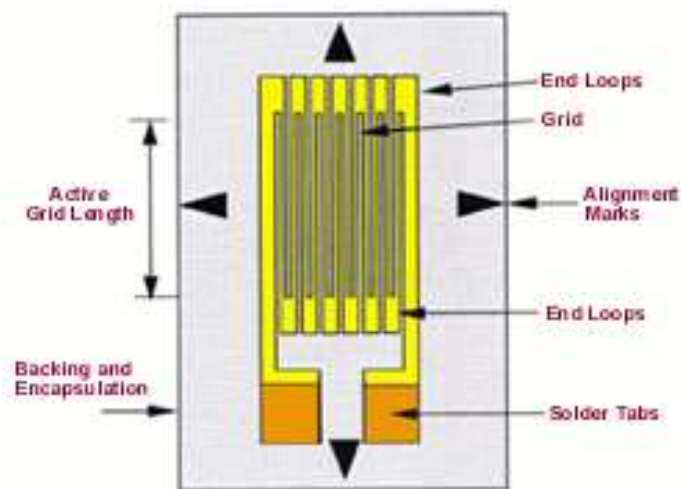


Figure 26 - Basic Strain Gauge Circuit (Dasar, 2013)

In order to interrogate a strain gauge, the gauge factor and ohms produced must be known (Dasar, 2013).

2.8.3.3.2 Interrogation

Strain gauges can be orientated in many way in order to read various types of strains. The following figure shows that orientating strain gauges longitudinally allows them to read bending strains or maximum principal strains (Inc, 2015a).

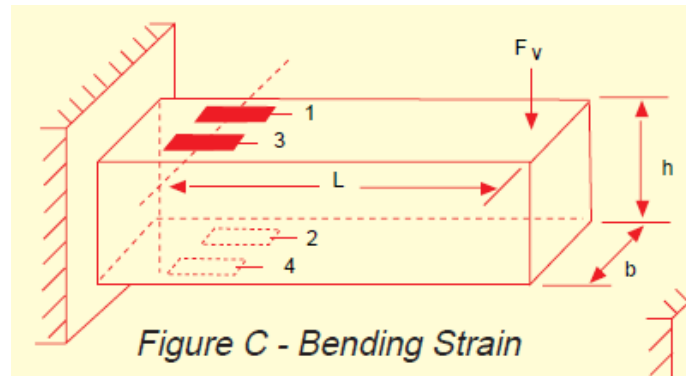


Figure 27 - How to Orientate Strain Gauges to Read Bending Strain (Inc, 2015a)

The following figure shows a strain gauge interrogator unit:



Figure 28 - Strain Gauge Interrogator Unit

The specifications of the strain gauge must be input into the strain gauge interrogator unit. After this the strain gauge must be fed into the interrogator unit using either a quarter, half or full bridge, depending on the strain gauge type. A quarter bridge is the most common configuration for strain gauges and is shown in the following figure (Inc, 2015a):

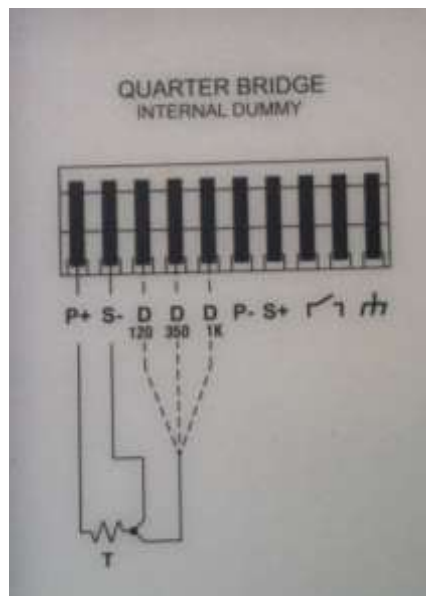


Figure 29 - Quarter Bridge Layout

2.8.4 Methods of Measuring Concrete Structural Health

To practically perform a static analysis of a beam's structural health, tests must be performed on hardened concrete. Such tests include compression tests and three point bending tests and can be performed via the SANS Machine.

2.8.4.1 Compression Tests

Compression tests are carried out on 28 day old cylindrical concrete specimens made of the same concrete as the beams as per the Australian standards guidelines. Two sizes of concrete cylinders can be used, either a cylinder with a diameter of 150 millimetres and a height of 300 millimetres, or a cylinder with a diameter of 100 millimetres and a height of 200 millimetres (Australia, 2002). The compression tests will be utilised to determine the compressive strength of the concrete. This will be done by applying an increasing compressive load to the specimens until they fail (Australia, 2002). The following figure shows the configuration of a general compression test:



Figure 30 - Configuration of a General Compression Test (Australia, 2002)

By recording the loads, deflections and observations regarding cracking, calculations can be performed to calculate the compressive strength of the concrete. This is a measure of concrete's capacity to resist crushing loads, and is calculated by dividing the load applied to the structure that causes failure by the contact surface area (Australia, 2002).

“It can be assumed that concrete fails in compression when the concrete strain reaches 0.003 (M. Nadim Hassoun, 2012).”

There are three modes of failure of standard concrete cylinders. Firstly, the specimen may fail under shear due to axial compression. Secondly, when concrete strength is high and lateral expansion is relatively unrestrained, separation of the specimen, splitting or columnar fracture may occur. Thirdly, a combination of shear and splitting failure may occur (M. Nadim Hassoun, 2012). This is shown in the below figure:

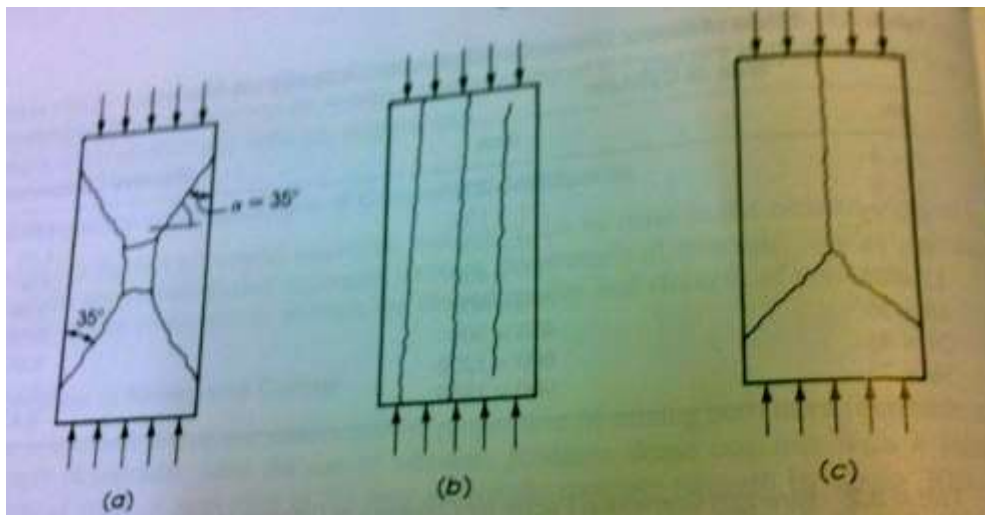


Figure 31 - Modes of Failure of Standard Concrete Cylinders (M. Nadim Hassoun, 2012)

2.8.4.2 Three Point Bending Tests

A three point bending test is when a beam is simply supported at a length of four times the width and loaded at the midspan until failure (Kopeliovich, 2012). The following figure demonstrates this configuration:

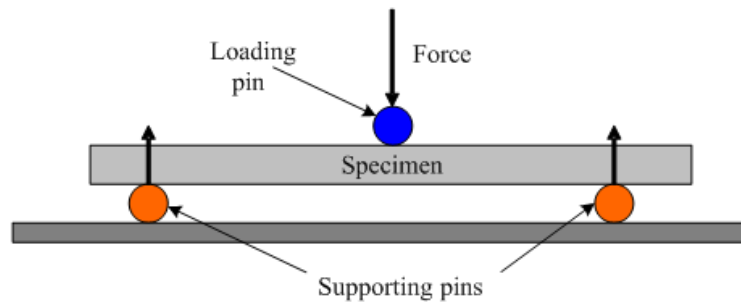


Figure 32 - Standard Configuration of a Three Point Bending Test (Kopeliovich, 2012)

By recording the loads, deflections and observations regarding cracking, calculations can be performed to determine the modulus of elasticity, cracking moment and ultimate moment capacity (M. Nadim Hassoun, 2012).

Cracks that may form throughout the concrete structure during this test may be of shear or flexural nature (M. Nadim Hassoun, 2012). In the following figure, examples of shear cracks in a concrete beam is shown on the left, and on the right is a picture of flexural cracks:

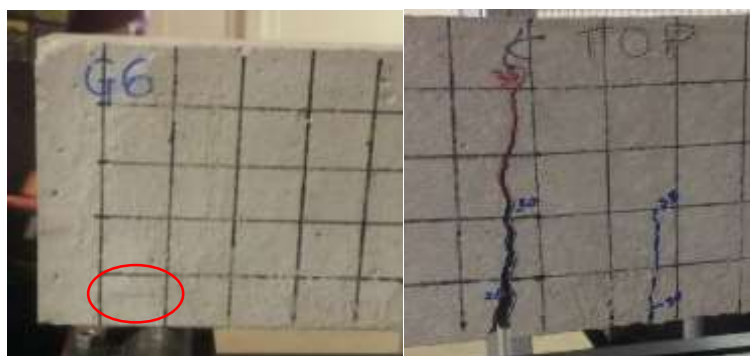


Figure 33 - Examples of Shear and Flexural Cracks

There are three types of flexural failure that may occur (M. Nadim Hassoun, 2012):

1. When steel reaches its yield strength before the concrete reaches its maximum strength. Failure thus occurs due to the yielding of steel reaching a high strain equal to or greater than 0.005.
2. When steel reaches its yield strength at the same time as concrete reaches its ultimate strength.
3. When concrete fails before the yield of steel. This is due to the presence of a high percentage of steel reinforcement. In this case, the concrete strength and its maximum strain of 0.003 are reached. The steel stress, however, is less than the yield strength, and its strain is equal to or less than 0.002.

Chapter 3: Dissertation Methodology

The following section will discuss the methodology of performing the theoretical and experimental analyses.

3.1 Design of Concrete Structure to be Analysed

The concrete structure chosen to be analysed was a concrete beam. The configuration of the chosen concrete beam is as follows:

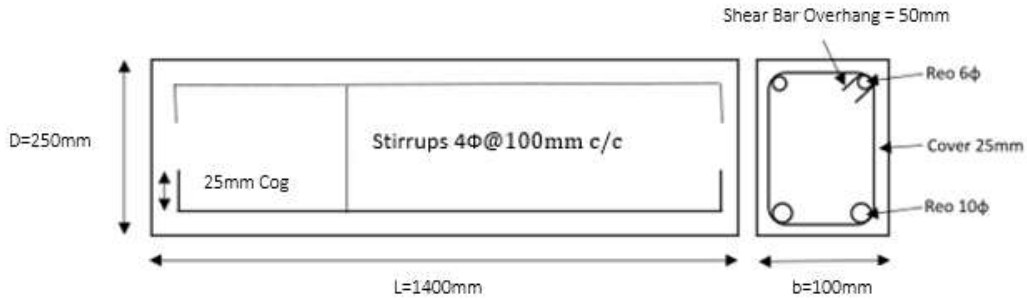


Figure 34 - Concrete Beam Structure

As per AS/NZS 3600-2009, for each concrete beam made, three test cylinders of 100 millimetre diameter and a height of 200 millimetres were also made and tested under compression.

The following table summarises information regarding reinforcement, stirrup, and concrete requirements:

Table 1 - Stirrup, Reinforcement and Concrete Requirements

Measurements & Volumes	
Length of T/B Reinforcement	1400mm
Length of Stirrup	600mm
No. of Stirrups	15
Volume of Concrete	0.0354m ³

High strength 40 MPa concrete was to be utilised. Refer to section 2.2 to view how the constituents of concrete influence concrete strength.

3.2 How the Concrete Structure will be Analysed

Three concrete beams of the above discussed structure will be made:

1. Control Beam – will be used to analyse curing temperatures over the 28 day curing period and to test the relevant properties of concrete under control conditions
2. Heated Beam – will be used to double check curing temperatures and compare relevant properties of the concrete after heat exposure to the properties of the control beam
3. Cracked Beam – will enable testing of FBG Sensors ability to recognise structural flaws within the concrete

Both the theoretical and experimental analyses will investigate:

- Two methods of encasing FBG Sensors embedded in the three beams as follows:
 1. Encasing to move with concrete (Concrete Encasing)
 2. Encasing to move with concrete (Concrete Encasing)
 3. Encasing to initiate crack propagation and prove that incorrect encasing can lead to false strain values (Aluminium Encasing)
- Curing temperatures
- Heating profile
- The modulus of elasticity
- The midpoint deflections
- The maximum principal strains
- The maximum principal stresses
- Tensile strength
- Flexural strength
- Compressive strength

3.3 Theoretical Analysis Techniques

This section will discuss the finite element analysis techniques and hand calculations utilised to theoretically analyse the concrete beam structure discussed above.

3.3.1 Finite Element Analysis Techniques

The program Abaqus/CAE was chosen to perform a finite element analysis of the above mentioned concrete beam structure. Refer to section 2.8.2 for details on this program.

3.3.1.1 Static Models

The program was used to first simulate a static analysis when the beam was under normal operating conditions, and then when the properties of the beam were deformed as expected due to heating. Both the control beam and heated beam models were then subjected to load. This load was applied to the top face of the beam via a strip across the width of the beam. This was to simulate the conditions of a three point bending test.

3.3.1.1.1 Control Beam

In order to create a three dimensional model of the concrete beam structure, the following information about concrete and steel were required for the program:

Concrete

- Mean value of modulus of elasticity of concrete at 28 days (ϵ_c)

$$\epsilon_c = 32800MPa$$

(As per AS/NZS 3600-2009 Table 3.1.2)

- Density of concrete (ρ_c)

$$\rho_c = 2400 \frac{kg}{m^3} = 2.4 \times 10^9 \frac{T}{mm^3}$$

(As per AS/NZS 3600-2009 Clause 3.1.3)

- Poisson's ratio for concrete (ϑ_c)

$$\vartheta_c = 0.2$$

(As per AS/NZS 3600-2009 Clause 3.1.5)

- Thermal conductivity of concrete (k_c)

$$k_c = 2.0 \times 10^{-9} \frac{mJ}{s.mm.K}$$

(As per (CLEAR, N/D))

Steel

- Mean value of modulus of elasticity of steel (ϵ_s)

$$\epsilon_s = 200 \times 10^3 MPa$$

(As per AS/NZS 3600-2009 Clause 3.2.2)

- Density of steel (ρ_s)

$$\rho_s = 7800 \frac{kg}{m^3} = 7.8 \times 10^9 \frac{T}{mm^3}$$

(As per (Civil, 2015))

- Poisson's ratio for steel (ϑ_s)

$$\vartheta_s = 0.3$$

(As per AS/NZS 3600-2009 Clause 3.1.5)

- Thermal conductivity of steel (k_s)

$$k_s = 52 \times 10^{-9} \frac{mJ}{s.mm.K}$$

(As per (CLEAR, N/D))

The control beam model was analysed in order to determine the position of the most critical stresses and strains. This information would contribute to deciding the optimal positioning of the FBG Sensors and strain gauges. The model was then further analysed to determine the theoretical maximum principal stresses and strains at the position of the FBG Sensors and strain gauges at various loads. These values were compared to theoretical calculations in order to validate that they were within a correct range. How these calculations were performed will be discussed in sections 3.3.2.2 and 3.3.2.3.

3.3.1.1.2 Heated Beam

For the heated beam model all inputs were the same except for the mean value of modulus of elasticity. These were declined by 25 percent as per the literature review (Association, 2002). The values utilised were as follows:

- Mean value of modulus of elasticity of concrete when heated to 200 degrees Celsius (E_c)

$$E_c = 24600MPa$$

(As per Association, 2002)

- Mean value of modulus of elasticity of steel when heated to 200 degrees Celsius (E_s)

$$E_s = 150 \times 10^3 MPa$$

(As per Association, 2002)

The model was then analysed to determine the theoretical maximum principal stresses and strains at the position of the FBG Sensors and strain gauges at various loads. These values were compared to theoretical calculations in order to validate that they were within a correct range. How these calculations were performed will be discussed in sections 3.3.2.2 and 3.3.2.3.

3.3.1.2 Thermal Model

The control beam model was further manipulated to conduct a thermal analysis of the concrete beam. A two kilowatt force at a temperature of 200°C was applied to the bottom face of the beam. This was to simulate the situation of flames lapping the bottom face of the beam as if it were in a roof structure of a building that was on fire.

This model was then utilised to predict the distribution of heat throughout the beams structure. This was further used to compare with the positioning of the FBG Sensors and thermocouples in order to predict the temperatures that they should record.

3.3.2 Calculations

Theoretical calculations were also performed so that the effects of the heat exposure on the structure integrity of the concrete beam could be predicted. Theoretical calculations included:

- Midpoint deflections
- Maximum principal strains (to compare to static models)
- Maximum principal stresses (to compare to static models)
- Tensile strength
- Flexural strength
- Compressive strength

3.3.2.1 Midpoint Deflections

The theoretical midpoint deflections of the control and heated beam specimens were calculated via use of the following equation (Australia, 2002):

$$\delta = \frac{PL_s^3}{48EI}$$

Where:

P = Applied Load (N)

E = Modulus of Elasticity (MPa)

$$I = \frac{bD^3}{12} \text{ (mm)}$$

$L_s = 4 \times b$ (mm)

δ = Midpoint Deflection (mm)

A length of four times the width of the beam was applied because this would be the positioning of the supports in the three point bending test. The modulus of elasticity values for the control and heated beam specimens as discussed in section 3.2.1.1 were utilised. Various loads were applied in increments of five Kilo Newtons.

3.3.2.2 *Maximum Principal Strains*

The theoretical maximum principal strains of the control and heated beam specimens were calculated via use of the following equation (Inc, 2015a):

$$e = \frac{\sigma}{E}$$

Where:

e = Maximum Principal Strain

σ = Maximum Principal Stress (MPa)

E = Modulus of Elasticity (MPa)

A length of four times the width of the beam was applied because this would be the positioning of the supports in the three point bending test. The modulus of elasticity values for the control and heated beam specimens as discussed in section 3.2.1.1 were utilised. Various loads were applied in increments of five Kilo Newtons.

3.3.2.3 *Maximum Principal Stresses*

The theoretical maximum principal stresses of the control and heated beam specimens were calculated via use of the following equation (Queensland, 2014):

$$\sigma = \frac{3PL_s}{2bD^2}$$

Where:

P = Applied Load (N)

b = Width of Beam (mm)

D = Depth of Beam (mm)

$L_s = 4 \times b$ (mm)

σ = Maximum Principal Stress (MPa)

A length of four times the width of the beam was applied because this would be the positioning of the supports in the three point bending test. The maximum principal stresses of the heated beam were assumed to be 80 percent of the maximum principal stresses of the control beam. This assumption was directly correlated from the literature stating that a 200 degree Celsius heat would cause a 20 percent reduction in tensile strength (Yao, 2006). Various loads were applied in order to compare these values with the values output by the static model.

3.3.2.4 Tensile Strength

Tensile strength is equal to the maximum principal stress a concrete specimen can handle. In order to determine this stress, the expected failure load of the beam was calculated from the theoretical ultimate moment capacity.

The theoretical ultimate moment capacity was calculated from the following equation (Queensland, 2014):

$$M_U = A_s f_y \left(d - \frac{A_s f_y}{\alpha_2 f'_c b} \right)$$

Where:

M_U = Ultimate Moment Capacity (MPa)

f'_c = Theoretical Compressive Strength (MPa)

b = Width of Beam (mm)

d = Depth of Beam - Cover (mm)

f_y = 500MPa

A_s = Area of Tensile Reinforcing Steel (mm²)

$\alpha_2 = 1.0 - 0.003 f'_c \quad 0.67 \leq \alpha_2 \leq 0.85$

The expected failure load was then calculated from the following equation (Queensland, 2014):

$$P_U = \frac{M_U \times 4}{L_s}$$

Where:

M_U = ultimate moment capacity (MPa)

P_U = ultimate load (expected failure load)(kN)

$L_s = 4 \times b$ (mm)

A length of four times the width of the beam was applied because this would be the positioning of the supports in the three point bending test. The maximum principal stress at the position of the strain gauges at this expected failure load was determined from the control and heated beam static models. This was applied as the theoretical tensile strength of each beam.

3.3.2.5 Flexural Strength

The flexural strength of the control beam was assumed to be 10 percent of the expected compressive strength of the beam. The flexural strength of the heated beam was then calculated to be 85 percent of the flexural strength of the control beam. This is because a 200 degree Celsius heat is expected to degrade the flexural strength of concrete by 15 percent (Association, 2002).

The theoretical load at which the each beam will fail due to flexure was calculated from the following equation (Queensland, 2014):

$$\text{Failure Load} = \text{Flexural Strength} \times b \times D$$

Where:

b = Width of Beam (mm)

D = Depth of Beam (mm)

Failure Load (N)

Flexural Strength (MPa)

3.3.2.6 Compressive Strength

The theoretical compressive strength of concrete can be determined via the proportional mix quantities. It was decided to use a mix quantity that produced a compressive strength of 40 Mega Pascals. It was assumed that the heating would cause a 10 percent reduction in the compressive strength of the heated specimens (Association, 2002).

The compressive strength of a concrete beam is experimentally determined via the use of Australian standard sized cylinders. The theoretical failure load of these cylinders when under compression was calculated from the following equation (Queensland, 2014):

$$\text{Failure Load} = f'c \times \frac{\pi \times di^2}{4}$$

Where:

$f'c$ = compressive strength of cylinder

di = diameter of cylinder

3.3.3 Information Purely from Literature

Theoretical assumptions about the behaviour of the FBG Sensors when encased utilising the two chosen techniques (which will be discussed in section 3.3.1) were purely based on literature. Refer to section 2.8.3.1.6 for the literature regarding this.

The theoretical curing temperatures and modulus of elasticity values were also based on literature review. It must be noted that the modulus of elasticity was assumed to decrease by 25 percent for the heated beam (Association, 2002).

3.4 Experimental Analysis Technique

The experimental analysis techniques will be discussed in the following section.

3.4.1 FBG Sensor Encasing Techniques

Two techniques of encasing an FBG Sensor were trialled. The first technique utilised a concrete encasing which was hoped to be able to move with the concrete and read accurate strain values. The second technique utilised aluminium encasing and was hoped to create an internal deficiency within the concrete structure so that the FBG Sensor could be proven to be capable of reading such a deficiency. This technique would also be utilised to prove that incorrect encasing can inhibit an FBG Sensors' ability to read accurate strains.

3.4.1.1 Concrete Encasing

A practical method of encasing that would not create a crack within the concrete or have the issue of picking up false strains was trialled. It was made as follows:

1. Coat the FBG Sensor fibre in liquid electrical tape leaving the sensor region bare and allow to set for 24 hours. This protects the fibre from corrosion and chemical attack.
2. Thread the FBG Sensor fibre inside zero tube but leave the 1mm sensor region of the fibre, and 0.5mm either side of that region bare. The zero tube protects the fibre from abrasion.
3. Thread the FBG Sensor encased in zero tube inside fibreglass sleeving, leaving the same region bare. Leaving the sensor region bare allows the sensor to be in direct contact with the concrete. The fibreglass sleeving provides further protection from abrasion as well as heat.
4. Cut a one 5mm long section of 20mm diameter electrical conduit. This will be utilised as the mould for encasing the sensor region of the FBG Sensor in concrete.
5. Oil conduit in order to prepare mould.
6. Tape (using duct tape) each end of the conduit mould securely shut.

7. Cut a hole in the tape at the centre on each end of the conduit mould. This hole should be 3mm in diameter.
8. Thread the FBG Sensor (encased as per step three) through the hole, leaving the bare sensor region in the centre of the conduit mould (central diameter and length).

An example of a moulds is shown in the below diagram:



Figure 35 - Method of Encasing FBG Sensor in Concrete Capsule Moulds

9. Lift the tape from one end of the conduit mould.
10. Pour same concrete mixture as will be used for concrete structures into the opened end of the conduit mould.
11. Tap side of conduit mould to compact concrete.
12. Repeat steps 10 and 11 until conduit mould is full of compacted concrete.
13. Replace tape on end of mould and leave in a safe place to set. If care is not taken the FBG Sensor could be broken.
14. After seven days remove mould and place FBG Sensor in concrete beam. At this point the concrete will have achieved 80 percent of its strength (Australia, 2002).
15. A thermocouple was then tied to the outside of the concrete capsule so that any temperatures recorded by the FBG Sensor could be validated.

It was believed that encasing the FBG Sensor in the same concrete as the structure that it would be embedded in would allow for it to move with the structure. Using electrical conduit as the mould created a ribbed surface which was hoped to encourage bonding. It was hoped that when the capsule is embedded in concrete this concrete should set in these ribbed areas.

3.4.1.2 Aluminium Encasing

A summary of the encasing technique to be used for the FBG Sensor to encourage crack propagation is as follows:

1. Thread the FBG Sensor fibre inside zero tube but leave the 1mm sensor region of the fibre, and 0.5mm either side of that region bare. The zero tube protects the fibre from abrasion.
2. Thread the FBG Sensor encased in zero tube inside fibreglass sleeving, leaving the same region bare. Leaving the sensor region bare allows the sensor to be in direct contact with the concrete. The fibreglass sleeving provides further protection from abrasion as well as heat.
3. Cut a 180 millimetre long, 15 millimetre wide strip of 1 millimetre thick aluminium.
4. Drill 1 millimetre holes at each corner of the aluminium.
5. Use epoxy to glue the FBG Sensor and a thermocouple in practically the same position on aluminium strip. The thermocouple was included so that any temperatures recorded by the FBG Sensor could be validated.
6. Tape the ends in order to ensure the FBG Sensor and thermocouple stay in place.
7. A 120 millimetre long, 15 millimetre wide strip of 1 millimetre thick aluminium was then cut and bent in a triangular shape with a peak of 5 millimetres.
8. This triangular strip of aluminium was placed over the rectangular strip of aluminium in order to fully encase the sensor (as per other metal encasing techniques).
9. This encasing was epoxy glued together.

Refer to the below schematic to view the encasing.



Figure 36 - Aluminium Encasing of FBG Sensor

The aluminium was used for housing the FBG Sensor as it will protect the FBG Sensor during construction of the beam. Since it is a foreign material with sharp edges it should create an internal crack within the structure which will allow the examination of this with the FBG Sensor. Aluminium also has less electrochemical activity than reinforcing steel. If the aluminium was to come into contact with the reinforcing steel, or react with it due to the concrete acting as an active electrolyte, corrosion of the aluminium would occur which would encourage internal crack propagation close to the FBG Sensor (Association, 2002).

The shape and material used for this encasing should not bond when embedded in concrete. This combined with its inflexible nature should prevent accurate strains being read. The encasing contained holes on each corner so that the housing could be tied in place using fishing line.

3.4.2 Placement of FBG Sensors, Strain gauges and Thermocouples

FBG Sensors, thermocouples and strain gauges were to be embedded in the concrete beams at locations determined from investigation of the results of the finite element analysis. For details on how this was analysed refer to section 5.1.6.

One FBG Sensor was to be placed in each of the three concrete beams at the position shown in the following figure:

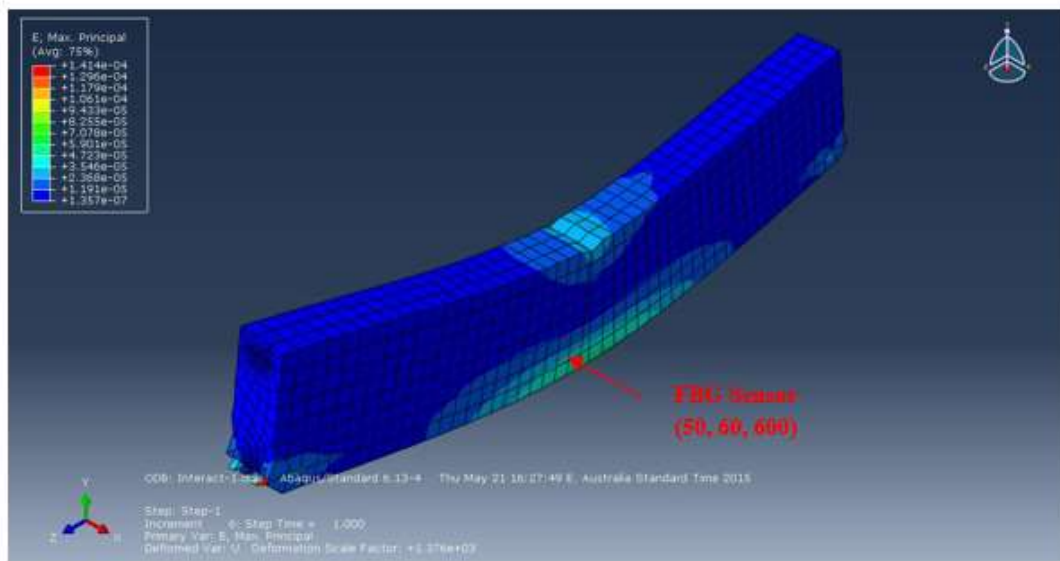


Figure 37 - Positioning of FBG Sensor

It can be seen that the FBG Sensor was to be placed at the z, y, z coordinates 50, 60, 600 (millimetres from axes). The FBG Sensor was placed longitudinally so that it could record maximum principal strains and be directly comparable to the theoretical static model. The FBG Sensor was to be tied in place via the use of fishing line wrapped around the reinforcement.

In order to validate the temperature readings recorded via the FBG Sensor, as well as give an overall temperature profile of the beam, four thermocouples were to be embedded in both the control and heated beams at the positions shown in the following figure:

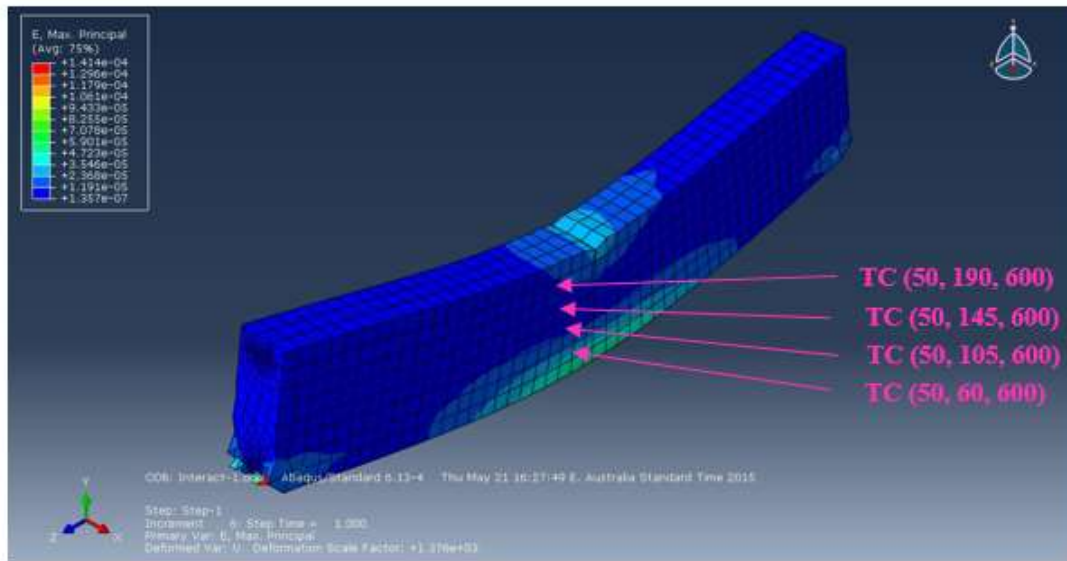


Figure 38 - Positioning of Thermocouples

It can be seen that the thermocouples (TC) were to be placed at the z, y, z coordinates 50, 60, 600; 50, 105, 600; 50, 145, 600; and 50, 190, 600 (millimetres from axes). They were to be tied in place via the use of fishing line wrapped around the reinforcement.

In order to validate the strain values recorded by the FBG Sensor, two strain gauges were to be surface mounted on the control and heated beams at the positions shown in the following figure:

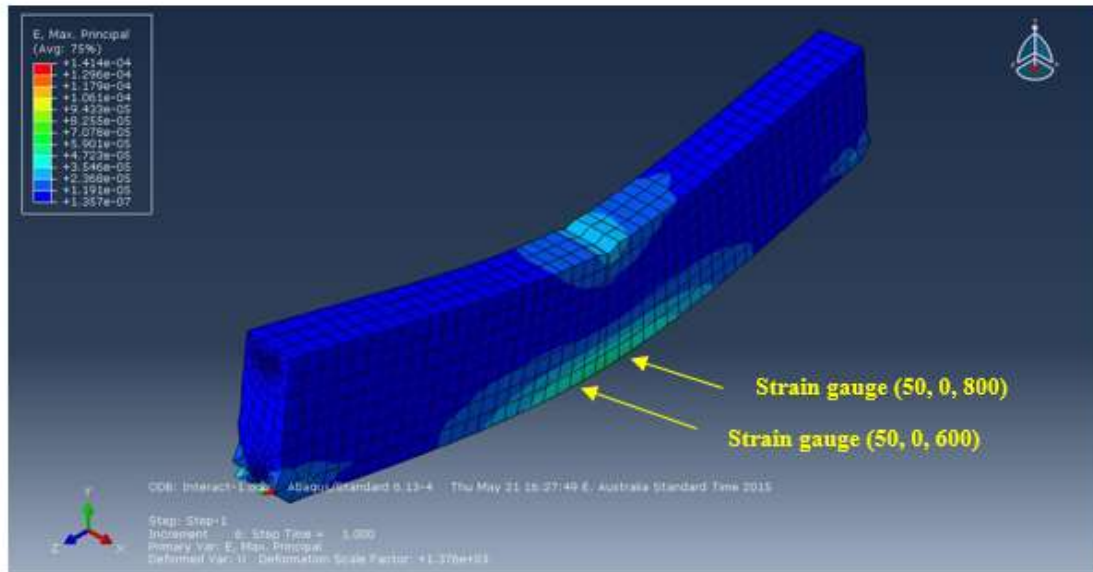


Figure 39 - Positioning of Strain gauges

It can be seen that the strain gauges (SG) were to be placed at the z, y, z coordinates 50, 0, 600 and 50, 0, 800 (millimetres from axes). They were to be placed longitudinally so that they could read maximum principal strains and be directly comparable to the FBG Sensor readings. It must be noted that the strain gauges were to be equally spaced from the centre of the beam. Due to the nature of the three point bending test, the strain gauges should thus record the same strain values.

The surface of the beam where the strain gauges were to be mounted was first smoothed via the use of sand paper. Then a thin layer of quick set epoxy was smoothed onto the surfaces. After the epoxy had dried the strain gauges were glued to this surface via the use of the quick set epoxy followed by sticky tape.

3.4.3 Casting of Concrete Structures

The concrete beam structures were cast using the following procedure:

1. Create concrete reinforcing cage as described in section 3.1 Ensure the ties used to secure the stirrups to the reinforcement bar are tied to the inside so that they do not protrude and cause corrosion.
2. Place concrete reinforcing cage in concrete beam mould ensuring 25mm cover.
3. Embed structure with FBG Sensors, thermocouples and strain gauges as appropriate for each beam as per section 3.3.2.
4. Mix concrete and subject it to the slump test as per section 2.4.1. Premix 40 MPa bags of concrete were utilised.
5. When concrete displays adequate slump pour into concrete beam mould and testing cylinders. Ensure the shear bar is methodically rotated in position to avoid weak spots forming.
6. Vibrate the concrete to remove excess air and avoid voids. The right balance of vibration must be applied as too little will lead to air in the concrete causing voids but too much will lead to separation of particles which leads to weaknesses forming. Refer to section 2.4 for more details.
7. Smooth top of mould.
8. Allow to cure for 28 days at uncontrolled temperatures.

The temperature changes of the control and heated beam specimens were recorded via the use of embedded FBG Sensors and compared to the results of embedded thermocouples. The thermocouples were numbered from the bottom of the beam upwards, starting with the control beam and then the heated beam. The control beam was to have thermocouples 0, 1, 2, and 3 embedded within it. The heated beam was to have thermocouples 4, 5, 6, and 7 embedded within it. Refer to section 3.3.3 for visual aids.

3.4.4 Sensor Calibration and Interrogation

How to calibrate and interrogate the FBG Sensors, thermocouples and strain gauges will be discussed in the following section:

3.4.4.1 FBG Sensors

FBG Sensors do not require calibration, all data can be correlated to the original wavelength of the FBG Sensor. Section 3.3.7 will discuss how temperatures and strains can be calculated from the FBG Sensor readings.

In order to record FBG Sensor readings, the FBG Sensor was first connected to a sml125 interrogation unit, and then interpreted via the use of the software program MOI Enlight. Refer to section 2.8.3.1.4 for more details.

The specifications of the FBG Sensor used is summarised in the following table:

Table 2 - Specifications of FBG Sensor

Specification	Description
CW	1550 +/- 0.3 nm
FBG Length	5mm
Reflectivity	>50%
Fibre Type	SMF – 28C Fibre
Recoat	None
Connector	FC/APC

3.4.4.2 Thermocouples

Type K thermocouples require calibration. This is generally done by recording the amf produced by the thermocouple at various temperatures, and correlating the recorded values to a calibration curve. From this calibration curve a calibration equation can be determined.

For this experiment the thermocouple readings were interrogated via the use of an NI cDAQ-9174, and then interpreted via the use of the software program LabVIEW. In order to use this program a script had to be written which had its own calibration curve and equation. The calibration was input by recording the amf produced at various temperatures which were measured via the use of a digital thermometer. Both the thermocouple and digital thermometer were placed in boiling water and the temperatures recorded at various increments as the water cooled. This calibration meant the script translated the thermocouple readings straight to temperatures. For more details on the capabilities of LabVIEW refer to section 2.8.3.2.2.

3.4.4.3 Strain Gauges

Strain gauges require calibration. The strain gauge interrogation unit used required the ohms, and gauge factor to be input. A quarter bridge was then used to take readings from the strain gauge and this too had to be input into the strain gauge interrogator unit. Strains had to be manually recorded as the function of the strain gauge interrogator unit used for recording was not working. Refer to section 2.8.3.3.2 for more details on the strain gauge equipment.

The strain gauges to be used had the following specifications:

Table 3 - Specifications of Strain Gauges to be used

Specification	Number
Gauge Factor	2.150
Ohm's	120

3.4.5 Heat Test

Heats are unpredictable, so thus, there is no exact way of simulating them (Han et al., 2013). The concrete beam structure was to be put in the situation where it was subjected to a heat of approximately 200 degrees Celsius within a concentrated area near the centre of its side face.

This type of heating was different to what was utilised in the theoretical thermal model. It was altered due to greater practicality. This meant that an Australian standardised and approved circular gas burner of 200 millimetre nominal diameter, attached to an Australian standardised and approved gas bottle was able to be utilised. The beam was propped up on its side via the use of Hebel blocks. These were chosen due to their non-conductive properties. The heat was then applied to the beam with the z position of the thermocouples and FBG Sensor at the centre of the heat cylinder. The heat was applied at approximately five millimetres from the face of the beam.

This method of heating meant the thermocouples and FBG Sensor were easily interrogated. The use of a kiln or oven would have been unsafe because the door would not have been able to be shut due to the need to connect the thermocouples and FBG Sensor to the relevant equipment for interrogation and recording.

The use of a circular gas burner also meant that the beam was subjected to partial heat, which was theoretically expected to have a greater detrimental effect to the concrete structure. This heat being subjected to the side face meant the whole 200 millimetre diameter heat was able to be in direct contact with the concrete. This also meant the thermocouples and FBG Sensor were closer to the heat source (only 50 millimetres away) and thus would be able to be used to detect greater heat variation.

As per AS/NZS 3600-2009, a building should be designed to withstand at least a 90 minute heat resistance. The concrete beam structure was thus subjected to heat for approximately 90 minutes.

Whilst the heating was being performed, a laser thermometer was used to determine the external temperature of the heat so that when an external temperature of 200 degrees Celsius was reached, the heating was stopped. At this point the laser thermometer was used to measure the distribution of heat at every one hundred millimetre interval along the length of the beam on the 'surface' (i.e. the side of the concrete beam not subjected to the heating).

During the heating test, a thermocouple was epoxy glued to this above mentioned surface of the beam at the same y and z position as the already embedded thermocouples. The thermocouples were numbered from the bottom of the beam to the top, starting with thermocouple zero and ending with thermocouple three. Thermocouple four was the thermocouple epoxy glued to the surface of the beam.

3.4.6 Structural Health Tests

Structural health tests will be performed on all concrete specimens using the SANS Machine. The machine will be used to perform compression tests and three point bending tests as described in section 2.9.4.

3.4.6.1 Three Point Bending Test

The three point bending test was performed to be performed to all three beams. For the control and heated beam specimens the SANS Machine would be utilised to record the applied loads, the midpoint deflections that these loads cause, and the times at which these loads were applied. At the same time the FBG Sensor would be connected to the sml125 interrogator and the program MOI Enlight would be utilised to record the peak and response data. The maximum principal strains as per the strain gauges were also recorded via the use of the blue box interrogator.

For the cracked beam specimen, the SANS Machine would be utilised to record the applied loads and times at which these load were applied. At the same time the FBG Sensor would be connected to the sml125 interrogator and the program MOI Enlight would be utilised to record the peak and response data. The comparison of these strains with the strains read from the control beam should be much lower, thus showing that the aluminium encasing has inhibited the FBG Sensors ability to read strains.

3.4.6.2 Compression Test

The compression test was to be performed to six Australian standardised cylinders. The first three were the control specimens, and the next three were the heated specimens. The heated specimens were to be heated using the same technique as what was to be used for the heated beam. Refer to section 3.4.5 for details. The SANS machine recorded the failure load of each cylinder, and from this the average compressive strength was able to be determined.

3.4.7 Calculations

The following section will discuss how temperatures and maximum principal strains were calculated from the FBG Sensor peak wavelengths. It will also discuss how the FBG Sensor and strain gauge strains were converted to stress and then tensile strength. How the modulus of elasticity, flexural strength, and compressive strength were able to be determined from the SANS Machine readings will also be discussed.

3.4.7.1 Temperature – FBG Sensor

The following equation was rearranged to give the change in temperature (Su and Han, 2014):

$$\Delta\lambda_B = \lambda_B \{(\alpha + \xi) \Delta T + (1 - p_e) \Delta\varepsilon\},$$

Where:

$\Delta\varepsilon$ = strain variation (equated to zero for this case)

ΔT = temperature change

α = coefficient of thermal expansion

ξ = thermo-optic coefficient

p_e = strain optic coefficient

$\Delta\lambda_B$ = change in wavelength

λ_B = original wavelength

The change in temperature was then correlated to an actual temperature by adding the change to the original temperature value.

3.4.7.2 Maximum Principal Strains – FBG Sensor

The following equation was rearranged to give the change in maximum principal strain (Su and Han, 2014):

$$\Delta\lambda_B = \lambda_B \{(\alpha + \xi) \Delta T + (1 - p_e) \Delta\varepsilon\},$$

Where:

$\Delta\varepsilon$ = strain variation

ΔT = temperature change (equated to zero for this case)

α = coefficient of thermal expansion

ξ = thermooptic coefficient

p_e = strain optic coefficient

$\Delta\lambda_B$ = change in wavelength

λ_B = original wavelength

The change in strain was then correlated to an actual strain by adding the change to the original strain value.

3.4.7.3 Maximum Principal Stresses

The experimental maximum principal stresses were calculated from the maximum principal strains via use of the following equation (Queensland, 2014):

$$\sigma = eE$$

Where:

e = Maximum Principal Strain

σ = Maximum Principal Stress (MPa)

E = Modulus of Elasticity (MPa)

3.4.7.4 Modulus of Elasticity

The experimental modulus of elasticity was calculated from the loads and deflections recorded from the SANS machine using the following equation (Australia, 2002):

$$E = \frac{PL_s^3}{48\delta I} \text{ (MPa)}$$

Where:

$$I = \frac{bd^3}{12} \text{ (mm}^4\text{)}$$

$$L_s = 4xb \text{ (mm)}$$

P = Applied Load (N) (Ultimate was used)

δ = Deflection (mm) (Ultimate was used)

E = Modulus of Elasticity (MPa)

3.3.7.5 Tensile Strength

The maximum principal stresses at each beams' respective failure load correlates to the experimental tensile strengths of each specimen (Yao, 2006).

3.4.7.6 Flexural Strength

The experimental flexural strength was determined from the following equation (Queensland, 2014):

$$\text{Flexural Strength} = \frac{P_U L_s}{bD}$$

Where:

P_U = Failure Load of Beam (N)

b = Width of beam (mm)

L_s = $4b$ (mm)

D = Depth of beam (mm)

3.4.7.7 Compressive Strength

The experimental compressive strength of each cylinder was calculated from the following equation (Queensland, 2014):

$$f'_c = \frac{P}{A} \text{ (MPa)}$$

Where:

$$A = \frac{\pi D^2}{4} \text{ (mm)} \text{ (Area of cylinder)}$$

P = failure load (N)

The average of the three cylinders for each scenario was then applied as the compressive strength of each respective beam.

Chapter 4: Project Organisation

The following chapter will discuss project timelines, resource requirements, risks and consequential effects.

4.1 Timelines

To organise timelines throughout this dissertation, a table has been produced. This table allows for expected time lines to be set out, and for these to be compared to the actual progress made. By keeping this chart up to date, an estimation of the work completed, and work still requiring completion can be achieved.

The figure below highlights the project timelines for this project.

Table 4 - Timelines

Task	Expected Completion Date	Actual Completion Date
Literature Review	31 st May	15 th October
Determination of Testing Techniques	30 th April	25 th April
Risk Management Plan	30 th April	26 th April
Determination of Method of Encasing	30 th April	5 th May
Determination of Resource Requirements	30 th April	5 th May
Stress and Strain Hand Calculations	10 th May	9 th May
FEA Analysis (Abaqus/CAE)	31 st May	20 th May
Comparison of FEA and Hand Calculation Results	31 st May	22 nd May
Hand Calculations (Deflections, Modulus of Elasticity, Strengths, etc.)	10 th June	12 th June
Analysis of Theoretical Results	28 th June	20 th June
Building of Test Specimens	1 st June	12 th August
Monitoring of Curing Temperatures	28 th June	9 th September
Heating Tests	29 th June	16 th September
Compression and Three Point Bending Tests	6 th July	18 th September
Analysis of Experimental Results	31 st July	30 th September
Comparison of Theoretical and Experimental Results	31 st August	15 th October

4.2 Resource Requirements

The resources necessary to complete this project and when they were required are detailed in the below table:

Table 5 - Resource Requirements

Resource	Description	When Required
Computer	For electronic production of dissertation	Throughout project
External hard drive	For file backup	Throughout project
Abaqus/CAE	For 3D computer modelling of concrete beam	April
SANS Machine	For compression and three point bending tests of concrete beams	August
FBG Sensors Replica Fibres	To embed in concrete samples to check methods of encasing FBG Sensors	May
Concrete Test Cylinder Moulds (3)	To mould concrete cylinders embedded with replica FBG Sensors	May
FBG Sensors (3)	To embed in three concrete beams to analyse strain and temperature	May
Thermocouples (8)	To embed in two concrete beams to analyse temperature.	May
Wire Strippers	For stripping thermocouples to reveal two dissimilar metals so they can be joined together	May
Soldering Iron	For joining thermocouple dissimilar metals together	May

Sm125	To log the readings of the FBG Sensors.	June-July
Micron Optics	To interpret the readings of the FBG Sensors.	June-July
NI cDAQ - 9174	To log the readings of the thermocouples	May-July
LabVIEW	To interpret the readings of the thermocouples	May-July
Kettle and Cup	To create varying temperature environments to calibrate thermocouples	May
Digital Thermometer	To read the temperature throughout the varying environments and calibrate the thermocouples to	May
Strain Gauges (4)	To put on concrete surface to analyse strain.	July
Data Interrogator	To log the readings of the strain gauges	July
Personal Protective Equipment (Safety Boots, Goggles Mask, and Riggers Gloves)	To ensure safety whilst testing.	May-July
Concrete Beam Moulds	To mould concrete beams.	June
Concrete Test Cylinder Moulds (9)	To mould concrete cylinders to test compressive strengths of beams	June

Grade 40 Cement Mix (320kg-13x20kg Bags)	To pour concrete samples and beams	May
Water (24.7L)	To pour concrete samples and beams	May and June
Beakers	To measure water proportions	May and June
Steel Reinforcement- 6xN10 (Ribbed Bars) 6xN6 (Smooth Bars)	To reinforce concrete beams	May
25m of R4 steel (smooth)	To make reinforcing stirrups	May
Wire Cutters	To cut stirrups to appropriate lengths	May
Steel Plate For Making Stirrups	To shape stirrups	May
300 Zip Ties	To hold steel reinforcement in place	May
Oil and Brush	To lubricate beam and cylinder moulds before pouring concrete	May and June
Vibrator	To rid concrete of air voids	June
Concrete Slump Test Equipment (Mould, Ruler and Bar)	To test concrete before pouring it into moulds	May and June
Cement Mixer	To mix cement and water	May and June
Wheelbarrow and Bucket	To transport concrete from cement mixer to moulds	May and June
Shovel and Spade	To mix and move concrete ingredients	May and June

Electrical Conduit (25m role with 20mm diameter)	To act as a mould for encasing FBG Sensor in concrete	May
Masking Tape	To plug off ends of electrical conduit mould	May
Aluminium	To encase FBG Sensor	May
Fast Set Epoxy	To glue FBG in place within aluminium encasing and to glue surface mounted strain gauges in place	May and July
Liquid Electrical Tape	To protect FBG Sensor from chemical and corrosion attack	May
Zero Tube (6m)	To protect FBG Sensor from abrasion	May
Fibreglass Sleeving (6m)	To protect FBG Sensor from heat	May
Safety Tape	To stop people entering areas where experimentation is occurring	June-July
Safety Glass	To protect by standers watching three point or compression bending tests	July
Good Quality Camera	To capture test results	May - July
Laser Interrogator	To check condition of FBG Sensors and replica fibres	May - July
Hebel Blocks	To prop up beam whilst subjecting it to heat	July

Australian Standardised Gas Heater	To simulate the situation of heat	July
Australian Standardised Lighter	To light gas heater	July
Infrared Thermometer with Dual Laser Targeting	To read temperatures of heat source and relative beam surface temperatures	July
Access to P2	To pour and store concrete beams	May-July
Access to P11	To subject concrete beams to compression and three point testing	July
Access to Z1	To make initial three cylinder moulds and store all concrete cylinders in fog room	May - July

4.3 Risk Register

With any technical investigation, there are a range of associated risks which may negatively impact the progress. The theoretical/simulation phase of this technical analysis was of insignificant consequence with a rare probability of injury. The physical testing phase of this technical analysis, however, contained a range of possible risks. These risks were analysed and their corresponding mitigating actions were decided.

The risk assessment deemed that the following personal protective equipment were necessary at various stages throughout the project:

- Safety Boots
- Safety Glasses
- Safety Mask
- Riggers Gloves
- Heat Protective Gloves
- Heat Protective Suit

Overall this project was identified as having low risks if mitigated appropriately. Refer to Appendix B for the risk assessment forms that were used to draw these conclusions.

4.4 Consequential Effects

This section analyses the effects of this technical investigation, and situations where its content may be able to be utilised or applied externally. The following are a list of the possible uses for the technical investigation findings:

- For further investigation into structural health monitoring of structures
- By engineers and construction workers for implementation in concrete structures around the world

When completing this technical investigation, a high level of integrity is thus required to ensure the presented findings are sufficient for industry utilisation.

Chapter 5: Models and Results

This chapter will detail the results of the theoretical and experimental analyses. It will discuss the following:

- The performance of the FBG Encasings
- The curing temperatures of the concrete
- The heating profile of the beam
- The midpoint deflections associated with loading the beam
- The modulus of elasticity of the beam
- The principal strains associated with loading the beam
- The principal stresses associated with loading the beam
- The tensile strength of the beam
- The flexural strength of the beam
- The compressive strength of the beam

All associated assumptions will also be discussed.

5.1 Theoretical Analysis

This section will discuss theoretically what should occur with the results. Any associated assumptions will be listed.

5.1.1 Performance of FBG Encasing Techniques

Theoretical assumptions about the performance of both the aluminium and concrete encasing techniques will be discussed in the following section.

5.1.1.1 Concrete Encasing

It is assumed that the concrete encasing will show the following characteristics:

- It will sufficiently protect the FBG Sensor from corrosion, chemical attack, abrasion, and heat
- It will be able to read accurate internal temperatures
- It will be flexible and will bond with the concrete beam, and so thus will be able to read accurate strains
- It will allow the FBG Sensor to identify any significant internal cracks

The concrete encasing is to be used for the control and heated beam specimens. Throughout the following sections in this theoretical analysis, the predicted readings the FBG Sensors encased in this way and embedded in these specimens will be discussed.

5.1.1.2 Aluminium Encasing

As per the literature review, it is assumed that the aluminium encasing will show the following characteristics:

- It will sufficiently protect the FBG Sensor from chemical attack, abrasion, and heat
- It will be able to read accurate internal temperatures
- It will be inflexible and will not bond with the concrete beam, and so thus will not be able to read accurate strains. The strains read by the FBG Sensor encased in aluminium or any other inflexible encasing (such as the commercially used stainless steel) is predicted to pick up strains much smaller than the actual strains experienced by the concrete (Biswas et al., 2010). How much smaller these strains are is unable to be accurately predicted.
- It will create an internal crack within the concrete beam
- It will allow the FBG Sensor to identify any significant internal cracks. An internal crack is picked up by an FBG Sensor and displayed as an interruption of the spectra (Tadros et al., 1997).

The aluminium encasing was to be used for the cracked beam specimen. It was used to conclude whether the aluminium encasing will create an internal crack, and determine whether an FBG Sensor can recognise the creation of such a crack. The only other characteristic of interest is the predicted inability of the FBG Sensor encased in this way to read accurate strains. Further theoretical characteristics regarding the cracked beam specimen are thus not of interest in this paper and will not be further discussed.

5.1.2 Concrete Curing Temperatures

The theoretical internal curing temperatures and assumptions associated with their formation will be discussed in the following section:

5.1.2.1 Theoretical Results

The theoretical internal curing temperatures are believed to be comparable to the normal weight concrete block of dimensions 1m^3 as shown in the below schematic:

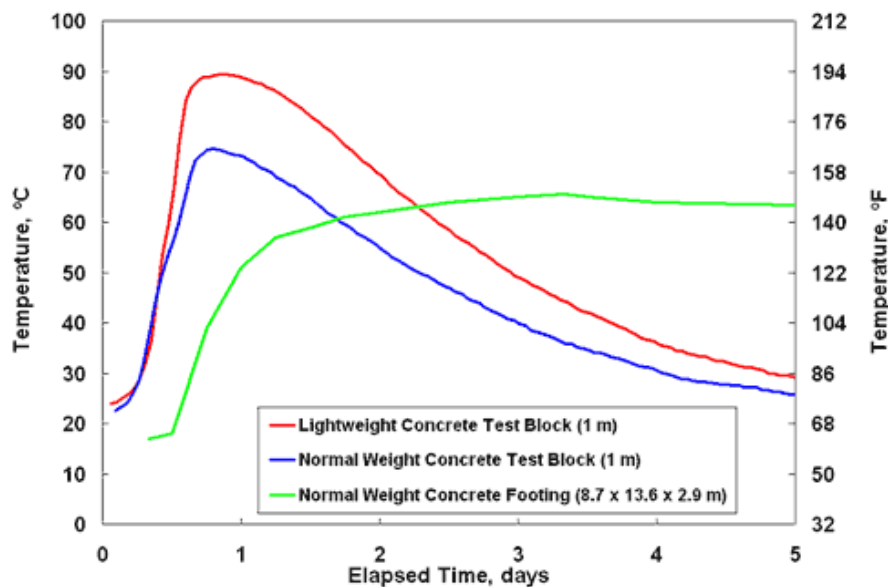


Figure 40 - Comparable Theoretical Internal Curing Temperatures ((APEE), 2005)

From the above figure it is suggested that the concrete beam specimens will show a rapid rise in internal temperature until it reaches a maximum temperature of approximately 75 degrees Celsius about 24 hours after pouring. After this point the internal temperature of the concrete beams are expected to decline until it reaches its approximate starting temperature of approximately 20 degrees Celsius about five days after pouring ((APEE), 2005).

5.1.2.2 Assumptions

The reliability of the results of this theoretical analysis are based on the following assumptions:

- The difference in size of the concrete block and concrete beam specimens will have negligible effect on the results
- The concrete beam specimens will be subjected to relatively similar external temperatures during pouring and curing
- The composition of the concrete used for the concrete block and concrete beam specimens are of comparable nature

5.1.3 Heating Profile of Beam

In order to determine the expected temperature profile of the concrete beam specimen when subjecting it to a maximum external heat of 200 degrees Celsius at a two kilowatt force, a three dimensional thermal model was created in Abaqus/CAE. The following section will discuss the results of this thermal analysis and any associated assumptions.

5.1.3.1 Theoretical Finite Element Thermal Analysis Results

The following figure shows the temperature profile of the reinforced concrete beam as predicted by the finite element analysis:

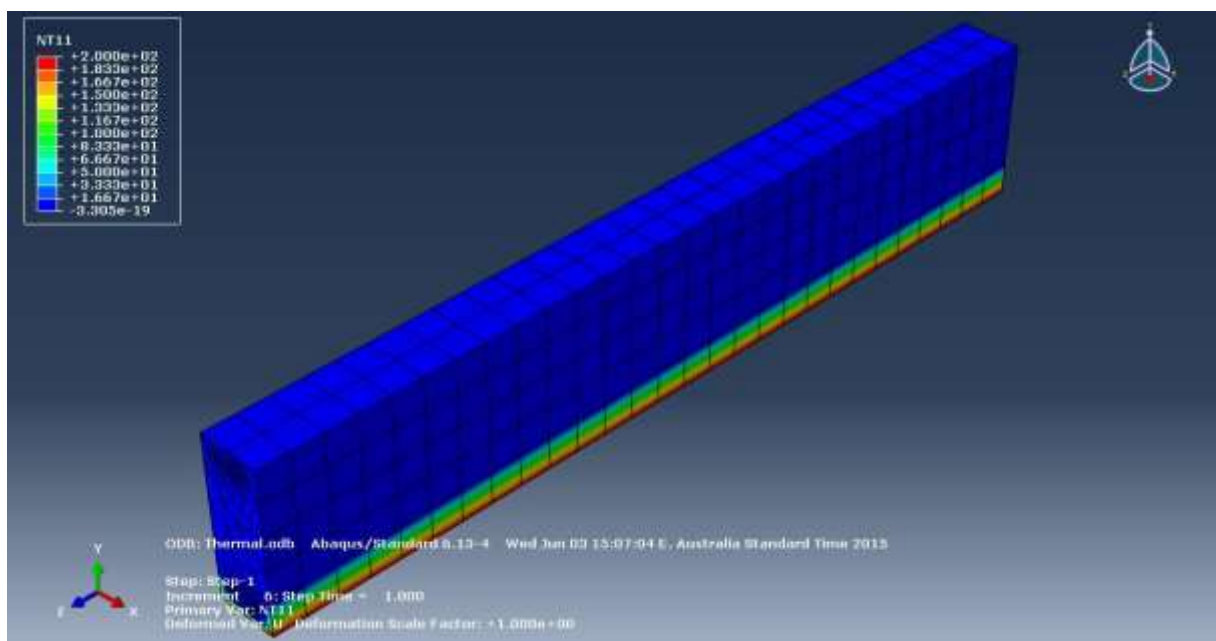


Figure 41 – Theoretical Temperature Profile of Reinforced Concrete Beam

In this schematic the heat is applied uniformly across the bottom face of the beam. The method of heating was in fact changed and unfortunately due to time constraints the model was unable to be altered.

The heating method was altered so that the heat was applied on the side face of the beam within a concentrated 200 millimetre circle. The maximum external heat and force was still estimated to be the same. This means the thermocouples and FBG Sensor were all 50millimetres from the heat source.

The model can, therefore, still be used to estimate the expected internal temperature of concrete 50 millimetres away from an external heat of 200 degrees Celsius at a 2 kilowatt force. The model suggested that the thermocouples and FBG Sensor should get a reading of approximately 92.4 degrees Celsius when subjected to such a heat.

5.1.3.2 Assumptions

The reliability of the results of this theoretical analysis are based on the following assumptions:

- The heat source will generate a heat of 200 degrees Celsius at a force of 2 kilowatts.
- The uniformity of the heating, although different to the experimental scenario, will not greatly affect the result of the model
- The theoretical concrete and reinforcing steel compositions are accurate and are thus shown to respond to the heat source appropriately
- It is appropriate to use the modulus of elasticity of steel and concrete under normal operating conditions (i.e.: not the values after exposed to an external temperature of 200 degrees Celsius)

5.1.4 Modulus of Elasticity of Beam

The following section will discuss the theoretical modulus of elasticity of the concrete beam specimen and any associated assumptions.

5.1.4.1 Theoretical Results

The theoretical modulus of elasticity of concrete is 32 800 Mega Pascals (Australia, 2009). The theoretical modulus of elasticity of concrete exposed to an external temperature of 200 degrees Celsius is 24 600 Mega Pascals, to represent a 25 percent decrease in elasticity as suggested by Association, 2002.

5.1.4.2 Assumptions

The reliability of the results of this theoretical analysis are based on the following assumptions:

- The value of modulus of elasticity provided by the Australian Standards is correct
- The modulus of elasticity will decrease by 25 percent when the beam is heated to 200 degrees Celsius (Association, 2002)
- The heat source will generate a heat of 200 degrees Celsius
- The method of heating is directly comparable to the results of Association, 2002

5.1.5 Midpoint Deflections Associated with Loading Beam

The following section will discuss the theoretical midpoint deflections that the concrete beam structures should display and the assumptions associated with their calculation.

5.1.5.1 Theoretical Results

The following graph displays the expected midpoint deflections of the control and heated beams when subjected to varying loads during the three point bending test:

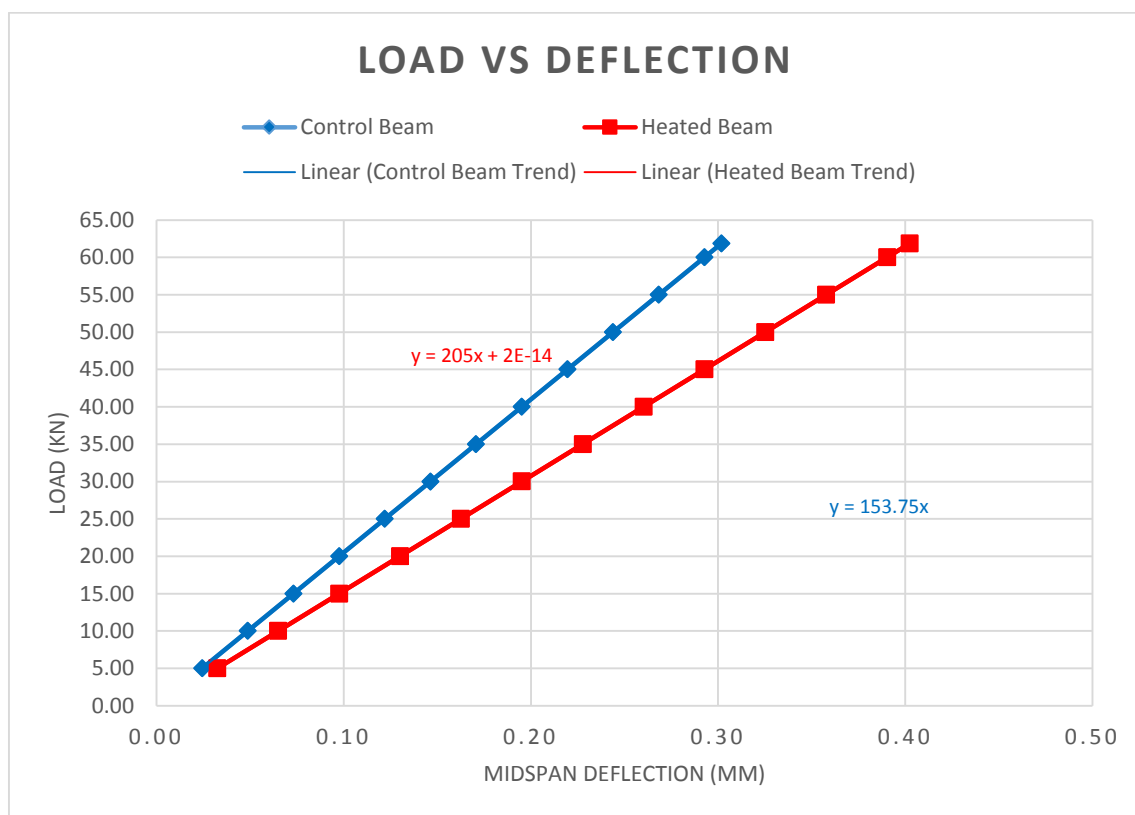


Figure 42 - Theoretical Midspan Deflections at Various Loads

In the above figure the blue line represents the control beam and the red line represents the heated beam. Theoretically speaking the heated beam is shown to display greater midspan deflections due to the heat exposure lowering the concrete's modulus of elasticity (Association, 2002). The maximum point was determined by calculating the theoretical ultimate moment capacity of the beam and thus the expected failure load of the beam. The expected failure load is 61.68 Kilo Newtons. Please refer to Appendix D1 for the table listing specific values displayed on the above graph.

5.1.5.2 Assumptions

The reliability of the results of this theoretical analysis are based on the following assumptions:

- The deflection of the concrete beam will follow the relationship of (Australia, 2002):

$$\delta = \frac{PLs^3}{48EI}$$

- The modulus of elasticity will decrease by 25 percent when the beam is heated to 200 degrees Celsius (Association, 2002)
- The heat source will generate a heat of 200 degrees Celsius
- The method of heating is directly comparable to the results of Association, 2002
- The theoretical ultimate moment capacity can be accurately calculated from the following equation (Queensland, 2014):

$$M_U = A_s f_y \left(d - \frac{A_s f_y}{\alpha_2 f'_c b} \right)$$

- The expected failure load can be calculated accurately from the following equation (Queensland, 2014):

$$P_U = \frac{M_U \times 4}{Ls}$$

5.1.6 Maximum Principal Strains Associated with Loading Beam and Appropriate Placement of FBG Sensor

In order to determine the theoretical maximum principal strains associated with loading the concrete beam structure via a three point bending test, a three dimensional static model was created in Abaqus/CAE. The reliability of these results were verified by checking that the values were within the range of hand calculations. All results and associated assumptions will be discussed in the following section.

5.1.6.1 Finite Element Analysis Static Model

The results of the three dimensional static model will be discussed in the following section.

5.1.6.1.1 Theoretical Results

The static model was first utilised to determine the optimum placement of the FBG Sensors within the concrete beam structure. This was deemed to be where the most significant maximum principal strain would be present in the beam due to three point bending. The following figure shows the maximum principal strain profile of the beam when loaded as per the static model:

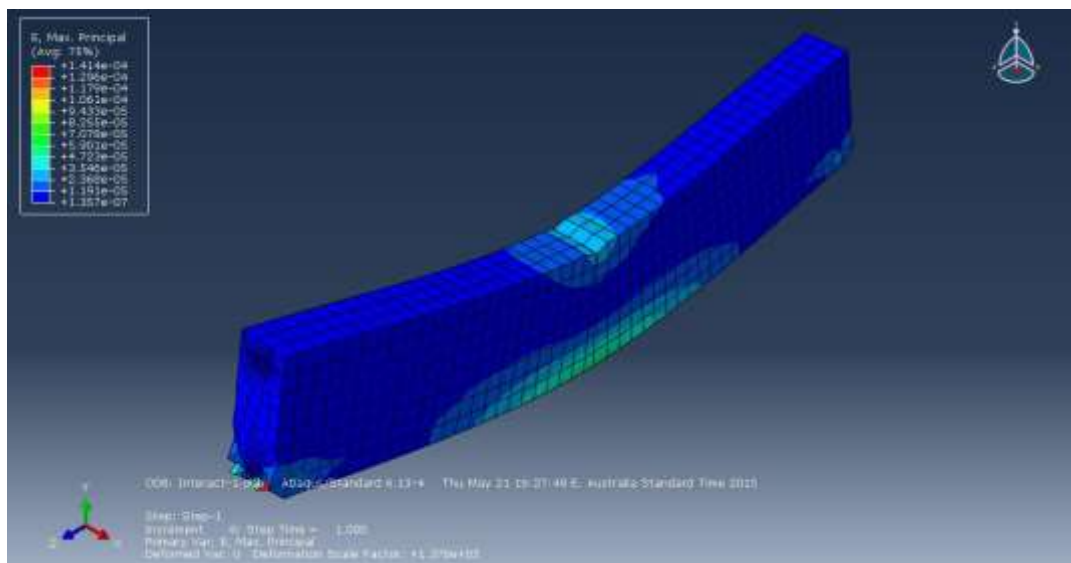


Figure 43 – Theoretical Maximum Principal Strain of Entire Beam Structure

From the above figure it can be concluded that the most significant maximum principal strains are throughout the central bottom region of the beam. The next figure shows the beam cut in half along its length:

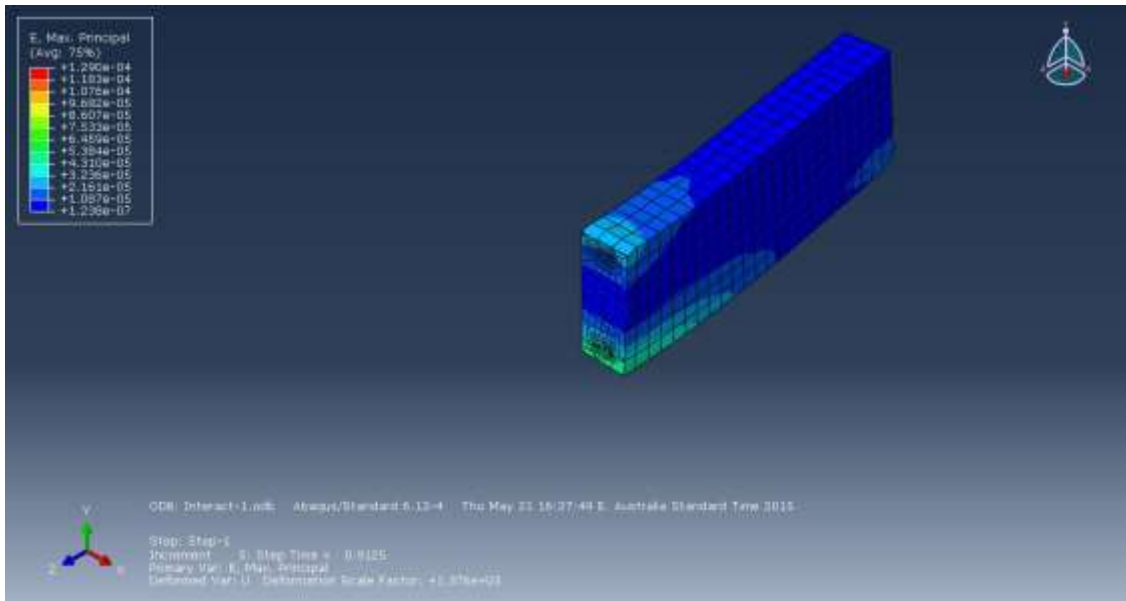


Figure 44 – Theoretical Maximum Principal Strain through Centre of Beam

It must be taken into account that in terms of reading temperature, the optimum placement of the FBG Sensor is as close to the centre of the beam as possible. There are also several other considerations in terms of getting appropriate strain readings when it comes to deciding the placement of the FBG Sensor.

In terms of y axis location, if the FBG Sensor is too far from the bottom of the beam, no strains will be read. Another factor that has to be taken into account is the fact that the reinforcing steel can interact with the FBG readings. It can create interference in the spectra and cause false strains to be read if the FBG Sensor is placed too closely to the reinforcing steel.

In terms of z axis location it was deemed safest to locate the FBG Sensor slightly away from the centre of the beam. Since the FBG Sensor was tied in place utilising fishing line and the surrounding reinforcing steel, it was deemed easiest to place the FBG Sensor 100 millimetres away from the centre of the beam at the next location of the next reinforcing stirrup.

After all of the above considerations, and some trial and error of strain readings in the static model, the ideal placement of the FBG Sensor was thus deemed to be at a position x, y, z of 50, 60, 600 (millimetres from axes).

One of the most important considerations to ensure the static model was displaying valid results was to ensure that the reinforcing steel and concrete were bonding adequately. Refer to Appendix D2 to view figures proving that this bonding did in fact occur.

As per the three dimensional static model created in Abaqus, the maximum principal strains associated with varying loads for the control and heated beams are displayed in the below graph:

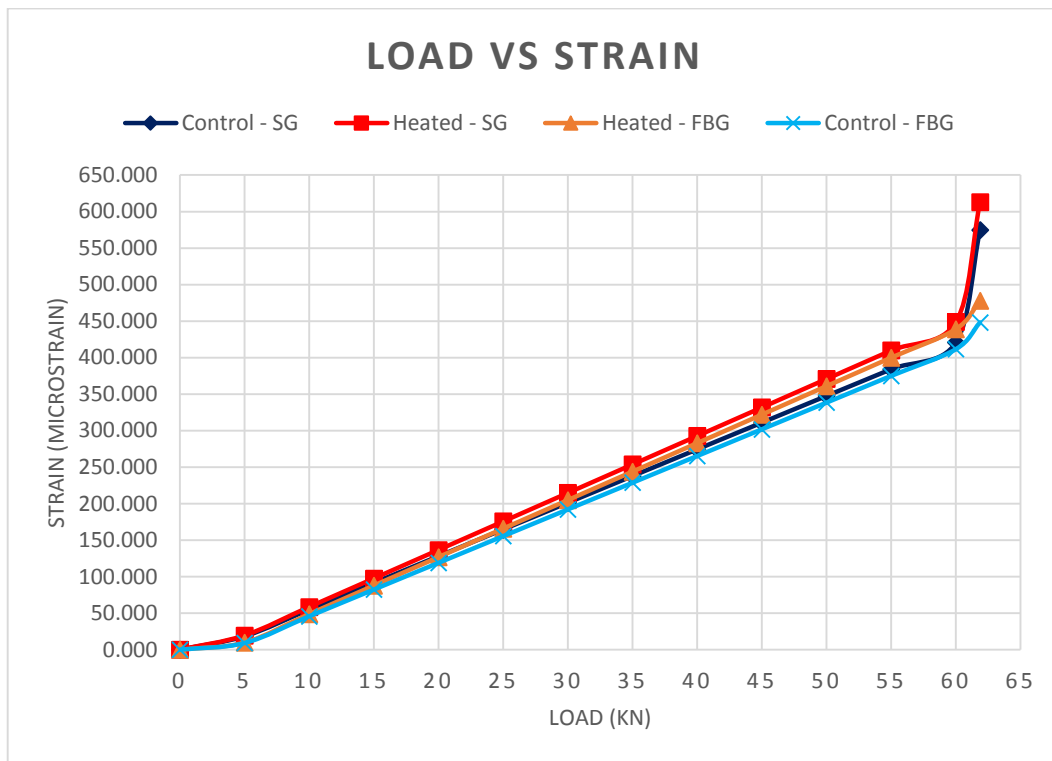


Figure 45 - Theoretical Maximum Principal Strains for Various Loads

In the above figure the dark blue line represents the strains at the location of the FBG Sensor in the control beam, the light blue line represents the strains at the location of the strain gauge on the control beam, the red line represents the strains at the location of the FBG Sensor in the heated beam, and the orange line represents the strains at the location of the strain gauge on the heated beam.

It can be seen that the heated beam specimen is predicted to incur greater maximum principal strains when loaded than the control beam specimen. This was predicted by applying a 25 percent reduction to the heated beam specimens modulus of elasticity, as suggested by the literature review (Association, 2002). It can also be seen that the strain gauges are predicted to record higher strain readings than the FBG Sensors because of their location.

The maximum point was determined by calculating the ultimate moment capacity of the beam and thus the expected failure load of the beam. The expected failure load is 61.68 Kilo Newtons. Please refer to Appendix D2 for a table listing specific values displayed on the above graph.

5.1.6.1.2 Assumptions

The reliability of the results of this theoretical analysis are based on the following assumptions:

- The value of modulus of elasticity provided by the Australian Standards is correct
- The modulus of elasticity will decrease by 25 percent when the beam is heated to 200 degrees Celsius (Association, 2002)
- The heat source will generate a heat of 200 degrees Celsius
- The method of heating is directly comparable to the results of Association, 2002
- The bonding between the reinforcing steel and concrete is adequate and thus the model behaves in a similar fashion to a real life concrete beam
- The load is applied in the three dimensional model in the same fashion as the load would be applied in a real life three point bending test
- The three dimensional model behaves in the same way as the concrete beams will when subjected to a three point bending test
- The results of the three dimensional model are accurate
- The FBG Sensors will be located at the specified location and will not move during pouring
- The theoretical ultimate moment capacity can be accurately calculated from the following equation (Queensland, 2014):

$$M_U = A_s f_y \left(d - \frac{A_s f_y}{\alpha_2 f' c b} \right)$$

- The expected failure load can be calculated accurately from the following equation (Queensland, 2014):

$$P_U = \frac{M_U \times 4}{L_s}$$

5.1.6.2 Hand Calculations

Whether the results of the static model were reasonable was checked via the use of hand calculations. The results of these calculations will be discussed in the following section.

5.1.6.2.1 Theoretical Results

The following graph displays the expected maximum principal strains of the control and heated beams when subjected to varying loads during the three point bending test:

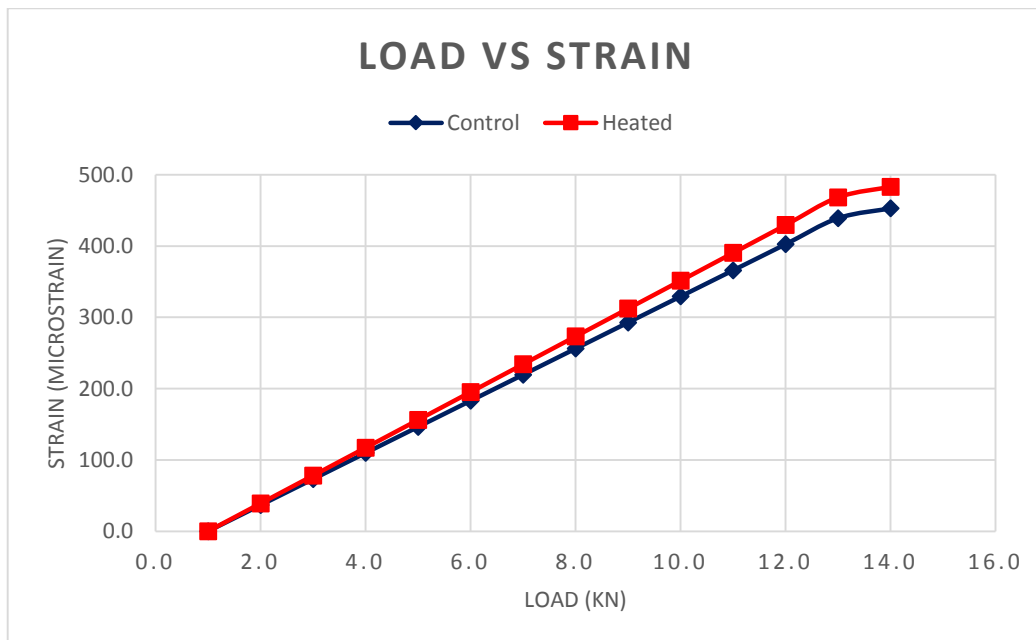


Figure 46 - Verification of Theoretical Maximum Principal Strains for Various Loads

In the above figure the blue line represents the control beam and the red line represents the heated beam. It must be noted that the hand calculations only represent midspan strains in order to predict whether the strains output by the three dimensional Abaqus model were reasonable. Since the hand calculated strains are consistently within the range of the strains predicted by the static model discussed in the above section, the theoretical model is assumed to be accurate. The maximum point was determined by calculating the theoretical ultimate moment capacity of the beam and thus the expected failure load of the beam. Please refer to Appendix D3 for a table listing specific values displayed on the above graph.

5.1.6.2.2 Assumptions

The reliability of the results of this theoretical analysis are based on the following assumptions:

- The maximum principal strains of the concrete beam will follow the relationship of (Queensland, 2014):

$$e = \frac{\sigma}{E}$$

- The value of modulus of elasticity provided by the Australian Standards is correct
- The modulus of elasticity will decrease by 25 percent when the beam is heated to 200 degrees Celsius (Association, 2002)
- The heat source will generate a heat of 200 degrees Celsius
- The method of heating is directly comparable to the results of Association, 2002
- The results are comparable even though the position of the FBG will be different to what is assumed for these calculations
- The control beam will be of a compressive strength of 40 Mega Pascals
- The heated beam will be of a compressive strength of 40 Mega Pascals before it is subjected to heat
- The theoretical ultimate moment capacity can be accurately calculated from the following equation (Queensland, 2014):

$$M_U = A_s f_y \left(d - \frac{A_s f_y}{\alpha_2 f'_{cb}} \right)$$

- The expected failure load can be calculated accurately from the following equation (Queensland, 2014):

$$P_U = \frac{M_U \times 4}{L_s}$$

5.1.7 Maximum Principal Stresses Associated with Loading Beam

In order to determine the theoretical maximum principal stresses associated with loading the concrete beam structure via a three point bending test, the same three dimensional static model discussed in section 5.1.6 was utilised. The reliability of these results were verified by checking that the values were within the range of hand calculations.

5.1.7.1 Finite Element Analysis Static Model

The results of the three dimensional static model will be discussed in the following section.

5.1.7.1.1 Theoretical Results

The profile of the maximum principal stresses throughout the beam structure and proof of the bonding of the reinforcing steel and concrete are shown in Appendix D3.

As per the three dimensional static model created in Abaqus, the maximum principal stresses associated with varying loads are displayed in the below graph:

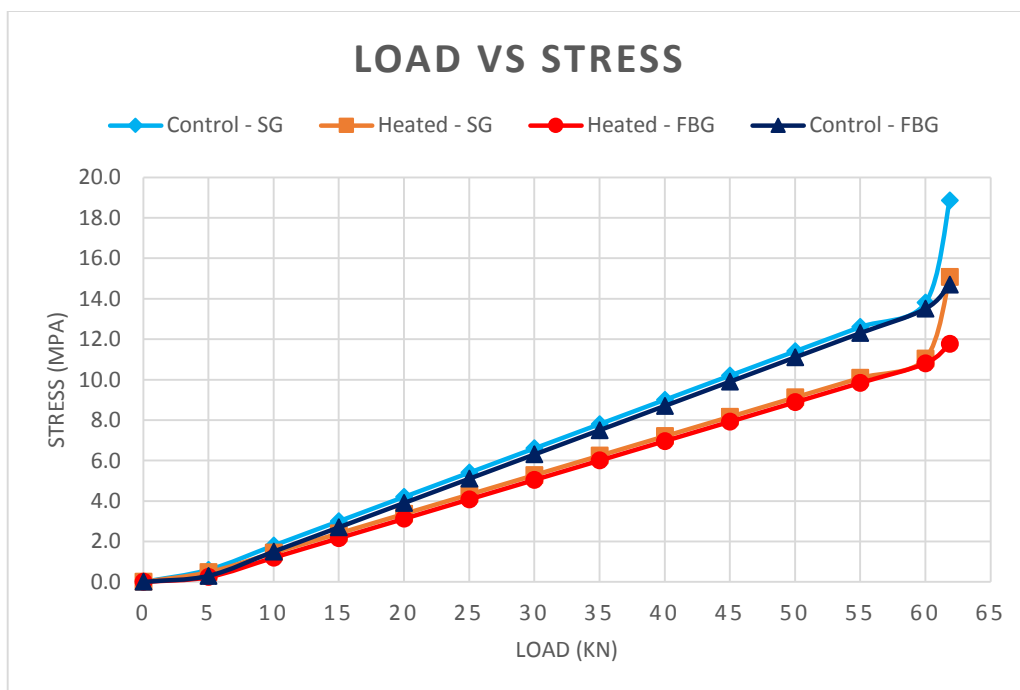


Figure 47 - Theoretical Maximum Principal Stresses for Various Loads

In the above figure the dark blue line represents the stresses at the location of the FBG Sensor in the control beam, the light blue line represents the stresses at the location of the strain gauge on the control beam, the red line represents the stresses at the location of the FBG Sensor in the heated beam, and the orange line represents the stresses at the location of the strain gauge on the heated beam.

It can be seen that the heated beam specimen is predicted to incur lesser maximum principal stresses when loaded than the control beam specimen. It can also be seen that the strain gauges are predicted to record higher stress readings than the FBG Sensors because of their location. The maximum point was determined by calculating the theoretical ultimate moment capacity of the beam and thus the expected failure load of the beam. The expected failure load is 61.68 Kilo Newtons. Please refer to Appendix D3 for a table listing specific values displayed on the above graph.

5.1.7.1.2 Assumptions

The reliability of the results of this theoretical analysis are based on the following assumptions:

- The value of modulus of elasticity provided by the Australian Standards is correct
- The modulus of elasticity will decrease by 25 percent when the beam is heated to 200 degrees Celsius (Association, 2002)
- The heat source will generate a heat of 200 degrees Celsius
- The method of heating is directly comparable to the results of Association, 2002
- The bonding between the reinforcing steel and concrete is adequate and thus the model behaves in a similar fashion to a real life concrete beam
- The load is applied in the three dimensional model in the same fashion as the load would be applied in a real life three point bending test
- The three dimensional model behaves in the same way as the concrete beams will when subjected to a three point bending test
- The results of the three dimensional model are accurate
- The FBG Sensors will be located at the specified location and will not move during pouring
- The control beam will be of a compressive strength of 40 Mega Pascals
- The heated beam will be of a compressive strength of 40 Mega Pascals before it is subjected to heat
- The theoretical ultimate moment capacity can be accurately calculated from the following equation (Queensland, 2014):

$$M_U = A_s f_y \left(d - \frac{A_s f_y}{\alpha_2 f'_c b} \right)$$

- The expected failure load can be calculated accurately from the following equation (Queensland, 2014):

$$P_U = \frac{M_U \times 4}{L_s}$$

5.1.7.2 Hand Calculations

The results of the static model were checked via the use of hand calculations. The results of these calculations will be discussed in the following section.

5.1.7.2.1 Theoretical Results

The following graph displays the expected maximum principal stresses of the control and heated beams when subjected to varying loads during the three point bending test:

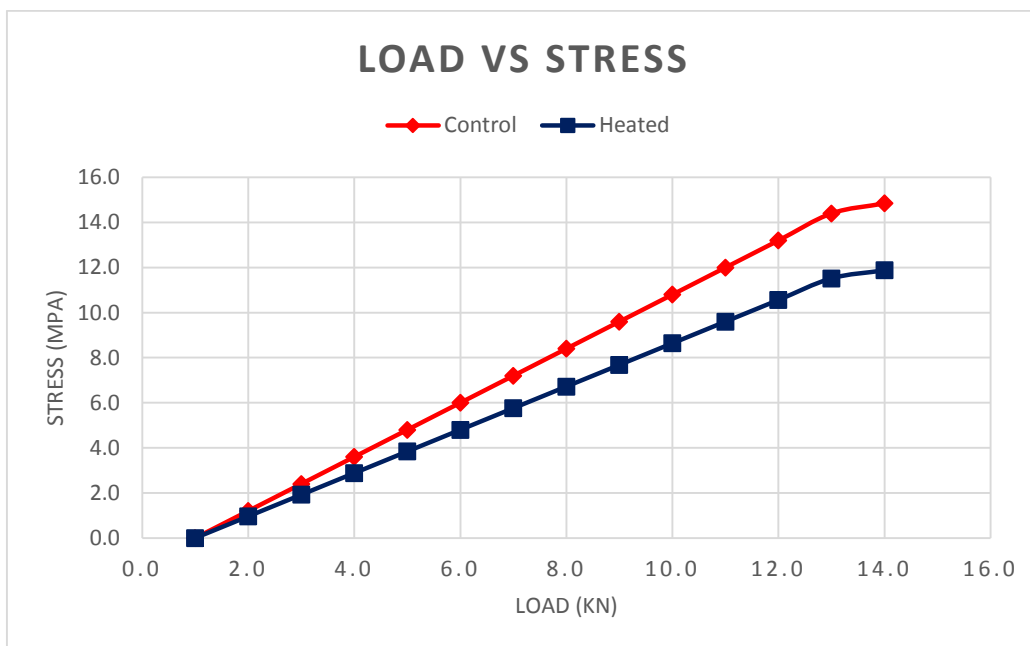


Figure 48 - Verification of Theoretical Maximum Principal Stresses for Various Loads

In the above figure the blue line represents the control beam and the red line represents the heated beam. It must be noted that the hand calculations only represent midspan stresses in order to predict whether the stresses output by the three dimensional Abaqus model were reasonable. Since the hand calculated stresses are consistently within the range of the stresses predicted by the static model discussed in the above section, the theoretical model is assumed to be accurate. The maximum point was determined by calculating the theoretical ultimate moment capacity of the beam and thus the expected failure load of the beam. Please refer to Appendix D3 for a table listing specific values displayed on the above graph.

5.1.7.2.2 Assumptions

The reliability of the results of this theoretical analysis are based on the following assumptions:

- The maximum principal stresses of the concrete beam will follow the relationship of (Queensland, 2014):

$$\sigma = \frac{3PL_s}{2bD^2}$$

- The maximum principal stress of the heated beam will be only 80 percent of the maximum principal stress of the control beam due to a 20 percent reduction in tensile strength (Yao, 2006)
- The value of modulus of elasticity provided by the Australian Standards is correct
- The modulus of elasticity will decrease by 25 percent when the beam is heated to 200 degrees Celsius (Association, 2002)
- The heat source will generate a heat of 200 degrees Celsius
- The method of heating is directly comparable to the results of Association, 2002
- The results are comparable even though the position of the FBG will be different to what is assumed for these calculations
- The theoretical ultimate moment capacity can be accurately calculated from the following equation (Queensland, 2014):

$$M_U = A_s f_y \left(d - \frac{A_s f_y}{\alpha_2 f'_c b} \right)$$

- The expected failure load can be calculated accurately from the following equation (Queensland, 2014):

$$P_U = \frac{M_U \times 4}{L_s}$$

5.1.8 Tensile Strength of Beam

The theoretical tensile strength of the control and heated beam specimens will be discussed in the following section.

5.1.8.1 Theoretical Results

The theoretical tensile strength of the control and heated concrete beam specimens was calculated by calculating the theoretical ultimate moment capacity of the beam and thus the expected failure load of the beam. The theoretical maximum principal stresses at these respective loads correlate to the theoretical tensile strengths of each specimen.

The theoretical tensile strengths are:

- Control Beam = 18.8 Mega Pascals
- Heated Beam = 15.1 Mega Pascals

These values correlate to the literature review which revealed that a beam subjected to a heat of 200 degree Celsius degrades in tensile strength by approximately 20 percent (Yao, 2006).

5.1.8.2 Assumptions

The reliability of the results of this theoretical analysis are based on the following assumptions:

- Yao 2006 is correct in their statement that subjecting concrete to a temperature of 200 degrees Celsius reduces concrete tensile strength by 20 percent
- The control beam will be of a compressive strength of 40 Mega Pascals
- The heated beam will be of a compressive strength of 40 Mega Pascals before it is subjected to heat
- The value of modulus of elasticity provided by the Australian Standards is correct
- The modulus of elasticity will decrease by 25 percent when the beam is heated to 200 degrees Celsius (Association, 2002)
- The value of modulus of elasticity provided by the Australian Standards is correct
- The modulus of elasticity will decrease by 25 percent when the beam is heated to 200 degrees Celsius (Association, 2002)
- The heat source will generate a heat of 200 degrees Celsius
- The method of heating is directly comparable to the results of Association, 2002
- The theoretical ultimate moment capacity can be accurately calculated from the following equation (Queensland, 2014):

$$M_U = A_s f_y \left(d - \frac{A_s f_y}{\alpha_2 f' c b} \right)$$

- The expected failure load can be calculated accurately from the following equation (Queensland, 2014):

$$P_U = \frac{M_U \times 4}{L_S}$$

5.1.9 Flexural Strength of Beam

The theoretical flexural strength of the control and heated beam specimens will be discussed in the following section.

5.1.9.1 Theoretical Results

The theoretical flexural strengths and thus the theoretical failure loads of the control and heated beam specimens are summarised in the following table:

Table 6 - Theoretical Flexural Strengths and Failure Loads

Flexural Strength (MPa)		Failure Load (kN)	
Control Beam	Heated Beam	Control Beam	Heated Beam
4	3.4	100	85

Based on the results of the theoretical analysis, the flexural strength of the heated beam will be reduced by 15 percent (Association, 2002). The theoretical failure loads in terms of flexural strength are higher than the theoretical failure loads in terms of tensile strength. It is thus suggested that the beams will fail due to tension before they fail due to flexure.

5.1.9.2 Assumptions

The reliability of the results of this theoretical analysis are based on the following assumptions:

- The control beam will be of a compressive strength of 40 Mega Pascals
- The heated beam will be of a compressive strength of 40 Mega Pascals before it is subjected to heat
- Flexural strength is equal to 10 percent of the compressive strength of the beam
- When the beam is heated to 200 degrees Celsius it will degrade in flexural strength by 15 percent (Association, 2002)
- The heat source will generate a heat of 200 degrees Celsius
- The method of heating is directly comparable to the results of Association, 2002
- The theoretical load at which each beam will fail due to flexure can be calculated from the following equation (Queensland, 2014):

$$\textit{Failure Load} = \textit{Flexural Strength} \times b \times D$$

5.1.10 Compressive Strength of Beam

The theoretical compressive strength of the control and heated beam specimens will be discussed in the following section.

5.1.10.1 Theoretical Results

The theoretical compressive strengths of the beams were calculated via the use of Australian standard sized cylinders. The theoretical compressive strengths and failure loads of the control and heated cylinder specimens are summarised in the following table:

Table 7 - Theoretical Compressive Strengths and Failure Loads

Compressive Strength (MPa)		Failure Load (kN)	
Control Cylinders	Heated Cylinders	Control Cylinders	Heated Cylinders
40	36	314	283

Based on the results of the theoretical analysis, the heated cylinders will require 31 Kilo Newtons less load in order for them to fail in compression. This is because of the heat exposure causing a 10 percent reduction in compressive strength (Yao, 2006, Association, 2002).

5.1.10.2 Assumptions

The reliability of the results of this theoretical analysis are based on the following assumptions:

- Yao 2006 is correct in their statement that subjecting concrete to a temperature of 200 degrees Celsius reduces concrete compressive strength by 10 percent
- The control cylinders will be of a compressive strength of 40 Mega Pascals
- The heated cylinders will be of a compressive strength of 40 Mega Pascals before it is subjected to heat
- The compressive strength of the cylinders can be directly correlated to the compressive strength of the beams
- The heat source will generate a heat of 200 degrees Celsius
- The method of heating is directly comparable to the results of Association, 2002
- Failure load is equal to (Queensland, 2014):

$$Failure\ Load = f'c \times \frac{\pi \times d^2}{4}$$

5.2 Experimental Analysis

This section will discuss what results were actually achieved via experimentation and any assumptions that were associated with them. It must be noted that the experimental design had to be altered from the theoretical design. The section titled performance of FBG Encasings will detail how and why this was the case.

5.2.1 Performance of FBG Encasing Techniques

The following section will detail the experimental performance of both the aluminium and concrete encasing techniques.

5.2.1.1 Concrete Encasing

When encasing the two FBG Sensors utilising the concrete encasing method, the fibre snapped in the bare sensor region, thus rendering the sensors inoperable. Although the method had been proven successful previously, via the use of replica fibres embedded in cylinders, the method failed with the real FBG Sensors. When testing replica fibres, fibreglass sleeving was unable to be used. The fibreglass sleeving was thus, a new variable which was not properly handled.

The addition of the fibreglass sleeving meant the addition of weight. Since the fibre was bare at the central sensor region, additional weight on either side of this region created downward forces. These downward forces lead to too much strain on the bare sensor region of the fibre, and thus the fragile glass fibre snapped before the method of encasing it in concrete was completed.

The fibreglass sleeving was, however, deemed necessary to protect FBG Sensors embedded in concrete structures. This is not only due to its high heat protective properties but also its ability to resist abrasion. The technique of encasing the FBG Sensor in concrete was thus modified successfully, but an inability to replace the broken FBG Sensors within the time constraints meant the modified method of concrete encasing could only be tested utilising replica fibres.

The modified method of concrete encasing is outlined as follows:

1. Coat the FBG Sensor fibre in liquid electrical tape and allow to set for 24 hours. This protects the fibre from corrosion and chemical attack.
2. Thread the FBG Sensor fibre inside zero tube but leave the 1mm sensor region of the fibre, and 0.5mm either side of that region bare. The zero tube protects the fibre from abrasion.
3. Thread the FBG Sensor encased in zero tube inside fibreglass sleeving, leaving the same region bare. Leaving the sensor region bare allows the sensor to be in direct contact with the concrete. The fibreglass sleeving provides further protection from abrasion as well as heat.
4. Cut a one 5mm long section of 20mm diameter electrical conduit. This will be utilised as the mould for encasing the sensor region of the FBG Sensor in concrete.
5. Cut the electrical conduit in half along its length.
6. Tape (using duct tape) the end of the conduit at the same height.
7. Oil conduit in order to prepare mould.

An example of two moulds is shown in the below diagram:



Figure 49 – Modified Concrete Capsule Moulds

8. Compact concrete in each side of the mould. Pack slightly higher than mould level.
9. Place the central region of the FBG Sensor in the centre of one half of the mould so that it stretches longitudinally along the 5mm length of the mould.
10. Press two mould halves together and tape tight.
11. After seven days remove mould and place FBG Sensor in concrete beam. At this point the concrete will have achieved 80 percent of its strength (Australia, 2002).

The following figure shows an infrared light shone through the replica fibre encased using this method at the seven day point when it is removed from its mould:

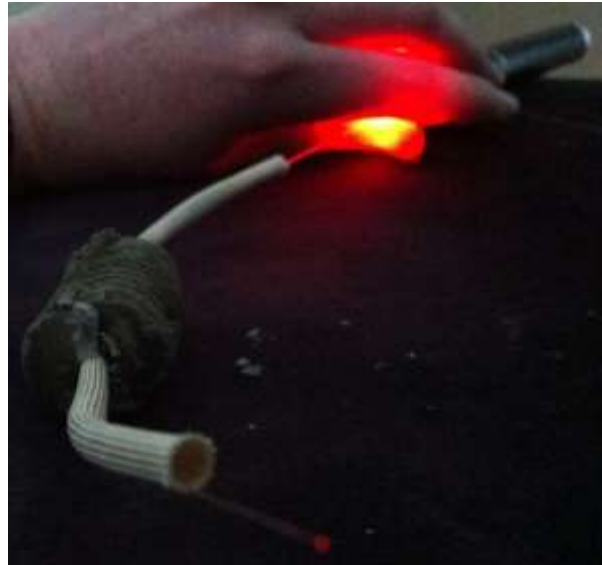


Figure 50 - Replica Fibre Shown to Survive Modified Method of Concrete Encasing

The fact that the end of the fibre displays the infrared light proves that the fibre is intact.

This encased replica fibre was then tied in position by wrapping fishing line around the central concrete encasing and then wrapping it around the reinforcement to fix it in place. This is shown in the following figure:



Figure 51 - Replica Fibre Tied in Position Using Fishing Line

After the concrete pour and compaction, the infrared light was again shone through the replica fibre. This is shown in the following two figures:



Figure 52 - Replica Fibre Shown to Survive Pouring and Compaction

The fact that the end of the fibre displays the infrared light proves that the fibre is intact.

The following picture shows the above figure zoomed out:



Figure 53 - Proof Replica Fibre is embedded in Concrete Beam

The above figure proves that the replica fibre with the infrared light shone through it is in fact embedded in the concrete beam.

The next figure shows the bonding of the concrete encasing when embedded in concrete:



Figure 54 - Concrete Encasing Shown to Bond when Embedded in Concrete

The concrete encased replica fibre is the darker region in the above figure, recognisable by its ribbed shape created by the electrical conduit mould. It is shown that appropriate bonding is occurring between the encasing and the concrete it is embedded in. This suggests that the encasing would thus move in relation to its surrounding concrete and thus allow an FBG Sensor inside of it to read accurate strain values.

As will be discussed in the following section, the fibreglass sleeving was used in the same way for the aluminium encasing as the concrete encasing. The fibreglass sleeving was proven to protect the FBG Sensor from heat, so thus the concrete encasing method would also protect an FBG Sensor from heat.

The aluminium encasing also proved that the FBG Sensor was capable of reading accurate temperatures and was able to identify the formation of internal cracks. It is suggested that an FBG Sensor encased in concrete would also have these capabilities.

5.2.1.2 Aluminium Encasing

Due to the initial concrete encasing technique breaking the FBG Sensor fibre, and thus rendering two of the three FBG Sensors inoperative, the experimental design had to be altered. Now only two beams were to be tested, as the specimen to be tested for internal cracks had to also become the specimen exposed to heat. This specimen was deemed the heated beam and had one FBG Sensor encased in aluminium.

Although the control beam was unable to have an FBG Sensor embedded in it, enough results were still able to be compiled via the use of the strain gauges, thermocouples, and strength tests to use it as a comparison to the heated beam. Almost all objectives were still able to be met, as will be displayed in the experimental analysis as well as chapter six.

The experimental analysis showed that the aluminium encasing performed in the ways theoretically expected. The aluminium encasing did in fact cause an internal crack which was successfully picked up by the FBG Sensor as an interruption of the spectra. The following schematic shows the FBG Sensor spectra first without a crack and then with a crack:

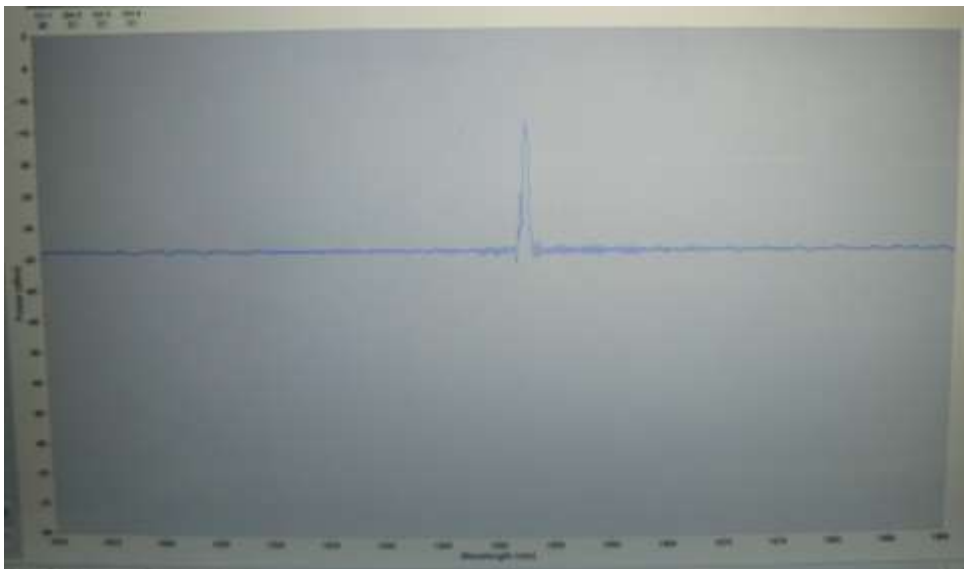


Figure 55 - Uninterrupted FBG Sensor Spectra

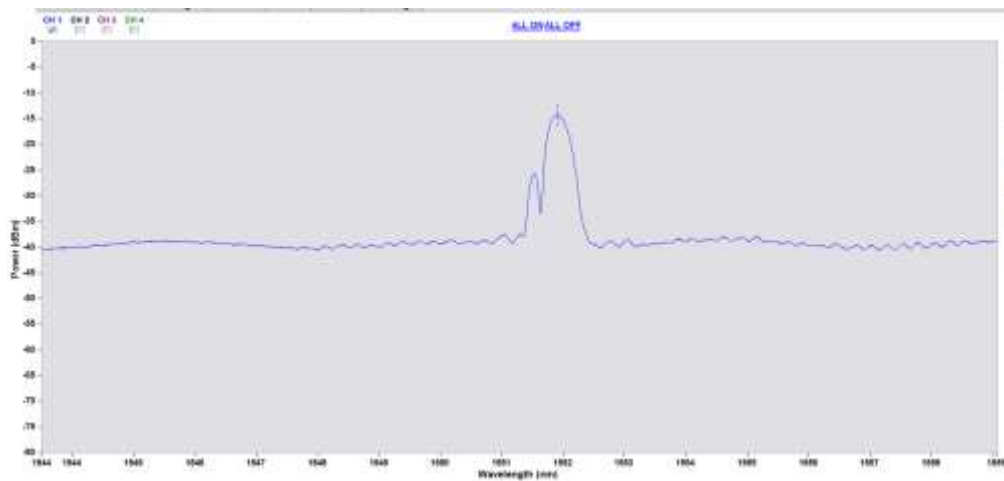


Figure 56 – Interrupted FBG Sensor Reading Suggesting Internal Crack within Beam

The FBG Sensor encased in aluminium was also able to read internal temperature variations, which was shown via shifts in wavelength during concrete curing and heating. When these shifts in wavelengths were converted to temperature readings, they were very similar to the readings of the thermocouples, thus suggesting the aluminium encasing allowed the sensor to read temperatures accurately. Refer to sections 5.2.2 and 5.2.3 for more details.

As expected, the aluminium encasing was believed to be inflexible and unable to bond with the concrete. This was suggested by the fact that the strains recorded by the FBG Sensor were very low in comparison to the theoretical strains and the strains picked up by the strain gauges. Refer to section 5.2.6 for more details.

The aluminium encasing was in fact proven to sufficiently protect the FBG Sensor from chemical attack, abrasion, and heat. This was demonstrated by the fact that the FBG Sensor was still alive after all experimentation. It is, however, as expected, unsuitable for general use due to its presence creating internal cracks and its inability to read appropriate strains.

5.2.2 Concrete Curing Temperatures

The internal curing temperatures as per the experimental analysis and assumptions associated with their validity will be discussed in the following section:

5.2.2.1 Experimental Results

The following schematic displays the experimental curing temperatures of Beam One over the first seven days of curing:

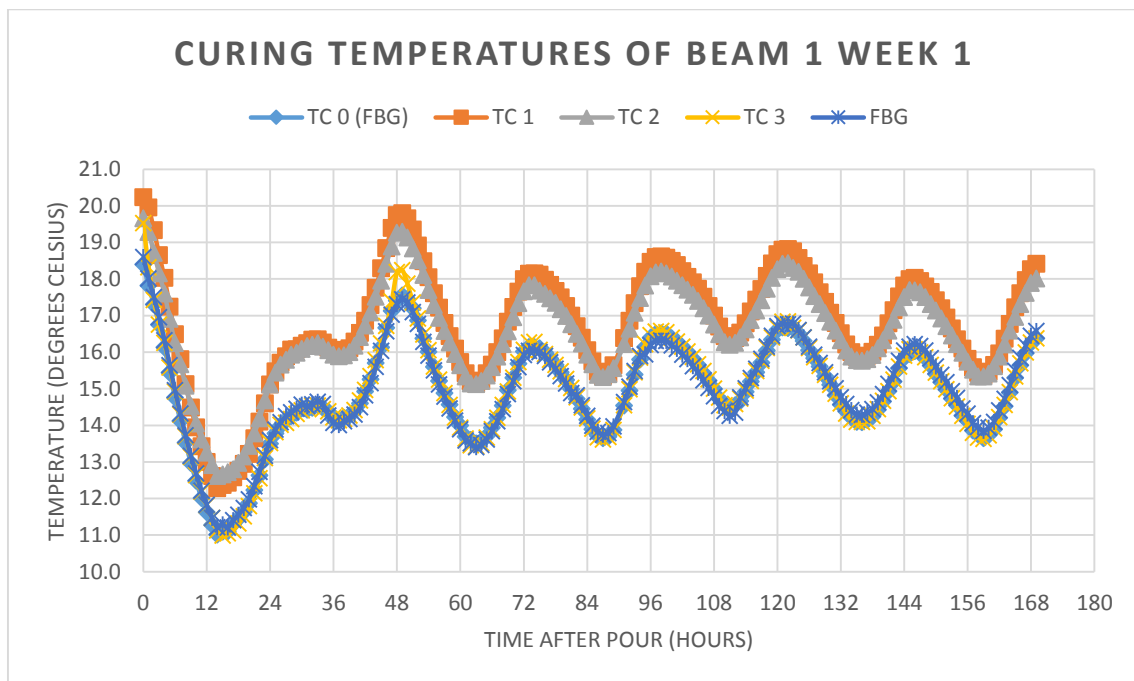


Figure 57 - Experimental Curing Temperatures of Beam One Week One

In the above graph, the blue lines represent the temperatures read by the FBG Sensor and TC 0 encased with the sensor. They are shown to have recorded relatively the same temperatures, thus suggesting their validity. The temperatures recorded by TC 3, displayed as a yellow line on the graph above, also displayed relatively the same temperatures. Since it was placed at the same distance from the centre of the beam, this is to be expected and suggests validity of results.

The orange and grey lines representing TC 1 and TC 2, recorded slightly higher temperatures (varying between one and two degrees higher) than the other thermocouples. This is suggested to be because they were placed closer to the centre of the beam, where more reactions would have been taking place and where less heat would escape. The fact that TC 1 and TC 2 display relatively similar results suggests their validity.

The general trend of the above schematic shows that the concrete initially cools and then presumably the main reactions between the cement and water occur between twelve and forty eight hours after pouring, which is shown by an increase in temperature. Throughout the curing period the temperatures seem to follow a day night trend. The temperatures decrease over night, reaching a low at approximately 9am. The temperatures then increase during the day reaching a high at approximately 8pm. This trend was unexpected, especially since the recorded temperatures are between a low range of 10 to 21 degrees Celsius.

After a week, one of the thermocouples was disconnected and another which had been calibrated the same was connected. The ambient temperature was then taken using TC 7.

Before the ambient temperature was taken, it was double checked whether the thermocouples could read temperature variation correctly. This was checked by placing the thermocouple in boiling water along with a digital thermometer and verifying that the thermocouple and digital thermometer readings were within a reasonable range throughout the cooling of the water. This had been done with the thermocouples embedded in the beam whilst in position before the concrete was poured.

A one week sample of the ambient temperature plotted with the curing temperatures is shown in the following schematic:

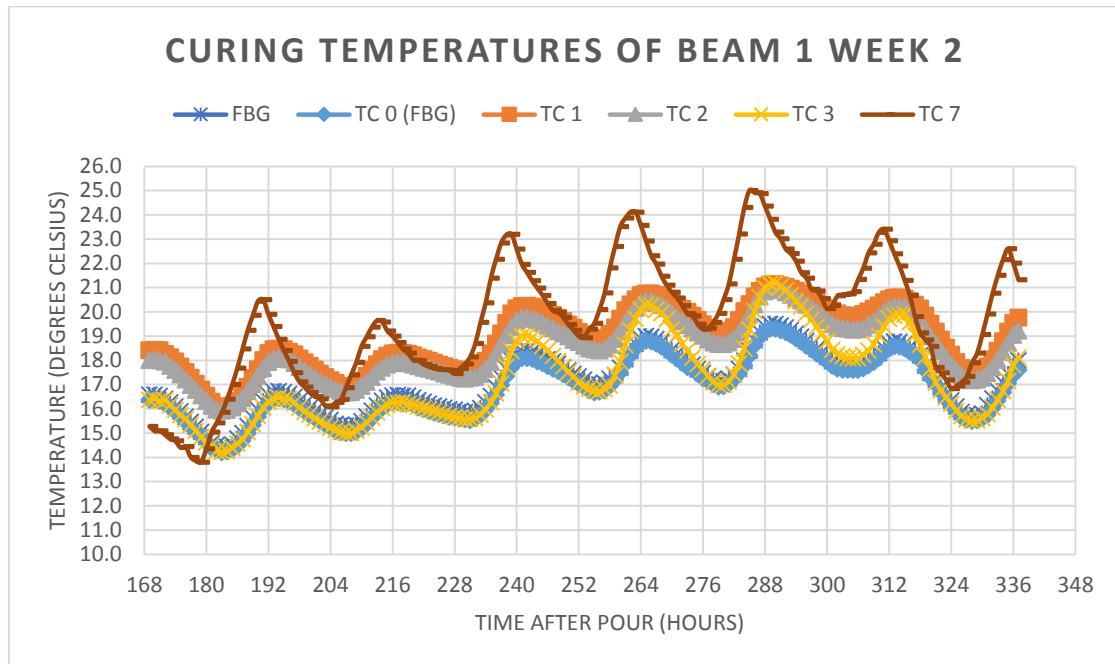


Figure 58 - Theoretical Curing Temperatures of Beam 1 Week 2

It can be seen that the curing temperatures do in fact follow the trend of the ambient temperature. Please refer to Appendix E1 for graphs and tables detailing the curing temperatures of the two beam specimens over 28 days.

5.2.2.2 Assumptions

The reliability of the results of this experimental analysis are based on the following assumptions:

- The thermocouples were calibrated accurately
- The natural calibration of the FBG Sensor was accurate
- The thermocouples were able to read precise temperatures when embedded in the concrete
- The FBG Sensor encased in aluminium was able to read precise temperatures when embedded in the concrete
- The NI CDAQ-9174 was interrogating the thermocouple data properly
- LabVIEW was recording the thermocouple data properly
- The sml125 was interrogating the FBG Sensor data properly
- MOI Enlight was recording the FBG Sensor data properly
- The recorded FBG Sensor wavelengths were manipulated correctly to produce temperatures
- It is accurate to use the following equation rearranged to give the change in temperature read by the FBG Sensor (Su and Han, 2014):

$$\Delta\lambda_B = \lambda_B \{(\alpha + \xi) \Delta T + (1 - p_e) \Delta\varepsilon\},$$

5.2.3 Heating Profile of Beam

The internal temperatures of the beam whilst it was heated was recorded via the thermocouples and FBG. Discussion surrounding the experimental temperature variations and any assumptions associated with them will take place in the following section.

5.2.3.1 Experimental Results

The following figure shows the temperature variation of the beam recorded over the time it was heated via the use of embedded thermocouples and the embedded FBG Sensor:

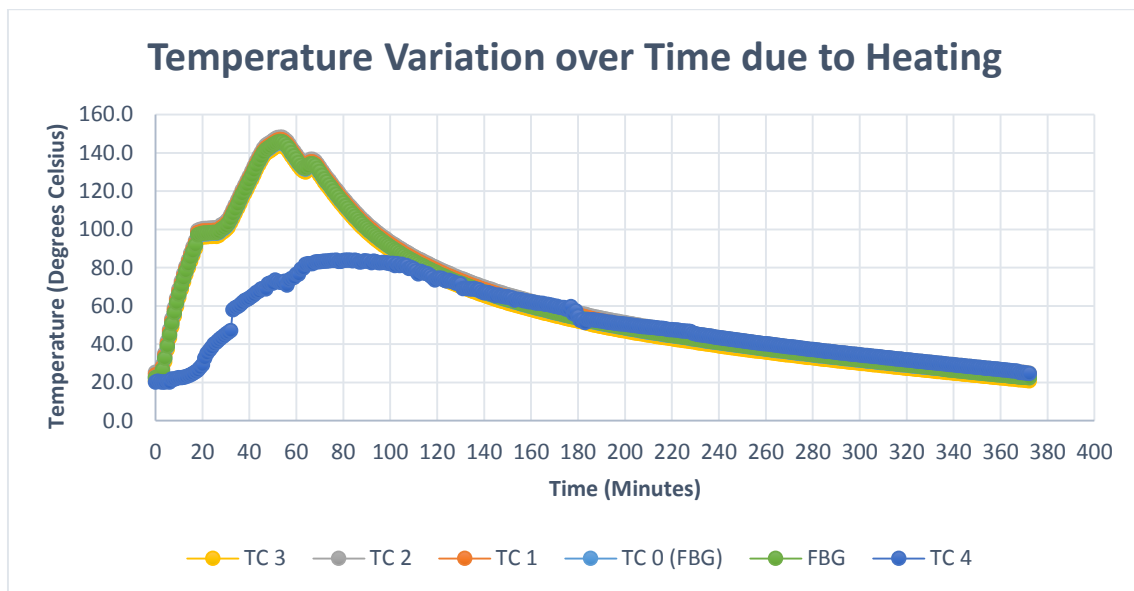


Figure 59 - Experimental Temperature Variation of Concrete Beam over Time due to Heating

It can be seen from the above schematic that the beam was subjected to a continuous heat for approximately one hour. After one hour it reached a maximum temperature of approximately 145 degrees Celsius. It then took a further approximately five hours after reaching the maximum temperature to cool back down to ambient temperature. Please refer to Appendix E2 to view the results displayed in the above graph in tabulated form.

The beam was heated on its side face so thus the FBG Sensor and the embedded thermocouples were the same distance from the heat source. The fact that they recorded practically the same temperatures suggests the accuracy of the results. Thermocouple four represented by the deep blue line was on the side surface of the beam, so thus an extra 50 millimetres from the heat source. This surface was shown to only reach a maximum of approximately 85 degrees Celsius.

A laser thermometer was used to estimate that the external heating temperature reached a maximum of approximately 200 degrees Celsius. When the heating source reached this temperature the thermometer was also used to record the surface temperatures of the side face of the beam. The temperature was recorded at every 100 millimetres along the length of the beam in order to gain an understanding of the spread in heat. The following table summarises the temperatures:

Table 8 - Surface Temperatures along the Length of the Side Face of the Beam Whilst at Maximum Temperature

Distance From End of Beam (mm)	Temperature (Degrees Celsius)
0	26.6, 26.5
100	27.0, 26.8
200	27.9, 27.7
300	30.2, 30.0
400	38.6, 38.3
500	57.9, 58.3
600	81.0, 81.2
700	83.9

5.2.3.2 Assumptions

The reliability of the results of this experimental analysis are based on the following assumptions:

- The thermocouples were calibrated accurately
- The natural calibration of the FBG Sensor was accurate
- The thermocouples were able to read precise temperatures when embedded in the concrete
- The FBG Sensor encased in aluminium was able to read precise temperatures when embedded in the concrete
- The NI CDAQ-9174 was interrogating the thermocouple data properly
- LabVIEW was recording the thermocouple data properly
- The sml125 was interrogating the FBG Sensor data properly
- MOI Enlight was recording the FBG Sensor data properly
- The recorded FBG Sensor wavelengths were manipulated correctly to produce temperatures
- The laser thermometer was reading accurate temperatures
- It is accurate to use the following equation rearranged to give the change in temperature recorded via the FBG Sensor (Su and Han, 2014):

$$\Delta\lambda_B = \lambda_B \{(\alpha + \xi) \Delta T + (1 - p_e) \Delta\varepsilon\},$$

5.2.4 Midpoint Deflections Associated with Loading Beam

The following section will discuss the midpoint deflections that the concrete beam displayed and the assumptions associated with the recording of the results.

5.2.4.1 Experimental Results

The following graph displays the midpoint deflections of the control and heated beams when subjected to varying loads during the three point bending test:

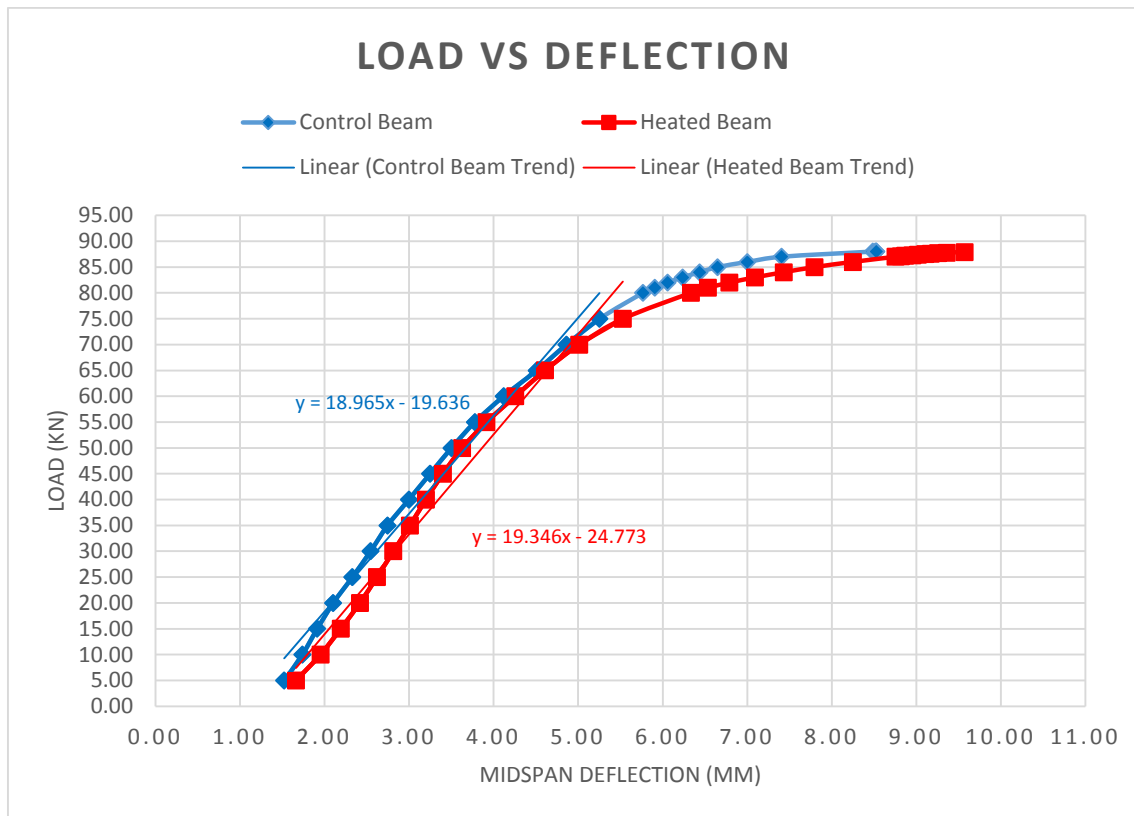


Figure 60 - Experimental Midpoint Deflections with Varying Loads

In the above figure the blue line represents the control beam and the red line represents the heated beam. The heated beam is shown to display slightly greater midspan deflections. This is believed to be due to the heat exposure lowering the concrete's modulus of elasticity (Association, 2002). Please refer to Appendix E3 for the table listing specific values displayed on the above graph.

5.2.4.2 Assumptions

The reliability of the results of this experimental analysis are based on the following assumptions:

- The SANS machine recorded the loads and their associated deflections accurately
- Each beam was placed on the SANS machine in the exact same position
- Each beam was loaded at exactly the midpoint
- Each beam was supported at exactly 500 millimetres from the centre
- The SANS Machine loaded each beam at the same rate
- The internal crack created by the aluminium encasing had minimal effect on the strength of the heated beam specimen

5.2.5 Modulus of Elasticity of Beam

The following section will discuss the theoretical modulus of elasticity of the concrete beam specimen and any associated assumptions.

5.2.5.1 Experimental Results

The experimental modulus of elasticity of the two concrete beam specimens were calculated to be:

- Control Beam = 1651.58 Mega Pascals
- Heated Beam = 1469.93 Mega Pascals

The heating of the concrete beam thus lead to an approximate degradation in modulus of elasticity of 11 percent.

5.2.5.2 Assumptions

The reliability of the results of this experimental analysis are based on the following assumptions:

- The experimental modulus of elasticity can accurately be determined from the following equation (Australia, 2002):

$$E = \frac{PL^3}{48\delta I} \text{ (MPa)}$$

- The SANS machine recorded the loads and their associated deflections accurately
- Each beam was placed on the SANS machine in the exact same position
- Each beam was loaded at exactly the midpoint
- Each beam was supported at exactly 500 millimetres from the centre
- The SANS Machine loaded each beam at the same rate
- The internal crack created by the aluminium encasing had minimal effect on the strength of the heated beam specimen

5.2.6 Principal Strains Associated with Loading Beam

The following section will discuss the experimental principal strains read via the surface mounted strain gauges and aluminium encased FBG Sensor.

5.2.6.1 Experimental Results

Resource limitations meant that only one strain gauge was able to be placed on the control beam. Two strain gauges were, however, still able to be placed on the heated beam specimen. As discussed previously, the control beam was unable to be embedded with any FBG Sensors, and the heated beam was embedded with an FBG Sensor encased in aluminium. The following graph shows the relative strain values read by the strain gauges and FBG Sensor at various loads throughout the three point bending test:

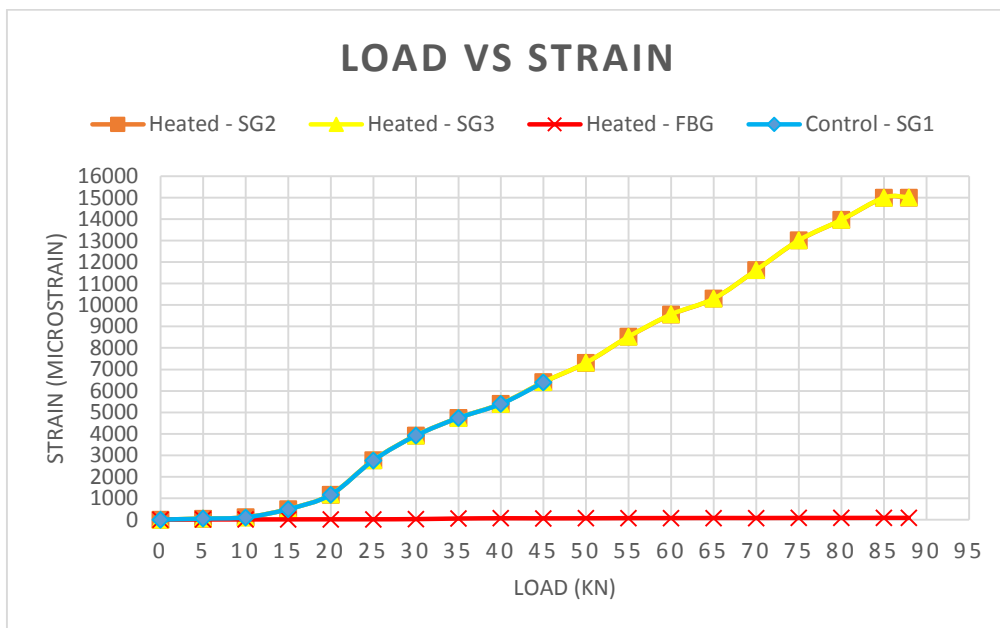


Figure 61 - Comparison of Maximum Principal Strains on Control and Heated Beams

In the above figure, the blue line represents the strain values read from the strain gauge surface mounted on the control beam; the orange and yellow lines represent the strain values read from the strain gauges surface mounted on the heated beam; and the red line represents the strain values read from the FBG Sensor encased in aluminium and embedded within the heated beam. Refer to Appendix E4 for specific tabulated values displayed in the above graph.

It can be seen that the strain gauge surface mounted on the control beam did not record any readings after a load of 45 Kilo Newtons. Investigation found that a crack had formed where the strain gauge was located, thus breaking it. Until this point though, the strains incurred on the control beam were relatively similar to those incurred on the heated beam.

The two strain gauges surface mounted on the heated beam specimen at the same distance from the centre of the beam were found to record very similar strain values, thus suggesting the validity of the results. They showed that the greater the load applied to the beam, the greater the maximum principal strain induced on the tensile side of the concrete beam.

If the FBG Sensor was encased appropriately, the strains read by the FBG Sensor should be in a similar range to those read via the strain gauges that were mounted on the same beam. This is due to the similar placement of each strain reading device. The strains read via the aluminium encased FBG Sensor embedded in the heated beam, however, were very low in comparison to those read via the strain gauges surface mounted on the heated beam. The next figure shows the strain values recorded by the FBG Sensor.

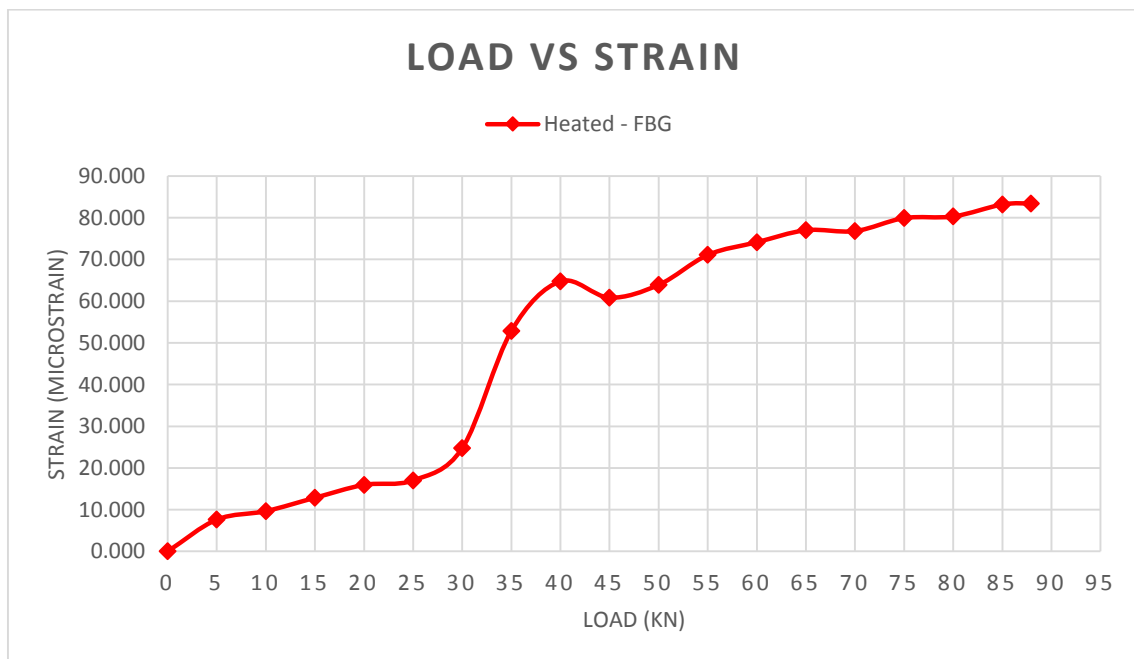


Figure 62 - Maximum Principal Strains Read by the FBG Sensor during the Three Point Bending Test

It can be seen that at the maximum load, a strain of 90 Microstrain was not even reached. The strain gauges, however, suggest that the concrete reached a strain greater than this after being loaded to approximately 10 Kilo Newtons. The strain gauge readings also suggest that at the maximum load, a strain of approximately 15,000 Microstrain should have been picked up by the FBG Sensor. Generally speaking, the FBG Sensor encased in the aluminium was unable to read more than one percent of the strain present.

This was expected, and thus proves that the inflexible nature of the encasing meant the FBG Sensor could not move with the concrete structure. This meant the FBG Sensors strain reading abilities were inhibited. The fact that this occurred, highlights the importance of properly encasing FBG Sensors.

5.2.6.2 Assumptions

The reliability of the results of this experimental analysis are based on the following assumptions:

- The strain gauges were calibrated accurately
- The natural calibration of the FBG Sensor was accurate
- The strain gauges were surface mounted appropriately to read maximum principal strains
- The FBG Sensor was embedded appropriately so that it would read maximum principal strains
- The sml125 was interrogating the FBG Sensor data properly
- MOI Enlight was recording the FBG Sensor data properly
- The strain gauge interrogator recorded the strains from the strain gauges accurately
- The SANS machine recorded the loads accurately
- Each beam was placed on the SANS machine in the exact same position
- Each beam was loaded at exactly the midpoint
- Each beam was supported at exactly 500 millimetres from the centre
- The SANS Machine loaded each beam at the same rate
- The internal crack created by the aluminium encasing had minimal effect on the maximum principal strains
- The following equation can be rearranged to give an accurate value of the change in strain of the FBG Sensor (Su and Han, 2014):

$$\Delta\lambda_B = \lambda_B \{(\alpha + \xi) \Delta T + (1 - p_e) \Delta\varepsilon\},$$

5.2.7 Principal Stresses Associated with Loading Beam

The following section will discuss the experimental principal stresses as calculated from the experimental strains.

5.2.7.1 Experimental Results

The maximum principal strains that were recorded and discussed in section 5.2.6, were converted to maximum principal stresses. The maximum principal stresses recorded for the control and heated beam specimens are shown in the below figure:

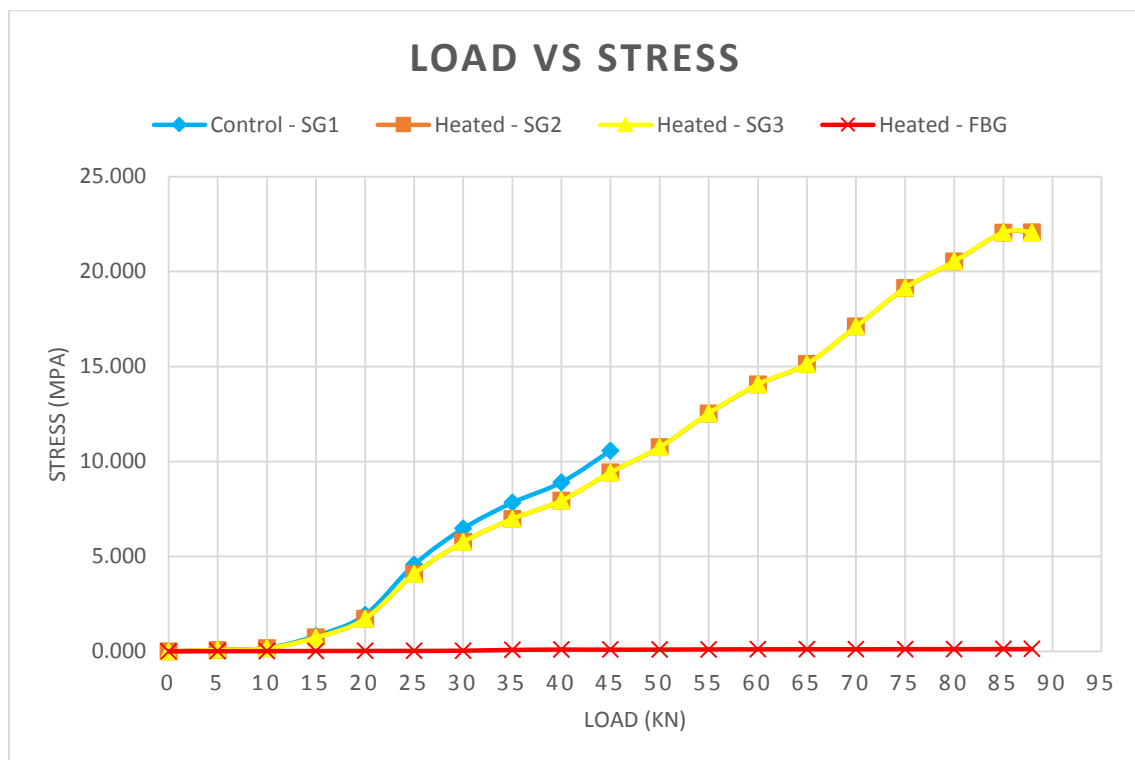


Figure 63 - Comparison of Maximum Principal Stresses of Control and Heated Beam Specimens

In the above figure, the blue line represents the stress values calculated from the strain gauge surface mounted on the control beam; the orange and yellow lines represent the stress values calculated from the strain gauges surface mounted on the heated beam; and the red line represents the stress values calculated from the FBG Sensor encased in aluminium and embedded within the heated beam. Refer to Appendix E4 for specific tabulated values displayed in the above graph.

The initial stress values for the control beam suggest that the applied load was inducing greater stress on the control beam than the heated beam. The relationship between load and stress, however, could have changed after more load was applied. The end result was in fact that the control beam withstood a slightly greater applied force (and suggested higher stress) than the heated beam, however, the difference was negligible. A confident conclusion regarding the effect of the heating on the stresses of the beam thus cannot be drawn.

The one conclusion that can be drawn is that FBG Sensor was unable to determine accurate stresses. The stress values calculated from the strains picked up by the FBG Sensor are extremely small, less than one Mega Pascal even. The following graph shows the apparent maximum principal stresses for various loads as calculated from the FBG Sensor readings:

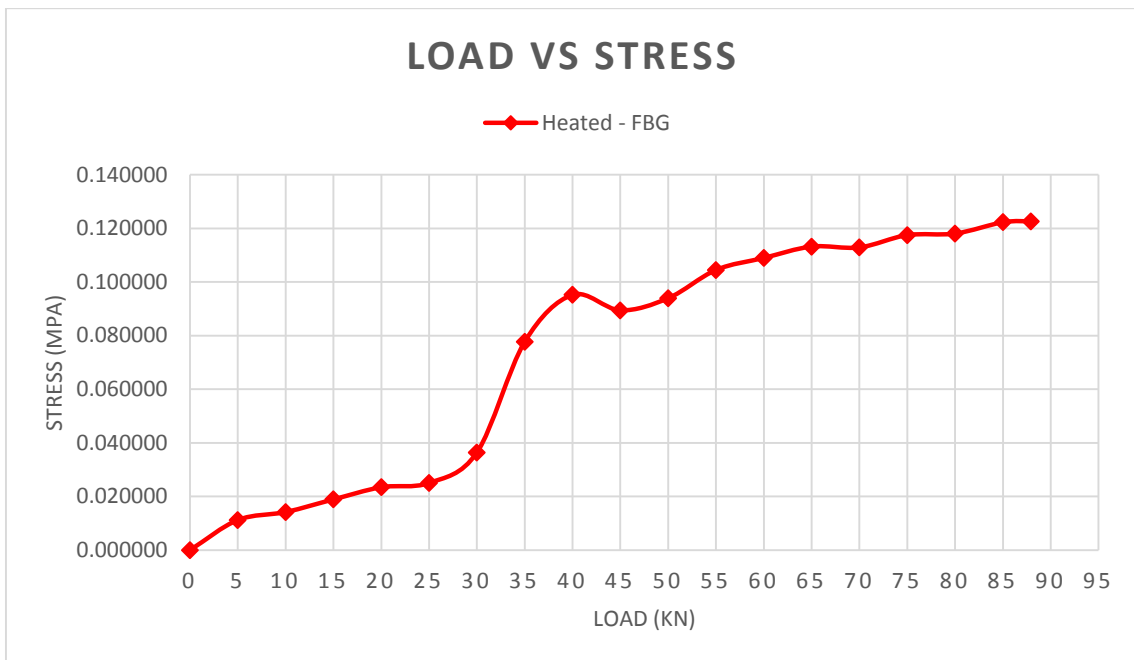


Figure 64 - Maximum Principal Stresses Read by FBG Sensor during the Three Point Bending Test

5.2.7.2 Assumptions

The reliability of the results of this experimental analysis are based on the following assumptions:

- The strain gauges were calibrated accurately
- The natural calibration of the FBG Sensor was accurate
- The strain gauges were surface mounted appropriately to read maximum principal strains
- The FBG Sensor was embedded appropriately so that it would read maximum principal strains
- The sml125 was interrogating the FBG Sensor data properly
- MOI Enlight was recording the FBG Sensor data properly
- The strain gauge interrogator recorded the strains from the strain gauges accurately
- The SANS machine recorded the loads accurately
- Each beam was placed on the SANS machine in the exact same position
- Each beam was loaded at exactly the midpoint
- Each beam was supported at exactly 500 millimetres from the centre
- The SANS Machine loaded each beam at the same rate
- The internal crack created by the aluminium encasing had minimal effect on the maximum principal strains
- The maximum principal strains of the concrete beam will follow the relationship of (Queensland, 2014):

$$e = \frac{\sigma}{E}$$

- The experimental modulus of elasticity of the control and heated beams were calculated correctly

5.2.8 Tensile Strength of Beam

The experimental tensile strength of the control and heated beam specimens, as calculated from their relative maximum principal stresses, will be discussed in the following section.

5.2.8.1 Experimental Results

The maximum principal stresses at each beams' respective failure load correlates to the experimental tensile strengths of each specimen. The strain gauge on the control beam broke after a load of 45 Kilo Newtons. This means the tensile strength of this beam could not be determined.

The heated beam, on the other hand, was estimated to have a tensile strength of 22.06 Mega Pascals. This was calculated as an average of the two principal stress values that correlate to the strain gauge readings (SG2 and SG3) at the failure load of 87.92 Kilo Newtons.

Since the strain gauge on the control beam broke before the maximum failure load, the percentage reduction in tensile strength caused from the heating could not be accurately determined. An approximation could, however, be applied by comparing the difference in the maximum principle stresses of the control and heated beam specimens when loaded to 45 Kilo Newtons. They are as follows:

- Control Beam = 10.57 Mega Pascals
- Heated Beam = 9.42 Mega Pascals

There is approximately a 10.92 percent reduction between the control beam maximum principal stress, and heated beam maximum principal stress at this load. It is thus approximated that the tensile strength of the concrete beam was reduced by 10.92 percent due to the heating.

5.2.8.2 Assumptions

The reliability of the results of this experimental analysis are based on the following assumptions:

- The SANS machine recorded the loads correctly
- The strain gauge interrogator read accurate strain values
- The strain gauge values were recorded at the exact loads indicated
- Each beam was placed on the SANS machine in the exact same position
- Each beam was loaded at exactly the midpoint
- Each beam was supported at exactly 500 millimetres from the centre
- The SANS Machine loaded each beam at the same rate
- The internal crack created by the aluminium encasing had minimal effect on the strength of the heated beam specimen
- The midspan deflections were recorded by the SANS Machine accurately
- The modulus of elasticity of each beam was calculated accurately
- The maximum principal stresses were calculated correctly from the maximum principal strains
- The positioning of the strain gauges were placed within the area where the maximum strains would of occurred due to loading
- The reduction in tensile strength can be approximated by comparing the maximum principal stresses at a load of 45 Kilo Newtons

5.2.9 Flexural Strength of Beam

The experimental flexural strength of the control and heated beam specimens, as determined from the three point bending test, will be discussed in the following section.

5.2.9.1 Experimental Results

The SANS Machine was used to perform the three point bending test to the control and heated beam specimens. This tests determined the failure load of each beam, and from this the flexural strength could be calculated. The flexural strength of each beam was:

- Control Beam = 3.522 Mega Pascals
- Heated Beam = 3.517 Mega Pascals

As can be seen, there was minimal reduction in flexural strength due to the heating of approximately 0.14 percent.

The following figure displays the flexural and shear cracking that occurred to the control beam due to the three point bending test:



Figure 65 - Flexural and Shear Cracking of Control Beam

The next figure displays the flexural and shear cracking that occurred to the heated beam due to the three point bending test:



Figure 66 - Flexural and Shear Cracking of Heated Beam

It can be seen that both beam specimens cracked and failed in similar fashions.

5.2.9.2 Assumptions

The reliability of the results of this experimental analysis are based on the following assumptions:

- The experimental flexural strength can be accurately determined from the following equation (Queensland, 2014):

$$\text{Flexural Strength} = \frac{P_U L_s}{bD}$$

- The SANS machine recorded the failure loads accurately
- Each beam was placed on the SANS machine in the exact same position
- Each beam was loaded at exactly the midpoint
- Each beam was supported at exactly 500 millimetres from the centre
- The SANS Machine loaded each beam at the same rate
- The internal crack created by the aluminium encasing had minimal effect on the strength of the heated beam specimen

5.2.10 Compressive Strength of Beam

The compressive strength of the heated and control beam specimens were determined by performing the compression test to cylinders made of the same concrete which had undergone the same conditions.

5.2.10.1 Experimental Results

In order to determine the experimental compressive strength difference between the control beam and heated beam, three cylinders were compressively loaded at 24 Newtons per second for each case. The heated cylinders were subjected to the same form of heating as the heated beam specimen. The following table summarises the loading failures, relative compressive strengths and the approximate reduction in compressive strength due to heating:

Table 9 - Experimental Compression Test Results

	Failure Loads (kN)		Compressive Strength (MPa)		Reduction in Strength (%)
	Control Cylinders	Heated Cylinders	Control Cylinders	Heated Cylinders	
Cylinder 1	220	173	28.0	22.0	21.6
Cylinder 2	224	179	28.5	22.7	20.2
Cylinder 3	235	181	29.9	23.0	23.2
Average	226	177	28.8	22.6	21.7

From the above table it can be concluded that in terms of experimental results, the average compressive strength of the control beam was 28.8 Mega Pascals, and the average compressive strength of the heated beam was 22.6 Mega Pascals. The experimental analysis thus showed a 21.7 percent reduction in compressive strength due to this specific heat exposure.

The following figure displays one of the cylinders failing under the hydraulic loading:



Figure 67 - Concrete Cylinder under Compression Tests at Failure Load

The next figure shows the cracking planes of a control cylinder specimen on the left, and a heated cylinder specimen on the right, after they were subjected to the compression test:



Figure 68 - Failure Planes of Control and Heated Concrete Cylinders

5.2.10.2 Assumptions

The reliability of the results of this experimental analysis are based on the following assumptions:

- Compressive strength can accurately be calculated from the following equation (Queensland, 2014):

$$f'c = \frac{P}{A} \text{ (MPa)}$$

- The SANS machine recorded the failure loads accurately
- Each cylinder was placed on the SANS machine in the exact same position
- The SANS Machine loaded each cylinder at the same rate
- The compressive strength of the cylinders is directly comparable to the compressive strength of the concrete beams

Chapter 6: Discussion and Recommendations

The following section will compare the theoretical and experimental results, discuss whether the aims of the research were met, and list any limitations and suggested improvements.

6.1 Discussion of Theoretical and Experimental Results

The following section will compare the theoretical and experimental results and recommend as to why any variances have occurred.

6.1.1 Concrete Curing Temperatures

The theoretical analysis suggested that the concrete would show a rapid rise in internal temperature until reaching a maximum temperature of approximately 75 degrees Celsius about 24 hours after pouring. After this point the internal temperature of the concrete beams were expected to decline until reaching their approximate starting temperature about five days after pouring (Australia, 2002).

Experimentally, however, the internal temperature of the concrete initially declined, reaching a low of approximately 10 degrees Celsius. After twelve hours the temperature of the concrete began to rise, and after forty eight hours it returned to its approximate starting temperature. After this point, the temperature of the concrete seemed to follow the trend of the ambient temperature.

It must be noted that the concrete was poured on a cold night that had an ambient temperature of approximately eight degrees Celsius. The water that was used to mix the concrete was at an approximate temperature of four degrees Celsius. The concrete mixture also had a high cement to aggregate content, in order to ensure high grade strength was achieved. Yadav, 2015, stated that these factors can inhibit internal temperature rise within a curing concrete specimen.

Yadav, 2015, also suggested that internal temperature rise within a curing concrete specimen can be inhibited by cement fineness and unideal cement composition. It was unable to be confirmed whether these were contributing factors, but it is suggested that they in fact were.

Although there are explanations as to why the internal temperature rise within the concrete beams was inhibited, it is still unknown as to why the temperatures recorded were consistently low, being between approximately 10 to 23 degrees Celsius.

6.1.2 Heating Profile of Beam

The experimental heating method was altered to the method theoretically modelled in Abaqus/CAE. An external heat of 200 degrees Celsius was, however, still utilised. Assuming this heat would be applied at an apparent force of 2 Kilo Watts, it was theoretically expected that the FBG Sensor would read a maximum temperature of approximately 92.4 degrees Celsius.

Experimentally, however, the FBG Sensor read a much higher maximum temperature of 145 degrees Celsius. This could be due to the fact that the heat source actually applied the heat at a higher force, but it is more likely because the three dimensional model could not take into account if the heat was applied for a prolonged period. A temperature of 145 degrees Celsius after all was reached after the beam had been exposed to heat for approximately one hour.

6.1.3 Midpoint Deflections Associated with Loading Beam

The theoretical midspan deflections were much lower than the experimental midspan deflections. The theoretical deflections calculated were points of a millimetre, whereas the experimental deflections were between one and ten millimetres. This is believed to be due to the beam structure tested having a low shear span to depth ratio, thus meaning experimental deflections were recorded in terms of flexure as well as shear. The placement of the beam, machine error, and human error when recording may also have contributed to higher deflections than expected ((APEE), 2005).

It must also be noted that the equation utilised to theoretically calculate the midspan deflections of the beam is dependent on modulus of elasticity, and as discussed in the following section, the experimental modulus of elasticity values were much lower than theoretically expected (Australia, 2002).

6.1.4 Modulus of Elasticity of Beam

The following table compares the theoretical and experimental modulus of elasticity of both the control and heated beam specimens:

Table 10 - Comparison of Theoretical and Experimental Modulus of Elasticity

	Modulus of Elasticity (MPa)		Reduction (%)
	Control Beam	Heated Beam	
Theoretical	32800.00	24600.00	25
Experimental	1651.58	1469.93	11.00

From the above table it can be seen that in both the control and heated beam scenarios, the theoretical modulus of elasticity was much higher than the experimental modulus of elasticity. The experimental modulus of elasticity values calculated were dependent on the recorded deflection values. Since the recorded deflection values were much higher than theoretically expected, the experimental modulus of elasticity values were much lower than theoretically expected.

It must also be noted that the beam did not reach its full potential strength, meaning it would not have reached its full potential modulus of elasticity. Why the beam did not reach its full potential strength will be discussed when comparing the theoretical and experimental tensile, flexural and compressive strengths.

Theoretically speaking, exposing the concrete beam to a heat of approximately 200 degrees Celsius was expected to cause a degradation in modulus of elasticity of approximately 25 percent (Association, 2002). Experimentation, however, found that the heating only reduced the modulus of elasticity by 11 percent. It is suggested that this is due to the heat either not being applied for a sufficient length of time, or perhaps due to it not being applied to a large enough area ((APEE), 2005). The heating being applied to a partial area was theoretically expected to have the greatest detrimental effect on the concrete, but if not enough of the concrete was heated, the effects may not be as significant (Association, 2002).

6.1.5 Maximum Principal Strains Associated with Loading Beam

A comparison of the theoretical and experimental maximum principal strains, when the beam was loaded at 40 Kilo Newtons is shown in the below table:

Table 11 - Comparison of Theoretical and Experimental Strains

40 kN Applied Load	Strain (Micro strain)			
	Control - SG	Heated - SG	Control - FBG	Heated - FBG
Theoretical	274.39	292.68	265.24	282.93
Experimental	5390	5398.50	Unknown	64.75

From the above table, it can be viewed that the experimental strains recorded via the use of strain gauges for the control and heated beam specimens were much higher than theoretically expected. This is believed to be due to the beam structure tested having a low shear span to depth ratio, thus meaning experimental strains were influenced via flexure and shear ((APEE), 2005). The three dimensional theoretical model would not of taken both of these pressures into account but rather would of behaved how a more stable beam structure should behave. The placement of the beam, machine error, and human error when recording may also have contributed to higher strains than expected ((APEE), 2005).

It must be noted that the experimental design was altered due to the initial concrete encasing design failing. An FBG Sensor was thus unable to be embedded within the control beam, meaning no strain value were read for the experimental Control FBG Sensor scenario.

This also meant that the heated beam had an FBG Sensor embedded within it that was encased using the aluminium technique. The above table shows that the experimental strains read from the FBG Sensor for the heated beam were significantly lower than what was theoretically expected.

Considering the strain gauges recorded strains significantly higher than theoretically expected, it can be concluded that the aluminium encasing inhibited the FBG Sensors ability to read accurate strains. It is believed that the aluminium encasing was inflexible and did not bond with the concrete appropriately. Having limited movement means the FBG Sensor could only read a low range of strains. If the FBG Sensor was encased using a method that allowed the FBG Sensor to move with concrete structure, it would have been able to read much higher, much more accurate strains (Biswas et al., 2010).

6.1.6 Maximum Principal Stresses Associated with Loading Beam

A comparison of the theoretical and experimental maximum principal stresses, when the beam was loaded at 40 Kilo Newtons is shown in the below table:

Table 12 - Comparison of Theoretical and Experimental Stresses

40 kN Applied Load	Stress (MPa)			
	Control - SG	Heated - SG	Control - FBG	Heated - FBG
Theoretical	274.39	292.68	265.24	282.93
Experimental	5390	5398.50	Unknown	64.75

Explanation for variances in the theoretical and experimental results can be directly related to those reasons discussed in section 6.1.5. This is because the theoretical maximum principal stresses were estimated using the same three dimensional static model. The experimental maximum principal stresses were also calculated by multiplying the maximum principal strain values recorded by the experimental modulus of elasticity of each beam.

It must be noted that the experimental modulus of elasticity values were much lower than those used in the three dimensional model. This would have also contributed to a variance in the theoretical and experimental maximum principal stresses. This in combination with high maximum principal strain values would actually have brought the theoretical and experimental maximum principal stresses closer in value. Reasoning for variances in the theoretical and experimental modulus of elasticity values were discussed in section 6.1.4.

6.1.7 Tensile Strength of Beam

The following table compares the theoretical and experimental tensile strengths of the control and heated beam specimens:

Table 13 - Comparison of Theoretical and Experimental Tensile Strengths

	Tensile Strength (MPa)		Strength Reduction (%)
	Control Beam	Heated Beam	
Theoretical	18.848	15.078	20.00
Experimental	unknown	22.06	10.92

The experimental tensile strength of the control beam could not be determined. Using the maximum principal strains recorded, an approximation was applied to estimate that the experimental tensile strength of the control beam was 10.92 percent higher than the heated beam, thus giving it a tensile strength of 24.47 Mega Pascals.

From the above tabulated and estimated values, it can be concluded that the theoretical tensile strengths of the concrete beam are lower than the experimental tensile strengths. This is mainly because experimentally the beams were able to handle a greater ultimate load, but also because the experimental maximum principal stresses were larger due to the beam experiencing flexural and shear stresses ((APEE), 2005).

It must be noted that the theoretical calculation of the ultimate load did not take into account the ability of the compressive reinforcing steel, and reinforcing stirrups to enhance the beams ability to carry load (Queensland, 2014). This suggests why the theoretical ultimate failure load was calculated to be lower than what occurred experimentally.

The theoretical strength reduction caused by the heating, on the other hand, was greater than what occurred experimentally. It is suggested that this is due to the heat either not being applied for a sufficient length of time, or perhaps due to it not being applied to a large enough area. The heating being applied to a partial area was theoretically expected to have the greatest detrimental effect on the concrete, but if not enough of the concrete was heated, the effects may not be as significant.

6.1.8 Flexural Strength of Beam

The following table compares the theoretical and experimental flexural strengths of the control and heated beam specimens:

Table 14 - Comparison of Theoretical and Experimental Flexural Strengths

	Flexural Strength (MPa)		Strength Reduction (%)
	Control Beam	Heated Beam	
Theoretical	4.00	3.40	15.00
Experimental	3.522	3.517	0.14

From the above table it can be viewed that the theoretical flexural strengths were calculated to be greater than the flexural strengths that occurred experimentally. This is because the theoretical tensile strengths were calculated as ten percent of the expected compressive strength of the beams, and the beams did not reach their full potential compressive strength. Why this occurred will be discussed in the following section.

The experimental flexural strength reduced by less than one percent after the beam was heated. This reduction in strength is so marginal that it cannot be concluded that the heating caused any reduction in flexural strength. Theoretically the flexural strength was expected to reduce by 15 percent (Association, 2002). It is suggested that this did not occur because the heat either was not applied for a sufficient length of time, or perhaps it was not applied to a large enough area ((APEE), 2005). The heating being applied to a partial area was theoretically expected to have the greatest detrimental effect on the concrete, but if not enough of the concrete was heated, the effects may not be as significant (Association, 2002).

6.1.9 Compressive Strength of Beam

The following table compares the theoretical and experimental compressive strengths of the control and heated cylinder specimens:

Table 15 - Comparison of Theoretical and Experimental Compressive Strengths

	Compressive Strength (MPa)		Strength Reduction (%)
	Control Cylinders	Heated Cylinders	
Theoretical	40.00	36.00	10.00
Experimental	28.80	22.60	21.53

The theoretical compressive strengths were considerably higher than those recorded experimentally. This is believed to be due to the low curing temperatures reducing the rate at which hydration occurred, and thus inhibiting the concrete's ability to reach its full potential strength (Australia, 2002). It could also be due to the fact that the concreting was not performed by an experienced professional. This very well could of lead to not only the concrete being compacted ineffectively but also potentially inconsistently (Australia, 2002).

Inconsistency in compaction could explain why experimentally the reduction in strength caused by the heating was more than twice than was theoretically anticipated (Australia, 2002). It must also be noted that the heated cylinders specimens may not have been the best representation of the heated beam specimens' compressive strength. This is suggested because a greater percentage of the cylinders surface areas would have been in direct contact with the heat source than that of the concrete beam. It is proposed that if the same percentage of surface area was heated in both cases, the percentage reduction in compressive strength between the control and heated specimens would have been less (Association, 2002, Australia, 2002).

6.1.10 Performance of FBG Sensor Encasing Techniques

The following section will discuss whether the aluminium and concrete encasing methods performed as theoretically anticipated.

6.1.10.1 Aluminium Encasing

Experimentation proved that the aluminium encasing performed as theoretically expected. The behaviour of the aluminium encasing is summarised as follows:

- It sufficiently protected the FBG Sensor from chemical attack, abrasion, and heat
- It was able to read accurate internal temperatures
- It was inflexible and did not bond with the concrete beam, and so thus was not be able to read accurate strains
- It created an internal crack within the concrete beam
- It allowed the FBG Sensor to identify any significant internal cracks

6.1.10.2 Concrete Encasing

When performing the theoretical analysis, it was not expected that the method of concrete encasing would fail and break the FBG Sensor. The method was, however, modified and tested via the utilisation of replica fibres. Experimentation suggested that an FBG Sensor encased in this way would perform as theoretically expected of the initial method of concrete encasing.

Experimentation with replica fibres indicated that the modified method of concrete encasing should:

- Firstly, not break the FBG Sensor when encasing it
- Protect the FBG Sensor from corrosion, chemical attack, and abrasion
- Ensure the FBG Sensors' survival throughout pouring, compaction, vibration and other methods utilised when making a concrete beam
- Protect the FBG Sensor from heat
- Allow the FBG Sensor to read accurate internal temperatures
- Be flexible and bond with the concrete beam, and so thus allowing the FBG Sensor to read accurate strains
- Allow the FBG Sensor to identify the formation of any significant internal cracks

6.2 Comparison with the Aim of the Research

The objectives of the investigation are summarised as follows:

1. Conduct an extensive literature review on the behaviour of concrete when curing, when loaded, and when subjected to heat. Also include an overview of structural health monitoring techniques with a focus on FBG Sensors, strain gauges, thermocouples, three point bending tests, and compression tests.
2. Determine an appropriate testing temperature and method of heating.
3. Model a chosen concrete beam structure using Abaqus 3D finite element analysis in order to predict structural and thermal behaviours and thus determine appropriate placement of FBG
4. Sensors, strain gauges and thermocouples.
5. Perform relevant hand calculations to theoretically analyse the effects of temperature on the chosen beam structure.
6. Design a method for placing FBG Sensors within the concrete beam structures.
7. Build two concrete beam structures with embedded FBG Sensors and thermocouples.
8. Monitor internal temperature changes of the two concrete beam structures for 28 days as they cure.
9. Keep one beam as the control and with the other simulate the situation of heat and monitor the temperature variation inside the structure using embedded FBG sensor(s) & thermocouples.

10. Carry out compression and three point bending tests to concrete specimens.

11. Analyse experimental data.

12. Submit an academic dissertation on the project findings.

As time permits:

13. Analyse a third concrete beam structure with a deliberately made internal crack.

It is believed that all of the objectives were attempted. Objectives six, eight and twelve were not fully met, however, due to the initial design of the new method of encasing the FBG Sensor failing. This meant that the first control beam was only analysed via the use of thermocouples and strain gauges. The second beam was then a combination of beams two and three. This beam had an FBG Sensor embedded within it in such a way that it made an internal crack, and then this FBG Sensor was used to analyse the beam whilst curing and whilst subjected to heat.

It must also be noted with objective three that the method of heating was altered from that designed in the three dimensional thermal model. Information from this model, however, could still be used for a theoretical comparison.

In terms of objective five, although the initial method of encasing an FBG Sensor failed, it was modified and retested via the use of replica fibres. It was proven that it was a viable method that could have the enhanced capability of reading accurate strain values.

In terms of meeting the aim of this research, it is believed that a new method of encasing FBG Sensors in concrete in order to successfully embed them within a concrete structure was designed. Although it was unable to be tested with a real FBG Sensor, it is believed that it was proven that this method of encasing an FBG Sensor would be capable of predicting damage accumulation and conditions inside the concrete structure before, during and after a natural disaster such as a fire.

6.3 Limitations and Improvements

The largest limitation of this research paper is that the modified method of encasing FBG Sensor in concrete, discussed in section 5.2.1.1, was unable to be tested with real fibres. Having to perform the experimental analysis with the aluminium encasing meant that the maximum principal strains, maximum principal stresses and tensile strength could not be accurately determined via the use of the FBG Sensor. It also meant that the internal crack created by this encasing had an unknown influence on all FBG Sensor results. An improvement would thus be to perform the experimental analysis as planned in the methodology using the modified method of concrete encasing.

Another significant limitation of the analysis was the fact that the experimental analysis was not performed by an experienced professional. This meant that the concrete did not reach its full potential strength, and a variance between how well each specimen was made could have occurred and thus could have had an effect on the results recorded.

An additional limitation of this research paper was the fact that a beam with a low shear span to depth ratio was used. This meant that strains, stresses and deflections during the three point bending test were influenced by shear as well as flexure ((APEE), 2005). This caused a notable variance in the experimental and theoretical strains, stresses, deflections, and modulus of elasticity.

Chapter 7: Conclusion

The following section will summarise the overall conclusions, recommendations and any suggested further research.

7.1 Overall Conclusion

The first noteworthy conclusion that could be made from this research paper was, that FBG Sensors were proven to be capable of identifying internal deformations in concrete structures that cannot be seen via visual inspection. An interruption in their spectrum allows for the recognition of such deformations (Su and Han, 2014).

These sensors can also continuously real time monitor and record data relating to temperatures, strains, and vibrations. If a natural disaster occurs within an area, these sensors could allow for the determination of the extent a specific concrete structural elements are affected by such a disaster or just by long term use (Su and Han, 2014).

With the use of proper comparison technology, the data could be used to determine the structural health of concrete elements. The use of such technology could improve safety by early identification of structural flaws that may have otherwise been overlooked. They could also improve maintenance and natural disaster clean-up costs by ensuring unnecessary replacement of concrete structural elements does not occur (Su and Han, 2014).

Within this research paper it was proven that encasing an FBG Sensor in a foreign materials such as stainless steel, aluminium, or another metal could cause a reaction to occur between this material and the reinforcing steel. Such a reaction was proven to be capable of creating an internal structural deformity. It was also proven that encasing an FBG Sensor in such way inhibits the FBG Sensors ability to accurately read internal strains.

Literature and theoretical analysis suggested that encasing an FBG Sensor utilising the modified method of concrete encasing discussed in section 5.2.1.1 could eliminate the deficiencies of the current methods of FBG Sensor encasing. The main deficiency being the fact that the FBG Sensor encased in a metal is inflexible and unlikely to bond appropriately with a concrete structure it is embedded within.

The experimental analysis demonstrated that the modified method of concrete encasing was able to protect an FBG Sensor replica fibre throughout the processes of pouring, vibrating, compacting, and curing. This method of encasing was also proven to sufficiently bond with the concrete it was embedded within. This suggests that the modified concrete encasing method would be superior to other FBG Sensor encasing techniques in the fact that it would move with the concrete structure and thus read accurate strains. If this could be proven to be the case, this technique for encasing FBG Sensors could be utilised throughout industry for concrete structural health monitoring purposes.

7.2 Recommendations

The invention of an effective internal monitoring system to evaluate the integrity of concrete structures after natural disasters such as fires, floods and terrorist activities is of importance. If encased appropriately FBG Sensors are a viable method for in-situ structural health monitoring of concrete structures. The modified concrete encasing technique discussed in section 5.2.1.1 could take the use of FBG Sensors in structural health monitoring to a new level. The utilisation of this technique would, however, depend on necessity and affordability.

7.3 Further Research

If further time permitted it would have been beneficial to trial the modified method of encasing the FBG Sensors in concrete with real fibres. This method is outlined in section 5.2.1.1. Trialling of this method with real fibres would allow the determination of whether the flexibility of this encasing and its ability to bond with the concrete it is embedded in would in fact enable the FBG Sensor it encases to read accurate strains.

If FBG Sensors encased in this way are proven to have the enhanced ability of being able to read accurate strains, as well as the abilities to determine crack propagation and read accurate temperatures, they could be a viable option for use in industry for structural health monitoring.

Chapter 8: List of References

- (APEE), Portugese. Group. Of. IABSE. Structures and Extreme Events. IABSE Symposium, 2005 Lisbon, Portugal.
- ASSOCIATION, Portland. Cement. 2002. *Concrete Information - Types and Causes of Concrete Deterioration* [Online]. Available: http://www.cement.org/docs/default-source/fc_concrete_technology/durability/is536-types-and-causes-of-concrete-deterioration.pdf?sfvrsn=4 [Accessed March 8 2015].
- AUSTRALIA, Cement. And. Concrete. Association. Of. Australia. 2002. *Guide to Concrete Construction*, Sydney, Cement and Concrete Association of Australia and Standard Australia.
- AUSTRALIA, Standards. 2009. Concrete Structures. AS3600.
- BISWAS, P., BANDYOPADHYAY, S., KESAVAN, K., PARIVALLAL, S., SUNDARAM, B. A., RAVISANKAR, K. & DASGUPTA, K. 2010. Investigation on packages of fiber Bragg grating for use as embeddable strain sensor in concrete structure. *Sensors and Actuators A: Physical*, 157, 77-83.
- CIVIL, Web. 2015. *Rebar Properties* [Online]. Available: <http://www.webcivil.com/rcrebar.aspx> [Accessed 2 February 2015].
- CLEAR. N/D. *Thermal Conductivity* [Online]. Available: http://www.new-learn.info/packages/clear/thermal/buildings/building_fabric/properties/conductivity.html [Accessed 2 February 2015].
- CORPORATION, National. Instruments. 2015. *What Can You Do With LabVIEW* [Online]. Available: <http://www.ni.com/LabVIEW/why/>.
- DASAR, E. 2013. *Sensor Strain Gauge* [Online]. Available: <http://elektronika-dasar.web.id/komponen/sensor-tranducer/sensor-strain-gauge/> [Accessed 2 March 2015].
- ENGINEERING, Instrumentation. And. Control. N/D. *Explanation of Thermocouple with Circuit* [Online]. Available: <http://instrumentationandcontrollers.blogspot.com.au/2010/06/thermocouple-with-circuit.html> [Accessed 2 March 2015].
- ERDOGAN, T. 1997. Fiber Grating Spectra. *Journal of Lightwave Technology*, 15.
- GAO, W. Y., DAI, J.-G., TENG, J. G. & CHEN, G. M. 2013. Finite element modeling of reinforced concrete beams exposed to fire. *Engineering Structures*, 52, 488-501.
- GLIŠIĆ, B. 2000. FIBRE OPTIC SENSORS AND BEHAVIOUR IN CONCRETE AT EARLY AGE.
- GLISIC, D., VURPILLOT, S., KRONENBERG, P. & LLORET, S. 2001. Lessons learned in the use of fiber optic sensor for civil structural monitoring. *International Journal for Restoration of Buildings and Monuments*, 301-320.
- HAMERLINCK, R. 1991. *The Behaviour of Fire-Exposed Composite Steel/Concrete Slabs*, Eindhoven, A.F. Hamerlinck.
- HAN, L., TAN, Q. & SONG, T. 2013. Fire Performance of Steel Reinforced Concrete (SRC) Structures. *Procedia Engineering*, 62, 46-55.
- INC, Micron. Optics. 2009. *Optical Sensing Interrogator sm125* [Online]. Micron Optics Inc. Available: http://www.micronoptics.com/uploads/library/documents/datasheets/instruments/Micron_Optics_sm125.pdf [Accessed 1 April 2015].

- INC, Omega. Engineering. 2015a. *POSITIONING STRAIN GAGES TO MONITOR BENDING, AXIAL, SHEAR, AND TORSIONAL LOADS* [Online]. Available: <http://www.omega.com/faq/pressure/pdf/positioning.pdf>.
- INC, Omega. Engineering. 2015b. *Thermocouples* [Online]. Available: <http://www.omega.com/prodinfo/thermocouples.html> [Accessed March 26 2015].
- M. NADIM HASSOUN, 2012. *Structural Concrete - Theory & Design*, Hoboken, New Jersey, John Wiley & Sons Inc.
- MILLARD, G. 1996. *Testing of Concrete in Structures*, Cambridge, The University Press.
- QUEENSLAND, The. University. Of. S. 2014. *CIV3506 Concrete Structures Study Book*, Toowoomba, The University of Southern Queensland.
- SJ FOSTER, RF WARNER 2010. *Reinforced Concrete Basics 2E - Analysis and Design of Reinforced Concrete Structures*, Frenchs Forest NSW, Pearson Australia.
- SU, X & HAN, J. P. 2014. Structural Health Monitoring of Civil Infrastructure Using Optical Fiber Sensing Technology: A Comprehensive Review. *The Scientific World Journal*.
- SYSTEMS, D. 2015. *Abaqus/CAE* [Online]. Available: <http://www.3ds.com/products-services/simulia/products/abaqus/abaquscae/> [Accessed 10 February 2015].
- TADROS, R., RIZKALLA, S. H. & GUHA-THAKURTAD, A. 1997. Fibre Optic Bragg Grating Sensors for Bridge Monitoring. *Cement and Concrete Composites*, 21-33.
- YADAV, B. P. 2015. *Mass Concrete* [Online]. LinkedIn Corporation. Available: <http://www.slideshare.net/erbrijeshpyadav/mass-concrete> [Accessed 3 March 2015].
- YAO, Y. 2006. Residual stress–strain relationship for concrete after exposure to high temperatures. *Cement and Concrete Research*, 36.

Appendices

Appendix A - Project Specification

University of Southern Queensland
FACULTY OF ENGINEERING AND SURVEYING
ENG4111/4112 RESEARCH PROJECT
PROJECT SPECIFICATION

FOR: **AMY BERNIER**

TOPIC: **STRUCTURAL HEALTH MONITORING OF CONCRETE**

SUPERVISOR: **Dr. Jayantha Epaarachchi**

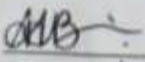
PROJECT AIM: **The aim of this research is to figure out a viable method of embedding fibre optic sensors within a concrete structure. This technique will be utilised to analyse the structural health of concrete under normal operating conditions, and when heated to simulate the extreme condition of a fire. Concrete will first be analysed as it cures. The structural health monitoring system will also be used to investigate the residual life/integrity of concrete when subjected to heat of a particular nature. The application will be used to predict damage accumulation and conditions inside the concrete structure before, during, and after such an event.**

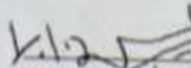
PROGRAMME: **ISSUE B, 25TH APRIL 2015**

1. Conduct an extensive literature review on the behaviour of concrete when curing, when loaded, and when subjected to heat. Also include an overview of structural health monitoring techniques with a focus on fibre optic sensors, strain gauges, thermocouples, three point bending tests, and compression tests.
2. Determine an appropriate testing temperature and method of heating.
3. Model a chosen concrete beam structure using Abaqus 3D finite element analysis in order to predict structural and thermal behaviours and thus determine appropriate placement of fibre optic sensors, strain gauges and thermocouples.
4. Perform relevant hand calculations to theoretically analyse the effects of temperature on the chosen beam structure.
5. Design a method for placing fibre optic sensors within the concrete beam structures.
6. Build two concrete beam structures with embedded fibre optic sensors and thermocouples.
7. Monitor internal temperature changes of the two concrete beam structures for 28 days as they cure.
8. Keep one beam as the control and with the other simulate the situation of heat and monitor the temperature variation inside the structure using embedded FBG sensor(s) & thermocouples.
9. Carry out compression and three point bending tests to concrete specimens.
10. Analyse experimental data.
11. Submit an academic dissertation on the project findings.


As time permits:

12. Analyse a third concrete beam structure with a deliberately made internal crack.

AGREED  (Student)
Date: 25/4/15

 (Supervisor)
Date: 25/4/15

Appendix B – Risk Assessment Documentation

	The University of Southern Queensland	USQSafe Enquiries: (07) 4631 2520 Facsimile: (07) 4631 2829
---	--	--

Date of Assessment: <u>26/4/15</u>	Due Date of Reassessment: _____
Assessors Names: <u>Amy Beemer</u> <u>Janantha Spasich</u>	
Substances: <u>Cement, (LPG Gas - off campus)</u>	
Location: <u>P2, P3, Z1</u>	Job: _____ Use: <u>create concrete beam</u> <u>Expose concrete beam to temperature increase</u>

1 USING THE MSDS AND LABEL, DETERMINE:

Hazards and Health Effects	Potential Routes of Exposure	MSDS Recommended Control Measures
Corrosive <input type="checkbox"/>	Inhalation <input checked="" type="checkbox"/>	Engineering <input type="checkbox"/>
Irritant <input type="checkbox"/>	Ingestion <input checked="" type="checkbox"/>	Isolation <input checked="" type="checkbox"/> (LPG Gas off campus)
Sensitising <input type="checkbox"/>	Skin/Eye <input checked="" type="checkbox"/>	PPE <input checked="" type="checkbox"/>
Carcinogenic <input type="checkbox"/>		Other <input type="checkbox"/>
Mutagenic <input type="checkbox"/>		
Teratogenic <input type="checkbox"/>		
Toxic <input checked="" type="checkbox"/>		
Asphyxiant <input type="checkbox"/>		
Flammable <input checked="" type="checkbox"/> (off campus)		
Other <input type="checkbox"/>		

2 INSPECT THE WORKPLACE AND EVALUATE THE EXPOSURE

	Yes	No
Is the substance used in the work environment?	<input checked="" type="checkbox"/>	<input type="checkbox"/>
Is the substance emitted or released into the work area?	<input checked="" type="checkbox"/>	<input type="checkbox"/>
Are staff or students exposed to the substance via any of the potential routes of exposure listed:		
• Inhalation	<input checked="" type="checkbox"/>	<input type="checkbox"/>
• Ingestion	<input type="checkbox"/>	<input checked="" type="checkbox"/>
• Skin Absorption	<input checked="" type="checkbox"/>	<input type="checkbox"/>
Have any employees experienced symptoms of exposure?	<input type="checkbox"/>	<input checked="" type="checkbox"/>
If YES, list these: _____		

Have any employees reported any health effects?	<input type="checkbox"/>	<input checked="" type="checkbox"/>
If YES, list these: _____		

Date Revised: May 2003 Page 1 of 4

Looking at the work process, location of workers and considering all persons with the potential for exposure, consider the following:

	Yes	No
Is there evidence of contamination?	<input type="checkbox"/>	<input checked="" type="checkbox"/>
• Dusts or fumes visible in the air or on surfaces	<input checked="" type="checkbox"/> (off campus)	<input type="checkbox"/>
• Substances visible on a person's skin or clothing	<input checked="" type="checkbox"/>	<input type="checkbox"/>
• Visible leaks, spills or residue	<input type="checkbox"/>	<input checked="" type="checkbox"/>
• Other	<input type="checkbox"/>	<input checked="" type="checkbox"/>
Is there direct contact with the substance?	<input type="checkbox"/>	<input checked="" type="checkbox"/>
Is there a potential for splashes?	<input checked="" type="checkbox"/>	<input type="checkbox"/>

What is the time exposure to the substance?

	Number of Times	Period of Each Time (minutes/hours)
• Per day	_____	_____
• Per week	_____	_____
• Per month	_____	_____
• Per year	<u>Cement - 4</u> <u>LPG Gas - 1 (off campus)</u>	<u>Cement - 1 hr</u> <u>LPG Gas - 1 hr</u>

	Yes	No
Is the substance used in concentrated form?	<input type="checkbox"/>	<input checked="" type="checkbox"/>
Is the substance diluted by the user?	<input type="checkbox"/>	<input checked="" type="checkbox"/>
Are the health effects different for diluted and undiluted?	<input type="checkbox"/>	<input checked="" type="checkbox"/>
If YES what are the health statements for UNDILUTED solution:	_____	

Are any of the following controls in place and are they properly maintained (cleaned, recorded, follow-up)?

	Present		Maintained	
	Yes	No	Yes	No
• Are there engineering controls in place?	<input checked="" type="checkbox"/>	<input type="checkbox"/>	<input checked="" type="checkbox"/>	<input type="checkbox"/>
• Are there gen. ventilation & local ventilation systems in place?	<input checked="" type="checkbox"/>	<input type="checkbox"/>	<input checked="" type="checkbox"/>	<input type="checkbox"/>
• Are workers trained in the proper use of the substance?	<input checked="" type="checkbox"/>	<input type="checkbox"/>	<input checked="" type="checkbox"/>	<input type="checkbox"/>
• Do work practices ensure safe handling?	<input checked="" type="checkbox"/>	<input type="checkbox"/>	<input checked="" type="checkbox"/>	<input type="checkbox"/>
• Is the appropriate PPE used?	<input checked="" type="checkbox"/>	<input type="checkbox"/>	<input checked="" type="checkbox"/>	<input type="checkbox"/>
• Are there facilities for changing and washing?	<input checked="" type="checkbox"/>	<input type="checkbox"/>	<input checked="" type="checkbox"/>	<input type="checkbox"/>
• Are good housekeeping practices in place?	<input checked="" type="checkbox"/>	<input type="checkbox"/>	<input checked="" type="checkbox"/>	<input type="checkbox"/>
• Are hazardous substances stored correctly	<input checked="" type="checkbox"/>	<input type="checkbox"/>	<input checked="" type="checkbox"/>	<input type="checkbox"/>
• Is waste disposed of properly	<input checked="" type="checkbox"/>	<input type="checkbox"/>	<input checked="" type="checkbox"/>	<input type="checkbox"/>

- Are there emergency procedures in place?
- Is there emergency equipment eg eye wash

3 EVALUATE THE RISK

	Low	High
Nature and severity of the hazard/s	<input checked="" type="checkbox"/>	<input type="checkbox"/>
Degree of exposure	<input checked="" type="checkbox"/>	<input type="checkbox"/>
Are existing control measures adequate?	<input type="checkbox"/>	<input checked="" type="checkbox"/> <i>yes adequate</i>

(for on-campus)

4 ASSESSMENT RESULTS

What is the conclusion about risks?

Conclusion 1	Risks not significant	<input type="checkbox"/>
Conclusion 2	Risks significant BUT effectively controlled	<input checked="" type="checkbox"/>
Conclusion 3	Risks significant and NOT adequately controlled	<input type="checkbox"/>
Conclusion 4	Uncertain about risks, expert opinion required	<input type="checkbox"/>

NOTE: Conclusion 3 and 4 require further action.

5 COMMENTS

Please provide any comments regarding the assessment. _____

Risk is not significant due to the infrequent use and small quantities held.

6 ACTIONS RESULTING FROM ASSESSMENT RESULTS
(only further actions that need to be carried out)

Requires no further action	<input type="checkbox"/>
Seek expert help	<input type="checkbox"/>
Requires appropriate control measures	<input checked="" type="checkbox"/>
Requires induction and training <i>(safety induction to work areas)</i>	<input checked="" type="checkbox"/>
Requires emergency procedures/first aid	<input type="checkbox"/>

If Risk is SIGNIFICANT can the substance be:

	Yes	No
Eliminated	<input type="checkbox"/>	<input checked="" type="checkbox"/>
Substituted (less hazardous substances)	<input type="checkbox"/>	<input checked="" type="checkbox"/>
Separated (eg relocated from workers)	<input type="checkbox"/>	<input checked="" type="checkbox"/>
Enclosed (isolated)	<input checked="" type="checkbox"/>	<input type="checkbox"/>
Controlled by ventilation/engineering controls	<input checked="" type="checkbox"/>	<input type="checkbox"/>
Isolated (eg restrict entry, organise job rotation, personnel not allowed to work alone)	<input checked="" type="checkbox"/>	<input type="checkbox"/>

Controlled by the use of PPE (this is to be used as a last resort only)

7 DO YOU BELIEVE AIR MONITORING IS REQUIRED?

Yes No

If the degree of exposure is high and the existing control measures are inadequate, then it is likely air monitoring is required.

8 DO YOU BELIEVE HEALTH SURVEILLANCE IS REQUIRED?

Yes No

If the degree of exposure is high and the substance is listed in column 1 of schedule 6 of the QLD Workplace Hazardous Substances Regulations then health surveillance will be required.

NOTE: THIS RISK ASSESSMENT IS ONLY RELEVANT ON THE CONDITION THAT ALL CONTROLS ARE IN PLACE AND USED AND ALL INSTRUCTIONS AS PROVIDED BY THE MSDS AND RISK ASSESSMENT ARE COMPLIED WITH.

SIGNATURE OF ASSESSOR/S:

AB

Date: 26/4/15

APPROVED BY:

[Signature]

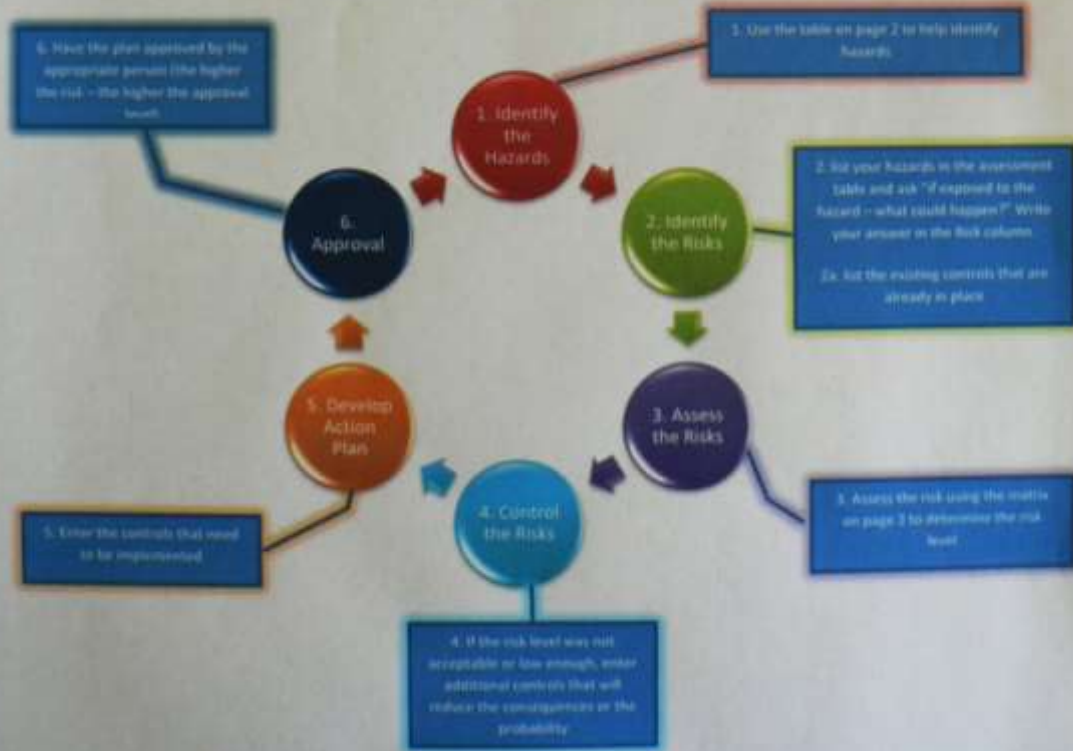
Date: 26/4/15



Generic Risk Management Plan

Workplace (Division/Faculty/Section): Engineering & Built Environment		
Assessment No (if applicable):	Assessment Date: 26/4/15	Review Date: (5 years maximum) 1/7/15
Context: What is being assessed? Describe the item, job, process, work arrangement, event etc: The safety risks involved with casting concrete beams, (3 cylinders) Subjecting them to strength tests & exposing them to heat		
Assessment Team – who is conducting the assessment?		
Assessor(s): Amy Bernier & Jayantha Epearachchi Others consulted: (eg elected health and safety representative, other personnel exposed to risks) Piumika Ariyadasa		

The Risk Management Process



Step 1 - Identify the hazards (use this table to help identify hazards then list all hazards in the risk table)

General Work Environment

<input type="checkbox"/> Sun exposure	<input type="checkbox"/> Water (creek, river, beach, dam)	<input type="checkbox"/> Sound / Noise
<input type="checkbox"/> Animals / Insects	<input type="checkbox"/> Storms / Weather/Wind/Lightning	<input checked="" type="checkbox"/> Temperature (heat, cold)
<input checked="" type="checkbox"/> Air Quality	<input type="checkbox"/> Lighting	<input type="checkbox"/> Uneven Walking Surface
<input checked="" type="checkbox"/> Trip Hazards	<input type="checkbox"/> Confined Spaces	<input type="checkbox"/> Restricted access/egress
<input type="checkbox"/> Pressure (Diving/Altitude)	<input type="checkbox"/> Smoke	<input type="checkbox"/>

Other/Details: *Air Quality - Cement, Trip - Thermocouple & sensor cords, Temperature-Heat*

Machinery, Plant and Equipment

<input type="checkbox"/> Machinery (fixed plant)	<input type="checkbox"/> Machinery (portable)	<input checked="" type="checkbox"/> Hand tools
<input type="checkbox"/> Laser (Class 2 or above)	<input type="checkbox"/> Elevated work platforms	<input type="checkbox"/> Traffic Control
<input type="checkbox"/> Non-powered equipment	<input type="checkbox"/> Pressure Vessel	<input type="checkbox"/> Electrical
<input checked="" type="checkbox"/> Vibration	<input checked="" type="checkbox"/> Moving Parts	<input type="checkbox"/> Acoustic/Noise
<input type="checkbox"/> Vehicles	<input type="checkbox"/> Trailers	<input type="checkbox"/> Hand tools

Other/Details: *Hand Tools - Preparation of reinforcement & concrete, vibrator - for concrete*

Manual Tasks / Ergonomics

<input type="checkbox"/> Manual tasks (repetitive, heavy)	<input type="checkbox"/> Working at heights	<input type="checkbox"/> Restricted space
<input checked="" type="checkbox"/> Vibration	<input checked="" type="checkbox"/> Lifting Carrying	<input type="checkbox"/> Pushing/pulling
<input type="checkbox"/> Reaching/Overstretching	<input type="checkbox"/> Repetitive Movement	<input type="checkbox"/> Bending
<input type="checkbox"/> Eye strain	<input type="checkbox"/> Machinery (portable)	<input type="checkbox"/> Hand tools

Other/Details: *Vibration of concrete in mould, Lifting-concrete beams via hand/machine*

Biological (e.g. hygiene, disease, infection)

<input type="checkbox"/> Human tissue/fluids	<input type="checkbox"/> Virus / Disease	<input type="checkbox"/> Food handling
<input type="checkbox"/> Microbiological	<input type="checkbox"/> Animal tissue/fluids	<input type="checkbox"/> Allergenic

Other/Details:

Chemicals Note: Refer to the label and Safety Data Sheet (SDS) for the classification and management of all chemicals.

<input checked="" type="checkbox"/> Non-hazardous chemical(s)	<input type="checkbox"/> 'Hazardous' chemical (Refer to a completed hazardous chemical risk assessment)
<input type="checkbox"/> Engineered nanoparticles	<input type="checkbox"/> Explosives
<input checked="" type="checkbox"/> Gas Cylinders	

Name of chemical(s) / Details: *Cement*

Critical Incident - resulting in:

<input type="checkbox"/> Lockdown	<input checked="" type="checkbox"/> Evacuation	<input type="checkbox"/> Disruption
<input type="checkbox"/> Public Image/Adverse Media Issue	<input type="checkbox"/> Violence	<input type="checkbox"/> Environmental Issue

Other/Details:

Radiation

<input type="checkbox"/> Ionising radiation	<input type="checkbox"/> Ultraviolet (UV) radiation	<input type="checkbox"/> Radio frequency/microwave
<input checked="" type="checkbox"/> Infrared (IR) radiation	<input type="checkbox"/> Laser (class 2 or above)	<input type="checkbox"/>

Other/Details: *IR - FBG Sensors & Pen for ensuring their survival*

Energy Systems - incident / issues involving:

<input type="checkbox"/> Electricity (incl. Mains and Solar)	<input checked="" type="checkbox"/> LPG Gas	<input type="checkbox"/> Gas / Pressurised containers
--	---	---

Other/Details: *LPG Gas bottle for heating*

Facilities / Built Environment

<input type="checkbox"/> Buildings and fixtures	<input type="checkbox"/> Driveway / Paths	<input checked="" type="checkbox"/> Workshops / Work rooms
<input type="checkbox"/> Playground equipment	<input type="checkbox"/> Furniture	<input type="checkbox"/> Swimming pool

Other/Details: *P2, P11, P3 & Z1*

People Issues

<input checked="" type="checkbox"/> Students	<input checked="" type="checkbox"/> Staff	<input type="checkbox"/> Visitors / Others
<input type="checkbox"/> Physical	<input type="checkbox"/> Psychological / Stress	<input type="checkbox"/> Contractors
<input type="checkbox"/> Fatigue	<input type="checkbox"/> Workload	<input type="checkbox"/> Organisational Change
<input type="checkbox"/> Workplace Violence/Bullying	<input type="checkbox"/> Inexperienced/new personnel	<input type="checkbox"/>

Other/Details:

Risk Matrix

Eg 1. Enter
Consequence

		Consequence				
Probability		Insignificant No Injury 0-\$5K	Minor First Aid \$5K-\$50K	Moderate Med Treatment \$50K-\$100K	Major Serious Injuries \$100K-\$250K	Catastrophic Death More than \$250K
Eg 2. Enter Probability	Almost Certain 1 in 2	M	H	S	S	S
	Likely 1 in 100	M	H	H	S	S
	Possible 1 in 1000	L	M	H	H	H
	Unlikely 1 in 10 000	L	L	M	M	M
	Rare 1 in 1 000 000	L	L	L	L	L
Recommended Action Guide						
S-High Risk - Full MS&P/MSF process						
M-Moderate Risk - Special Procedures Required (See USQSR)						
M-Moderate Risk - Risk Management Plan/Work Method Statement Required						
L-Low Risk - Use Routine Procedures						

Eg 3. Find
Action

Appendix C – Interrogation Unit Specifications

Specifications	sm125-200	sm125-500	sm125-700
Optical Properties			
Number of Optical Channels ¹	1	4	4
Scan Frequency	1 Hz	2 Hz	5 Hz
Wavelength Range	1520-1580 nm	1510-1590 nm	1510-1590 nm
Wavelength Accuracy ²	10 pm	1 pm	2.5 pm
Wavelength Stability ³	5pm	1 pm	2.5 pm
Wavelength Repeatability ⁴	1 pm at 1 Hz	0.5 pm at 1 Hz, 0.2 pm at 0.1 Hz	
Dynamic Range ⁵	40 dB	50 dB	30 dB
Typical FBG Sensor Capacity ^{6,7}	15	80	80
Full Spectrum Measurement		Included	
Internal Peak Detection Mode		Included	
sm041 Switch Compatible ¹	No	Yes	Yes
Optical Connectors	FC/APC (E2000 available)		
Data Processing Capabilities			
Interfaces	Ethernet - other interfaces available via an sp125 Sensing Processor Module		
Protocols	Custom Micron Optics protocol via Ethernet		
Remote Software	Spectral analysis, peak detection, data logger, peak tracking, and instrument control		
LabVIEW™ Source Code	Allows for customization of remote software		
Enhanced Data Management	ENLIGHT Sensing Analysis Software		
Mechanical, Environmental, Electrical Properties			
Dimensions; Weight	117 mm x 234 mm x 135 mm; 2 kg (4.5 lbs)		
Operating Temperature; Humidity	0° to 50° C; 0 to 90%, non-condensing		
Storage Temperature; Humidity	-20° to 70° C; 0 to 95%, non-condensing		
Input Voltage	7-36 VDC (100-240 VAC, 47-63 Hz), AC/DC converter included		
Power Consumption at 12V	20W typ, 30 Max		
Options			
8 or 16 Channel Expansion	Please see our 8 or 16 channel sm041 multiplexers		
Increased Scan Frequency ⁸	2, 5, or 10 Hz		
Notes:			
1. Expansion requires 4 integrated optical channels to operate an sm041-408 or sm041-416 switch type multiplexer.			
2. Per NIST Technical Note 1297, 1994 Edition, Section D.1.1.1, definition of "accuracy of measurement"			
3. Captures effects of long term use over full operating temperature range of the instrument.			
4. Per NIST Technical Note 1297, 1994 Edition, Section D.1.1.2, definition of "repeatability [of results of measurements]"			
5. Defined as laser launch power minus detection noise floor			
6. 10 Hz scan rate available with 40 nm (1525-1565nm) wavelength range.			
7. Assuming nominal wavelength range of +/- 2nm per FBG sensor			

Figure 69 - Optical Sensing Interrogator Specifications (Micron Optics Inc, 2009)

Appendix D – Additional Theoretical Analysis Results

Appendix D1 – Midpoint Deflections Associated with Loading Beam

Table 16 – Theoretical Midpoint Deflections Associated with Loading Beam

Control Beam		Heated Beam	
Load (kN)	Deflection (mm)	Load (kN)	Deflection (mm)
5.00	0.02	5.00	0.03
10.01	0.05	10.00	0.07
15.00	0.07	15.00	0.10
20.01	0.10	20.01	0.13
25.01	0.12	25.00	0.16
30.00	0.15	30.01	0.20
35.00	0.17	35.01	0.23
40.00	0.20	40.00	0.26
45.01	0.22	45.01	0.29
50.00	0.24	50.01	0.33
55.00	0.27	55.00	0.36
60.00	0.29	60.02	0.39
61.86	0.30	61.86	0.40

Appendix D2 – Maximum Principal Strains Associated with Loading Beam

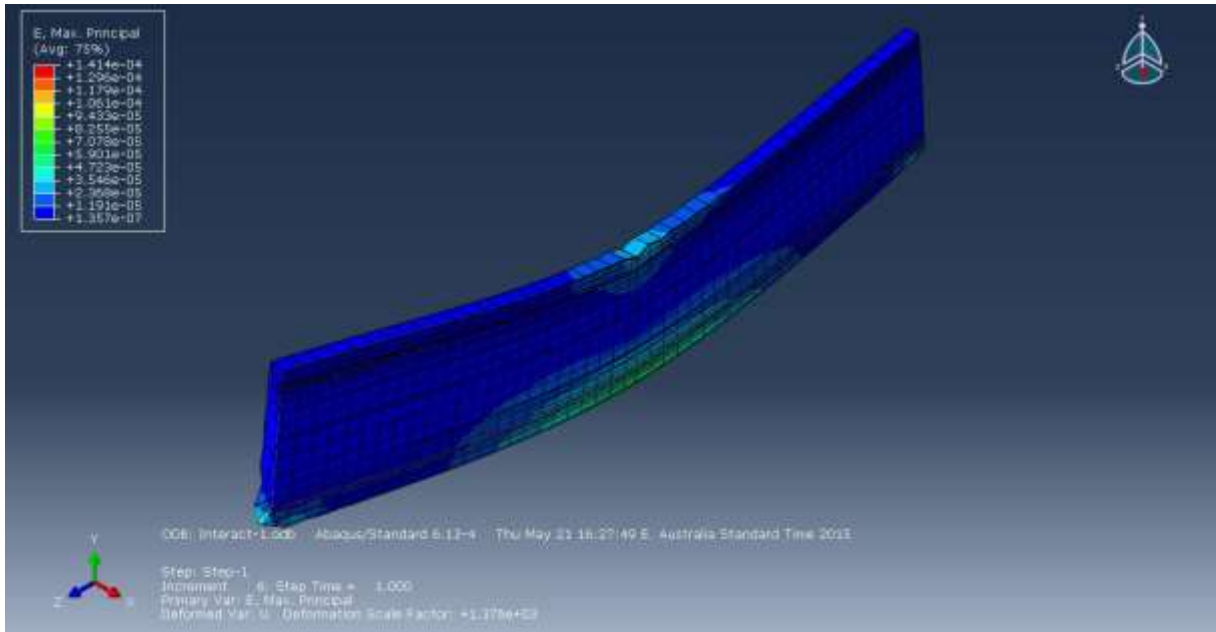


Figure 70 - Theoretical Maximum Principal Strain through Reinforcement Bars

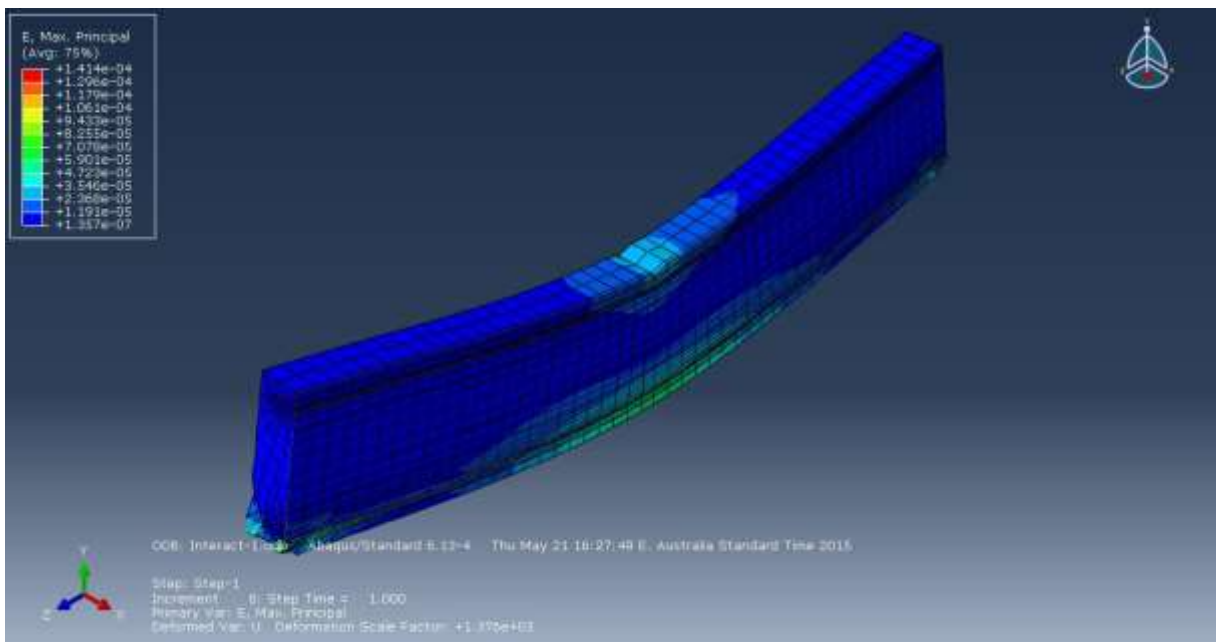


Figure 71 – Theoretical Maximum Principal Strain through Reinforcement Bars

Table 17 - Theoretical Maximum Principal Strains as Per Static Model

Load (kN)	Strain $\times 10^{-6}$			
	Control - SG	Heated - SG	Control - FBG	Heated - FBG
0.00	0.00	0.00	0.00	0.00
5.00	18.29	19.51	9.15	9.76
10.00	54.88	58.54	45.73	48.78
15.00	91.46	97.56	82.32	87.81
20.00	128.05	136.59	118.90	126.83
25.00	164.63	175.61	155.49	165.85
30.00	201.22	214.63	192.07	204.88
35.00	237.81	253.66	228.66	243.90
40.00	274.39	292.68	265.24	282.93
45.00	310.98	331.71	301.83	321.95
50.00	347.56	370.73	338.42	360.98
55.00	384.15	409.76	375.00	400.00
60.00	420.73	448.78	411.59	439.02
61.86	574.63	612.94	448.17	478.05

Table 18 - Validation of Theoretical Strains via Hand Calculations

Load (kN)	Strain x10⁻⁶	
	Control	Heated
0.00	0.00	0.00
5.00	36.59	39.02
10.00	73.17	78.05
15.00	109.76	117.07
20.00	146.34	156.10
25.00	182.93	195.12
30.00	219.51	234.15
35.00	256.10	273.17
40.00	292.68	312.20
45.00	329.27	351.22
50.00	365.85	390.24
55.00	402.44	429.27
60.00	439.02	468.29
61.86	452.63	482.81

Appendix D3 – Maximum Principal Stresses Associated with Loading Beam

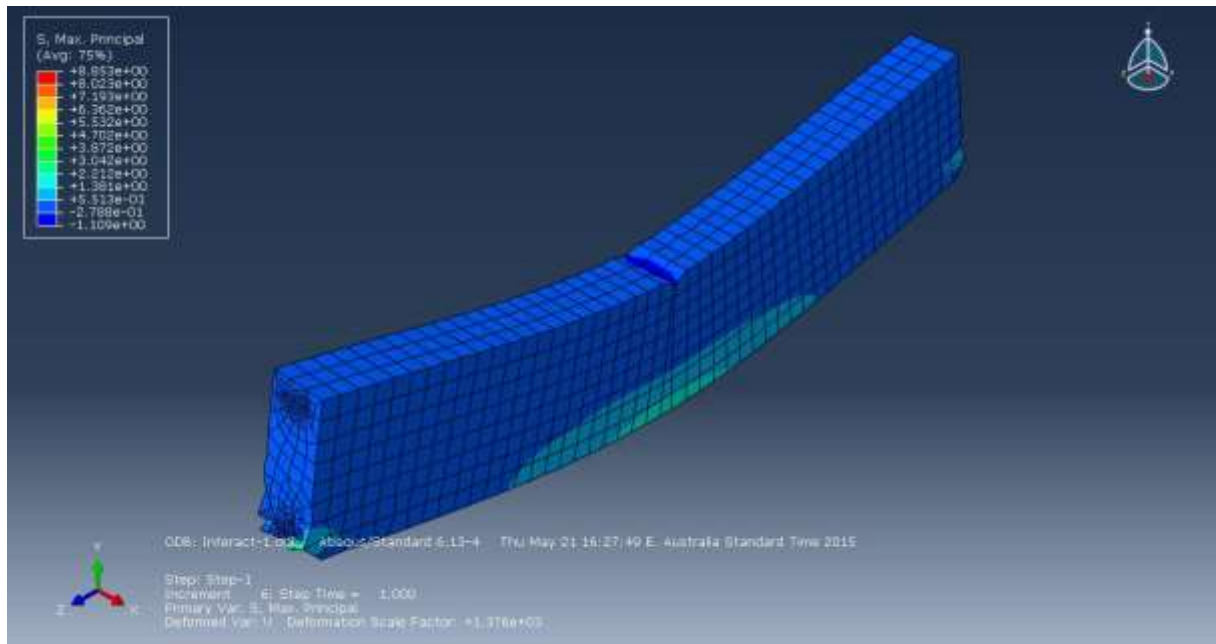


Figure 72 – Theoretical Maximum Principal Stress over Entire Beam Structure

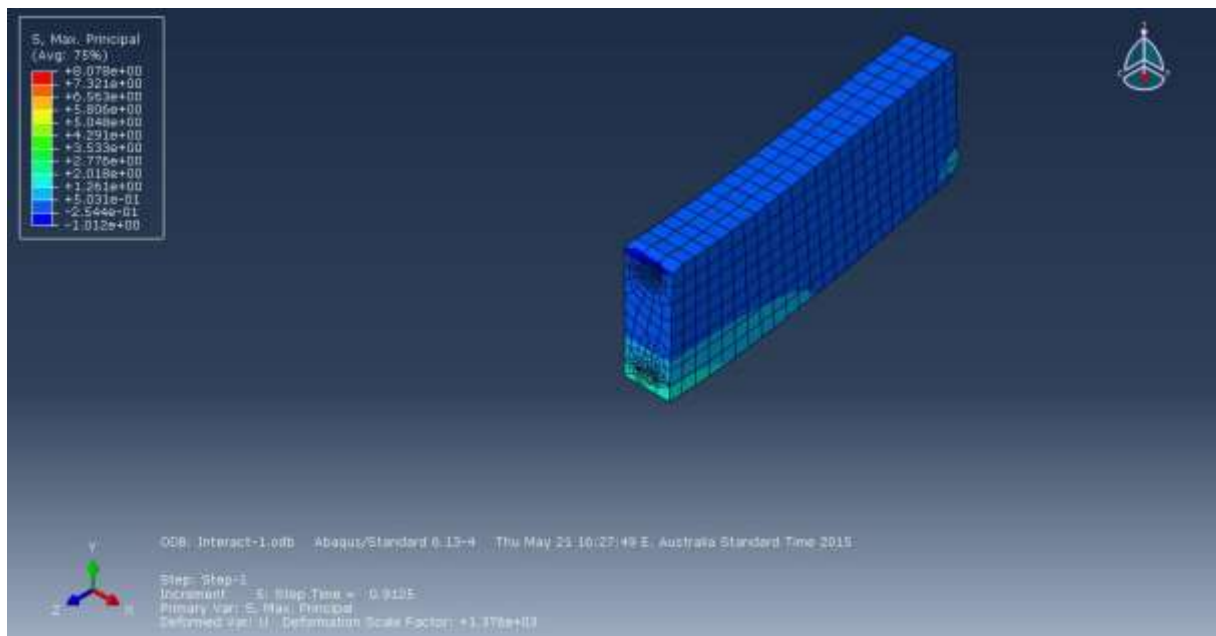


Figure 73 – Theoretical Maximum Principal Stress through Centre of Beam

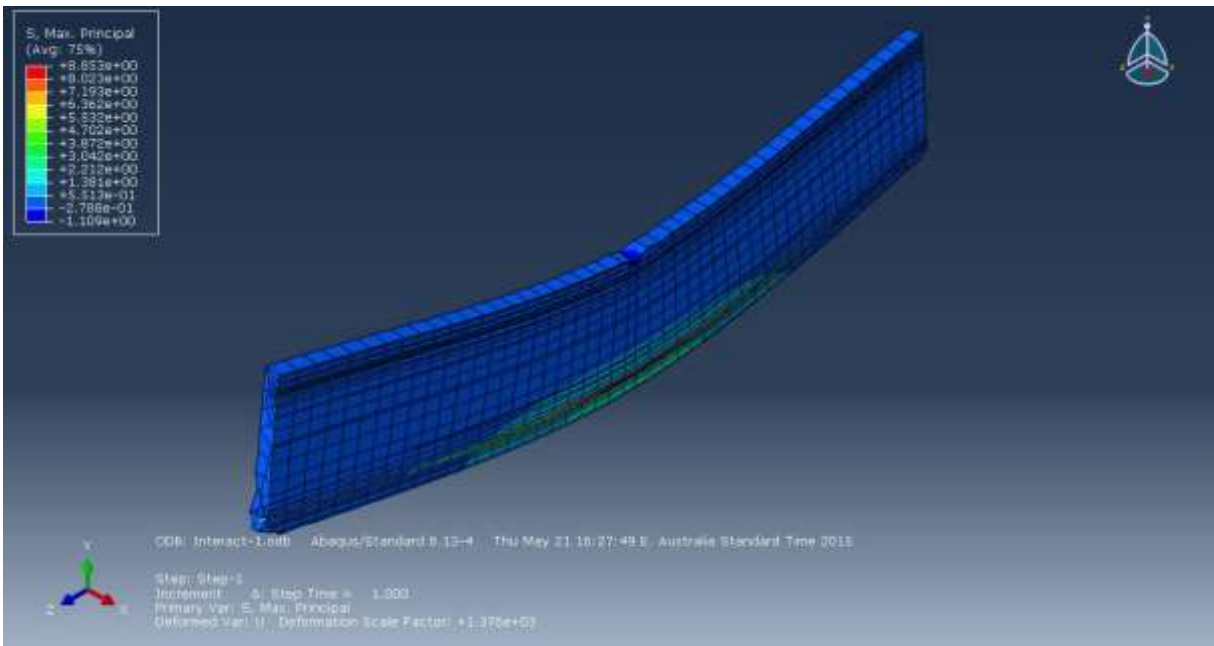


Figure 74 – Theoretical Maximum Principal Stress through Reinforcement

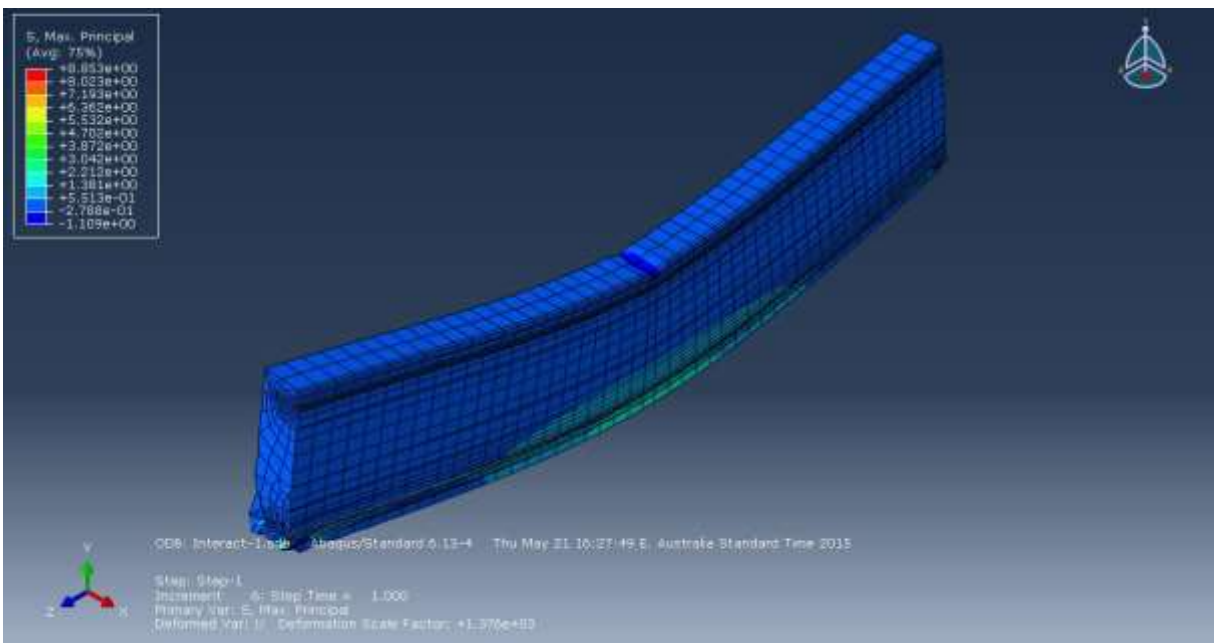


Figure 75 – Theoretical Maximum Principal Stress through Reinforcement

Table 19 – Theoretical Maximum Principal Stresses as Per Static Model

Load (kN)	Stress (MPa)			
	Control - SG	Heated - SG	Control - FBG	Heated - FBG
0.00	0.00	0.00	0.00	0.00
5.00	0.60	0.48	0.30	0.24
10.00	1.80	1.44	1.50	1.20
15.00	3.00	2.40	2.70	2.16
20.00	4.20	3.36	3.90	3.12
25.00	5.40	4.32	5.10	4.08
30.00	6.60	5.28	6.30	5.04
35.00	7.80	6.24	7.50	6.00
40.00	9.00	7.20	8.70	6.96
45.00	10.20	8.16	9.90	7.92
50.00	11.40	9.12	11.10	8.88
55.00	12.60	10.08	12.30	9.84
60.00	13.80	11.04	13.50	10.80
61.86	18.85	15.08	14.70	11.76

Table 20 - Validation of Theoretical Stresses via Hand Calculations

Load (kN)	Stress (MPa)	
	Control	Heated
0.00	0.00	0.00
5.00	1.20	0.96
10.00	2.40	1.92
15.00	3.60	2.88
20.00	4.80	3.84
25.00	6.00	4.80
30.00	7.20	5.76
35.00	8.40	6.72
40.00	9.60	7.68
45.00	10.80	8.64
50.00	12.00	9.60
55.00	13.20	10.56
60.00	14.40	11.52
61.86	14.85	11.88

Appendix E – Additional Experimental Analysis Results

Appendix E1 – Curing Temperatures of Beams

Table 21 - Experimental Curing Temperatures of Beam 1

Date	24 Hour Time	Beam 1 Curing Temperatures (Degrees Celsius)				
		TC 0 (FBG)	FBG	TC 1	TC 2	TC 3
12/08/2015	18:00	18.40	18.60	20.23	19.66	19.53
12/08/2015	19:00	17.82	18.02	19.95	19.28	18.32
12/08/2015	20:00	17.30	17.50	19.33	18.72	17.43
12/08/2015	21:00	16.75	16.95	18.66	18.15	16.75
12/08/2015	22:00	16.13	16.33	18.03	17.60	16.26
12/08/2015	23:00	15.44	15.64	17.24	16.91	15.58
12/08/2015	0:00	14.76	14.96	16.49	16.24	14.92
13/08/2015	1:00	14.12	14.32	15.81	15.67	14.30
13/08/2015	2:00	13.52	13.72	15.13	15.08	13.70
13/08/2015	3:00	12.97	13.17	14.49	14.53	13.14
13/08/2015	4:00	12.48	12.68	13.94	14.05	12.64
13/08/2015	5:00	12.01	12.21	13.43	13.62	12.18
13/08/2015	6:00	11.63	11.83	13.00	13.25	11.81
13/08/2015	7:00	11.27	11.47	12.61	12.91	11.47
13/08/2015	8:00	11.01	11.21	12.28	12.61	11.12
13/08/2015	9:00	11.09	11.29	12.37	12.66	10.99
13/08/2015	10:00	11.10	11.20	12.43	12.72	11.05
13/08/2015	11:00	11.30	11.40	12.58	12.80	11.12
13/08/2015	12:00	11.45	11.55	12.75	12.97	11.31
13/08/2015	13:00	11.64	11.74	12.94	13.14	11.51
13/08/2015	14:00	11.87	11.97	13.22	13.43	11.79
13/08/2015	15:00	12.23	12.33	13.65	13.78	12.14
13/08/2015	16:00	12.63	12.73	14.10	14.19	12.55
13/08/2015	17:00	13.07	13.17	14.60	14.68	13.10
13/08/2015	18:00	13.50	13.60	15.12	15.12	13.52
13/08/2015	19:00	13.78	13.88	15.47	15.44	13.81

13/08/2015	20:00	13.98	14.08	15.71	15.66	14.01
13/08/2015	21:00	14.15	14.25	15.89	15.79	14.07
13/08/2015	22:00	14.25	14.35	16.07	15.93	14.17
13/08/2015	23:00	14.35	14.45	16.08	15.99	14.31
13/08/2015	0:00	14.46	14.56	16.17	16.09	14.41
14/08/2015	1:00	14.42	14.52	16.24	16.17	14.49
14/08/2015	2:00	14.47	14.57	16.34	16.20	14.53
14/08/2015	3:00	14.54	14.64	16.35	16.24	14.54
14/08/2015	4:00	14.48	14.58	16.26	16.15	14.45
14/08/2015	5:00	14.37	14.27	16.12	16.06	14.38
14/08/2015	6:00	14.17	14.07	16.06	15.93	14.22
14/08/2015	7:00	14.11	14.01	15.98	15.89	14.14
14/08/2015	8:00	14.21	14.11	16.01	15.91	14.17
14/08/2015	9:00	14.27	14.17	16.10	16.00	14.26
14/08/2015	10:00	14.39	14.29	16.29	16.17	14.42
14/08/2015	11:00	14.60	14.50	16.52	16.41	14.68
14/08/2015	12:00	14.92	14.82	16.86	16.72	14.97
14/08/2015	13:00	15.25	15.15	17.28	17.08	15.35
14/08/2015	14:00	15.70	15.60	17.76	17.51	15.78
14/08/2015	15:00	16.13	16.03	18.29	17.95	16.23
14/08/2015	16:00	16.67	16.57	18.85	18.42	16.72
14/08/2015	17:00	17.13	17.03	19.39	18.89	17.38
14/08/2015	18:00	17.41	17.31	19.74	19.27	18.19
14/08/2015	19:00	17.55	17.45	19.80	19.29	18.24
14/08/2015	20:00	17.45	17.35	19.66	19.13	17.87
14/08/2015	21:00	17.20	17.10	19.35	18.83	17.35
14/08/2015	22:00	16.87	16.77	18.92	18.51	16.92
14/08/2015	23:00	16.38	16.28	18.49	18.11	16.48
14/08/2015	0:00	16.01	15.91	18.05	17.70	16.06
15/08/2015	1:00	15.60	15.50	17.61	17.29	15.61
15/08/2015	2:00	15.21	15.11	17.22	16.94	15.25
15/08/2015	3:00	14.88	14.78	16.80	16.58	14.88
15/08/2015	4:00	14.56	14.46	16.44	16.26	14.55
15/08/2015	5:00	14.23	14.13	16.10	15.95	14.21

15/08/2015	6:00	13.99	13.89	15.73	15.64	13.94
15/08/2015	7:00	13.69	13.59	15.43	15.33	13.64
15/08/2015	8:00	13.60	13.50	15.21	15.14	13.45
15/08/2015	9:00	13.50	13.40	15.14	15.12	13.43
15/08/2015	10:00	13.56	13.46	15.22	15.21	13.50
15/08/2015	11:00	13.71	13.61	15.42	15.36	13.67
15/08/2015	12:00	13.94	13.84	15.66	15.59	13.89
15/08/2015	13:00	14.21	14.11	16.00	15.88	14.20
15/08/2015	14:00	14.54	14.44	16.37	16.22	14.56
15/08/2015	15:00	14.96	14.86	16.83	16.57	14.93
15/08/2015	16:00	15.30	15.20	17.23	16.95	15.30
15/08/2015	17:00	15.68	15.58	17.65	17.34	15.73
15/08/2015	18:00	16.02	15.92	17.99	17.66	16.06
15/08/2015	19:00	16.14	16.04	18.15	17.82	16.26
15/08/2015	20:00	16.14	16.04	18.15	17.83	16.28
15/08/2015	21:00	16.10	16.00	18.12	17.68	16.06
15/08/2015	22:00	16.00	15.90	17.98	17.59	15.95
15/08/2015	23:00	15.82	15.72	17.84	17.47	15.79
15/08/2015	0:00	15.65	15.55	17.67	17.34	15.65
16/08/2015	1:00	15.45	15.35	17.50	17.18	15.48
16/08/2015	2:00	15.24	15.14	17.26	16.99	15.27
16/08/2015	3:00	14.98	14.88	16.99	16.76	15.02
16/08/2015	4:00	14.72	14.82	16.71	16.50	14.77
16/08/2015	5:00	14.45	14.55	16.40	16.23	14.48
16/08/2015	6:00	14.16	14.26	16.05	15.93	14.18
16/08/2015	7:00	13.89	13.99	15.75	15.67	13.91
16/08/2015	8:00	13.72	13.82	15.46	15.38	13.67
16/08/2015	9:00	13.64	13.74	15.34	15.32	13.61
16/08/2015	10:00	13.69	13.79	15.42	15.39	13.68
16/08/2015	11:00	13.87	13.97	15.64	15.57	13.87
16/08/2015	12:00	14.53	14.63	16.39	16.22	14.54
16/08/2015	13:00	14.95	15.05	16.86	16.64	14.99
16/08/2015	14:00	15.38	15.48	17.34	17.08	15.44
16/08/2015	15:00	15.80	15.90	17.81	17.47	15.85

16/08/2015	16:00	16.14	15.94	18.20	17.82	16.21
16/08/2015	17:00	16.40	16.20	18.47	18.07	16.47
16/08/2015	18:00	16.50	16.30	18.60	18.18	16.56
16/08/2015	19:00	16.52	16.32	18.61	18.21	16.58
16/08/2015	20:00	16.51	16.31	18.58	18.16	16.54
16/08/2015	21:00	16.38	16.18	18.49	18.06	16.40
16/08/2015	22:00	16.29	16.09	18.38	17.95	16.29
16/08/2015	23:00	16.13	15.93	18.21	17.83	16.14
16/08/2015	0:00	16.01	15.81	18.06	17.70	16.02
17/08/2015	1:00	15.81	15.61	17.91	17.57	15.87
17/08/2015	2:00	15.65	15.45	17.73	17.40	15.67
17/08/2015	3:00	15.43	15.23	17.51	17.20	15.48
17/08/2015	4:00	15.22	15.02	17.26	17.00	15.26
17/08/2015	5:00	14.99	14.79	17.00	16.75	15.00
17/08/2015	6:00	14.73	14.53	16.70	16.49	14.76
17/08/2015	7:00	14.59	14.39	16.44	16.27	14.55
17/08/2015	8:00	14.46	14.26	16.34	16.20	14.48
17/08/2015	9:00	14.55	14.35	16.38	16.25	14.59
17/08/2015	10:00	14.66	14.76	16.53	16.40	14.73
17/08/2015	11:00	14.91	15.01	16.79	16.62	14.95
17/08/2015	12:00	15.19	15.29	17.11	16.87	15.21
17/08/2015	13:00	15.45	15.55	17.43	17.14	15.49
17/08/2015	14:00	15.71	15.81	17.72	17.42	15.76
17/08/2015	15:00	16.05	16.15	18.08	17.73	16.11
17/08/2015	16:00	16.34	16.44	18.42	18.03	16.40
17/08/2015	17:00	16.61	16.71	18.68	18.27	16.66
17/08/2015	18:00	16.67	16.77	18.80	18.41	16.83
17/08/2015	19:00	16.66	16.76	18.82	18.43	16.84
17/08/2015	20:00	16.68	16.78	18.76	18.30	16.67
17/08/2015	21:00	16.51	16.61	18.57	18.20	16.59
17/08/2015	22:00	16.30	16.40	18.36	18.01	16.40
17/08/2015	23:00	16.05	16.15	18.15	17.77	16.11
17/08/2015	0:00	15.83	15.93	17.91	17.53	15.86
18/08/2015	1:00	15.60	15.70	17.63	17.32	15.62

18/08/2015	2:00	15.35	15.45	17.38	17.07	15.38
18/08/2015	3:00	15.10	15.20	17.07	16.83	15.11
18/08/2015	4:00	14.82	15.02	16.80	16.58	14.86
18/08/2015	5:00	14.57	14.77	16.51	16.32	14.60
18/08/2015	6:00	14.38	14.58	16.21	16.05	14.32
18/08/2015	7:00	14.22	14.42	16.00	15.88	14.15
18/08/2015	8:00	14.09	14.29	15.87	15.78	14.09
18/08/2015	9:00	14.08	14.28	15.86	15.76	14.09
18/08/2015	10:00	14.14	14.34	15.90	15.81	14.11
18/08/2015	11:00	14.24	14.44	16.01	15.92	14.26
18/08/2015	12:00	14.42	14.62	16.20	16.10	14.44
18/08/2015	13:00	14.66	14.86	16.45	16.33	14.67
18/08/2015	14:00	14.93	15.13	16.79	16.58	14.93
18/08/2015	15:00	15.20	15.40	17.15	16.89	15.25
18/08/2015	16:00	15.56	15.76	17.52	17.23	15.61
18/08/2015	17:00	15.84	16.04	17.82	17.50	15.90
18/08/2015	18:00	15.95	16.15	17.99	17.70	16.08
18/08/2015	19:00	16.02	16.22	18.03	17.69	16.08
18/08/2015	20:00	15.97	16.17	17.94	17.63	15.99
18/08/2015	21:00	15.84	16.04	17.80	17.50	15.86
18/08/2015	22:00	15.63	15.83	17.65	17.31	15.65
18/08/2015	23:00	15.40	15.60	17.42	17.14	15.44
18/08/2015	0:00	15.18	15.38	17.20	16.92	15.20
19/08/2015	1:00	14.98	15.18	16.94	16.71	14.98
19/08/2015	2:00	14.73	14.93	16.65	16.46	14.74
19/08/2015	3:00	14.55	14.75	16.35	16.22	14.52
19/08/2015	4:00	14.26	14.46	16.10	15.98	14.26
19/08/2015	5:00	14.12	14.32	15.81	15.74	14.04
19/08/2015	6:00	13.85	14.05	15.59	15.51	13.79
19/08/2015	7:00	13.75	13.95	15.43	15.34	13.66
19/08/2015	8:00	13.65	13.85	15.37	15.34	13.63
19/08/2015	9:00	13.73	13.93	15.47	15.42	13.72
19/08/2015	10:00	13.89	14.09	15.65	15.61	13.92
19/08/2015	11:00	14.21	14.41	15.96	15.87	14.23

19/08/2015	12:00	14.52	14.72	16.36	16.21	14.55
19/08/2015	13:00	14.90	15.10	16.77	16.59	14.91
19/08/2015	14:00	15.30	15.50	17.23	16.96	15.33
19/08/2015	15:00	15.64	15.84	17.61	17.31	15.69
19/08/2015	16:00	15.98	16.18	17.97	17.62	16.00
19/08/2015	17:00	16.25	16.45	18.27	17.89	16.26
19/08/2015	18:00	16.38	16.58	18.41	18.01	16.37
19/08/2015	19:00	16.38	16.58	18.43	18.05	16.41
19/08/2015	20:00	16.33	16.53	18.41	17.99	16.34
19/08/2015	21:00	16.21	16.41	18.26	17.94	16.36
19/08/2015	22:00	16.07	16.27	18.12	17.77	16.15
19/08/2015	23:00	15.89	16.09	17.95	17.60	15.95
19/08/2015	0:00	15.70	15.90	17.74	17.41	15.74
20/08/2015	1:00	15.47	15.67	17.52	17.20	15.58
20/08/2015	2:00	15.26	15.46	17.28	16.98	15.34
20/08/2015	3:00	15.06	15.26	17.03	16.78	15.09
20/08/2015	4:00	14.85	15.05	16.79	16.55	14.83
20/08/2015	5:00	14.64	14.84	16.54	16.32	14.62
20/08/2015	6:00	14.38	14.58	16.30	16.12	14.48
20/08/2015	7:00	14.31	14.51	16.11	15.97	14.25
20/08/2015	8:00	14.21	14.41	16.01	15.92	14.22
20/08/2015	9:00	14.24	14.44	16.03	15.95	14.25
20/08/2015	10:00	14.32	14.52	16.14	16.05	14.39
20/08/2015	11:00	14.48	14.78	16.31	16.22	14.56
20/08/2015	12:00	14.70	15.00	16.57	16.44	14.74
20/08/2015	13:00	14.99	15.29	16.89	16.73	15.05
20/08/2015	14:00	15.33	15.63	17.26	17.02	15.37
20/08/2015	15:00	15.67	15.97	17.63	17.36	15.72
20/08/2015	16:00	16.02	16.32	18.00	17.68	16.05
20/08/2015	17:00	16.27	16.57	18.30	17.92	16.29
20/08/2015	18:00	16.41	16.71	18.45	18.06	16.41
20/08/2015	19:00	16.43	16.73	18.49	18.10	16.46
20/08/2015	20:00	16.39	16.69	18.46	18.07	16.42
20/08/2015	21:00	16.30	16.60	18.35	18.03	16.40

20/08/2015	22:00	16.19	16.49	18.24	17.89	16.25
20/08/2015	23:00	16.03	16.33	18.08	17.72	16.05
20/08/2015	0:00	15.89	16.19	17.92	17.56	15.88
21/08/2015	1:00	15.74	16.04	17.78	17.42	15.76
21/08/2015	2:00	15.61	15.91	17.61	17.28	15.60
21/08/2015	3:00	15.48	15.78	17.45	17.14	15.48
21/08/2015	4:00	15.34	15.64	17.31	17.01	15.36
21/08/2015	5:00	15.24	15.54	17.18	16.90	15.22
21/08/2015	6:00	15.08	15.38	17.06	16.80	15.13
21/08/2015	7:00	15.03	15.33	16.95	16.72	15.04
21/08/2015	8:00	15.00	15.30	16.88	16.68	15.01
21/08/2015	9:00	15.00	15.30	16.89	16.69	15.00
21/08/2015	10:00	15.05	15.35	16.95	16.78	15.10
21/08/2015	11:00	15.18	15.48	17.12	16.93	15.24
21/08/2015	12:00	15.38	15.68	17.37	17.11	15.43
21/08/2015	13:00	15.62	15.92	17.61	17.30	15.65
21/08/2015	14:00	15.83	16.13	17.83	17.53	15.86
21/08/2015	15:00	16.03	16.33	18.05	17.69	16.04
21/08/2015	16:00	16.17	16.47	18.19	17.83	16.18
21/08/2015	17:00	16.25	16.55	18.28	17.89	16.25
21/08/2015	18:00	16.27	16.57	18.31	17.92	16.25
21/08/2015	19:00	16.23	16.53	18.30	17.93	16.28
21/08/2015	20:00	16.24	16.54	18.27	17.87	16.20
21/08/2015	21:00	16.17	16.47	18.21	17.82	16.16
21/08/2015	22:00	16.06	16.36	18.11	17.76	16.10
21/08/2015	23:00	15.99	16.29	18.04	17.69	16.03
21/08/2015	0:00	15.91	16.21	17.98	17.65	15.97
22/08/2015	1:00	15.84	16.14	17.90	17.59	15.92
22/08/2015	2:00	15.79	16.09	17.83	17.53	15.85
22/08/2015	3:00	15.73	16.03	17.75	17.46	15.78
22/08/2015	4:00	15.67	15.97	17.69	17.40	15.71
22/08/2015	5:00	15.66	15.96	17.63	17.33	15.67
22/08/2015	6:00	15.60	15.90	17.57	17.28	15.63
22/08/2015	7:00	15.56	15.86	17.53	17.24	15.58

22/08/2015	8:00	15.53	15.83	17.52	17.29	15.59
22/08/2015	9:00	15.61	15.91	17.61	17.31	15.62
22/08/2015	10:00	15.73	16.03	17.75	17.44	15.76
22/08/2015	11:00	15.97	16.27	17.99	17.64	15.98
22/08/2015	12:00	16.24	16.54	18.28	17.93	16.26
22/08/2015	13:00	16.59	16.89	18.69	18.28	16.64
22/08/2015	14:00	16.98	17.28	19.11	18.65	17.05
22/08/2015	15:00	17.34	17.64	19.54	19.03	17.73
22/08/2015	16:00	17.71	18.01	19.93	19.38	18.38
22/08/2015	17:00	17.96	18.26	20.15	19.63	18.80
22/08/2015	18:00	18.08	18.38	20.24	19.74	19.00
22/08/2015	19:00	18.08	18.38	20.25	19.77	19.01
22/08/2015	20:00	18.06	18.36	20.22	19.71	18.93
22/08/2015	21:00	17.96	18.26	20.15	19.64	18.77
22/08/2015	22:00	17.87	18.17	20.07	19.54	18.59
22/08/2015	23:00	17.75	18.05	19.99	19.42	18.40
22/08/2015	0:00	17.65	17.95	19.87	19.32	18.18
23/08/2015	1:00	17.56	17.86	19.76	19.20	17.97
23/08/2015	2:00	17.42	17.72	19.62	19.11	17.75
23/08/2015	3:00	17.29	17.59	19.47	18.98	17.51
23/08/2015	4:00	17.15	17.45	19.34	18.84	17.33
23/08/2015	5:00	17.03	17.33	19.18	18.74	17.09
23/08/2015	6:00	16.90	17.20	19.06	18.60	16.93
23/08/2015	7:00	16.77	17.07	18.92	18.49	16.83
23/08/2015	8:00	16.67	16.97	18.84	18.44	16.76
23/08/2015	9:00	16.70	17.00	18.85	18.41	16.72
23/08/2015	10:00	16.76	17.06	18.93	18.48	16.81
23/08/2015	11:00	16.94	17.24	19.09	18.64	16.97
23/08/2015	12:00	17.19	17.39	19.36	18.88	17.39
23/08/2015	13:00	17.49	17.69	19.71	19.18	17.94
23/08/2015	14:00	17.85	18.05	20.07	19.54	18.63
23/08/2015	15:00	18.19	18.39	20.31	19.87	19.22
23/08/2015	16:00	18.48	18.68	20.52	20.16	19.71
23/08/2015	17:00	18.70	18.90	20.68	20.37	20.09

23/08/2015	18:00	18.79	18.99	20.75	20.45	20.29
23/08/2015	19:00	18.77	18.97	20.75	20.44	20.27
23/08/2015	20:00	18.68	18.88	20.70	20.35	20.09
23/08/2015	21:00	18.56	18.76	20.59	20.28	19.95
23/08/2015	22:00	18.41	18.61	20.49	20.15	19.69
23/08/2015	23:00	18.24	18.44	20.38	19.95	19.28
23/08/2015	0:00	18.07	18.27	20.26	19.78	19.05
24/08/2015	1:00	17.89	18.09	20.12	19.61	18.69
24/08/2015	2:00	17.72	17.92	20.00	19.45	18.40
24/08/2015	3:00	17.62	17.82	19.84	19.30	18.12
24/08/2015	4:00	17.44	17.64	19.67	19.14	17.83
24/08/2015	5:00	17.27	17.47	19.49	19.01	17.63
24/08/2015	6:00	17.15	17.35	19.33	18.85	17.35
24/08/2015	7:00	17.02	17.22	19.18	18.73	17.12
24/08/2015	8:00	16.91	17.11	19.10	18.67	16.99
24/08/2015	9:00	16.93	17.13	19.12	18.66	16.99
24/08/2015	10:00	17.04	17.24	19.21	18.74	17.12
24/08/2015	11:00	17.21	17.41	19.37	18.88	17.41
24/08/2015	12:00	17.45	17.65	19.66	19.14	17.87
24/08/2015	13:00	17.78	17.98	20.03	19.48	18.49
24/08/2015	14:00	18.20	18.40	20.32	19.88	19.26
24/08/2015	15:00	18.63	18.83	20.63	20.30	20.03
24/08/2015	16:00	18.95	19.15	20.86	20.64	20.59
24/08/2015	17:00	19.19	19.39	21.04	20.85	20.99
24/08/2015	18:00	19.30	19.50	21.12	20.95	21.15
24/08/2015	19:00	19.30	19.50	21.13	20.95	21.19
24/08/2015	20:00	19.23	19.43	21.09	20.90	21.04
24/08/2015	21:00	19.15	19.35	21.03	20.80	20.88
24/08/2015	22:00	19.05	19.25	20.95	20.69	20.68
24/08/2015	23:00	18.91	19.11	20.87	20.57	20.44
24/08/2015	0:00	18.77	18.97	20.76	20.46	20.22
25/08/2015	1:00	18.60	18.80	20.66	20.29	19.94
25/08/2015	2:00	18.44	18.64	20.53	20.16	19.67
25/08/2015	3:00	18.27	18.47	20.40	19.98	19.38

25/08/2015	4:00	18.14	18.34	20.28	19.81	19.10
25/08/2015	5:00	17.95	18.15	20.15	19.66	18.78
25/08/2015	6:00	17.77	17.97	20.03	19.49	18.43
25/08/2015	7:00	17.65	17.85	19.94	19.38	18.25
25/08/2015	8:00	17.61	17.81	19.86	19.33	18.16
25/08/2015	9:00	17.60	17.80	19.85	19.30	18.10
25/08/2015	10:00	17.60	17.80	19.83	19.26	18.09
25/08/2015	11:00	17.60	17.80	19.83	19.28	18.08
25/08/2015	12:00	17.66	17.86	19.91	19.35	18.22
25/08/2015	13:00	17.78	17.98	20.02	19.46	18.40
25/08/2015	14:00	17.93	18.13	20.13	19.60	18.67
25/08/2015	15:00	18.10	18.30	20.27	19.78	19.02
25/08/2015	16:00	18.31	18.51	20.40	19.98	19.40
25/08/2015	17:00	18.49	18.69	20.52	20.14	19.71
25/08/2015	18:00	18.57	18.77	20.58	20.22	19.84
25/08/2015	19:00	18.56	18.76	20.60	20.22	19.87
25/08/2015	20:00	18.49	18.69	20.54	20.21	19.90
25/08/2015	21:00	18.35	18.55	20.44	20.06	19.58
25/08/2015	22:00	18.20	18.40	20.29	19.81	19.05
25/08/2015	23:00	18.01	18.21	20.13	19.58	18.64
25/08/2015	0:00	17.59	17.79	19.84	19.30	18.14
26/08/2015	1:00	17.28	17.48	19.51	18.99	17.64
26/08/2015	2:00	17.00	17.20	19.18	18.68	17.09
26/08/2015	3:00	16.69	16.89	18.85	18.39	16.77
26/08/2015	4:00	16.39	16.59	18.52	18.10	16.47
26/08/2015	5:00	16.14	16.34	18.24	17.83	16.21
26/08/2015	6:00	15.89	16.09	17.93	17.58	15.93
26/08/2015	7:00	15.66	15.86	17.68	17.39	15.70
26/08/2015	8:00	15.55	15.75	17.53	17.23	15.57
26/08/2015	9:00	15.50	15.70	17.47	17.18	15.52
26/08/2015	10:00	15.53	15.73	17.48	17.20	15.52
26/08/2015	11:00	15.61	15.81	17.56	17.29	15.62
26/08/2015	12:00	15.75	16.15	17.74	17.47	15.79
26/08/2015	13:00	16.03	16.43	18.04	17.72	16.05

26/08/2015	14:00	16.34	16.74	18.39	18.01	16.37
26/08/2015	15:00	16.67	17.07	18.78	18.35	16.72
26/08/2015	16:00	17.04	17.44	19.18	18.72	17.15
26/08/2015	17:00	17.39	17.79	19.55	19.05	17.79
26/08/2015	18:00	17.59	17.99	19.77	19.22	18.12
26/08/2015	19:00	17.62	18.02	19.87	19.33	18.27
26/08/2015	20:00	17.58	17.98	19.78	19.25	18.14
26/08/2015	21:00	17.46	17.86	19.67	19.14	17.94
26/08/2015	22:00	17.34	17.74	19.52	19.03	17.69
26/08/2015	23:00	17.15	17.55	19.34	18.83	17.38
26/08/2015	0:00	16.97	17.37	19.16	18.64	17.00
27/08/2015	1:00	16.81	17.21	18.97	18.48	16.81
27/08/2015	2:00	16.66	17.06	18.79	18.33	16.67
27/08/2015	3:00	16.53	16.93	18.64	18.19	16.53
27/08/2015	4:00	16.36	16.76	18.48	18.05	16.39
27/08/2015	5:00	16.24	16.64	18.33	17.90	16.24
27/08/2015	6:00	16.11	16.51	18.19	17.78	16.15
27/08/2015	7:00	16.02	16.42	18.05	17.67	15.99
27/08/2015	8:00	15.90	16.30	17.94	17.57	15.91
27/08/2015	9:00	15.87	16.27	17.86	17.56	15.90
27/08/2015	10:00	15.87	16.27	17.84	17.53	15.87
27/08/2015	11:00	15.86	16.26	17.85	17.53	15.86
27/08/2015	12:00	15.89	16.29	17.86	17.54	15.88
27/08/2015	13:00	15.88	16.28	17.89	17.58	15.90
27/08/2015	14:00	15.89	16.29	17.91	17.62	15.94
27/08/2015	15:00	15.91	16.31	17.97	17.65	15.96
27/08/2015	16:00	15.95	16.35	17.98	17.69	16.03
27/08/2015	17:00	15.98	16.38	18.02	17.70	16.05
27/08/2015	18:00	16.03	16.43	18.02	17.69	16.05
27/08/2015	19:00	16.01	16.41	18.02	17.69	16.03
27/08/2015	20:00	16.00	16.40	18.00	17.68	16.00
27/08/2015	21:00	15.95	16.35	17.96	17.64	15.97
27/08/2015	22:00	15.95	16.35	17.93	17.60	15.93
27/08/2015	23:00	15.88	16.28	17.88	17.56	15.90

27/08/2015	0:00	15.80	16.20	17.82	17.49	15.82
28/08/2015	1:00	15.76	16.16	17.74	17.41	15.74
28/08/2015	2:00	15.68	16.08	17.65	17.33	15.68
28/08/2015	3:00	15.60	16.00	17.53	17.21	15.54
28/08/2015	4:00	15.43	15.83	17.41	17.10	15.49
28/08/2015	5:00	15.30	15.70	17.26	16.97	15.34
28/08/2015	6:00	15.16	15.56	17.11	16.86	15.22
28/08/2015	7:00	15.10	15.50	16.99	16.76	15.08
28/08/2015	8:00	15.04	15.44	16.92	16.73	15.03
28/08/2015	9:00	15.02	15.42	16.91	16.71	15.05
28/08/2015	10:00	15.08	15.48	16.98	16.76	15.09
28/08/2015	11:00	15.14	15.54	17.04	16.83	15.17
28/08/2015	12:00	15.24	15.64	17.17	16.97	15.30
28/08/2015	13:00	15.39	15.79	17.32	17.10	15.45
28/08/2015	14:00	15.55	15.95	17.50	17.26	15.57
28/08/2015	15:00	15.76	16.16	17.72	17.43	15.76
28/08/2015	16:00	15.98	16.38	17.97	17.64	15.99
28/08/2015	17:00	16.17	16.37	18.17	17.82	16.17
28/08/2015	18:00	16.24	16.44	18.28	17.91	16.29
28/08/2015	19:00	16.18	16.38	18.22	17.86	16.22
28/08/2015	20:00	16.08	16.28	18.09	17.75	16.13
28/08/2015	21:00	15.89	16.09	17.93	17.59	15.98
28/08/2015	22:00	15.69	15.89	17.74	17.41	15.79
28/08/2015	23:00	15.48	15.68	17.52	17.19	15.57
28/08/2015	0:00	15.27	15.47	17.29	17.00	15.29
29/08/2015	1:00	15.10	15.30	17.01	16.74	15.07
29/08/2015	2:00	14.92	15.12	16.79	16.53	14.85
29/08/2015	3:00	14.68	14.88	16.57	16.35	14.64
29/08/2015	4:00	14.49	14.69	16.32	16.12	14.43
29/08/2015	5:00	14.31	14.51	16.11	15.93	14.23
29/08/2015	6:00	14.08	14.28	15.93	15.77	14.08
29/08/2015	7:00	14.05	14.25	15.75	15.63	13.94
29/08/2015	8:00	13.94	14.14	15.68	15.65	13.96
29/08/2015	9:00	14.08	14.28	15.82	15.75	14.08

29/08/2015	10:00	14.27	14.47	16.06	15.98	14.29
29/08/2015	11:00	14.65	14.85	16.42	16.32	14.64
29/08/2015	12:00	15.06	15.26	16.94	16.72	15.06
29/08/2015	13:00	15.50	15.70	17.42	17.17	15.55
29/08/2015	14:00	15.87	16.07	17.81	17.49	15.87
29/08/2015	15:00	16.08	16.28	18.13	17.82	16.22
29/08/2015	16:00	16.17	16.37	18.18	17.84	16.21
29/08/2015	17:00	16.16	16.36	18.18	17.81	16.17
29/08/2015	18:00	16.04	16.24	18.09	17.71	16.06
29/08/2015	19:00	15.91	16.11	17.97	17.61	15.97
29/08/2015	20:00	15.79	15.99	17.85	17.48	15.85
29/08/2015	21:00	15.66	15.86	17.72	17.35	15.70
29/08/2015	22:00	15.54	15.74	17.57	17.23	15.57
29/08/2015	23:00	15.41	15.61	17.39	17.12	15.48
29/08/2015	0:00	15.28	15.48	17.29	16.98	15.34
30/08/2015	1:00	15.13	15.33	17.11	16.83	15.20
30/08/2015	2:00	14.98	15.18	16.90	16.66	15.07
30/08/2015	3:00	14.83	15.03	16.71	16.51	14.87
30/08/2015	4:00	14.64	14.84	16.52	16.32	14.67
30/08/2015	5:00	14.46	14.66	16.29	16.12	14.48
30/08/2015	6:00	14.28	14.48	16.01	15.90	14.24
30/08/2015	7:00	14.11	14.31	15.82	15.70	13.99
30/08/2015	8:00	13.93	14.13	15.68	15.62	13.93
30/08/2015	9:00	13.90	14.10	15.66	15.57	13.92
30/08/2015	10:00	13.94	14.14	15.68	15.58	13.91
30/08/2015	11:00	13.99	14.19	15.75	15.65	13.99
30/08/2015	12:00	14.08	14.28	15.86	15.78	14.11
30/08/2015	13:00	14.23	14.43	16.01	15.92	14.25
30/08/2015	14:00	14.40	14.60	16.19	16.10	14.42
30/08/2015	15:00	14.63	14.83	16.44	16.29	14.61
30/08/2015	16:00	14.85	15.05	16.68	16.48	14.83
30/08/2015	17:00	15.07	15.27	16.90	16.70	15.06
30/08/2015	18:00	15.20	15.40	17.02	16.76	15.09
30/08/2015	19:00	15.12	15.32	16.93	16.70	15.04

30/08/2015	20:00	14.99	15.19	16.82	16.60	14.94
30/08/2015	21:00	14.83	15.03	16.62	16.41	14.74
30/08/2015	22:00	14.64	14.84	16.39	16.20	14.54
30/08/2015	23:00	14.30	14.50	16.11	15.97	14.34
30/08/2015	0:00	14.06	14.26	15.86	15.74	14.13
31/08/2015	1:00	13.87	14.07	15.62	15.52	13.87
31/08/2015	2:00	13.64	13.84	15.36	15.29	13.65
31/08/2015	3:00	13.40	13.60	15.10	15.05	13.44
31/08/2015	4:00	13.16	13.36	14.87	14.85	13.22
31/08/2015	5:00	12.98	13.18	14.69	14.68	12.99
31/08/2015	6:00	12.79	12.99	14.41	14.46	12.81
31/08/2015	7:00	12.67	12.87	14.26	14.34	12.65
31/08/2015	8:00	12.71	12.91	14.25	14.33	12.63
31/08/2015	9:00	12.80	13.00	14.33	14.42	12.73
31/08/2015	10:00	12.89	13.09	14.47	14.58	12.90
31/08/2015	11:00	13.10	13.30	14.72	14.80	13.12
31/08/2015	12:00	13.38	13.58	15.02	15.06	13.39
31/08/2015	13:00	13.65	13.85	15.36	15.36	13.68
31/08/2015	14:00	14.00	14.20	15.71	15.66	13.99
31/08/2015	15:00	14.34	14.54	16.07	15.96	14.33
31/08/2015	16:00	14.69	14.89	16.48	16.32	14.68
31/08/2015	17:00	14.98	15.18	16.83	16.67	15.05
31/08/2015	18:00	15.17	15.37	17.00	16.77	15.13
31/08/2015	19:00	15.20	15.40	17.05	16.81	15.13
31/08/2015	20:00	15.15	15.35	16.96	16.71	15.03
31/08/2015	21:00	14.99	15.19	16.82	16.63	14.97
31/08/2015	22:00	14.89	15.09	16.68	16.49	14.82
31/08/2015	23:00	14.70	14.90	16.49	16.33	14.67
31/08/2015	0:00	14.46	14.66	16.28	16.14	14.48
1/09/2015	1:00	14.27	14.47	16.08	15.94	14.32
1/09/2015	2:00	14.06	14.26	15.87	15.76	14.15
1/09/2015	3:00	13.89	14.09	15.64	15.56	13.94
1/09/2015	4:00	13.69	13.79	15.44	15.36	13.76
1/09/2015	5:00	13.51	13.61	15.24	15.19	13.57

1/09/2015	6:00	13.34	13.44	15.02	15.03	13.35
1/09/2015	7:00	13.36	13.46	14.97	14.95	13.24
1/09/2015	8:00	13.29	13.39	14.93	14.94	13.25
1/09/2015	9:00	13.30	13.40	14.96	14.95	13.26
1/09/2015	10:00	13.36	13.46	15.04	15.02	13.35
1/09/2015	11:00	13.50	13.60	15.17	15.20	13.49
1/09/2015	12:00	13.73	13.83	15.42	15.42	13.74
1/09/2015	13:00	14.01	14.11	15.74	15.69	14.01
1/09/2015	14:00	14.35	14.45	16.09	15.97	14.31
1/09/2015	15:00	14.68	14.78	16.48	16.33	14.69
1/09/2015	16:00	15.08	15.18	16.92	16.69	15.05
1/09/2015	17:00	15.40	15.50	17.28	17.07	15.49
1/09/2015	18:00	15.58	15.68	17.53	17.31	15.72
1/09/2015	19:00	15.62	15.72	17.58	17.29	15.66
1/09/2015	20:00	15.58	15.68	17.52	17.24	15.60
1/09/2015	21:00	15.44	15.54	17.41	17.13	15.52
1/09/2015	22:00	15.24	15.34	17.22	16.96	15.36
1/09/2015	23:00	15.05	15.15	17.01	16.77	15.16
1/09/2015	0:00	14.87	14.97	16.80	16.57	14.93
2/09/2015	1:00	14.65	14.75	16.58	16.36	14.71
2/09/2015	2:00	14.46	14.56	16.36	16.17	14.50
2/09/2015	3:00	14.28	14.38	16.16	15.99	14.29
2/09/2015	4:00	14.08	14.18	15.93	15.80	14.13
2/09/2015	5:00	13.94	14.04	15.76	15.64	13.95
2/09/2015	6:00	13.82	13.92	15.58	15.48	13.81
2/09/2015	7:00	13.75	13.85	15.47	15.46	13.76
2/09/2015	8:00	13.87	13.97	15.58	15.57	13.88
2/09/2015	9:00	14.05	14.05	15.79	15.76	14.05
2/09/2015	10:00	14.47	14.47	16.24	16.13	14.47
2/09/2015	11:00	14.93	14.93	16.76	16.58	14.93
2/09/2015	12:00	15.44	15.34	17.34	17.09	15.46
2/09/2015	13:00	15.98	15.88	17.97	17.63	15.99
2/09/2015	14:00	16.55	16.45	18.59	18.19	16.58
2/09/2015	15:00	17.08	16.98	19.21	18.74	17.23

2/09/2015	16:00	17.57	17.47	19.73	19.20	18.08
2/09/2015	17:00	17.88	17.78	20.07	19.53	18.64
2/09/2015	18:00	18.05	17.95	20.20	19.69	18.90
2/09/2015	19:00	18.08	17.98	20.23	19.74	18.99
2/09/2015	20:00	18.03	17.93	20.20	19.69	18.87
2/09/2015	21:00	17.94	17.84	20.14	19.59	18.71
2/09/2015	22:00	17.78	17.68	20.03	19.47	18.50
2/09/2015	23:00	17.62	17.52	19.90	19.36	18.23
2/09/2015	0:00	17.50	17.70	19.72	19.19	17.96
3/09/2015	1:00	17.35	17.55	19.55	19.05	17.68
3/09/2015	2:00	17.19	17.39	19.38	18.91	17.43
3/09/2015	3:00	17.07	17.27	19.21	18.75	17.14
3/09/2015	4:00	16.92	17.12	19.10	18.62	16.94
3/09/2015	5:00	16.83	17.03	18.97	18.52	16.85
3/09/2015	6:00	16.78	16.98	18.89	18.46	16.79
3/09/2015	7:00	16.70	16.90	18.85	18.44	16.78
3/09/2015	8:00	16.66	16.86	18.80	18.37	16.73
3/09/2015	9:00	16.54	16.74	18.66	18.27	16.62
3/09/2015	10:00	16.46	16.66	18.57	18.17	16.50
3/09/2015	11:00	16.43	16.63	18.50	18.09	16.43
3/09/2015	12:00	16.38	16.58	18.48	18.13	16.46
3/09/2015	13:00	16.47	16.67	18.56	18.19	16.52
3/09/2015	14:00	16.56	16.76	18.69	18.29	16.63
3/09/2015	15:00	16.72	16.92	18.84	18.40	16.75
3/09/2015	16:00	16.88	17.08	18.99	18.52	16.87
3/09/2015	17:00	16.95	17.15	19.11	18.69	17.10
3/09/2015	18:00	17.03	17.23	19.09	18.61	16.97
3/09/2015	19:00	16.88	17.08	18.95	18.46	16.80
3/09/2015	20:00	16.69	16.89	18.73	18.26	16.57
3/09/2015	21:00	16.48	16.68	18.46	18.01	16.26
3/09/2015	22:00	16.21	16.41	18.16	17.71	15.94
3/09/2015	23:00	15.81	16.01	17.74	17.36	15.60
3/09/2015	0:00	15.51	15.61	17.36	16.98	15.27
4/09/2015	1:00	15.14	15.24	16.96	16.67	14.92

4/09/2015	2:00	14.76	14.86	16.54	16.33	14.64
4/09/2015	3:00	14.53	14.63	16.27	16.07	14.33
4/09/2015	4:00	14.26	14.36	15.99	15.81	14.04
4/09/2015	5:00	13.85	13.95	15.58	15.52	13.84
4/09/2015	6:00	13.62	13.72	15.32	15.29	13.60
4/09/2015	7:00	13.58	13.68	15.19	15.14	13.43
4/09/2015	8:00	13.48	13.58	15.12	15.12	13.43
4/09/2015	9:00	13.51	13.61	15.20	15.19	13.51
4/09/2015	10:00	13.64	13.74	15.35	15.35	13.67
4/09/2015	11:00	13.85	13.95	15.60	15.60	13.91
4/09/2015	12:00	14.19	14.29	15.95	15.89	14.21
4/09/2015	13:00	14.62	14.72	16.40	16.30	14.67
4/09/2015	14:00	15.10	15.20	16.93	16.75	15.13
4/09/2015	15:00	15.63	15.73	17.53	17.27	15.64
4/09/2015	16:00	16.14	16.24	18.11	17.78	16.17
4/09/2015	17:00	16.51	16.61	18.55	18.14	16.53
4/09/2015	18:00	16.75	16.85	18.83	18.38	16.76
4/09/2015	19:00	16.88	16.98	18.97	18.50	16.87
4/09/2015	20:00	16.91	17.01	19.01	18.52	16.89
4/09/2015	21:00	16.81	16.91	18.95	18.51	16.86
4/09/2015	22:00	16.70	16.80	18.85	18.40	16.76
4/09/2015	23:00	16.53	16.63	18.69	18.25	16.62
4/09/2015	0:00	16.36	16.46	18.51	18.08	16.44
5/09/2015	1:00	16.18	16.28	18.30	17.88	16.23
5/09/2015	2:00	15.98	16.08	18.09	17.70	16.03
5/09/2015	3:00	15.79	15.89	17.86	17.51	15.86
5/09/2015	4:00	15.59	15.69	17.65	17.31	15.68
5/09/2015	5:00	15.41	15.51	17.41	17.13	15.51
5/09/2015	6:00	15.33	15.33	17.20	16.92	15.25
5/09/2015	7:00	15.11	15.11	17.06	16.84	15.16
5/09/2015	8:00	15.17	15.17	17.08	16.87	15.18
5/09/2015	9:00	15.20	15.20	17.18	16.96	15.26
5/09/2015	10:00	15.42	15.42	17.36	17.12	15.45
5/09/2015	11:00	15.67	15.67	17.64	17.37	15.72

5/09/2015	12:00	16.03	16.03	18.01	17.71	16.07
5/09/2015	13:00	16.40	16.60	18.45	18.09	16.44
5/09/2015	14:00	16.85	17.05	18.95	18.53	16.90
5/09/2015	15:00	17.35	17.55	19.51	19.02	17.72
5/09/2015	16:00	17.84	18.04	20.04	19.50	18.58
5/09/2015	17:00	18.24	18.44	20.34	19.88	19.30
5/09/2015	18:00	18.44	18.64	20.49	20.10	19.66
5/09/2015	19:00	18.47	18.67	20.52	20.12	19.69
5/09/2015	20:00	18.39	18.59	20.47	20.07	19.54
5/09/2015	21:00	18.25	18.45	20.38	19.90	19.27
5/09/2015	22:00	18.00	18.20	20.22	19.76	18.96
5/09/2015	23:00	17.80	18.00	20.06	19.55	18.60
5/09/2015	0:00	17.59	17.79	19.89	19.31	18.15
6/09/2015	1:00	17.34	17.54	19.63	19.07	17.80
6/09/2015	2:00	17.09	17.29	19.37	18.84	17.32
6/09/2015	3:00	16.85	17.05	19.08	18.58	16.93
6/09/2015	4:00	16.59	16.79	18.78	18.33	16.71
6/09/2015	5:00	16.36	16.56	18.52	18.09	16.41
6/09/2015	6:00	16.13	16.33	18.20	17.82	16.14
6/09/2015	7:00	15.96	16.16	18.03	17.68	15.99
6/09/2015	8:00	15.97	16.17	17.97	17.66	15.99
6/09/2015	9:00	16.00	16.20	18.07	17.75	16.06
6/09/2015	10:00	16.20	16.40	18.27	17.94	16.26
6/09/2015	11:00	16.49	16.69	18.60	18.21	16.55
6/09/2015	12:00	16.83	17.03	18.95	18.54	16.89
6/09/2015	13:00	17.26	17.46	19.42	18.93	17.52
6/09/2015	14:00	17.65	17.85	19.85	19.31	18.19
6/09/2015	15:00	17.99	18.19	20.16	19.65	18.82
6/09/2015	16:00	18.31	18.51	20.38	19.97	19.41
6/09/2015	17:00	18.57	18.77	20.58	20.20	19.83
6/09/2015	18:00	18.67	18.87	20.67	20.33	20.03
6/09/2015	19:00	18.69	18.89	20.67	20.34	20.06
6/09/2015	20:00	18.63	18.83	20.64	20.27	19.92
6/09/2015	21:00	18.51	18.61	20.56	20.19	19.78

6/09/2015	22:00	18.36	18.46	20.45	20.04	19.48
6/09/2015	23:00	18.16	18.26	20.31	19.87	19.16
6/09/2015	0:00	17.97	18.07	20.18	19.66	18.78
7/09/2015	1:00	17.77	17.87	20.05	19.48	18.42
7/09/2015	2:00	17.60	17.70	19.86	19.31	18.12
7/09/2015	3:00	17.43	17.53	19.66	19.13	17.84
7/09/2015	4:00	17.28	17.38	19.49	18.95	17.54
7/09/2015	5:00	17.09	17.19	19.31	18.80	17.28
7/09/2015	6:00	16.96	17.06	19.14	18.64	16.97
7/09/2015	7:00	16.82	16.92	18.98	18.53	16.87
7/09/2015	8:00	16.79	16.89	18.95	18.54	16.87
7/09/2015	9:00	16.84	16.94	19.02	18.59	16.90
7/09/2015	10:00	16.98	17.08	19.16	18.73	17.08
7/09/2015	11:00	17.21	17.31	19.41	18.97	17.52
7/09/2015	12:00	17.55	17.65	19.78	19.27	18.09
7/09/2015	13:00	17.95	18.05	20.13	19.63	18.77
7/09/2015	14:00	18.33	18.43	20.41	19.99	19.46
7/09/2015	15:00	18.68	18.78	20.66	20.36	20.08
7/09/2015	16:00	18.97	19.07	20.88	20.64	20.58
7/09/2015	17:00	19.18	19.28	21.03	20.83	20.97
7/09/2015	18:00	19.25	19.35	21.09	20.90	21.09
7/09/2015	19:00	19.21	19.31	21.08	20.87	21.05
7/09/2015	20:00	19.10	19.20	20.99	20.75	20.81
7/09/2015	21:00	18.94	19.04	20.88	20.65	20.60
7/09/2015	22:00	18.76	18.86	20.76	20.47	20.25
7/09/2015	23:00	18.54	18.64	20.60	20.25	19.83
7/09/2015	0:00	18.30	18.40	20.44	20.01	19.45
8/09/2015	1:00	18.04	18.14	20.27	19.77	18.98
8/09/2015	2:00	17.82	17.92	20.10	19.53	18.54
8/09/2015	3:00	17.59	17.69	19.88	19.31	18.22
8/09/2015	4:00	17.38	17.48	19.67	19.10	17.82
8/09/2015	5:00	17.16	17.26	19.42	18.90	17.50
8/09/2015	6:00	16.97	17.07	19.17	18.67	17.03
8/09/2015	7:00	16.86	16.96	19.02	18.58	16.91

8/09/2015	8:00	16.87	16.97	19.03	18.59	16.90
8/09/2015	9:00	16.94	17.04	19.12	18.67	16.99
8/09/2015	10:00	17.11	17.21	19.31	18.84	17.29
8/09/2015	11:00	17.37	17.47	19.57	19.08	17.75
8/09/2015	12:00	17.68	17.78	19.91	19.36	18.29
8/09/2015	13:00	17.96	18.06	20.15	19.65	18.82
8/09/2015	14:00	18.24	18.34	20.35	19.91	19.28
8/09/2015	15:00	18.47	18.57	20.51	20.13	19.68
8/09/2015	16:00	18.67	18.77	20.67	20.34	20.08
8/09/2015	17:00	18.87	18.97	20.85	20.60	20.54
8/09/2015	18:00	18.88	18.98	20.82	20.58	20.60
8/09/2015	19:00	18.75	18.85	20.69	20.39	20.21
8/09/2015	20:00	18.49	18.59	20.49	20.06	19.55
8/09/2015	21:00	18.14	18.24	20.23	19.68	18.79
8/09/2015	22:00	17.67	17.77	19.83	19.23	17.91
8/09/2015	23:00	17.21	17.31	19.37	18.83	17.18
8/09/2015	0:00	16.74	16.84	18.85	18.40	16.71
9/09/2015	1:00	16.27	16.37	18.41	18.01	16.39
9/09/2015	2:00	16.00	16.10	18.02	17.64	16.00
9/09/2015	3:00	15.61	15.51	17.64	17.30	15.66
9/09/2015	4:00	15.28	15.18	17.26	16.98	15.38
9/09/2015	5:00	14.99	14.89	16.92	16.70	15.11
9/09/2015	6:00	14.77	14.67	16.64	16.43	14.77
9/09/2015	7:00	14.72	14.62	16.50	16.30	14.60
9/09/2015	8:00	14.62	14.52	16.43	16.27	14.57
9/09/2015	9:00	14.63	14.53	16.46	16.30	14.61
9/09/2015	10:00	14.72	14.82	16.55	16.40	14.74
9/09/2015	11:00	14.88	15.08	16.77	16.62	14.96
9/09/2015	12:00	15.24	15.44	17.19	16.99	15.34

Table 22 - Experimental Curing Temperatures of Beam 2

Date	24 Hour Time	Beam 2 Curing Temperatures (Degrees Celsius)		
		TC 4	TC 5	TC 6
12/08/2015	18:00	21.95	18.87	21.80
12/08/2015	19:00	21.31	21.02	20.71
12/08/2015	20:00	20.94	20.42	20.02
12/08/2015	21:00	20.42	19.77	19.32
12/08/2015	22:00	19.90	19.13	18.58
12/08/2015	23:00	19.38	18.45	17.78
12/08/2015	0:00	18.78	17.80	17.01
13/08/2015	1:00	18.00	17.17	16.29
13/08/2015	2:00	17.32	16.65	15.69
13/08/2015	3:00	16.59	16.07	15.03
13/08/2015	4:00	16.00	15.59	14.48
13/08/2015	5:00	15.40	15.12	13.95
13/08/2015	6:00	14.98	14.79	13.54
13/08/2015	7:00	14.51	14.42	13.15
13/08/2015	8:00	14.27	14.24	12.86
13/08/2015	9:00	14.45	14.31	12.88
13/08/2015	10:00	14.53	14.41	13.01
13/08/2015	11:00	14.67	14.43	13.08
13/08/2015	12:00	14.91	14.66	13.30
13/08/2015	13:00	15.22	14.87	13.54
13/08/2015	14:00	15.59	15.17	13.87
13/08/2015	15:00	16.20	15.67	14.45
13/08/2015	16:00	16.85	16.19	14.98
13/08/2015	17:00	17.47	16.70	15.67
13/08/2015	18:00	18.10	17.22	16.31
13/08/2015	19:00	18.61	17.68	16.82
13/08/2015	20:00	18.95	18.02	17.23
13/08/2015	21:00	19.13	18.24	17.43
13/08/2015	22:00	19.23	18.38	17.57

13/08/2015	23:00	19.39	18.50	17.76
13/08/2015	0:00	19.48	18.61	17.81
14/08/2015	1:00	19.49	18.68	17.91
14/08/2015	2:00	19.53	18.75	18.01
14/08/2015	3:00	19.43	18.60	17.88
14/08/2015	4:00	19.31	18.46	17.68
14/08/2015	5:00	19.27	18.41	17.64
14/08/2015	6:00	19.17	18.33	17.54
14/08/2015	7:00	19.04	18.14	17.32
14/08/2015	8:00	18.94	18.01	17.18
14/08/2015	9:00	18.98	18.05	17.20
14/08/2015	10:00	19.09	18.19	17.39
14/08/2015	11:00	19.25	18.37	17.57
14/08/2015	12:00	19.42	18.58	17.83
14/08/2015	13:00	19.62	18.85	18.13
14/08/2015	14:00	19.85	19.10	18.45
14/08/2015	15:00	20.08	19.39	18.81
14/08/2015	16:00	20.40	19.71	19.12
14/08/2015	17:00	20.63	20.05	19.54
14/08/2015	18:00	20.79	20.32	19.94
14/08/2015	19:00	20.80	20.27	19.90
14/08/2015	20:00	20.67	20.14	19.69
14/08/2015	21:00	20.49	19.90	19.42
14/08/2015	22:00	20.31	19.63	19.03
14/08/2015	23:00	20.09	19.42	18.79
14/08/2015	0:00	19.81	19.06	18.36
15/08/2015	1:00	19.58	18.78	18.09
15/08/2015	2:00	19.34	18.48	17.73
15/08/2015	3:00	19.09	18.13	17.31
15/08/2015	4:00	18.74	17.80	16.95
15/08/2015	5:00	18.36	17.51	16.60
15/08/2015	6:00	17.94	17.17	16.21
15/08/2015	7:00	17.52	16.82	15.81
15/08/2015	8:00	17.17	16.51	15.49

15/08/2015	9:00	17.10	16.48	15.45
15/08/2015	10:00	17.26	16.62	15.59
15/08/2015	11:00	17.54	16.80	15.80
15/08/2015	12:00	17.84	17.05	16.07
15/08/2015	13:00	18.25	17.37	16.45
15/08/2015	14:00	18.72	17.66	16.83
15/08/2015	15:00	19.20	18.16	17.26
15/08/2015	16:00	19.48	18.51	17.68
15/08/2015	17:00	19.79	18.92	18.19
15/08/2015	18:00	20.02	19.20	18.65
15/08/2015	19:00	20.11	19.43	18.86
15/08/2015	20:00	20.11	19.40	18.87
15/08/2015	21:00	20.12	19.40	18.75
15/08/2015	22:00	20.04	19.32	18.70
15/08/2015	23:00	19.95	19.23	18.65
15/08/2015	0:00	19.83	19.08	18.44
16/08/2015	1:00	19.74	18.98	18.33
16/08/2015	2:00	19.57	18.76	18.08
16/08/2015	3:00	19.35	18.51	17.79
16/08/2015	4:00	19.13	18.22	17.46
16/08/2015	5:00	18.83	17.91	17.11
16/08/2015	6:00	18.38	17.57	16.68
16/08/2015	7:00	17.99	17.24	16.33
16/08/2015	8:00	17.47	16.81	15.84
16/08/2015	9:00	17.39	16.72	15.72
16/08/2015	10:00	17.49	16.80	15.82
16/08/2015	11:00	17.87	17.05	16.07
16/08/2015	12:00	18.82	17.74	16.83
16/08/2015	13:00	19.21	18.23	17.35
16/08/2015	14:00	19.57	18.66	17.87
16/08/2015	15:00	19.93	19.09	18.38
16/08/2015	16:00	20.19	19.42	18.82
16/08/2015	17:00	20.37	19.64	19.12
16/08/2015	18:00	20.42	19.74	19.24

16/08/2015	19:00	20.44	19.79	19.21
16/08/2015	20:00	20.42	19.79	19.20
16/08/2015	21:00	20.34	19.69	19.10
16/08/2015	22:00	20.27	19.63	19.05
16/08/2015	23:00	20.16	19.50	18.93
16/08/2015	0:00	20.06	19.37	18.78
17/08/2015	1:00	19.96	19.28	18.69
17/08/2015	2:00	19.83	19.11	18.47
17/08/2015	3:00	19.69	18.94	18.28
17/08/2015	4:00	19.51	18.69	17.97
17/08/2015	5:00	19.31	18.44	17.70
17/08/2015	6:00	19.04	18.09	17.31
17/08/2015	7:00	18.63	17.73	16.90
17/08/2015	8:00	18.52	17.67	16.82
17/08/2015	9:00	18.70	17.76	16.90
17/08/2015	10:00	18.90	17.87	17.03
17/08/2015	11:00	19.15	18.13	17.29
17/08/2015	12:00	19.38	18.42	17.61
17/08/2015	13:00	19.55	18.71	17.93
17/08/2015	14:00	19.78	19.00	18.27
17/08/2015	15:00	20.06	19.30	18.63
17/08/2015	16:00	20.32	19.62	19.01
17/08/2015	17:00	20.50	19.84	19.33
17/08/2015	18:00	20.58	20.00	19.50
17/08/2015	19:00	20.57	19.95	19.47
17/08/2015	20:00	20.54	19.92	19.40
17/08/2015	21:00	20.42	19.77	19.25
17/08/2015	22:00	20.34	19.69	19.11
17/08/2015	23:00	20.16	19.51	18.89
17/08/2015	0:00	20.01	19.33	18.73
18/08/2015	1:00	19.79	19.03	18.38
18/08/2015	2:00	19.63	18.84	18.16
18/08/2015	3:00	19.41	18.57	17.86
18/08/2015	4:00	19.23	18.34	17.59

18/08/2015	5:00	19.03	18.08	17.28
18/08/2015	6:00	18.57	17.69	16.82
18/08/2015	7:00	18.27	17.39	16.51
18/08/2015	8:00	18.09	17.30	16.41
18/08/2015	9:00	18.13	17.31	16.39
18/08/2015	10:00	18.26	17.38	16.46
18/08/2015	11:00	18.40	17.49	16.56
18/08/2015	12:00	18.63	17.62	16.70
18/08/2015	13:00	18.90	17.83	16.99
18/08/2015	14:00	19.19	18.15	17.26
18/08/2015	15:00	19.42	18.52	17.71
18/08/2015	16:00	19.69	18.82	18.07
18/08/2015	17:00	19.91	19.08	18.42
18/08/2015	18:00	19.99	19.19	18.63
18/08/2015	19:00	20.03	19.24	18.65
18/08/2015	20:00	20.01	19.21	18.58
18/08/2015	21:00	19.93	19.11	18.44
18/08/2015	22:00	19.83	19.08	18.39
18/08/2015	23:00	19.70	18.93	18.23
18/08/2015	0:00	19.53	18.71	18.01
19/08/2015	1:00	19.36	18.48	17.76
19/08/2015	2:00	19.14	18.21	17.42
19/08/2015	3:00	18.89	17.91	17.08
19/08/2015	4:00	18.53	17.64	16.78
19/08/2015	5:00	18.17	17.33	16.42
19/08/2015	6:00	17.79	17.04	16.10
19/08/2015	7:00	17.48	16.77	15.77
19/08/2015	8:00	17.43	16.76	15.74
19/08/2015	9:00	17.58	16.84	15.87
19/08/2015	10:00	17.86	17.06	16.10
19/08/2015	11:00	18.35	17.33	16.40
19/08/2015	12:00	18.81	17.72	16.80
19/08/2015	13:00	19.17	18.16	17.24
19/08/2015	14:00	19.48	18.56	17.74

19/08/2015	15:00	19.78	18.93	18.19
19/08/2015	16:00	20.01	19.19	18.62
19/08/2015	17:00	20.20	19.49	18.92
19/08/2015	18:00	20.30	19.57	19.06
19/08/2015	19:00	20.27	19.61	19.08
19/08/2015	20:00	20.32	19.66	19.05
19/08/2015	21:00	20.22	19.55	18.97
19/08/2015	22:00	20.13	19.44	18.82
19/08/2015	23:00	20.02	19.32	18.70
19/08/2015	0:00	19.86	19.14	18.48
20/08/2015	1:00	19.69	18.91	18.23
20/08/2015	2:00	19.53	18.72	18.01
20/08/2015	3:00	19.34	18.46	17.70
20/08/2015	4:00	19.17	18.24	17.44
20/08/2015	5:00	19.00	18.01	17.18
20/08/2015	6:00	18.62	17.71	16.84
20/08/2015	7:00	18.32	17.46	16.56
20/08/2015	8:00	18.26	17.40	16.51
20/08/2015	9:00	18.40	17.48	16.55
20/08/2015	10:00	18.55	17.59	16.70
20/08/2015	11:00	18.78	17.77	16.91
20/08/2015	12:00	19.03	17.98	17.16
20/08/2015	13:00	19.26	18.22	17.48
20/08/2015	14:00	19.59	18.59	17.82
20/08/2015	15:00	19.79	18.92	18.31
20/08/2015	16:00	20.04	19.26	18.71
20/08/2015	17:00	20.26	19.54	19.00
20/08/2015	18:00	20.37	19.69	19.10
20/08/2015	19:00	20.34	19.69	19.17
20/08/2015	20:00	20.31	19.64	19.12
20/08/2015	21:00	20.28	19.63	19.06
20/08/2015	22:00	20.24	19.58	18.96
20/08/2015	23:00	20.13	19.46	18.85
20/08/2015	0:00	20.01	19.30	18.68

21/08/2015	1:00	19.91	19.18	18.52
21/08/2015	2:00	19.77	18.98	18.31
21/08/2015	3:00	19.67	18.87	18.18
21/08/2015	4:00	19.57	18.73	18.02
21/08/2015	5:00	19.46	18.59	17.87
21/08/2015	6:00	19.38	18.49	17.74
21/08/2015	7:00	19.24	18.31	17.55
21/08/2015	8:00	19.24	18.28	17.48
21/08/2015	9:00	19.26	18.29	17.51
21/08/2015	10:00	19.30	18.38	17.64
21/08/2015	11:00	19.43	18.55	17.81
21/08/2015	12:00	19.57	18.67	17.98
21/08/2015	13:00	19.80	18.89	18.16
21/08/2015	14:00	19.90	19.10	18.45
21/08/2015	15:00	20.05	19.30	18.68
21/08/2015	16:00	20.17	19.45	18.83
21/08/2015	17:00	20.22	19.55	18.88
21/08/2015	18:00	20.25	19.60	19.02
21/08/2015	19:00	20.19	19.51	18.96
21/08/2015	20:00	20.19	19.52	18.93
21/08/2015	21:00	20.15	19.47	18.86
21/08/2015	22:00	20.07	19.42	18.81
21/08/2015	23:00	20.06	19.36	18.76
21/08/2015	0:00	19.97	19.30	18.69
22/08/2015	1:00	19.91	19.22	18.61
22/08/2015	2:00	19.89	19.18	18.53
22/08/2015	3:00	19.85	19.11	18.46
22/08/2015	4:00	19.79	19.06	18.38
22/08/2015	5:00	19.78	19.00	18.31
22/08/2015	6:00	19.74	18.94	18.25
22/08/2015	7:00	19.72	18.92	18.22
22/08/2015	8:00	19.66	18.88	18.19
22/08/2015	9:00	19.77	18.90	18.13
22/08/2015	10:00	19.86	19.03	18.32

22/08/2015	11:00	20.02	19.24	18.64
22/08/2015	12:00	20.29	19.55	19.02
22/08/2015	13:00	20.61	19.95	19.46
22/08/2015	14:00	20.93	20.37	19.93
22/08/2015	15:00	21.24	20.78	20.40
22/08/2015	16:00	21.50	21.13	20.80
22/08/2015	17:00	21.69	21.37	21.08
22/08/2015	18:00	21.76	21.47	21.18
22/08/2015	19:00	21.73	21.46	21.18
22/08/2015	20:00	21.66	21.41	21.10
22/08/2015	21:00	21.60	21.31	20.98
22/08/2015	22:00	21.48	21.19	20.81
22/08/2015	23:00	21.40	21.08	20.70
22/08/2015	0:00	21.29	20.99	20.54
23/08/2015	1:00	21.23	20.89	20.46
23/08/2015	2:00	21.13	20.76	20.34
23/08/2015	3:00	21.07	20.72	20.26
23/08/2015	4:00	21.00	20.59	20.11
23/08/2015	5:00	20.83	20.37	19.89
23/08/2015	6:00	20.78	20.30	19.79
23/08/2015	7:00	20.73	20.22	19.73
23/08/2015	8:00	20.60	20.14	19.63
23/08/2015	9:00	20.62	20.03	19.52
23/08/2015	10:00	20.71	20.10	19.62
23/08/2015	11:00	20.82	20.27	19.84
23/08/2015	12:00	21.04	20.54	20.16
23/08/2015	13:00	21.32	20.88	20.54
23/08/2015	14:00	21.62	21.29	20.97
23/08/2015	15:00	21.88	21.63	21.35
23/08/2015	16:00	22.11	21.92	21.71
23/08/2015	17:00	22.27	22.12	21.94
23/08/2015	18:00	22.32	22.21	22.04
23/08/2015	19:00	22.31	22.18	21.98
23/08/2015	20:00	22.22	22.09	21.89

23/08/2015	21:00	22.07	21.95	21.73
23/08/2015	22:00	21.99	21.82	21.55
23/08/2015	23:00	21.87	21.66	21.37
23/08/2015	0:00	21.76	21.55	21.23
24/08/2015	1:00	21.62	21.37	21.04
24/08/2015	2:00	21.49	21.21	20.85
24/08/2015	3:00	21.27	20.92	20.60
24/08/2015	4:00	21.18	20.86	20.47
24/08/2015	5:00	21.08	20.73	20.31
24/08/2015	6:00	21.02	20.58	20.13
24/08/2015	7:00	20.93	20.50	20.03
24/08/2015	8:00	20.81	20.40	19.93
24/08/2015	9:00	20.80	20.29	19.90
24/08/2015	10:00	20.95	20.40	19.89
24/08/2015	11:00	21.03	20.55	20.17
24/08/2015	12:00	21.26	20.84	20.50
24/08/2015	13:00	21.58	21.21	20.93
24/08/2015	14:00	21.94	21.67	21.42
24/08/2015	15:00	22.26	22.10	21.89
24/08/2015	16:00	22.49	22.42	22.26
24/08/2015	17:00	22.64	22.63	22.53
24/08/2015	18:00	22.72	22.72	22.63
24/08/2015	19:00	22.72	22.71	22.63
24/08/2015	20:00	22.64	22.64	22.55
24/08/2015	21:00	22.57	22.54	22.42
24/08/2015	22:00	22.45	22.42	22.29
24/08/2015	23:00	22.40	22.34	22.12
24/08/2015	0:00	22.24	22.26	22.05
25/08/2015	1:00	22.20	22.13	21.89
25/08/2015	2:00	22.03	21.88	21.65
25/08/2015	3:00	21.90	21.75	21.49
25/08/2015	4:00	21.70	21.50	21.23
25/08/2015	5:00	21.63	21.38	21.03
25/08/2015	6:00	21.49	21.16	20.77

25/08/2015	7:00	21.36	21.11	20.78
25/08/2015	8:00	21.34	21.02	20.69
25/08/2015	9:00	21.34	21.00	20.55
25/08/2015	10:00	21.34	20.98	20.54
25/08/2015	11:00	21.37	20.98	20.51
25/08/2015	12:00	21.37	21.01	20.66
25/08/2015	13:00	21.46	21.14	20.81
25/08/2015	14:00	21.61	21.31	21.02
25/08/2015	15:00	21.78	21.51	21.23
25/08/2015	16:00	21.96	21.73	21.51
25/08/2015	17:00	22.10	21.90	21.67
25/08/2015	18:00	22.15	21.95	21.76
25/08/2015	19:00	22.12	21.95	21.73
25/08/2015	20:00	22.06	21.87	21.70
25/08/2015	21:00	21.92	21.75	21.54
25/08/2015	22:00	21.77	21.53	21.29
25/08/2015	23:00	21.65	21.38	21.05
25/08/2015	0:00	21.44	21.16	20.82
26/08/2015	1:00	21.20	20.87	20.48
26/08/2015	2:00	21.00	20.58	20.13
26/08/2015	3:00	20.74	20.27	19.79
26/08/2015	4:00	20.53	19.99	19.47
26/08/2015	5:00	20.32	19.72	19.15
26/08/2015	6:00	20.07	19.41	18.79
26/08/2015	7:00	19.90	19.13	18.52
26/08/2015	8:00	19.81	19.02	18.36
26/08/2015	9:00	19.74	18.96	18.27
26/08/2015	10:00	19.77	18.96	18.25
26/08/2015	11:00	19.82	19.01	18.32
26/08/2015	12:00	19.91	19.14	18.50
26/08/2015	13:00	20.13	19.37	18.75
26/08/2015	14:00	20.41	19.68	19.09
26/08/2015	15:00	20.63	20.02	19.51
26/08/2015	16:00	20.93	20.42	19.96

26/08/2015	17:00	21.23	20.74	20.36
26/08/2015	18:00	21.33	20.91	20.64
26/08/2015	19:00	21.40	21.00	20.67
26/08/2015	20:00	21.32	20.93	20.59
26/08/2015	21:00	21.22	20.81	20.48
26/08/2015	22:00	21.16	20.75	20.34
26/08/2015	23:00	21.06	20.64	20.21
26/08/2015	0:00	20.94	20.51	20.03
27/08/2015	1:00	20.80	20.33	19.86
27/08/2015	2:00	20.69	20.19	19.68
27/08/2015	3:00	20.56	20.02	19.49
27/08/2015	4:00	20.46	19.87	19.31
27/08/2015	5:00	20.36	19.74	19.18
27/08/2015	6:00	20.25	19.61	19.01
27/08/2015	7:00	20.13	19.45	18.82
27/08/2015	8:00	20.00	19.28	18.65
27/08/2015	9:00	19.96	19.23	18.59
27/08/2015	10:00	19.96	19.19	18.52
27/08/2015	11:00	19.96	19.20	18.55
27/08/2015	12:00	20.00	19.23	18.56
27/08/2015	13:00	19.96	19.21	18.55
27/08/2015	14:00	19.97	19.27	18.64
27/08/2015	15:00	19.96	19.26	18.65
27/08/2015	16:00	20.04	19.35	18.70
27/08/2015	17:00	20.04	19.33	18.74
27/08/2015	18:00	20.09	19.36	18.72
27/08/2015	19:00	20.10	19.38	18.72
27/08/2015	20:00	20.08	19.37	18.72
27/08/2015	21:00	20.04	19.33	18.71
27/08/2015	22:00	20.01	19.27	18.62
27/08/2015	23:00	19.98	19.21	18.58
27/08/2015	0:00	19.97	19.22	18.58
28/08/2015	1:00	19.91	19.14	18.48
28/08/2015	2:00	19.80	19.01	18.33

28/08/2015	3:00	19.77	18.96	18.27
28/08/2015	4:00	19.68	18.89	18.20
28/08/2015	5:00	19.60	18.77	18.05
28/08/2015	6:00	19.45	18.58	17.84
28/08/2015	7:00	19.32	18.38	17.62
28/08/2015	8:00	19.30	18.35	17.59
28/08/2015	9:00	19.32	18.37	17.60
28/08/2015	10:00	19.36	18.42	17.65
28/08/2015	11:00	19.43	18.48	17.71
28/08/2015	12:00	19.50	18.57	17.83
28/08/2015	13:00	19.60	18.72	17.98
28/08/2015	14:00	19.68	18.84	18.13
28/08/2015	15:00	19.83	18.99	18.34
28/08/2015	16:00	20.04	19.24	18.56
28/08/2015	17:00	20.16	19.43	18.80
28/08/2015	18:00	20.22	19.54	18.99
28/08/2015	19:00	20.22	19.54	18.94
28/08/2015	20:00	20.17	19.48	18.88
28/08/2015	21:00	20.05	19.36	18.75
28/08/2015	22:00	19.97	19.26	18.62
28/08/2015	23:00	19.79	19.07	18.40
28/08/2015	0:00	19.65	18.85	18.12
29/08/2015	1:00	19.42	18.53	17.79
29/08/2015	2:00	19.26	18.32	17.53
29/08/2015	3:00	19.10	18.11	17.30
29/08/2015	4:00	18.85	17.86	17.01
29/08/2015	5:00	18.57	17.64	16.74
29/08/2015	6:00	18.26	17.40	16.47
29/08/2015	7:00	17.99	17.14	16.19
29/08/2015	8:00	17.89	17.13	16.20
29/08/2015	9:00	18.19	17.27	16.30
29/08/2015	10:00	18.46	17.50	16.59
29/08/2015	11:00	18.90	17.82	17.06
29/08/2015	12:00	19.34	18.28	17.51

29/08/2015	13:00	19.71	18.75	18.07
29/08/2015	14:00	19.99	19.12	18.46
29/08/2015	15:00	20.10	19.43	18.81
29/08/2015	16:00	20.12	19.45	18.91
29/08/2015	17:00	20.16	19.47	18.84
29/08/2015	18:00	20.17	19.51	18.89
29/08/2015	19:00	20.06	19.36	18.73
29/08/2015	20:00	19.99	19.29	18.65
29/08/2015	21:00	19.89	19.15	18.46
29/08/2015	22:00	19.77	18.99	18.30
29/08/2015	23:00	19.67	18.84	18.13
29/08/2015	0:00	19.57	18.76	18.03
30/08/2015	1:00	19.46	18.61	17.85
30/08/2015	2:00	19.33	18.44	17.64
30/08/2015	3:00	19.17	18.22	17.42
30/08/2015	4:00	19.02	18.03	17.20
30/08/2015	5:00	18.76	17.82	16.97
30/08/2015	6:00	18.49	17.55	16.65
30/08/2015	7:00	18.21	17.32	16.41
30/08/2015	8:00	18.15	17.27	16.36
30/08/2015	9:00	18.12	17.26	16.32
30/08/2015	10:00	18.14	17.26	16.31
30/08/2015	11:00	18.20	17.31	16.36
30/08/2015	12:00	18.31	17.37	16.47
30/08/2015	13:00	18.48	17.53	16.63
30/08/2015	14:00	18.68	17.65	16.77
30/08/2015	15:00	18.91	17.82	16.95
30/08/2015	16:00	19.11	18.07	17.19
30/08/2015	17:00	19.31	18.28	17.51
30/08/2015	18:00	19.32	18.35	17.63
30/08/2015	19:00	19.34	18.37	17.61
30/08/2015	20:00	19.27	18.29	17.52
30/08/2015	21:00	19.14	18.12	17.30
30/08/2015	22:00	19.01	17.96	17.13

30/08/2015	23:00	18.72	17.79	16.94
30/08/2015	0:00	18.51	17.62	16.72
31/08/2015	1:00	18.15	17.33	16.40
31/08/2015	2:00	17.87	17.10	16.12
31/08/2015	3:00	17.60	16.88	15.88
31/08/2015	4:00	17.34	16.73	15.69
31/08/2015	5:00	17.12	16.52	15.46
31/08/2015	6:00	16.66	16.15	15.03
31/08/2015	7:00	16.43	15.96	14.81
31/08/2015	8:00	16.38	15.87	14.74
31/08/2015	9:00	16.47	15.97	14.81
31/08/2015	10:00	16.73	16.12	14.99
31/08/2015	11:00	16.99	16.34	15.23
31/08/2015	12:00	17.34	16.60	15.53
31/08/2015	13:00	17.66	16.87	15.89
31/08/2015	14:00	18.06	17.13	16.20
31/08/2015	15:00	18.52	17.48	16.61
31/08/2015	16:00	18.99	17.86	17.03
31/08/2015	17:00	19.23	18.20	17.41
31/08/2015	18:00	19.37	18.37	17.62
31/08/2015	19:00	19.33	18.38	17.67
31/08/2015	20:00	19.33	18.35	17.57
31/08/2015	21:00	19.28	18.32	17.54
31/08/2015	22:00	19.21	18.22	17.43
31/08/2015	23:00	19.09	18.06	17.24
31/08/2015	0:00	18.91	17.89	17.04
1/09/2015	1:00	18.68	17.74	16.88
1/09/2015	2:00	18.47	17.57	16.67
1/09/2015	3:00	18.15	17.34	16.41
1/09/2015	4:00	17.94	17.16	16.21
1/09/2015	5:00	17.71	17.00	16.00
1/09/2015	6:00	17.40	16.71	15.71
1/09/2015	7:00	17.28	16.57	15.51
1/09/2015	8:00	17.25	16.56	15.53

1/09/2015	9:00	17.31	16.60	15.57
1/09/2015	10:00	17.38	16.66	15.60
1/09/2015	11:00	17.56	16.76	15.72
1/09/2015	12:00	17.83	16.98	15.98
1/09/2015	13:00	18.09	17.20	16.29
1/09/2015	14:00	18.55	17.51	16.60
1/09/2015	15:00	18.99	17.88	17.05
1/09/2015	16:00	19.32	18.27	17.55
1/09/2015	17:00	19.54	18.67	17.96
1/09/2015	18:00	19.73	18.84	18.14
1/09/2015	19:00	19.73	18.90	18.24
1/09/2015	20:00	19.73	18.90	18.21
1/09/2015	21:00	19.68	18.87	18.19
1/09/2015	22:00	19.57	18.75	18.04
1/09/2015	23:00	19.41	18.55	17.81
1/09/2015	0:00	19.25	18.35	17.57
2/09/2015	1:00	19.11	18.17	17.35
2/09/2015	2:00	18.93	17.96	17.12
2/09/2015	3:00	18.69	17.77	16.88
2/09/2015	4:00	18.35	17.50	16.59
2/09/2015	5:00	18.16	17.33	16.39
2/09/2015	6:00	17.84	17.06	16.09
2/09/2015	7:00	17.73	17.01	16.00
2/09/2015	8:00	17.93	17.08	16.08
2/09/2015	9:00	18.13	17.24	16.35
2/09/2015	10:00	18.71	17.64	16.83
2/09/2015	11:00	19.23	18.15	17.40
2/09/2015	12:00	19.65	18.68	18.03
2/09/2015	13:00	20.08	19.27	18.71
2/09/2015	14:00	20.56	19.86	19.37
2/09/2015	15:00	20.98	20.45	20.02
2/09/2015	16:00	21.38	20.95	20.57
2/09/2015	17:00	21.61	21.26	20.95
2/09/2015	18:00	21.71	21.41	21.12

2/09/2015	19:00	21.73	21.42	21.11
2/09/2015	20:00	21.68	21.37	21.06
2/09/2015	21:00	21.55	21.26	20.93
2/09/2015	22:00	21.40	21.14	20.83
2/09/2015	23:00	21.39	21.06	20.67
2/09/2015	0:00	21.24	20.92	20.49
3/09/2015	1:00	21.10	20.73	20.27
3/09/2015	2:00	20.98	20.55	20.10
3/09/2015	3:00	20.86	20.41	19.97
3/09/2015	4:00	20.79	20.34	19.84
3/09/2015	5:00	20.74	20.22	19.70
3/09/2015	6:00	20.69	20.13	19.55
3/09/2015	7:00	20.61	20.10	19.60
3/09/2015	8:00	20.57	20.03	19.55
3/09/2015	9:00	20.48	19.94	19.42
3/09/2015	10:00	20.42	19.83	19.27
3/09/2015	11:00	20.42	19.80	19.21
3/09/2015	12:00	20.36	19.78	19.24
3/09/2015	13:00	20.44	19.83	19.27
3/09/2015	14:00	20.53	19.91	19.40
3/09/2015	15:00	20.64	20.02	19.49
3/09/2015	16:00	20.73	20.15	19.69
3/09/2015	17:00	20.80	20.28	19.84
3/09/2015	18:00	20.85	20.31	19.83
3/09/2015	19:00	20.71	20.12	19.66
3/09/2015	20:00	20.58	19.96	19.46
3/09/2015	21:00	20.39	19.65	19.13
3/09/2015	22:00	20.18	19.40	18.76
3/09/2015	23:00	19.94	19.10	18.44
3/09/2015	0:00	19.74	18.86	18.13
4/09/2015	1:00	19.44	18.45	17.70
4/09/2015	2:00	19.22	18.24	17.45
4/09/2015	3:00	18.96	17.87	17.03
4/09/2015	4:00	18.64	17.60	16.72

4/09/2015	5:00	18.27	17.41	16.51
4/09/2015	6:00	17.91	17.15	16.21
4/09/2015	7:00	17.75	16.96	15.97
4/09/2015	8:00	17.65	16.89	15.90
4/09/2015	9:00	17.68	16.96	15.97
4/09/2015	10:00	17.90	17.08	16.09
4/09/2015	11:00	18.14	17.22	16.29
4/09/2015	12:00	18.51	17.52	16.62
4/09/2015	13:00	18.96	17.89	17.16
4/09/2015	14:00	19.38	18.36	17.72
4/09/2015	15:00	19.81	18.92	18.34
4/09/2015	16:00	20.24	19.46	18.93
4/09/2015	17:00	20.55	19.86	19.32
4/09/2015	18:00	20.69	20.06	19.58
4/09/2015	19:00	20.76	20.18	19.69
4/09/2015	20:00	20.78	20.27	19.76
4/09/2015	21:00	20.70	20.18	19.70
4/09/2015	22:00	20.69	20.17	19.65
4/09/2015	23:00	20.59	20.05	19.53
4/09/2015	0:00	20.45	19.88	19.33
5/09/2015	1:00	20.28	19.67	19.08
5/09/2015	2:00	20.15	19.49	18.89
5/09/2015	3:00	19.99	19.30	18.65
5/09/2015	4:00	19.83	19.09	18.43
5/09/2015	5:00	19.68	18.88	18.16
5/09/2015	6:00	19.46	18.54	17.78
5/09/2015	7:00	19.33	18.44	17.70
5/09/2015	8:00	19.38	18.43	17.64
5/09/2015	9:00	19.45	18.55	17.80
5/09/2015	10:00	19.59	18.69	18.01
5/09/2015	11:00	19.85	18.96	18.24
5/09/2015	12:00	20.08	19.27	18.72
5/09/2015	13:00	20.38	19.67	19.23
5/09/2015	14:00	20.76	20.15	19.76

5/09/2015	15:00	21.19	20.71	20.37
5/09/2015	16:00	21.59	21.23	20.96
5/09/2015	17:00	21.94	21.66	21.39
5/09/2015	18:00	22.02	21.83	21.63
5/09/2015	19:00	22.05	21.84	21.60
5/09/2015	20:00	21.95	21.78	21.52
5/09/2015	21:00	21.86	21.67	21.35
5/09/2015	22:00	21.67	21.47	21.15
5/09/2015	23:00	21.56	21.30	20.97
5/09/2015	0:00	21.42	21.14	20.77
6/09/2015	1:00	21.23	20.91	20.54
6/09/2015	2:00	21.05	20.67	20.24
6/09/2015	3:00	20.85	20.42	19.95
6/09/2015	4:00	20.65	20.17	19.66
6/09/2015	5:00	20.46	19.90	19.34
6/09/2015	6:00	20.17	19.50	18.90
6/09/2015	7:00	20.04	19.34	18.72
6/09/2015	8:00	20.04	19.30	18.66
6/09/2015	9:00	20.01	19.33	18.77
6/09/2015	10:00	20.23	19.51	18.98
6/09/2015	11:00	20.49	19.78	19.31
6/09/2015	12:00	20.75	20.14	19.76
6/09/2015	13:00	21.09	20.59	20.21
6/09/2015	14:00	21.42	21.00	20.67
6/09/2015	15:00	21.69	21.35	21.09
6/09/2015	16:00	21.97	21.72	21.45
6/09/2015	17:00	22.15	21.97	21.74
6/09/2015	18:00	22.23	22.06	21.87
6/09/2015	19:00	22.21	22.07	21.84
6/09/2015	20:00	22.13	21.99	21.76
6/09/2015	21:00	22.06	21.94	21.65
6/09/2015	22:00	21.94	21.77	21.48
6/09/2015	23:00	21.82	21.61	21.30
6/09/2015	0:00	21.64	21.42	21.13

7/09/2015	1:00	21.50	21.25	20.92
7/09/2015	2:00	21.37	21.08	20.69
7/09/2015	3:00	21.23	20.90	20.54
7/09/2015	4:00	21.11	20.74	20.32
7/09/2015	5:00	20.96	20.56	20.14
7/09/2015	6:00	20.86	20.41	19.97
7/09/2015	7:00	20.75	20.24	19.75
7/09/2015	8:00	20.71	20.19	19.71
7/09/2015	9:00	20.72	20.15	19.73
7/09/2015	10:00	20.85	20.29	19.88
7/09/2015	11:00	21.05	20.57	20.21
7/09/2015	12:00	21.30	20.88	20.57
7/09/2015	13:00	21.63	21.29	21.02
7/09/2015	14:00	21.96	21.71	21.47
7/09/2015	15:00	22.24	22.08	21.90
7/09/2015	16:00	22.48	22.39	22.23
7/09/2015	17:00	22.62	22.59	22.47
7/09/2015	18:00	22.67	22.63	22.55
7/09/2015	19:00	22.63	22.61	22.50
7/09/2015	20:00	22.50	22.47	22.34
7/09/2015	21:00	22.42	22.35	22.15
7/09/2015	22:00	22.23	22.16	21.99
7/09/2015	23:00	22.10	21.94	21.69
7/09/2015	0:00	21.95	21.82	21.55
8/09/2015	1:00	21.80	21.63	21.34
8/09/2015	2:00	21.61	21.41	21.09
8/09/2015	3:00	21.43	21.16	20.81
8/09/2015	4:00	21.25	20.95	20.54
8/09/2015	5:00	21.08	20.71	20.29
8/09/2015	6:00	20.86	20.40	19.93
8/09/2015	7:00	20.77	20.28	19.79
8/09/2015	8:00	20.74	20.23	19.73
8/09/2015	9:00	20.83	20.28	19.82
8/09/2015	10:00	20.99	20.47	20.03

8/09/2015	11:00	21.17	20.73	20.30
8/09/2015	12:00	21.40	21.01	20.68
8/09/2015	13:00	21.64	21.31	21.00
8/09/2015	14:00	21.83	21.58	21.31
8/09/2015	15:00	22.01	21.81	21.60
8/09/2015	16:00	22.19	22.03	21.88
8/09/2015	17:00	22.35	22.34	22.16
8/09/2015	18:00	22.36	22.31	22.19
8/09/2015	19:00	22.28	22.16	22.02
8/09/2015	20:00	22.04	21.86	21.61
8/09/2015	21:00	21.76	21.48	21.19
8/09/2015	22:00	21.41	21.07	20.73
8/09/2015	23:00	21.07	20.62	20.24
8/09/2015	0:00	20.81	20.32	19.85
9/09/2015	1:00	20.54	20.01	19.50
9/09/2015	2:00	20.25	19.63	19.05
9/09/2015	3:00	20.00	19.29	18.67
9/09/2015	4:00	19.72	18.96	18.28
9/09/2015	5:00	19.47	18.63	17.91
9/09/2015	6:00	19.23	18.30	17.48
9/09/2015	7:00	19.11	18.09	17.28
9/09/2015	8:00	19.02	18.01	17.20
9/09/2015	9:00	19.05	18.04	17.21
9/09/2015	10:00	19.12	18.09	17.28
9/09/2015	11:00	19.30	18.31	17.50
9/09/2015	12:00	19.52	18.59	17.83

Table 23 - Ambient Temperatures Whilst Curing (Started after 1 week)

Date	24 Hour Time	Ambient Temperature (Degrees Celsius)
		TC 7
20/08/2015	5:00	14.35
20/08/2015	6:00	15.04
20/08/2015	7:00	15.42
20/08/2015	8:00	15.85
20/08/2015	9:00	16.39
20/08/2015	10:00	17.00
20/08/2015	11:00	17.68
20/08/2015	12:00	18.46
20/08/2015	13:00	19.24
20/08/2015	14:00	19.85
20/08/2015	15:00	20.44
20/08/2015	16:00	20.50
20/08/2015	17:00	19.90
20/08/2015	18:00	19.39
20/08/2015	19:00	18.87
20/08/2015	20:00	18.41
20/08/2015	21:00	17.96
20/08/2015	22:00	17.49
20/08/2015	23:00	17.12
20/08/2015	0:00	16.90
21/08/2015	1:00	16.67
21/08/2015	2:00	16.51
21/08/2015	3:00	16.41
21/08/2015	4:00	16.13
21/08/2015	5:00	16.08
21/08/2015	6:00	16.27
21/08/2015	7:00	16.38
21/08/2015	8:00	16.87
21/08/2015	9:00	17.40

21/08/2015	10:00	17.92
21/08/2015	11:00	18.58
21/08/2015	12:00	18.97
21/08/2015	13:00	19.37
21/08/2015	14:00	19.64
21/08/2015	15:00	19.58
21/08/2015	16:00	19.21
21/08/2015	17:00	19.00
21/08/2015	18:00	18.73
21/08/2015	19:00	18.47
21/08/2015	20:00	18.29
21/08/2015	21:00	18.01
21/08/2015	22:00	17.99
21/08/2015	23:00	17.83
21/08/2015	0:00	17.74
22/08/2015	1:00	17.67
22/08/2015	2:00	17.62
22/08/2015	3:00	17.61
22/08/2015	4:00	17.59
22/08/2015	5:00	17.45
22/08/2015	6:00	17.66
22/08/2015	7:00	17.85
22/08/2015	8:00	18.14
22/08/2015	9:00	18.69
22/08/2015	10:00	19.56
22/08/2015	11:00	20.37
22/08/2015	12:00	21.39
22/08/2015	13:00	22.16
22/08/2015	14:00	22.84
22/08/2015	15:00	23.17
22/08/2015	16:00	23.20
22/08/2015	17:00	22.58
22/08/2015	18:00	21.96
22/08/2015	19:00	21.62

22/08/2015	20:00	21.28
22/08/2015	21:00	20.97
22/08/2015	22:00	20.68
22/08/2015	23:00	20.34
22/08/2015	0:00	20.05
23/08/2015	1:00	19.97
23/08/2015	2:00	19.77
23/08/2015	3:00	19.48
23/08/2015	4:00	19.24
23/08/2015	5:00	18.99
23/08/2015	6:00	18.94
23/08/2015	7:00	19.28
23/08/2015	8:00	19.53
23/08/2015	9:00	20.09
23/08/2015	10:00	20.78
23/08/2015	11:00	21.81
23/08/2015	12:00	22.69
23/08/2015	13:00	23.51
23/08/2015	14:00	23.86
23/08/2015	15:00	24.11
23/08/2015	16:00	24.11
23/08/2015	17:00	23.56
23/08/2015	18:00	22.92
23/08/2015	19:00	22.32
23/08/2015	20:00	21.96
23/08/2015	21:00	21.46
23/08/2015	22:00	21.10
23/08/2015	23:00	20.80
23/08/2015	0:00	20.57
24/08/2015	1:00	20.26
24/08/2015	2:00	19.92
24/08/2015	3:00	19.83
24/08/2015	4:00	19.48
24/08/2015	5:00	19.28

24/08/2015	6:00	19.32
24/08/2015	7:00	19.57
24/08/2015	8:00	19.94
24/08/2015	9:00	20.51
24/08/2015	10:00	21.14
24/08/2015	11:00	22.16
24/08/2015	12:00	23.21
24/08/2015	13:00	24.31
24/08/2015	14:00	25.01
24/08/2015	15:00	24.91
24/08/2015	16:00	24.87
24/08/2015	17:00	24.35
24/08/2015	18:00	23.81
24/08/2015	19:00	23.28
24/08/2015	20:00	23.01
24/08/2015	21:00	22.59
24/08/2015	22:00	22.40
24/08/2015	23:00	22.08
24/08/2015	0:00	21.62
25/08/2015	1:00	21.38
25/08/2015	2:00	20.93
25/08/2015	3:00	20.86
25/08/2015	4:00	20.54
25/08/2015	5:00	20.13
25/08/2015	6:00	20.26
25/08/2015	7:00	20.66
25/08/2015	8:00	20.71
25/08/2015	9:00	20.74
25/08/2015	10:00	20.83
25/08/2015	11:00	21.33
25/08/2015	12:00	21.80
25/08/2015	13:00	22.43
25/08/2015	14:00	22.79
25/08/2015	15:00	23.28

25/08/2015	16:00	23.41
25/08/2015	17:00	22.94
25/08/2015	18:00	22.39
25/08/2015	19:00	21.89
25/08/2015	20:00	21.29
25/08/2015	21:00	20.68
25/08/2015	22:00	19.80
25/08/2015	23:00	19.13
25/08/2015	0:00	18.84
26/08/2015	1:00	18.58
26/08/2015	2:00	17.70
26/08/2015	3:00	17.48
26/08/2015	4:00	17.19
26/08/2015	5:00	16.84
26/08/2015	6:00	16.94
26/08/2015	7:00	17.09
26/08/2015	8:00	17.34
26/08/2015	9:00	17.90
26/08/2015	10:00	18.29
26/08/2015	11:00	19.06
26/08/2015	12:00	19.90
26/08/2015	13:00	20.76
26/08/2015	14:00	21.50
26/08/2015	15:00	22.15
26/08/2015	16:00	22.60
26/08/2015	17:00	22.01
26/08/2015	18:00	21.32
26/08/2015	19:00	20.58
26/08/2015	20:00	20.23
26/08/2015	21:00	19.90
26/08/2015	22:00	19.32
26/08/2015	23:00	19.05
26/08/2015	0:00	18.86
27/08/2015	1:00	18.57

27/08/2015	2:00	18.37
27/08/2015	3:00	18.17
27/08/2015	4:00	18.14
27/08/2015	5:00	17.81
27/08/2015	6:00	17.61
27/08/2015	7:00	17.77
27/08/2015	8:00	18.00
27/08/2015	9:00	18.00
27/08/2015	10:00	17.86
27/08/2015	11:00	18.05
27/08/2015	12:00	18.07
27/08/2015	13:00	18.34
27/08/2015	14:00	18.41
27/08/2015	15:00	18.48
27/08/2015	16:00	18.52
27/08/2015	17:00	18.36
27/08/2015	18:00	18.27
27/08/2015	19:00	18.09
27/08/2015	20:00	18.09
27/08/2015	21:00	17.94
27/08/2015	22:00	17.76
27/08/2015	23:00	17.67
27/08/2015	0:00	17.40
28/08/2015	1:00	17.44
28/08/2015	2:00	17.00
28/08/2015	3:00	16.86
28/08/2015	4:00	16.80
28/08/2015	5:00	16.60
28/08/2015	6:00	16.44
28/08/2015	7:00	16.44
28/08/2015	8:00	16.89
28/08/2015	9:00	17.30
28/08/2015	10:00	17.62
28/08/2015	11:00	18.01

28/08/2015	12:00	18.42
28/08/2015	13:00	18.75
28/08/2015	14:00	19.36
28/08/2015	15:00	19.86
28/08/2015	16:00	20.00
28/08/2015	17:00	19.33
28/08/2015	18:00	18.54
28/08/2015	19:00	17.93
28/08/2015	20:00	17.43
28/08/2015	21:00	17.11
28/08/2015	22:00	16.62
28/08/2015	23:00	16.02
28/08/2015	0:00	15.73
29/08/2015	1:00	15.38
29/08/2015	2:00	15.10
29/08/2015	3:00	14.69
29/08/2015	4:00	14.65
29/08/2015	5:00	14.48
29/08/2015	6:00	14.45
29/08/2015	7:00	15.08
29/08/2015	8:00	15.99
29/08/2015	9:00	16.87
29/08/2015	10:00	18.08
29/08/2015	11:00	19.37
29/08/2015	12:00	20.06
29/08/2015	13:00	20.05
29/08/2015	14:00	19.94
29/08/2015	15:00	18.89
29/08/2015	16:00	18.30
29/08/2015	17:00	17.95
29/08/2015	18:00	17.74
29/08/2015	19:00	17.52
29/08/2015	20:00	17.08
29/08/2015	21:00	17.07

29/08/2015	22:00	16.89
29/08/2015	23:00	16.70
29/08/2015	0:00	16.53
30/08/2015	1:00	16.00
30/08/2015	2:00	15.82
30/08/2015	3:00	15.40
30/08/2015	4:00	14.85
30/08/2015	5:00	14.68
30/08/2015	6:00	14.08
30/08/2015	7:00	14.59
30/08/2015	8:00	15.24
30/08/2015	9:00	15.48
30/08/2015	10:00	15.87
30/08/2015	11:00	16.27
30/08/2015	12:00	16.67
30/08/2015	13:00	17.00
30/08/2015	14:00	17.49
30/08/2015	15:00	18.03
30/08/2015	16:00	18.27
30/08/2015	17:00	17.42
30/08/2015	18:00	16.66
30/08/2015	19:00	16.02
30/08/2015	20:00	15.56
30/08/2015	21:00	14.75
30/08/2015	22:00	14.47
30/08/2015	23:00	14.24
30/08/2015	0:00	14.27
31/08/2015	1:00	13.49
31/08/2015	2:00	13.37
31/08/2015	3:00	12.99
31/08/2015	4:00	12.77
31/08/2015	5:00	12.51
31/08/2015	6:00	12.28
31/08/2015	7:00	13.14

31/08/2015	8:00	13.86
31/08/2015	9:00	14.39
31/08/2015	10:00	15.21
31/08/2015	11:00	15.92
31/08/2015	12:00	16.61
31/08/2015	13:00	17.16
31/08/2015	14:00	17.96
31/08/2015	15:00	18.53
31/08/2015	16:00	18.77
31/08/2015	17:00	17.97
31/08/2015	18:00	17.22
31/08/2015	19:00	16.61
31/08/2015	20:00	16.06
31/08/2015	21:00	15.87
31/08/2015	22:00	15.52
31/08/2015	23:00	14.88
31/08/2015	0:00	14.64
1/09/2015	1:00	14.52
1/09/2015	2:00	14.21
1/09/2015	3:00	13.94
1/09/2015	4:00	13.67
1/09/2015	5:00	13.78
1/09/2015	6:00	13.83
1/09/2015	7:00	14.15
1/09/2015	8:00	14.50
1/09/2015	9:00	15.02
1/09/2015	10:00	15.53
1/09/2015	11:00	16.29
1/09/2015	12:00	17.03
1/09/2015	13:00	17.81
1/09/2015	14:00	18.54
1/09/2015	15:00	19.35
1/09/2015	16:00	19.69
1/09/2015	17:00	18.89

1/09/2015	18:00	18.21
1/09/2015	19:00	17.65
1/09/2015	20:00	17.03
1/09/2015	21:00	16.75
1/09/2015	22:00	16.16
1/09/2015	23:00	15.55
1/09/2015	0:00	15.25
2/09/2015	1:00	14.98
2/09/2015	2:00	14.74
2/09/2015	3:00	14.65
2/09/2015	4:00	14.33
2/09/2015	5:00	14.18
2/09/2015	6:00	14.81
2/09/2015	7:00	15.79
2/09/2015	8:00	16.70
2/09/2015	9:00	18.21
2/09/2015	10:00	19.39
2/09/2015	11:00	20.43
2/09/2015	12:00	21.47
2/09/2015	13:00	22.65
2/09/2015	14:00	23.34
2/09/2015	15:00	23.71
2/09/2015	16:00	23.40
2/09/2015	17:00	22.81
2/09/2015	18:00	22.39
2/09/2015	19:00	21.58
2/09/2015	20:00	21.29
2/09/2015	21:00	20.73
2/09/2015	22:00	20.50
2/09/2015	23:00	19.97
2/09/2015	0:00	19.48
3/09/2015	1:00	19.40
3/09/2015	2:00	19.17
3/09/2015	3:00	19.24

3/09/2015	4:00	19.24
3/09/2015	5:00	19.13
3/09/2015	6:00	19.31
3/09/2015	7:00	19.26
3/09/2015	8:00	18.82
3/09/2015	9:00	18.91
3/09/2015	10:00	19.12
3/09/2015	11:00	19.34
3/09/2015	12:00	19.77
3/09/2015	13:00	20.15
3/09/2015	14:00	20.51
3/09/2015	15:00	20.76
3/09/2015	16:00	20.73
3/09/2015	17:00	19.78
3/09/2015	18:00	18.81
3/09/2015	19:00	18.05
3/09/2015	20:00	17.22
3/09/2015	21:00	16.53
3/09/2015	22:00	16.00
3/09/2015	23:00	15.18
3/09/2015	0:00	14.85
4/09/2015	1:00	14.62
4/09/2015	2:00	14.28
4/09/2015	3:00	13.90
4/09/2015	4:00	13.30
4/09/2015	5:00	13.44
4/09/2015	6:00	13.69
4/09/2015	7:00	14.39
4/09/2015	8:00	14.92
4/09/2015	9:00	15.57
4/09/2015	10:00	16.29
4/09/2015	11:00	17.27
4/09/2015	12:00	18.46
4/09/2015	13:00	19.61

4/09/2015	14:00	20.77
4/09/2015	15:00	21.66
4/09/2015	16:00	21.58
4/09/2015	17:00	21.12
4/09/2015	18:00	20.65
4/09/2015	19:00	20.30
4/09/2015	20:00	19.61
4/09/2015	21:00	18.97
4/09/2015	22:00	18.68
4/09/2015	23:00	17.98
4/09/2015	0:00	17.52
5/09/2015	1:00	17.20
5/09/2015	2:00	17.07
5/09/2015	3:00	16.70
5/09/2015	4:00	16.36
5/09/2015	5:00	15.94
5/09/2015	6:00	16.64
5/09/2015	7:00	17.25
5/09/2015	8:00	17.82
5/09/2015	9:00	18.46
5/09/2015	10:00	19.23
5/09/2015	11:00	20.36
5/09/2015	12:00	21.32
5/09/2015	13:00	22.34
5/09/2015	14:00	23.50
5/09/2015	15:00	24.17
5/09/2015	16:00	24.37
5/09/2015	17:00	23.63
5/09/2015	18:00	22.96
5/09/2015	19:00	21.76
5/09/2015	20:00	21.02
5/09/2015	21:00	20.55
5/09/2015	22:00	19.92
5/09/2015	23:00	19.47

5/09/2015	0:00	19.09
6/09/2015	1:00	18.90
6/09/2015	2:00	18.15
6/09/2015	3:00	17.86
6/09/2015	4:00	17.83
6/09/2015	5:00	17.18
6/09/2015	6:00	17.78
6/09/2015	7:00	18.32
6/09/2015	8:00	18.94
6/09/2015	9:00	19.79
6/09/2015	10:00	20.78
6/09/2015	11:00	21.63
6/09/2015	12:00	22.86
6/09/2015	13:00	23.32
6/09/2015	14:00	23.72
6/09/2015	15:00	24.09
6/09/2015	16:00	24.00
6/09/2015	17:00	23.41
6/09/2015	18:00	22.86
6/09/2015	19:00	22.51
6/09/2015	20:00	21.96
6/09/2015	21:00	21.28
6/09/2015	22:00	20.64
6/09/2015	23:00	20.50
6/09/2015	0:00	20.07
7/09/2015	1:00	19.74
7/09/2015	2:00	19.45
7/09/2015	3:00	19.25
7/09/2015	4:00	19.05
7/09/2015	5:00	19.06
7/09/2015	6:00	19.10
7/09/2015	7:00	19.61
7/09/2015	8:00	20.06
7/09/2015	9:00	20.69

7/09/2015	10:00	21.66
7/09/2015	11:00	22.65
7/09/2015	12:00	23.59
7/09/2015	13:00	24.39
7/09/2015	14:00	24.60
7/09/2015	15:00	24.84
7/09/2015	16:00	24.67
7/09/2015	17:00	24.11
7/09/2015	18:00	23.45
7/09/2015	19:00	22.66
7/09/2015	20:00	22.44
7/09/2015	21:00	21.71
7/09/2015	22:00	21.31
7/09/2015	23:00	20.91
7/09/2015	0:00	20.27
8/09/2015	1:00	20.02
8/09/2015	2:00	19.46
8/09/2015	3:00	19.28
8/09/2015	4:00	18.82
8/09/2015	5:00	18.50
8/09/2015	6:00	19.08
8/09/2015	7:00	19.83
8/09/2015	8:00	20.38
8/09/2015	9:00	21.05
8/09/2015	10:00	21.85
8/09/2015	11:00	22.62
8/09/2015	12:00	23.31
8/09/2015	13:00	23.67
8/09/2015	14:00	23.86
8/09/2015	15:00	24.02
8/09/2015	16:00	24.52
8/09/2015	17:00	23.10
8/09/2015	18:00	21.45
8/09/2015	19:00	20.38

8/09/2015	20:00	19.10
8/09/2015	21:00	18.21
8/09/2015	22:00	17.51
8/09/2015	23:00	16.82
8/09/2015	0:00	16.52
9/09/2015	1:00	16.33
9/09/2015	2:00	15.82
9/09/2015	3:00	15.36
9/09/2015	4:00	15.38
9/09/2015	5:00	15.16
9/09/2015	6:00	15.56
9/09/2015	7:00	15.89
9/09/2015	8:00	16.42
9/09/2015	9:00	16.97
9/09/2015	10:00	17.61
9/09/2015	11:00	19.82
9/09/2015	12:00	21.66

Appendix E2 – Heating Temperatures

Table 24 - Experimental Heating Temperatures

		Temperature (Degrees Celsius)					
Time (Minutes)	Time (Hours)	TC (FBG) 0	FBG	TC 1	TC 2	TC 3	TC 4
0	0.00	22.5	22.4	24.0	25.3	21.0	20.2
1	0.02	22.6	22.5	24.0	25.3	21.0	20.7
2	0.03	23.0	22.9	24.5	25.7	21.4	20.3
3	0.05	26.5	26.7	28.0	29.2	24.9	20.2
4	0.07	32.5	32.7	34.0	35.2	30.9	20.1
5	0.08	38.8	39.0	40.3	41.5	37.2	20.4
6	0.10	44.8	45.0	46.2	47.5	43.2	20.2
7	0.12	50.5	50.7	52.0	53.3	49.0	21.8
8	0.13	56.1	56.4	57.6	58.9	54.6	21.7
9	0.15	61.3	61.6	62.7	64.0	59.7	22.2
10	0.17	65.9	66.2	67.3	68.6	64.3	22.6
11	0.18	70.2	70.5	71.7	73.0	68.7	22.5
12	0.20	74.1	74.4	75.6	76.9	72.6	22.6
13	0.22	77.8	78.1	79.3	80.6	76.3	23.0
14	0.23	81.4	81.7	82.8	84.1	79.8	23.5
15	0.25	84.8	85.1	86.3	87.6	83.3	24.1
16	0.27	88.0	88.4	89.4	90.7	86.4	24.7
17	0.28	91.4	91.8	92.9	94.2	89.9	25.5
18	0.30	96.7	97.1	98.2	99.5	95.2	26.3
19	0.32	97.2	97.6	98.7	99.9	95.6	27.7
20	0.33	97.6	98.0	99.1	100.3	96.0	29.1
21	0.35	97.7	98.1	99.1	100.4	96.1	32.6
22	0.37	97.7	98.1	99.1	100.4	96.1	35.1
23	0.38	97.8	98.2	99.3	100.6	96.3	36.8
24	0.40	97.9	98.3	99.3	100.6	96.3	38.4
25	0.42	98.0	98.4	99.5	100.7	96.4	40.0
26	0.43	97.9	98.3	99.4	100.6	96.3	41.1

27	0.45	98.4	98.8	99.8	101.1	96.8	42.2
28	0.47	99.5	100.0	101.0	102.3	98.0	43.2
29	0.48	100.3	100.8	101.8	103.0	98.7	44.2
30	0.50	101.3	101.8	102.7	104.0	99.7	45.2
31	0.52	102.6	103.1	104.0	105.3	101.0	46.1
32	0.53	105.0	105.5	106.4	107.7	103.4	47.1
33	0.55	107.5	108.0	108.9	110.2	105.9	58.0
34	0.57	109.9	110.4	111.4	112.7	108.3	58.9
35	0.58	112.5	113.0	114.0	115.3	111.0	59.7
36	0.60	115.1	115.6	116.6	117.9	113.5	60.5
37	0.62	117.8	118.3	119.3	120.5	116.2	61.6
38	0.63	120.2	120.7	121.7	123.0	118.7	62.7
39	0.65	122.6	123.1	124.1	125.4	121.1	63.3
40	0.67	125.0	125.5	126.5	127.8	123.5	64.0
41	0.68	127.6	128.1	129.0	130.3	126.0	65.1
42	0.70	130.2	130.7	131.6	132.9	128.6	65.8
43	0.72	132.8	133.3	134.3	135.6	131.3	67.1
44	0.73	135.3	135.8	136.8	138.1	133.8	67.7
45	0.75	137.4	137.9	138.9	140.2	135.9	68.9
46	0.77	139.5	140.0	141.0	142.3	138.0	69.1
47	0.78	141.2	141.7	142.6	143.9	139.6	68.9
48	0.80	142.0	142.5	143.5	144.7	140.4	71.4
49	0.82	142.7	143.2	144.2	145.5	141.2	72.0
50	0.83	143.7	144.2	145.2	146.5	142.2	71.9
51	0.85	144.5	145.0	145.9	147.2	142.9	73.5
52	0.87	145.2	145.7	146.6	147.9	143.6	72.9
53	0.88	145.4	145.9	146.9	148.2	143.9	72.4
54	0.90	145.3	145.7	146.8	148.1	143.8	72.1
55	0.92	144.5	144.9	146.0	147.3	143.0	72.9
56	0.93	143.3	143.7	144.8	146.0	141.7	70.8
57	0.95	141.7	142.1	143.2	144.5	140.2	73.5
58	0.97	139.8	140.2	141.2	142.5	138.2	74.4
59	0.98	138.0	138.4	139.4	140.7	136.4	74.8
60	1.00	136.3	136.7	137.8	139.0	134.7	76.6

61	1.02	134.6	135.0	136.1	137.3	133.0	76.6
62	1.03	133.0	133.4	134.5	135.8	131.4	79.1
63	1.05	131.9	132.3	133.4	134.7	130.4	79.7
64	1.07	131.4	131.8	132.9	134.2	129.9	81.7
65	1.08	132.5	132.9	133.9	135.2	130.9	82.0
66	1.10	133.8	134.2	135.2	136.5	132.2	82.0
67	1.12	133.9	134.3	135.3	136.6	132.3	82.1
68	1.13	133.0	133.4	134.4	135.7	131.4	82.9
69	1.15	131.6	132.0	133.0	134.3	130.0	83.0
70	1.17	129.8	130.2	131.3	132.6	128.2	83.0
71	1.18	127.9	128.2	129.4	130.6	126.3	83.2
72	1.20	126.1	126.4	127.6	128.9	124.6	83.4
73	1.22	124.5	124.8	126.0	127.3	123.0	83.4
74	1.23	123.0	123.3	124.4	125.7	121.4	83.5
75	1.25	121.4	121.7	122.8	124.1	119.8	83.7
76	1.27	119.7	120.0	121.2	122.4	118.1	83.8
77	1.28	118.1	118.4	119.5	120.8	116.5	83.9
78	1.30	116.5	116.8	118.0	119.3	115.0	83.2
79	1.32	115.0	115.3	116.5	117.7	113.4	83.3
80	1.33	113.5	113.8	115.0	116.2	111.9	83.8
81	1.35	112.0	112.3	113.5	114.8	110.5	83.9
82	1.37	110.6	110.9	112.1	113.4	109.1	83.9
83	1.38	109.2	109.5	110.7	112.0	107.7	83.9
84	1.40	107.9	108.2	109.3	110.6	106.3	83.5
85	1.42	106.5	106.8	108.0	109.2	104.9	83.9
86	1.43	105.2	105.4	106.7	108.0	103.7	83.6
87	1.45	103.9	104.1	105.4	106.7	102.3	82.9
88	1.47	102.7	102.9	104.2	105.5	101.2	83.0
89	1.48	101.5	101.7	103.0	104.3	99.9	83.6
90	1.50	100.4	100.6	101.9	103.1	98.8	83.4
91	1.52	99.3	99.5	100.8	102.0	97.7	83.2
92	1.53	98.2	98.4	99.7	101.0	96.7	82.5
93	1.55	97.2	97.4	98.7	100.0	95.7	83.4
94	1.57	96.2	96.4	97.7	99.0	94.6	83.1

95	1.58	95.2	95.4	96.7	97.9	93.6	82.5
96	1.60	94.3	94.5	95.7	97.0	92.7	82.6
97	1.62	93.4	93.6	94.9	96.1	91.8	82.7
98	1.63	92.5	92.7	93.9	95.2	90.9	82.5
99	1.65	91.6	91.8	93.0	94.3	90.0	82.4
100	1.67	90.8	91.0	92.2	93.5	89.2	82.0
101	1.68	89.9	90.1	91.4	92.7	88.4	82.2
102	1.70	89.1	89.3	90.6	91.9	87.6	81.0
103	1.72	88.3	88.5	89.8	91.1	86.8	82.0
104	1.73	87.6	87.8	89.0	90.3	86.0	81.0
105	1.75	86.8	87.0	88.2	89.5	85.2	81.7
106	1.77	86.0	86.2	87.5	88.7	84.4	81.0
107	1.78	85.3	85.5	86.7	88.0	83.7	81.1
108	1.80	84.6	84.8	86.1	87.3	83.0	79.5
109	1.82	83.9	84.1	85.4	86.6	82.3	80.0
110	1.83	83.2	83.4	84.7	86.0	81.6	79.4
111	1.85	82.5	82.7	84.0	85.3	80.9	78.2
112	1.87	81.9	82.1	83.4	84.6	80.3	76.8
113	1.88	81.2	81.4	82.7	84.0	79.7	78.0
114	1.90	80.6	80.8	82.1	83.4	79.1	77.4
115	1.92	80.0	80.2	81.5	82.8	78.4	77.1
116	1.93	79.4	79.6	80.9	82.1	77.8	76.7
117	1.95	78.8	79.0	80.3	81.5	77.2	75.8
118	1.97	78.2	78.4	79.7	81.0	76.6	74.8
119	1.98	77.6	77.8	79.1	80.3	76.0	73.5
120	2.00	77.0	77.2	78.5	79.7	75.4	74.4
121	2.02	76.4	76.6	77.9	79.1	74.8	74.5
122	2.03	75.8	76.0	77.3	78.6	74.3	74.4
123	2.05	75.3	75.5	76.8	78.0	73.7	73.4
124	2.07	74.8	75.0	76.2	77.5	73.2	73.1
125	2.08	74.2	74.4	75.7	77.0	72.7	73.3
126	2.10	73.7	73.9	75.2	76.5	72.2	72.9
127	2.12	73.2	73.4	74.7	75.9	71.6	72.6
128	2.13	72.7	72.9	74.1	75.4	71.1	71.9

129	2.15	72.2	72.4	73.6	74.9	70.6	71.7
130	2.17	71.7	71.9	73.2	74.4	70.1	71.6
131	2.18	71.2	71.4	72.7	74.0	69.7	69.0
132	2.20	70.7	70.9	72.2	73.5	69.1	69.2
133	2.22	70.2	70.4	71.7	73.0	68.7	69.1
134	2.23	69.7	69.9	71.2	72.5	68.2	68.9
135	2.25	69.3	69.5	70.7	72.0	67.7	68.8
136	2.27	68.8	69.0	70.3	71.6	67.3	69.0
137	2.28	68.4	68.6	69.9	71.2	66.8	68.4
138	2.30	67.9	68.1	69.4	70.7	66.4	68.3
139	2.32	67.5	67.7	69.0	70.3	65.9	67.3
140	2.33	67.1	67.3	68.6	69.8	65.5	66.9
141	2.35	66.7	66.9	68.1	69.4	65.1	67.0
142	2.37	66.3	66.5	67.7	69.0	64.7	66.9
143	2.38	65.8	66.0	67.3	68.6	64.3	66.4
144	2.40	65.4	65.6	66.9	68.2	63.9	65.9
145	2.42	65.0	65.2	66.4	67.7	63.4	65.4
146	2.43	64.6	64.8	66.1	67.3	63.0	65.7
147	2.45	64.2	64.4	65.7	67.0	62.7	65.2
148	2.47	63.8	64.0	65.3	66.6	62.3	65.0
149	2.48	63.5	63.7	64.9	66.2	61.9	64.7
150	2.50	63.1	63.3	64.6	65.9	61.5	64.8
151	2.52	62.7	62.9	64.2	65.5	61.2	64.2
152	2.53	62.4	62.6	63.9	65.1	60.8	64.1
153	2.55	62.1	62.3	63.5	64.8	60.5	63.1
154	2.57	61.8	62.0	63.2	64.5	60.2	63.5
155	2.58	61.4	61.6	62.8	64.1	59.8	63.3
156	2.60	61.0	61.2	62.5	63.7	59.4	63.1
157	2.62	60.7	60.9	62.1	63.4	59.1	62.7
158	2.63	60.3	60.5	61.8	63.1	58.7	62.7
159	2.65	60.0	60.2	61.5	62.7	58.4	62.1
160	2.67	59.6	59.8	61.1	62.4	58.1	62.2
161	2.68	59.3	59.5	60.8	62.1	57.7	61.9
162	2.70	59.0	59.2	60.5	61.7	57.4	61.4

163	2.72	58.6	58.8	60.1	61.4	57.1	61.5
164	2.73	58.4	58.6	59.8	61.1	56.8	61.3
165	2.75	58.1	58.3	59.5	60.8	56.5	61.3
166	2.77	57.8	58.0	59.2	60.5	56.2	60.7
167	2.78	57.4	57.6	58.9	60.2	55.9	60.9
168	2.80	57.1	57.3	58.6	59.9	55.6	60.4
169	2.82	56.8	57.0	58.3	59.6	55.3	60.2
170	2.83	56.5	56.6	58.0	59.3	55.0	59.8
171	2.85	56.2	56.3	57.7	59.0	54.7	59.8
172	2.87	55.9	56.0	57.4	58.7	54.4	59.3
173	2.88	55.6	55.7	57.1	58.4	54.1	59.2
174	2.90	55.3	55.4	56.8	58.1	53.8	59.2
175	2.92	55.0	55.1	56.5	57.8	53.5	58.4
176	2.93	54.7	54.8	56.2	57.5	53.2	58.2
177	2.95	54.5	54.6	56.0	57.3	52.9	59.7
178	2.97	54.2	54.3	55.7	57.0	52.7	55.9
179	2.98	54.0	54.1	55.4	56.7	52.4	57.5
180	3.00	53.6	53.7	55.1	56.4	52.1	54.6
181	3.02	53.4	53.5	54.9	56.2	51.8	52.4
182	3.03	53.1	53.2	54.6	55.9	51.6	52.7
183	3.05	52.8	52.9	54.3	55.6	51.3	51.2
184	3.07	52.5	52.7	54.0	55.2	50.9	52.9
185	3.08	52.1	52.3	53.6	54.9	50.6	52.8
186	3.10	51.8	52.0	53.3	54.6	50.3	52.7
187	3.12	51.5	51.7	53.0	54.3	50.0	52.6
188	3.13	51.3	51.5	52.8	54.0	49.7	52.4
189	3.15	51.0	51.2	52.5	53.8	49.5	52.2
190	3.17	50.8	51.0	52.3	53.5	49.2	52.1
191	3.18	50.5	50.7	52.0	53.3	49.0	51.9
192	3.20	50.3	50.5	51.8	53.0	48.7	51.7
193	3.22	50.0	50.2	51.5	52.8	48.5	51.5
194	3.23	49.8	50.0	51.3	52.6	48.2	51.4
195	3.25	49.6	49.8	51.0	52.3	48.0	51.2
196	3.27	49.3	49.5	50.8	52.1	47.8	50.9

197	3.28	49.1	49.3	50.6	51.9	47.6	50.8
198	3.30	48.9	49.1	50.4	51.6	47.3	50.6
199	3.32	48.7	48.9	50.2	51.5	47.1	50.6
200	3.33	48.4	48.6	49.9	51.2	46.9	50.4
201	3.35	48.2	48.4	49.7	51.0	46.7	50.2
202	3.37	48.0	48.2	49.5	50.8	46.4	50.1
203	3.38	47.8	48.0	49.2	50.5	46.2	49.9
204	3.40	47.6	47.8	49.0	50.3	46.0	49.8
205	3.42	47.4	47.6	48.8	50.1	45.8	49.6
206	3.43	47.2	47.4	48.6	49.9	45.6	49.5
207	3.45	46.9	47.1	48.4	49.7	45.4	49.3
208	3.47	46.7	46.9	48.2	49.5	45.2	49.1
209	3.48	46.5	46.7	48.0	49.3	44.9	49.1
210	3.50	46.3	46.5	47.8	49.1	44.8	49.0
211	3.52	46.1	46.3	47.6	48.9	44.5	48.7
212	3.53	45.9	46.1	47.4	48.6	44.3	48.7
213	3.55	45.7	45.9	47.2	48.5	44.2	48.6
214	3.57	45.5	45.7	47.0	48.3	44.0	48.4
215	3.58	45.3	45.5	46.8	48.1	43.8	48.3
216	3.60	45.2	45.4	46.6	47.9	43.6	48.2
217	3.62	45.0	45.2	46.5	47.7	43.4	48.0
218	3.63	44.8	45.0	46.3	47.5	43.2	47.8
219	3.65	44.6	44.8	46.1	47.3	43.0	47.7
220	3.67	44.4	44.6	45.9	47.2	42.9	47.6
221	3.68	44.2	44.4	45.7	47.0	42.6	47.5
222	3.70	44.0	44.2	45.5	46.8	42.5	47.4
223	3.72	43.8	44.0	45.3	46.6	42.3	47.2
224	3.73	43.7	43.9	45.2	46.5	42.1	47.0
225	3.75	43.5	43.7	45.0	46.3	42.0	47.0
226	3.77	43.3	43.5	44.8	46.1	41.8	46.8
227	3.78	43.2	43.4	44.6	45.9	41.6	46.8
228	3.80	43.0	43.2	44.4	45.7	41.4	46.5
229	3.82	42.8	43.0	44.2	45.5	41.2	45.7
230	3.83	42.6	42.8	44.0	45.3	41.0	45.4

231	3.85	42.4	42.6	43.8	45.1	40.8	45.1
232	3.87	42.2	42.4	43.7	44.9	40.6	44.9
233	3.88	42.0	42.2	43.5	44.7	40.4	44.8
234	3.90	41.8	42.0	43.3	44.6	40.2	44.6
235	3.92	41.6	41.8	43.1	44.4	40.1	44.4
236	3.93	41.4	41.6	42.9	44.2	39.9	44.2
237	3.95	41.2	41.4	42.7	44.0	39.7	44.0
238	3.97	41.1	41.3	42.5	43.8	39.5	43.8
239	3.98	40.9	41.1	42.3	43.6	39.3	43.6
240	4.00	40.7	40.9	42.2	43.4	39.1	43.5
241	4.02	40.5	40.7	42.0	43.3	39.0	43.3
242	4.03	40.3	40.5	41.8	43.1	38.8	43.1
243	4.05	40.2	40.4	41.6	42.9	38.6	42.9
244	4.07	40.0	40.2	41.4	42.7	38.4	42.7
245	4.08	39.8	40.0	41.3	42.6	38.3	42.6
246	4.10	39.6	39.8	41.1	42.4	38.1	42.4
247	4.12	39.5	39.7	41.0	42.2	37.9	42.2
248	4.13	39.3	39.5	40.8	42.1	37.8	42.1
249	4.15	39.2	39.4	40.6	41.9	37.6	41.9
250	4.17	39.0	39.2	40.5	41.7	37.4	41.7
251	4.18	38.8	39.0	40.3	41.6	37.3	41.6
252	4.20	38.7	38.9	40.1	41.4	37.1	41.4
253	4.22	38.5	38.7	40.0	41.2	36.9	41.3
254	4.23	38.3	38.5	39.8	41.1	36.8	41.1
255	4.25	38.2	38.4	39.6	40.9	36.6	40.9
256	4.27	38.0	38.2	39.5	40.8	36.5	40.8
257	4.28	37.9	38.1	39.3	40.6	36.3	40.6
258	4.30	37.7	37.9	39.2	40.5	36.1	40.5
259	4.32	37.5	37.7	39.0	40.3	36.0	40.3
260	4.33	37.4	37.6	38.9	40.1	35.8	40.2
261	4.35	37.2	37.4	38.7	40.0	35.7	40.0
262	4.37	37.1	37.3	38.6	39.8	35.5	39.8
263	4.38	36.9	37.1	38.4	39.7	35.4	39.7
264	4.40	36.8	37.0	38.2	39.5	35.2	39.5

265	4.42	36.6	36.8	38.1	39.4	35.1	39.4
266	4.43	36.5	36.7	37.9	39.2	34.9	39.2
267	4.45	36.3	36.5	37.8	39.1	34.8	39.1
268	4.47	36.2	36.4	37.6	38.9	34.6	38.9
269	4.48	36.0	36.2	37.5	38.8	34.5	38.8
270	4.50	35.9	36.1	37.3	38.6	34.3	38.6
271	4.52	35.7	35.9	37.2	38.5	34.2	38.5
272	4.53	35.6	35.8	37.0	38.3	34.0	38.3
273	4.55	35.4	35.6	36.9	38.2	33.9	38.2
274	4.57	35.3	35.5	36.7	38.0	33.7	38.0
275	4.58	35.1	35.3	36.6	37.9	33.6	37.9
276	4.60	35.0	35.2	36.4	37.7	33.4	37.7
277	4.62	34.8	35.0	36.3	37.6	33.3	37.6
278	4.63	34.7	34.9	36.1	37.4	33.1	37.4
279	4.65	34.5	34.7	36.0	37.3	33.0	37.3
280	4.67	34.4	34.6	35.8	37.1	32.8	37.1
281	4.68	34.2	34.4	35.7	37.0	32.7	37.0
282	4.70	34.1	34.3	35.6	36.8	32.5	36.9
283	4.72	33.9	34.1	35.4	36.7	32.4	36.7
284	4.73	33.8	34.0	35.3	36.6	32.2	36.6
285	4.75	33.7	33.9	35.1	36.4	32.1	36.4
286	4.77	33.5	33.7	35.0	36.3	32.0	36.3
287	4.78	33.4	33.6	34.9	36.1	31.8	36.1
288	4.80	33.2	33.4	34.7	36.0	31.7	36.0
289	4.82	33.1	33.3	34.6	35.9	31.5	35.9
290	4.83	33.0	33.2	34.4	35.7	31.4	35.7
291	4.85	32.8	33.0	34.3	35.6	31.3	35.6
292	4.87	32.7	32.9	34.2	35.4	31.1	35.5
293	4.89	32.6	32.8	34.0	35.3	31.0	35.3
294	4.90	32.4	32.6	33.9	35.2	30.9	35.2
295	4.92	32.3	32.5	33.8	35.0	30.7	35.1
296	4.94	32.2	32.4	33.6	34.9	30.6	34.9
297	4.95	32.0	32.2	33.5	34.8	30.5	34.8
298	4.97	31.9	32.1	33.4	34.6	30.3	34.6

299	4.99	31.8	32.0	33.2	34.5	30.2	34.5
300	5.00	31.6	31.8	33.1	34.4	30.1	34.4
301	5.02	31.5	31.7	33.0	34.2	29.9	34.2
302	5.04	31.4	31.6	32.8	34.1	29.8	34.1
303	5.05	31.2	31.4	32.7	34.0	29.7	34.0
304	5.07	31.1	31.3	32.6	33.8	29.5	33.9
305	5.09	31.0	31.2	32.4	33.7	29.4	33.7
306	5.10	30.8	31.0	32.3	33.6	29.3	33.6
307	5.12	30.7	30.9	32.2	33.4	29.1	33.5
308	5.14	30.6	30.8	32.0	33.3	29.0	33.3
309	5.15	30.4	30.6	31.9	33.2	28.9	33.2
310	5.17	30.3	30.5	31.8	33.0	28.7	33.1
311	5.19	30.2	30.4	31.6	32.9	28.6	32.9
312	5.20	30.0	30.2	31.5	32.8	28.5	32.8
313	5.22	29.9	30.1	31.4	32.7	28.3	32.7
314	5.24	29.8	30.0	31.2	32.5	28.2	32.5
315	5.25	29.6	29.8	31.1	32.4	28.1	32.4
316	5.27	29.5	29.7	31.0	32.3	27.9	32.3
317	5.29	29.4	29.6	30.8	32.1	27.8	32.1
318	5.30	29.2	29.4	30.7	32.0	27.7	32.0
319	5.32	29.1	29.3	30.6	31.9	27.6	31.9
320	5.34	29.0	29.2	30.5	31.7	27.4	31.8
321	5.35	28.9	29.1	30.3	31.6	27.3	31.6
322	5.37	28.7	28.9	30.2	31.5	27.2	31.5
323	5.39	28.6	28.8	30.1	31.3	27.0	31.4
324	5.40	28.5	28.7	29.9	31.2	26.9	31.2
325	5.42	28.3	28.5	29.8	31.1	26.8	31.1
326	5.44	28.2	28.4	29.7	31.0	26.6	31.0
327	5.45	28.1	28.3	29.6	30.8	26.5	30.8
328	5.47	28.0	28.2	29.4	30.7	26.4	30.7
329	5.49	27.8	28.0	29.3	30.6	26.3	30.6
330	5.50	27.7	27.9	29.2	30.4	26.1	30.5
331	5.52	27.6	27.8	29.0	30.3	26.0	30.3
332	5.54	27.4	27.6	28.9	30.2	25.9	30.2

333	5.55	27.3	27.5	28.8	30.1	25.7	30.1
334	5.57	27.2	27.4	28.6	29.9	25.6	29.9
335	5.59	27.1	27.3	28.5	29.8	25.5	29.8
336	5.60	26.9	26.8	28.4	29.7	25.4	29.7
337	5.62	26.8	26.7	28.3	29.5	25.2	29.6
338	5.64	26.7	26.6	28.1	29.4	25.1	29.4
339	5.65	26.5	26.4	28.0	29.3	25.0	29.3
340	5.67	26.4	26.3	27.9	29.2	24.9	29.2
341	5.69	26.3	26.2	27.8	29.0	24.7	29.1
342	5.70	26.2	26.1	27.6	28.9	24.6	28.9
343	5.72	26.0	25.9	27.5	28.8	24.5	28.8
344	5.74	25.9	25.8	27.4	28.7	24.4	28.7
345	5.75	25.8	25.7	27.3	28.5	24.2	28.6
346	5.77	25.7	25.6	27.1	28.4	24.1	28.4
347	5.79	25.5	25.4	27.0	28.3	24.0	28.3
348	5.80	25.4	25.3	26.9	28.2	23.9	28.2
349	5.82	25.3	25.2	26.8	28.0	23.7	28.0
350	5.84	25.2	25.1	26.6	27.9	23.6	27.9
351	5.85	25.0	24.9	26.5	27.8	23.5	27.8
352	5.87	24.9	24.8	26.4	27.7	23.4	27.7
353	5.89	24.8	24.7	26.3	27.5	23.2	27.6
354	5.90	24.7	24.6	26.1	27.4	23.1	27.4
355	5.92	24.5	24.4	26.0	27.3	23.0	27.3
356	5.94	24.4	24.3	25.9	27.2	22.9	27.2
357	5.95	24.3	24.2	25.8	27.0	22.7	27.1
358	5.97	24.2	24.1	25.6	26.9	22.6	26.9
359	5.99	24.0	23.9	25.5	26.8	22.5	26.8
360	6.00	23.9	23.8	25.4	26.7	22.4	26.7
361	6.02	23.8	23.7	25.3	26.6	22.2	26.6
362	6.04	23.7	23.6	25.2	26.1	22.1	26.4
363	6.05	23.6	23.5	25.0	26.0	22.0	26.3
364	6.07	23.4	23.3	24.9	25.9	21.9	26.2
365	6.09	23.3	23.2	24.8	25.8	21.8	26.1
366	6.10	23.2	23.1	24.7	25.6	21.6	26.0

367	6.12	23.1	23.0	24.5	25.5	21.5	25.8
368	6.14	22.9	22.8	24.4	25.4	21.4	25.2
369	6.15	22.8	22.7	24.3	25.3	21.3	25.1
370	6.17	22.7	22.6	24.2	25.1	21.1	25.0
371	6.19	22.6	22.6	24.1	25.0	21.0	24.8
372	6.20	22.5	22.6	23.9	24.9	20.9	24.7

Appendix E3 – Midpoint Deflections

Table 25 - Experimental Midpoint Deflections Associated with Loading Beam

Control Beam		Heated Beam	
Load (kN)	Deflection (mm)	Load (kN)	Deflection (mm)
5.00	1.52	5.00	1.66
10.01	1.74	10.00	1.95
15.00	1.91	15.00	2.19
20.01	2.10	20.01	2.42
25.01	2.33	25.00	2.62
30.00	2.54	30.01	2.82
35.00	2.75	35.01	3.01
40.00	3.00	40.00	3.20
45.01	3.25	45.01	3.40
50.00	3.50	50.01	3.63
55.00	3.78	55.00	3.92
60.00	4.12	60.02	4.26
65.00	4.51	65.01	4.61
70.00	4.86	70.01	5.01
75.00	5.25	75.00	5.53
80.01	5.77	80.01	6.33
81.00	5.91	81.01	6.54
82.00	6.06	82.00	6.79
83.01	6.24	83.01	7.09
84.01	6.44	84.01	7.43
85.01	6.65	85.00	7.80
86.00	7.00	86.01	8.25
87.00	7.41	87.00	8.75
88.00	8.49	87.10	8.82
88.02	8.51	87.21	8.87
88.03	8.53	87.31	8.96
88.05	8.53	87.40	9.02

		87.50	9.11
		87.60	9.17
		87.70	9.26
		87.80	9.36
		87.92	9.57

Appendix E4 – Maximum Principal Strains Associated with Loading Beam

Table 26 - Experimental Maximum Principal Strains

Load (kN)	Strain $\times 10^{-6}$			
	Control SG1	Heated SG2	Heated SG3	Heated FBG
0	0	0	0	0.000
5	49	48	51	7.616
10	108	111	108	9.649
15	492	496	495	12.855
20	1163	1165	1169	15.951
25	2763	2769	2773	17.022
30	3914	3917	3921	24.755
35	4740	4742	4745	52.849
40	5390	5399	5401	64.750
45	6401	6407	6411	60.841
50		7311	7316	63.904
55		8523	8531	71.068
60		9556	9568	74.123
65		10298	10301	77.002
70		11632	11634	76.801
75		13012	13020	79.914
80		13967	13973	80.299
85		15001	15009	83.186
87.92		15004	15014	83.404
88.05				

Appendix E5 – Maximum Principal Stresses Associated with Loading Beam

Table 27 - Experimental Maximum Principal Stresses

Load (kN)	Stress (MPa)			
	Control SG1	Heated SG2	Heated SG3	Heated FBG
0	0.000	0.000	0.000	0.000000
5	0.081	0.071	0.075	0.011194
10	0.178	0.163	0.159	0.014184
15	0.813	0.729	0.728	0.018895
20	1.921	1.712	1.718	0.023447
25	4.563	4.070	4.076	0.025021
30	6.464	5.758	5.764	0.036388
35	7.828	6.970	6.975	0.077684
40	8.902	7.936	7.939	0.095177
45	10.572	9.418	9.424	0.089432
50		10.747	10.754	0.093935
55		12.528	12.540	0.104465
60		14.047	14.064	0.108955
65		15.137	15.142	0.113187
70		17.098	17.101	0.112892
75		19.127	19.138	0.117468
80		20.531	20.539	0.118034
85		22.050	22.062	0.122278
87.92		22.055	22.070	0.122598
88.05				